

REMAINING USEFUL LIFE ESTIMATIONS APPLIED ON THE SIZING AND THE PROGNOSIS OF LITHIUM ION BATTERY ENERGY STORAGE SYSTEMS

Mikel Arrinda Martinez

Supervisors:

Eñaut Muxika Olasagasti

Mikel Oyarbide Urquizu



A thesis submitted for the degree of Doctoral Program in Engineering

at Electronics and Computer Science Department

Mondragon Unibertsitatea

February 2020

STATEMENT OF ORIGINALITY

I hereby declare that the research recorded in this thesis and the thesis itself was developed entirely by me at CIDETEC's Energy Storage System Unit with the collaboration of the Department of Electronics and Computer Science at the University of Mondragon.

The software used to perform the simulations was developed entirely by me on MATLAB except to the electric battery model, the thermal battery model and the sizing simulation environment for the Micro-grid use case. The electric and thermal battery models have been developed by my CIDETEC's colleagues Gorka Vertiz and Mikel Oyarbide. The foundation of the developed sizing simulation environment for the Micro-grid use case was the Simulink block that VUB had to evaluate different eolic and solar power plant sizing configurations along with an ideal Energy Storage System.

Acknowledgments

First of all, I would like to thank Eñaut Muxika for his help during these years conducting the thesis work as my director. You are one of the teachers I admired the most back at the university and it has been a pleasure to work with you. I would like to thank Mikel Oyarbide for his technical advices and for helping me when there were problems to go ahead. His support as co-director and as fellow researcher at CIDETEC has been fundamental on the development of this thesis and cannot be measured. This thesis is partly yours as well Mikel.

I want to thank as well my colleges that have given me great advises and have contributed on the development of this thesis. Thanks Cesar, Urtzi and Lander for all the extra work you have done on the lab due to me and for all the discussions we had, they have been nourishments for this thesis. Thanks Denis for providing the computer science point of view that I lacked when I started the thesis, the obtained cleanliness and universality on the developed tools is all thanks to your advice. Thanks Gorka for your explanations of the mechanical and thermal aspects that my electronic brain couldn't reach to completely understand. Thanks Iratxe for your unconditional predisposition to answer all the questions I had about the chemical aspects even though having so much work and so little time. I can't forget many other people from CIDETEC, Haritz, Iosu, Nerea, Ivan, Aitor, Cristina, Iker, Manex, Igor, Julen... thank you because it is so nice being with you every day.

I want to acknowledge CIDETEC research centre for their support during this work and for the opportunity to collaborate with them, it has been a pleasure for me.

I would also like to show my gratitude to the MOBI research centre and to the VUB University. Specially, I would like to acknowledge the people working in the department conducted by professor Coosemans. I felt part of the team since the first day and I had very good experiences working there. I also had the chance to experience how a huge university such as VUB manages research projects and how the integration of different disciplines could be done in such a good synergy.

I want to thank each member of the jury for coming to this event and for giving me their point of view about the developed work.

Nire familia eta lagunak eskertzea gustatuko litzaidake. Nire gurasoak bereziki eskertu nahiko nebazan, beti hor egon direlako behar izan dodazanean. Gaur nazen modukoa izatera heldu izana eurengatik izan da batez ere. Mila esker bixoi. Nire izeko, osaba eta lehengusu andanari eskerrak, beti hor daudelako eta espero denbora luzerako egotea. Nere amamak goian bego, jada hemen ez egon arren, euren irakatsiak eta oroitzapenak aurrera egiten laguntzen didatelako. Nire lagunei, nire oihu eta xelebrekeriak jasaten dabezalako, eta ala ere, nere alboan jarraitzen dabelako. Mila esker, zuei esker tentsio eta momentu txar guztiak puff batean desagertzen dira.

Nire neskalagun petralari eta oin nirea den bere familiari eskerrak ere. Adri, beti limitera daramadazu, baina beti maitasun eta intentzio onekaz beterik. Zuri esker nire limiteak gainditu eta pertsona hobea bilakatzen ari nazela argi daukat, mila esker. Tesia be, zer izango zan zu gabe, nahiago ez pentsa. Eta mila esker Josi, Maria, izeko, osaba eta lehengusu berri guztiei. Familia handituz doia, eta berarekin batera maite dodazanenganako nire esker ona.

Azkenik, nire ikasketa prozesuan eragina izan duten pertsonak aipatu nahiko nukeen. Lehendabizi, nire aita dago duda barik, non txikitatik miretsi izan dodan bere prestutasuna bai etxeko edo baserriko konponketak egiterakoan. Nire lehengusuak be eragin nabarmena izan dute, non arlo teknikoiez eztabaidatzeko aukera izan dodan txiki txikitatik. Eta bukatzeko, aipamen berezia egin nahiko nuke Javi teknori, goian bego, non berarekin ikastolan iragandako denbora izan baitzen ingeniariatza bat egiteko erabakia hartzearen arrazoi nagusia. Mila esker Javi.

Mila esker denoi!

Abstract

The present thesis develops an accurate sizing tool for the most relevant lithium ion battery energy storage system applications considering the aging and the remaining useful life. The developed tool involves firstly, the construction of the aging models of the lithium ion battery health indicators; secondly, the calculation of the end of life based on the evolution of the modelled health indicators; thirdly, the calculation of the levelized cost of the most relevant applications of lithium ion battery energy storage systems; and fourthly, the minimization of the committed error with the constructed aging models supported by electrode level data and prognosis algorithms. The methodology behind the construction and calculation of all the elements integrated on the sizing tool is described throughout the chapters of this thesis.

Firstly, the end of life state of the battery is determined as a combined threshold of all the health indicators of interest. Its calculation requires the implementation of an electro-thermal model in a simulation environment defined by the end of life criteria specified by the application requirements.

Secondly, the evolution of health indicators of interest are modelled based on the most relevant stress factors. The methodology to acquire the aging data and the construction of the posterior empirical models are presented. The validation of the constructed models based on the acquired data is performed based on three aspects: the accuracy describing the observed cases, the correctness of interpolations and the real life applicability.

Thirdly, the simulation environments for lithium ion battery energy storage systems applied on an electric vehicle application and on a stationary application are developed where the levelized cost of different battery solution sizes is calculated. The simulation environment integrates the already developed electric-thermal model, end of life map and aging models.

Fourthly, the error done by the constructed aging models is minimized by focusing on the errors done when extrapolating in time and when facing odd events. On one hand, electrode level data is analysed to generate data artificially and reduce the errors when extrapolating in time. On the other hand, a prognosis stochastic algorithm is selected and employed with real life data to deal with the effect that odd events have on the evolution of the health indicators.

The validity of many assumptions made for the development of the end of life map, the aging models, the simulation environment used on the sizing tool, the artificial data generator and the real time prognosis tool are proved experimentally.

CONTENTS LIST

STATEMENT OF ORIGINALITY	I
ACKNOWLEDGMENTS	III
ABSTRACT	V
LIST OF ILLUSTRATIONS	IX
LIST OF TABLES	XIII
ABBREVIATIONS	XVII
GLOSSARY	XIX
1 INTRODUCTION	1
1.1 BACKGROUND	2
1.1.1 <i>Lithium-ion battery</i>	3
1.1.2 <i>Remaining useful life</i>	10
1.2 OBJECTIVES AND SCOPE	11
1.3 METHODOLOGY AND STRUCTURE OF THE THESIS	12
1.4 SCIENTIFIC CONTRIBUTIONS	15
2 END OF LIFE CALCULATION FRAMEWORK	17
2.1 INTRODUCTION	18
2.2 METHODOLOGY	18
2.3 HEALTH INDICATORS	20
2.4 APPLICATION REQUIREMENTS	21
2.4.1 <i>High-Energy application</i>	21
2.4.2 <i>High-Power application</i>	22
2.5 SIMULATION	23
2.5.1 <i>Battery model</i>	23
2.5.2 <i>End of Life mapping algorithm</i>	26
2.6 RESULTS	28
2.7 VALIDATION	29
2.8 CONCLUSIONS	33
3 AGING: TESTING AND MODELLING	35
3.1 INTRODUCTION	36
3.2 AGING TESTING METHODOLOGY	37
3.2.1 <i>Accelerated Aging Tests</i>	37
3.2.2 <i>Aging Characterization Tests</i>	42
3.3 AGING MODEL	51
3.3.1 <i>Study of the State of the Art</i>	51
3.3.2 <i>Proposal of Modelling Methodology</i>	58
3.4 VALIDATION	60
3.4.1 <i>Methodology validation on a High-Energy Application</i>	60
3.4.2 <i>Methodology validation on a High-Power Application</i>	78
3.4.3 <i>Hypothesis validation</i>	93
3.5 CONCLUSIONS	99
4 SIZING ENERGY STORAGE SYSTEMS	103
4.1 INTRODUCTION	104
4.2 SIMULATION ENVIRONMENT	104
4.3 APPLICATIONS	105

4.3.1	<i>Electric vehicle application</i>	106
4.3.2	<i>Stationary application</i>	107
4.4	VALIDATION	109
4.4.1	<i>High-Energy Electric Vehicle application</i>	110
4.4.2	<i>High-Power Electric Vehicle application</i>	112
4.4.3	<i>Micro-grid stationary application</i>	114
4.4.4	<i>Hypotheses validation</i>	120
4.5	CONCLUSIONS	129
5	MODEL ACCURACY IMPROVEMENT	131
5.1	INTRODUCTION	132
5.2	ON-FIELD REMAINING USEFUL LIFE PROGNOSIS.....	133
5.2.1	<i>Evaluation Methodology</i>	133
5.2.2	<i>Stochastic algorithms</i>	141
5.2.3	<i>Evaluation</i>	152
5.2.4	<i>Comparison</i>	165
5.2.5	<i>Validation</i>	167
5.3	SUDDEN PERFORMANCE DECAY PREDICTION	169
5.3.1	<i>Electrode level data acquisition</i>	170
5.3.2	<i>Electrode level health indicator estimation</i>	171
5.3.3	<i>Electrode level health indicator modelling</i>	173
5.3.4	<i>Artificial data generation</i>	174
5.3.5	<i>Validation</i>	175
5.4	CONCLUSIONS.....	176
6	CONCLUSION AND FUTURE RESEARCH LINES.....	179
6.1	CONCLUSION.....	180
6.2	FUTURE WORK.....	181
	REFERENCES	183
	ANNEX 1: UN-SYNTHESIZED EVALUATION METRICS.	191

LIST OF ILLUSTRATIONS

Figure 1: Specific power and specific energy of different battery types [7].	2
Figure 2: Spider diagram of the characteristics of NCA cathode, NMC cathode, LMO cathode, LCO cathode, LTO anode and LFP cathode [11].	5
Figure 3: Possible degradation mechanisms [28].	6
Figure 4: Trends in the capacity fading as a function of cycle number for the five degradation modes: 4.5% LLI, 4.5% LAM at lithiated positive electrode, 16.5% LAM at delithiated positive electrode, 27.0% LAM at delithiated negative electrode, and 4.0% LAM at lithiated negative electrode, respectively, as predicted for C/25, in comparison with test data. All simulations are based on 5% capacity fade in a High-Power LFP/graphite cell using the 'Alawa model [27].	8
Figure 5: Lithium plating evidences on the OCV profile on discharge [15].	9
Figure 6: Structure of the thesis.	12
Figure 7: The black-box diagram of the methodology on a top view.	14
Figure 8: Application profile: voltage response and the SOC evolution of the battery.	21
Figure 9: Voltage and SOC response of the battery under the first Testing Input.	22
Figure 10: Voltage and SOC response of the battery under the second Testing Input.	23
Figure 11: a) Equivalent electric model; b) Equivalent thermal model.	24
Figure 12: The obtained EOL map in terms of the resistance increase and the capacity decrease on the High-Energy example of use.	29
Figure 13: The obtained EOL map in terms of the resistance increase and the capacity decrease on the High-Power example of use.	29
Figure 14: The OCV values at fresh state and aged state of the High-Energy battery.	30
Figure 15: Charge transfer impedance at fresh state and aged state of the High-Energy battery.	30
Figure 16: Difference between the estimated voltage and the measured one at fresh state and aged state of the High-Energy battery.	31
Figure 17: Temperature profile with initial resistance and with the resistance of EOL applied on the electric model set up with the resistance of EOL of the proposed High-Energy application.	32
Figure 18: Validation of the EOL mapping of the High-Energy application. The blue circles represent the batteries that have fulfilled the operation profile and the red x symbols are the ones that have not fulfilled the operation profile.	33
Figure 19: Different stress factors and their hypothetical influence (blue mesh) on lithium ion batteries' aging [68].	38
Figure 20: Methods of statistical design of experiments (DOE)[72].	40
Figure 21: Capacity characterization test applied on a SAMSUNG INR 21700 48G lithium ion cell. A) Voltage profile and B) Current profile.	44
Figure 22: A relaxation test applied on an A123 SYSTEMS APR 18650 M1 lithium ion cell. A) Voltage profile and B) Current profile.	45
Figure 23: Open Circuit Voltage characterization test at a continuous low current applied on a SAMSUNG ICR 18650 26F lithium ion cell. A) Voltage profile and B) Current profile.	45
Figure 24: A hysteresis characterization test applied on an A123 SYSTEMS APR 18650 M1 lithium ion cell. A) Voltage profile and B) Current profile.	46
Figure 25: Pulse current test applied on an A123 SYSTEMS APR 18650 M1 lithium ion cell. A) Voltage profile and B) Current profile.	46
Figure 26: Electrochemical Impedance Spectroscopy applied on a SAMSUNG ICR 18650 26F lithium ion cell.	47
Figure 27: EIS test run with different sinusoidal currents.	47
Figure 28: The Nyquist plot is divided into high, mid and low frequency sections [14].	47
Figure 29: Impedance spectra at 0°C at different SOC of A) a new cell and B) an aged cell [21].	48
Figure 30: A Hybrid Peak Pulse Characterization test applied on a certain lithium ion cell. A) Voltage profile and B) Current profile.	49
Figure 31: The current profile and the SOC evolution of the battery at BOL. The positive current values represent the discharge while the negative values represent the charge.	60
Figure 32: Relative dischargeable capacity values of the tested batteries under the calendar aging test matrix.	65

Figure 33: Relative dischargeable capacity values of the tested batteries under the cycling aging matrix.	66
Figure 34: Relative pure ohmic resistance values of the tested batteries at 50% SOC under the calendar aging matrix.	66
Figure 35: Relative pure ohmic resistance values of the tested batteries at 50% SOC under the cycling aging matrix.	66
Figure 36: Aging trends of the dischargeable capacity decrease at different calendar conditions.	69
Figure 37: Aging trends of the pure ohmic resistance increase at different calendar conditions.	70
Figure 38: Aging trends of the dischargeable capacity decrease at different cycling conditions.	70
Figure 39: Aging trends of the pure ohmic resistance increase at different cycling conditions.	71
Figure 40: The dischargeable capacity map based on Calendar aging model interpolations.	72
Figure 41: The pure ohmic resistance map based on calendar aging model interpolations.	73
Figure 42: The dischargeable capacity map based on cycling aging model interpolations.	73
Figure 43: The pure ohmic resistance map based on cycling aging model interpolations.	73
Figure 44: Aging trends of the dischargeable capacity decrease at different cycling conditions ones rebuilt the model from scratch.	75
Figure 45: The dischargeable capacity map based on cycling aging model interpolations ones rebuilt the model from scratch.	75
Figure 46: Dischargeable capacity evolution of the real High-Energy application use profile tested at three different temperatures: 10°C, 25°C and 45°C.	76
Figure 47: Pure ohmic resistance evolution of the real High-Energy application use profile tested at three different temperatures: 10°C, 25°C and 45°C.	77
Figure 48: Application profile: current profile and the SOC evolution of the battery under that current profile at BOL. The positive values on the current profile represent the discharge current values while the negative values represent the charge current values.	78
Figure 49: Relative dischargeable capacity values of the tested batteries under the calendar aging test matrix.	84
Figure 50: Relative dischargeable capacity values of the tested batteries under the cycling aging matrix.	84
Figure 51: Relative pure ohmic resistance values of the tested batteries at 50% SOC under the calendar aging matrix.	84
Figure 52: Relative pure ohmic resistance values of the tested batteries at 50% SOC under the cycling aging matrix.	85
Figure 53: Aging trends of the dischargeable capacity decrease at different calendar conditions.	87
Figure 54: Aging trends of the pure ohmic resistance increase at different calendar conditions.	88
Figure 55: Aging trends of the dischargeable capacity decrease at different cycling conditions.	88
Figure 56: Aging trends of the pure ohmic resistance increase at different cycling conditions.	89
Figure 57: The dischargeable capacity map based on Calendar aging model interpolations.	90
Figure 58: The pure ohmic resistance map based on calendar aging model interpolations.	90
Figure 59: The dischargeable capacity map based on cycling aging model interpolations.	91
Figure 60: The pure ohmic resistance map based on cycling aging model interpolations.	91
Figure 61: Dischargeable capacity evolution of the real High-Power application use profile tested at three different temperatures: 10°C, 25°C and 45°C.	92
Figure 62: Pure ohmic resistance evolution of the real High-Power application use profile tested at three different temperatures: 10°C, 25°C and 45°C.	92
Figure 63: Comparison of the effect of low temperatures on the dischargeable capacity decay under static operation conditions and dynamic operation conditions.	93
Figure 64: Current profiles of the tested real life cycles. A) has a mean current of 3120 mA and b) has a mean current of 2080 mA.	94
Figure 65: Dischargeable capacity evolution of tests 4, 8 and 11.	95
Figure 66: Pure ohmic resistance evolution of tests 4, 8 and 11.	95
Figure 67: Comparison of the observed dischargeable capacity evolution in the test 11 (blue dotted line) and the estimated dischargeable capacity with the complete aging model (red line).	96
Figure 68: Comparison of the observed pure ohmic resistance evolution in the test 11 (blue dotted line) and the estimated pure ohmic resistance with the complete aging model (red line).	97

Figure 69: Dischargeable capacity evolution of the tests 5, 6, 7, 13 and 14.	97
Figure 70: Pure ohmic resistance evolution of the tests 5, 6, 7, 13 and 14.	97
Figure 71: Average current values of each cycle done at tests 5, 6, 7, 13 and 14.	98
Figure 72: Average temperature values of each cycle done on the tests 5, 6, 7, 13 and 14.	98
Figure 73: Time of discharge on each cycle done on the tests 5, 6, 7, 13 and 14.	98
Figure 74: End of Discharge voltage on each cycle done on the tests 5, 6, 7, 13 and 14.	98
Figure 75: Current profiles of the different sizing options on the High-Energy application.	110
Figure 76: EOL maps of the different sizing options on the High-Energy application.	111
Figure 77: Replacement events on the High-Energy Electric Vehicle application.	112
Figure 78: Current profiles of the different sizing options on the High-Power application.	113
Figure 79: EOL maps of the different sizing options on the High-Power application.	113
Figure 80: Replacement events on the High-Power Electric Vehicle application.	114
Figure 81: Green Energy Campus's electrical Micro-Grid design [100].	115
Figure 82: The demand on Zellik on 2017 with an interval of 15 min.	116
Figure 83: The energy demand from the Thermal Management System.	116
Figure 84: Wind Power generation of a 3,3MW wind turbine.	117
Figure 85: Efficiency of SIEMENS sinvert 200 MS [105].	118
Figure 86: Replacement events on the Micro-grid stationary application.	119
Figure 87: LCOE results. The blue part of each bar represents the LCOE contribution of the solar and wind power plants and the yellow part represents the contribution of the BESS on the selected BESS size.	120
Figure 88: BESS contribution on the LCOE of the whole energy generation plant of the evaluated micro-grid.	120
Figure 89: The covered time at island mode by the energy generation plant.	120
Figure 90: Dischargeable capacity evolution of the tests 8, 9 and 10.	122
Figure 91: Pure ohmic resistance evolution of the tests 8, 9 and 10.	122
Figure 92: Comparison of the observed dischargeable capacity evolution in the test 9 (blue dotted line) and the estimated dischargeable capacity with the complete aging model (red line).	123
Figure 93: Comparison of the observed pure ohmic resistance evolution in the test 9 (blue dotted line) and the estimated pure ohmic resistance with the complete aging model (red line).	123
Figure 94: Dischargeable capacity evolution of the tests 1, 2, 3, 8 and 12.	123
Figure 95: Pure ohmic resistance evolution of the tests 1, 2, 3, 8 and 12.	124
Figure 96: Comparison of the observed dischargeable capacity evolution in the test 12 (blue dotted line) and the estimated dischargeable capacity with the complete aging model (red line).	125
Figure 97: Comparison of the observed pure ohmic resistance evolution in the test 12 (blue dotted line) and the estimated pure ohmic resistance with the complete aging model (red line).	125
Figure 98: Dischargeable capacity evolution of the tests 5, 6, 7 and 8.	125
Figure 99: Pure ohmic resistance evolution of the tests 5, 6, 7 and 8.	126
Figure 100: Comparison of the observed dischargeable capacity evolution in the test with dynamic operation conditions (dots) and the estimated one with the complete aging model (stars).	127
Figure 101: Comparison of the observed pure ohmic resistance evolution in the test with dynamic operation conditions (dots) and the estimated one with the complete aging model (stars).	127
Figure 102: Elapsed concept on cumulative aging model [109].	127
Figure 103: Comparison of the observed dischargeable capacity evolution in the test with dynamic operation conditions (dots) and the estimated one with the corrected complete aging model (stars).	128
Figure 104: Comparison of the observed pure ohmic resistance evolution in the test with dynamic operation conditions (dots) and the estimated one with the complete aging model (stars).	128
Figure 105: Qualitative response	138
Figure 106: Example of the trial-instant figure	139
Figure 107: The input data of the evaluated stochastic algorithm.	153
Figure 108: PH and α - λ accuracy visualization of the evaluated Particle Filter	161
Figure 109: PH and α - λ accuracy visualization of the evaluated Gaussian Process	162
Figure 110: PH and α - λ accuracy visualization of the evaluated Extended Kalman Filter	163

Figure 111: PH and α - λ accuracy visualization of the evaluated stochastic Unscented Kalman Filter	164
Figure 112: Illustrative example of the Remaining Useful Life predictions that are out of the displayed window.	166
Figure 113: Conflicting points.....	167
Figure 114: Correction of the calculated aging path of the pure ohmic resistance evolution of test 8 with a Particle Filter prognosis algorithm.....	169
Figure 115: The different degradation modes of a lithium ion cell [31].	170
Figure 116: Charge full-cell and half-cell OCV profiles of a fresh SAMSUNG 18650 26F battery.	171
Figure 117: Discharge full-cell and Half-cell OCV of a fresh SAMSUNG 18650 26F battery.	171
Figure 118: Evolution of the Electrode level Health Indicators. The blue line refers to Test 5, the red line refers to Test 6, the yellow line refers to Test 7 and the purple line refers to Test 8.	173
Figure 119: Models of the health indicators obtained from the Half-cell data. A) refers to the scaling factor of the anode at discharge and B) refers to the scaling factor of the cathode at charge.	174
Figure 120: Aging master curve of tests 5, 6 and 7 taken from test 7.....	174
Figure 121: Lengthened data sets of test 5 and 6.....	175
Figure 122: Comparison of the observed dischargeable capacity evolution in the test with dynamic operation conditions (dots) and the estimated one with the complete aging model (stars) with artificial data points.....	176

LIST OF TABLES

Table 1: Various developed rechargeable lithium metal battery systems [10]	4
Table 2: Patents related lithium ion batteries [10].	4
Table 3: High-Energy battery specifications.....	21
Table 4: High-Power battery specifications	22
Table 5: The first order RC equivalent circuit model [60]	24
Table 6: Pulse characterization test used on the parametrization of the equivalent electric circuit	25
Table 7: The second order RC equivalent circuit model [59]	25
Table 8: Specific heat capacity test.....	25
Table 9: Entropic factor tests	26
Table 10: The calculation of the EOL threshold pure ohmic resistance increase	26
Table 11: The initialization of the CV controller.....	27
Table 12: Pure ohmic resistance homogeneity at different SOH of the High-Energy battery	32
Table 13: Testing cases possibilities on the initial test matrix.....	40
Table 14: Comprehending the generic effect of the stress factors on the aging trend.....	41
Table 15: Dischargeable capacity calculation [11]	44
Table 16: Proposed Capacity characterization test.....	49
Table 17: Proposed Impedance characterization test.....	49
Table 18: Proposed long Aging Check-up Test	50
Table 19: The parameters of the aging model proposed by Sarasketa [11]	52
Table 20: The parameters of the aging model proposed by Xu [83]	53
Table 21: The parameters if the calendar aging model proposed by Sarasketa [11].....	53
Table 22: The parameters of the calendar aging model proposed by Wang et al. [87]	54
Table 23: Parameters of the calendar aging model proposed by Grolleau et al. [33]	54
Table 24: Parameters of the calendar aging model proposed by Xu [83]	55
Table 25: The parameters of the cycling aging model proposed by Wang et al. [87]	56
Table 26: The parameters of the cycling aging model proposed by Sarasketa [11]	56
Table 27: The parameters of the cycling aging model proposed by Käbitz et al. [30].....	56
Table 28: The parameters of the cycling aging model proposed by Wang et al. [49]	57
Table 29: The parameters of the cycling aging model proposed by Xu [83]	57
Table 30: Mathematical expressions for different lithium ion chemistries reported on the literature ...	58
Table 31: The parameters that gather the effect of all the stress factors	59
Table 32: The parameters that describes the evolution of a selected health indicator	59
Table 33: High-Energy battery specifications.....	60
Table 34: Testing cases possibilities on the first stage of the aging test matrix design on a High-Energy application.....	60
Table 35: Stress factors of calendar and cycling aging.....	61
Table 36: The Red testing cases. The levels of the stress factors that are in red describe the most probable operation condition defined on the application requirements	62
Table 37: The Red testing cases after a first iteration with the lab. The levels of the stress factors that are in red describe the most probable operation condition defined on the application requirements. The blue values are the ones modified after the first iteration with the lab	62
Table 38: Aging test matrix to characterize the calendar aging	63
Table 39: The reduced testing cases on the cycling operation mode	63
Table 40: The Aging test matrix to characterize the cycling aging with 26 testing cases. The cases that are in red are the selected ones as the final ones	64
Table 41: Aging test matrix to characterize the cycling aging	65
Table 42: Applicable mathematical expressions to the obtained data from the aging test matrix.....	66
Table 43: Fitting RMSE of the dischargeable capacity evolution data with the proposed cycling aging models.....	67
Table 44: Fitting RMSE of the pure ohmic resistance evolution data with the proposed cycling aging models.....	67
Table 45: Fitting RMSE of the dischargeable capacity evolution data with the proposed calendar aging models.....	67

Table 46: Fitting RMSE of the pure ohmic resistance evolution data with the proposed calendar aging models.....	67
Table 47: The applicable mathematical expressions to link the stress factors and the free variables designed on the calendar aging model	68
Table 48: The applicable mathematical expressions to link the stress factors and the free variables designed on the cycling aging model.	68
Table 49: The mean RMSE values of each combination of the proposed mathematical expressions	69
Table 50: Parameters of the calendar aging model of the dischargeable capacity evolution	69
Table 51: Parameters of the calendar aging model of the pure ohmic resistance evolution.....	70
Table 52: Parameters of the cycling aging model of the dischargeable capacity evolution	70
Table 53: Parameters of the cycling aging model of the pure ohmic resistance evolution.....	71
Table 54: RMSE between the response of the model and the data used to construct the model	71
Table 55: Interpolation cases possibilities on the aging model validation process of a High-Energy application	72
Table 56: The mean RMSE values of each combination of the proposed mathematical expressions ones rebuilt the model from scratch	74
Table 57: Parameters of the corrected dischargeable capacity evolution cycling aging model	74
Table 58: RMSE between the response of the model and the data used to construct the linear model	75
Table 59: The mean stress factor values that represent the operation condition of the proposed High-Power application use case	76
Table 60: Root Mean Square Error between the measured and estimated values of the real life cycle aging health indicators (dischargeable capacity and pure ohmic resistance)	76
Table 61: High-Power battery specifications	78
Table 62: Testing cases possibilities on the first stage of the aging test matrix design on a High-Power application	78
Table 63: Stress factors of calendar and cycling aging.....	79
Table 64: The Red testing cases. The levels of the stress factors that are in red describe the most probable operation condition defined on the application requirements	80
Table 65: The Red testing cases after a first iteration with the lab. The levels of the stress factors that are in red describe the most probable operation condition defined on the application requirements. The blue values are the ones modified after the first iteration with the lab	80
Table 66: The Aging test matrix to characterize the calendar aging with 6 testing cases. The cases that are in red are the selected ones as the final ones	81
Table 67: The reduced testing cases on the cycling operation mode	81
Table 68: The Aging test matrix to characterize the cycling aging with 26 testing cases. The cases that are in red are the selected ones as the final ones	82
Table 69: Aging test matrix to characterize the calendar aging	83
Table 70: Aging test matrix to characterize the cycling aging	83
Table 71: Applicable mathematical expressions to the obtained data from the aging test matrix.....	85
Table 72: Fitting RMSE of the dischargeable capacity evolution data with the proposed cycling aging models.....	85
Table 73: Fitting RMSE of the pure ohmic resistance evolution data with the proposed cycling aging models.....	85
Table 74: Fitting RMSE of the dischargeable capacity evolution data with the proposed calendar aging models.....	86
Table 75: Fitting RMSE of the pure ohmic resistance evolution data with the proposed calendar aging models.....	86
Table 76: The applicable mathematical expressions to link the stress factors and the free variables designed on the calendar aging model of the High-Power application	86
Table 77: The applicable mathematical expressions to link the stress factors and the free variables designed on the cycling aging model of the High-Energy application	86
Table 78: The mean RMSE values of each combination of the proposed mathematical expressions	87
Table 79: Parameters of the calendar aging model of the dischargeable capacity evolution	87
Table 80: Parameters of the calendar aging model of the pure ohmic resistance evolution.....	88

Table 81: Parameters of the cycling aging model of the dischargeable capacity evolution	88
Table 82: Parameters of the cycling aging model of the pure ohmic resistance evolution.....	89
Table 83: RMSE between the response of the model and the data used to construct the model	89
Table 84: Interpolation cases possibilities on the validation process of a High-Energy application....	90
Table 85: The mean stress factor values that represent the operation condition of the proposed High-Power application use case	92
Table 86: Root Mean Square Error between the measured and estimated values of the real life cycle aging health indicators (dischargeable capacity and pure ohmic resistance)	92
Table 87: SAMSUNG's ICR18650-26F battery specifications	93
Table 88: Aging test matrix design to validate the main hypotheses done on the aging model development.....	94
Table 89: Selection of mathematical expressions that can be applied to describe the aging trend of the selected health indicators.....	96
Table 90: Fitting RMSE of the dischargeable capacity evolution data extracted from the proposed test number 4 and test number 8	96
Table 91: Fitting RMSE of the pure ohmic resistance evolution data extracted from the proposed test number 4 and test number 8	96
Table 92: Parameters of the complete aging model	96
Table 93: A fictitious example of the sizing activity of an entire bus fleet with N bus lines	107
Table 94: The Levelized Cost of Energy equation	108
Table 95: Characteristics of the High-Energy minimum sizing option introduced on the sizing activity	110
Table 96: Cost values taken into account on BESS CI calculation	111
Table 97: Sizing simulation results of the High-Energy Electric Vehicle application.....	112
Table 98: Characteristics of the High-Power minimum sizing option introduced on the sizing activity	112
Table 99: Cost values taken into account on BESS CI calculation	113
Table 100: Sizing simulation results of the High-Power Electric Vehicle application	114
Table 101: The Levelized Cost of Energy equation adapted to the proposed stationary application.....	115
Table 102: Joule losses on the BESS	117
Table 103: Cost values of an average solar and wind power plant on Belgium [103].....	118
Table 104: Cost values taken into account on BESS CI calculation	119
Table 105: LCOE simulation results of the Micro-grid stationary application	119
Table 106: SAMSUNG's ICR18650-26F battery specifications	121
Table 107: Aging test matrix design to validate the main hypotheses done on the aging model development.....	121
Table 108: Parameters of the complete aging model	122
Table 109: Selection of mathematical expressions to describe the aging trend	124
Table 110: Fitting RMSE of the dischargeable capacity evolution data extracted from the proposed test number 1, 2 and 3	124
Table 111: Fitting RMSE of the pure ohmic resistance evolution data extracted from the proposed test number 1, 2 and 3	124
Table 112: Parameters of the complete aging model	125
Table 113: Selection of mathematical expressions to describe the aging trend	126
Table 114: Fitting RMSE of the dischargeable capacity evolution data extracted from the proposed test number 5, 6 and 7	126
Table 115: Fitting RMSE of the pure ohmic resistance evolution data extracted from the proposed test number 5, 6 and 7	126
Table 116: Parameters of the complete aging model	126
Table 117: Parameters of the corrected complete aging model	128
Table 118: Set of metrics that quantifies the correctness	134
Table 119: The prediction Root Mean Square Error	135
Table 120: The Relative Accuracy	135
Table 121: The probability of predicting the real RUL	135
Table 122: The PDF width	136

Table 123: Set of metrics that quantifies the timeliness	136
Table 124: The Prognosis Horizon fulfilment criterion	136
Table 125: The Prognosis Horizon.....	136
Table 126: The Convergence of the Relative Accuracy	137
Table 127: Set of metrics that quantifies the computational performance	137
Table 128: The α - λ accuracy boundary fulfilment criterion	138
Table 129: Reference values of the unified set of metrics	139
Table 130: Proposed trial matrix to separate input uncertainty effect on algorithm's evaluation.	140
Table 131: The Linear Optimizing Combination Resampling method.....	144
Table 132: The Gaussian Process.....	147
Table 133: The covariance functions of the Gaussian Process	147
Table 134: The Bayesian inference on a Gaussian Process	148
Table 135: The Bayesian Inference on a Gaussian Process considering a Gaussian noise on the measurements	149
Table 136: Space Model used in Kalman Filter [44]	150
Table 137: Sigma point calculation by Symmetric Unscented Transformation	151
Table 138: The proposed capacity decay models.....	153
Table 139: Trial matrix definition for every algorithm under evaluation.....	154
Table 140: Affecting parameters on the Particle Filter	154
Table 141: Hyper-parameters on the Particle Filter with basic resampling methods	154
Table 142: Grid Search Optimization grid on the Particle Filter with basic resampling methods.....	155
Table 143: Hyper-parameters on the Gaussian Process with Neural Network covariance function.	156
Table 144: Grid Search Optimization grid on the Gaussian Process with a Neural Network covariance function.....	156
Table 145: Hyper-parameters on the Extended Kalman Filter.....	157
Table 146: Grid Search Optimization grid on the Extended Kalman Filter.....	157
Table 147: Hyper-parameters on the Unscented Kalman Filter.....	158
Table 148: Grid Search Optimization grid on the Unscented Kalman Filter.....	158
Table 149: Simulation variables	159
Table 150: The obtained evaluation metrics of Particle Filter on all training data sets	161
Table 151: The obtained evaluation metrics of Gaussian Process on all training data sets	162
Table 152: The obtained evaluation metrics of Extended Kalman Filter on all training data sets.....	163
Table 153: The obtained evaluation metrics of Unscented Kalman Filter on all the training data sets	164
Table 154: The average evaluation metrics of the evaluated 4 stochastic algorithms.....	165
Table 155: The mathematical framework to apply the Particle Filter on test 8	168
Table 156: Affecting parameters on the Particle Filter	168
Table 157: Hyper-parameters on the Particle Filter applied on the validation	169
Table 158: Convolution of both electrode level OCV profiles.....	172
Table 159: Scaling equation.....	175
Table 160: Scaling variables of test 5 and 6	175
Table 161: Selection of mathematical expressions that can be applied to describe the aging trend of the dischargeable capacity evolution	175
Table 162: Fitting RMSE of the lengthened dischargeable capacity evolution data sets of the tests 5 and 6	175
Table 163: Parameters of the reconstructed complete aging model.....	176
Table 164: The obtained evaluation metrics on all the tests and training data sets with the evaluated Particle Filter configuration.....	193
Table 165: The obtained evaluation metrics on all the tests and training data sets with the evaluated Gaussian Process configuration	196
Table 166: The obtained evaluation metrics on all the tests and training data sets with the evaluated Extended Kalman Filter.....	199
Table 167: The obtained evaluation metrics on all the tests and training data sets with the evaluated Unscented Kalman Filter.....	202

ABBREVIATIONS

AAT	Accelerated Aging Test
ACT	Aging Check-up Test
BESS	Battery Energy Storage System
BOL	Beginning of Life
CC	Constant Current
CV	Constant Voltage
DOD	Depth of Discharge
DOE	Design of Experiment
EIS	Electrochemical Impedance Spectroscopy
EOL	End of Life
GP	Gaussian Process
HPPC	Hybrid Peak Pulse Characterization
LAM	Loss of Active Material
LCO	Lithium Cobalt Oxide
LFP	Lithium Iron Phosphate
LLI	Loss of Lithium Inventory
LMO	Lithium Manganese Oxide
LTO	Lithium Titanate Oxide
NCA	Lithium Nickel Cobalt Aluminium Oxide
NMC	Lithium Nickel Manganese Cobalt Oxide
OCV	Open Circuit Voltage
PF	Particle Filter
PI	Proportional Integral
RUL	Remaining Useful Life
SEI	Solid Electrolyte Interphase
SOC	State of Charge
SOH	State of Health
SPI	Solid Permeable Interphase

GLOSSARY

Constant Current (CC): A charge or discharge done with a constant current all along the operation period. This operation mode usually is cut off when reaching a certain voltage level.

Constant Voltage (CV): A charging or discharging mode where a voltage is fixed and the current is controlled to keep constant this voltage value. The limiting variable is the voltage. This operation mode usually is cut off when reducing the current to $C/20$ or $C/25$.

Open Circuit Voltage (OCV): The OCV of a battery is the potential difference between the positive electrode and the negative electrode when no current flows and the electrode potentials are at equilibrium. It is measured at the terminals of the battery when the battery voltage reaches an electrochemical equilibrium.

State of charge (SOC): The SOC represents the relative stored energy. This relative value is given in terms of the total dischargeable energy. It is usually given on percentages. The upper SOC, 100% SOC, is defined by the end of charge voltage and the lower SOC, 0% SOC, is defined by the end of discharge voltage. These voltages are defined by the safety operation window of the battery and changes with the battery chemistry.

State of Health (SOH): The SOH reflect the relative general condition that a battery is on a specific time instant. It also represents the relative performance level compared with a fresh battery. It is often used as a relative value of the dischargeable capacity, where the relativity is done with the nominal dischargeable capacity.

Depth of Discharge (DOD): The DOD represents the relative discharged energy on a continuous operation. This relative value is given in terms of the total dischargeable energy. It is usually given on percentages. It can be expressed as the difference of SOC between two time instants. As consequence, the maximum DOD would be a change of SOC from 100% to 0%, a 100% DOD. The DOD is 0% when the SOC is the same on the evaluated two time instants.

Current rate (C-rate): The C-rate is the relative current measured on the battery terminals. This relative value is given in terms of the nominal current of the battery. The nominal current is usually expressed by a C and the C-rate as a multiple of it: 2C, 1C, C/20 etc.

Remaining Useful Life (RUL): The RUL represents the required time to reach a particular future event or state. That future event or state used to be the End of Life.

End of Life (EOL): The EOL can be defined as the fact of something not working, or stopping working as well as it should. The EOL used on this thesis is related with the second term. The EOL is the state of health of the system at which the application requirements cannot be fulfilled.

Prognostics: Prognostics is the science of making predictions.

Levelized cost: The levelized cost of a system is the total cost of that system on its entire lifespan.

CHAPTER 1:

1 Introduction

This chapter introduces the problematic that has motivated this thesis and gives some basic information about lithium ion batteries and remaining useful life prognosis. Then, the main objective is presented together with the followed methodology and the structure of the thesis. Finally, the scientific contributions are listed.

1.1 Background

Two of the main concerns of today’s society are, on one hand, the protection of the environment and on the other hand, the search for high efficiencies mainly related with cost and energy savings [1]. On this social context, the main environmentally harmful systems have been gradually replaced by sustainable alternatives, which are more efficient and more environmentally friendly. Specially, there are two environmentally sustainable initiatives that are specially having and will have huge impact on the preservation of the environment: the electric mobility and the renewable energy generation. The substitution of inner combustion engines and traditional power plants with electric engines and solar, wind or hydroelectric power plants will suppose an approximate 40% decrease of worldwide greenhouse gas emissions [2].

Nonetheless, the sustainable alternatives on the mobility and energy generation sectors show some technical challenges when comparing them to the original systems that they replace. On one hand, there is a technical challenge balancing the energy generation with renewable energy generation power plants and the energy demand. The electricity is generated to cover the instantaneous energy demand. However, the solar and wind power plants cannot generate energy at will. The energy generated by these renewable energy generation plants is conditioned by the weather conditions. On the other hand, there is a technical challenge in the energy supply for the electric mobility. The mobility until now has been powered by petrol, which can be stored on a simple petrol tank. The electric mobility, in contrast, is powered by electricity, which requires a special “tank”.

In this context, energy storage systems are the key technological solution to the electric mobility and the renewable energy power plants. Firstly, the energy storage systems are themselves the special tank required on the electric vehicles and secondly, they can be used to compensate the imbalance on the energy generation-demand by saving the energy generation surplus and using the storage energy to cover the energy demand that these renewable energy generation power plants cannot cover. In addition to this, the energy storage systems are also key technological solutions on maximizing the efficiency of any energy generation plant. The chance of storing energy loosens the restrictions on the energy generation imposed by the energy demand. The power plants can be exploited at their maximum efficiency on a certain period time where the energy surplus resultant from the imbalance between the energy generation-demand is used to charge the energy storage system, which afterwards can be poured to the grid at will.

There are many kind of Energy Storage Systems available on the market but specifically, lithium ion battery based Energy Storage Systems are positioning first in the market [3][4]. The main reason behind this is that lithium ion batteries has an unrivalled performance potential comparing with the rest battery technologies that are nowadays available on the market, see Figure 1. A lithium ion battery has a high “energy-to-weight” ratio (lithium has the greatest electrochemical potential and provides the largest energy density per weight of all metals [5]) and low self-discharge loss; it can have a cycle life of around 10,000 and an efficiency of around 100%; it has no ‘memory effect’ [6].

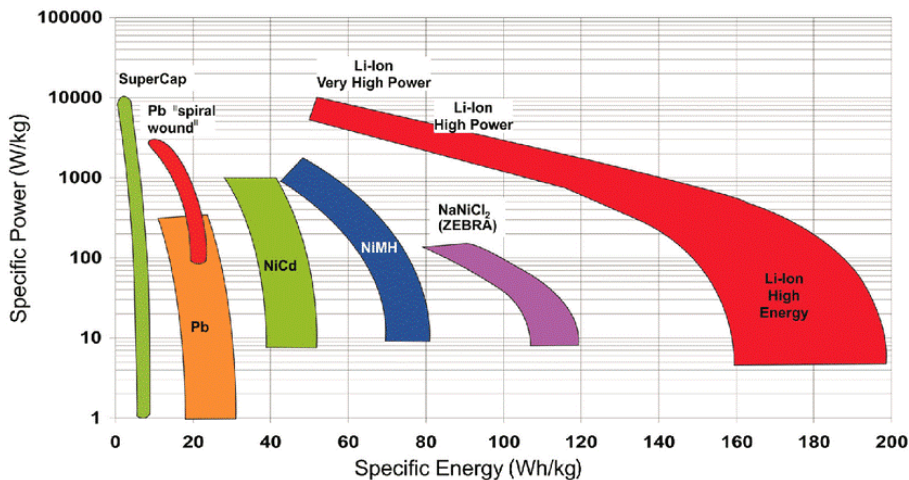


Figure 1: Specific power and specific energy of different battery types [7].

Each Energy Storage solution is designed to fulfil the requirements imposed by the application. These requirements are always, at least, the minimum electrical performance (the maximum power and energy values demanded by the application) and the time period that the application is expected to be functioning (the lifespan). The minimum electric performance determines the smallest size of the Energy Storage solution that will be able to fulfil the requirements imposed by the application. Then, the expected lifespan of the application is considered to determine the final size of the Energy Storage System. Historically, energy storage systems have been designed for lifespans much higher than the required ones without a real efficiency or cost evaluation. They have been continually oversized. The goal of old designs was the achievement of hardwearing robust systems that could always fulfil the requirements imposed by the application (for example, there is an operative 100 years hydro storage system in Cuenca, Spain, which was expected to work only 20 years). Nowadays, the designs are based on finding the best efficiency in terms of energy, economical cost and environmental cost along the whole useful life of the system. However, the current designs of Energy Storage Systems done with wrong lifespan estimations or without any lifespan estimation are often leading to unexpected replacements of the energy storage system. The sustainability of those solutions goes drastically down when facing these kinds of unexpected events, as well as their economic profitability. This is why, the accurate estimation of the lifespan (prognosis) applied on the sizing process is essential to assure the sustainability and viability of these solutions.

In addition to this, the accurate estimation of the lifespan of the solution is interesting for economic and environmental cost saving objectives. Firstly, accurate lifespan estimations enable failure prevention in a more controllable manner. In this way, an effective maintenance can be administered when it is needed in order to correct impending faults without permanently damaging battery as traditional protection circuits do [8]. Secondly, accurate lifespan estimations can be used to meet the lifespan requirement of the solution by adjusting the stress generated by the operation conditions and prevent unexpected replacements.

The improvement on the efficiency and the reduction on the cost of the whole energy storage system based on accurate lifespan estimation have motivated to develop this thesis titled “REMAINING USEFUL LIFE ESTIMATIONS APPLIED ON THE SIZING AND THE PROGNOSIS OF LITHIUM ION BATTERY ENERGY STORAGE SYSTEMS”. In addition to this, the generation of this thesis is also motivated by the high interest that actually exists around prognosis and predictive maintenance tools applicable to the industry.

1.1.1 Lithium-ion battery

A lithium battery is an electrochemical energy storage system technology. This technology has less than 40 years of development. Pioneer work with the lithium battery began in 1912 under G.N. Lewis but it was not until the early 1970s that the first non-rechargeable lithium batteries became commercially available [5]. Attempts to develop rechargeable lithium batteries followed in the 1980s, focusing on the lithium metal as the negative electrode because of high specific capacity of the metal [9] (see Table 1).

In 1980s, it was found that cycling causes changes on the lithium electrode. These transformations, which are part of normal wear and tear (aging), reduce the thermal stability, causing potential thermal runaway conditions. When this occurs, the cell temperature quickly approaches the melting point of lithium, resulting in a violent reaction called “venting with flame” [5].

System	Voltage	Wh/kg	Wh/l	Company
Li/TiS ₂	2.1	130	280	'78 Exxon
LiAl/TiS ₂				'79 Hitachi
Li/LiAlCl ₄ -SO ₂ /C	3.2	63	208	'81-85 Duracell
Li/V ₂ O ₅	1.5	10	40	'89 Tohsiba
Li/NbSe ₃	2.0	95	250	'83-86 Bell Lab
LiAl/Polyaniline	3.0	-	180	'87 Bridgestone
LiAl/Polypyrrole	3.0	-	180	'89 Kanebo
Li/Al/Polyacene	3.0	-	-	'91 Kanebo/Seiko
Li/MoS ₂	1.8	52	140	'87 MoLi

Li/CDMO (Li_xMnO₂)	3.0	-	-	'89 Sanyo
Li/Li_{0.3}MnO₂	3.0	50	140	'89 Tadiran
Li/VO_x	3.2	200	300	'90 HydroQuebec

Table 1: Various developed rechargeable lithium metal battery systems [10]

The safety issues caused the industry to concentrate on carbon and lithium intercalated electrode instead of using lithium metal (research shifted to non-metallic lithium battery using lithium ions) because carbon electrodes offer a more stable morphology than the lithium metal ones (see the first developed patents in the lithium ion battery field in Table 2) [11]. Although slightly lower in energy density than lithium metal, the lithium ion is safe (providing certain precautions) [5]. In 1991, the Sony Corporation commercialized the first lithium ion battery. Sony's original version of lithium ion used coke, a product of coal, as the negative electrode. Since 1997, most lithium ions (including Sony's) have shifted to graphite anodes [5].

Patents	Patents No. and application date	Name	Company
Transition metal oxides as cathode, LiCoO₂	US 4,302,518 (1980/3/31)	J.B. Goodenough	United Kingdom Atomic Energy Authority
Graphite/Li in nonaqueous solvents	Japan 1769661 (1981/6/18)	H. Ikeda, K. Narukawa, H. Nakashima	Sanyo
Graphite/Li in nonaqueous solvents	US 4,423,125 (1982/9/13)	S. Basu	Bell Telephone Laboratories, Inc.
Graphite/Li in molten salt	US 4,304,825 (1980/11/21)	S. Basu	Bell Telephone Laboratories, Inc.
Graphitized mesophase carbon	Japan 2,943,287 (Sept. 1990)	Kawagoe, Ogino	Bridgestone
Li-ion battery (battery based on carbonous material)	Japan 1989293 (1985/5/10)	A. Yoshino, K. Jitsuchika, T. Nakajima	Asahi Chemical Ind.
Carbonous/Li nonaqueous	US 4,959,281 (1989/8/29)	N. Nishi	Sony Co.
Additives for Gr vinylene carbonate	Japan 3059832 (1992/7/27)	M. Fujimoto, M. Takahashi, A. Nishio	Sanyo
Additives for Gr vinylene carbonate	US 5,626,981 (May 6, 1997)	A. Simon, J-P. Boeueve	Saft
Additives of propane sulton	US 6,033,809 (1997/8/22)	S. Hamamoto, A. Hidaka, K. Abe	Ube

Table 2: Patents related lithium ion batteries [10].

1.1.1.1 Most Common Lithium Ion Battery Configurations

The lithium ion cell is compound by several elements: a cathode, an anode, an electrolyte, a binder, a separator and two current collectors. The cell level performance is governed by secondary conditions and interactions between those components [12], which means that the selection of each element can generate huge changes on the behaviour of the lithium ion cell.

LTO has low energy density (capacity of LTO is 170mAh/g) [12], high cycling stability (low volume change during cycling) and high thermal stability (stable up to 1000 °C and no restriction imposed to lithium ion diffusion at low temperatures); the Peukert relationship is linear [13][14]. Moreover, it is reported that the surface area of the anode in LTO batteries is 100 times larger than graphite, which results in a reduction in the internal resistance and increase of the power capabilities of the LTO battery (Figure 2.a) [12].

At lower temperatures, lithium plating is unlikely to happen due to the high lithiation voltage of LTO [15]. Besides, the surface layer that may exist on LTO do not seem to exhibit a distinctive electrochemical signature, thus not contributing to the energy barrier for lithium ion transport [12], which leads to a high rate charge and discharge capability [14].

The NMC cathode belongs to a mixed metal oxide layered oxide framework cathode. In the case of mixed metal oxides, there is a positive synergy between their constituting elements (combining the

nickel, manganese and cobalt metals enhances each other strengths [14]). NMC exhibits high capacity, minimal cationic disorder and extended thermal stability [12]. It has good overall performance and excels on specific energy. This battery is the preferred candidate for the electric mobility sector and has the lowest self-heating rate (Figure 2.b) [14].

LFP has become attractive for specific industrial and stationary applications because of its higher power density and long cycle and calendar live [12]. It has an excellent safety and long life span. LFP batteries has a higher self-discharge than other Li-ion batteries, which can cause balancing issues with aging [14] and a lower energy density than cobalt (operating low voltage: 3.2v.) but it can provide higher currents (greater power) (Figure 2.c).

NCA delivers high stable capacity, because doping with aluminium enhances charge retention, facilitating maximum utilization of the active transition metal [12]. It shares similarities with NMC as high specific energy, high specific power and a long life span (it is widely used in the automotive industry) but has lower safety and higher cost (Figure 2.d).

LMO exhibits good thermal stability and rate capability; oxygen release usually occurs at temperatures higher than for layered materials, indicating the robustness of spinels [12]; manganese is much cheaper, safer and has a higher cell voltage (its structure enables higher rate of ion exchange between electrodes) and lower internal impedance than cobalt but it has less energy density (Figure 2.e) [14]. Nonetheless, LMO has some serious concerns to be taken into account: electrolyte oxidation (at 4.0V), metal dissolution (due to disproportionation reactions) and Jahn-Teller distortion. Because of this, pure lithium manganese batteries are no longer common today [14].

LCO belongs to the two-dimensional layered materials family ($LiMO_2, M = Co, Ni, Mn$). It shows satisfactory performance at room temperature with intercalation and deintercalation of 0.5 lithium per unit formula; however, the use is limited to 60°C due to the structural instability in the deeply charged state and fragile cobalt oxygen unions (the intermediate oxidation state of cobalt in charged state makes the crystal susceptible to releasing oxygen due to metal dissolution in the electrolyte, in a process that is aggravated beyond 60°C) [12]. It has excellent specific energy but offers moderate specific power, safety and life span (Figure 2.f) [14].

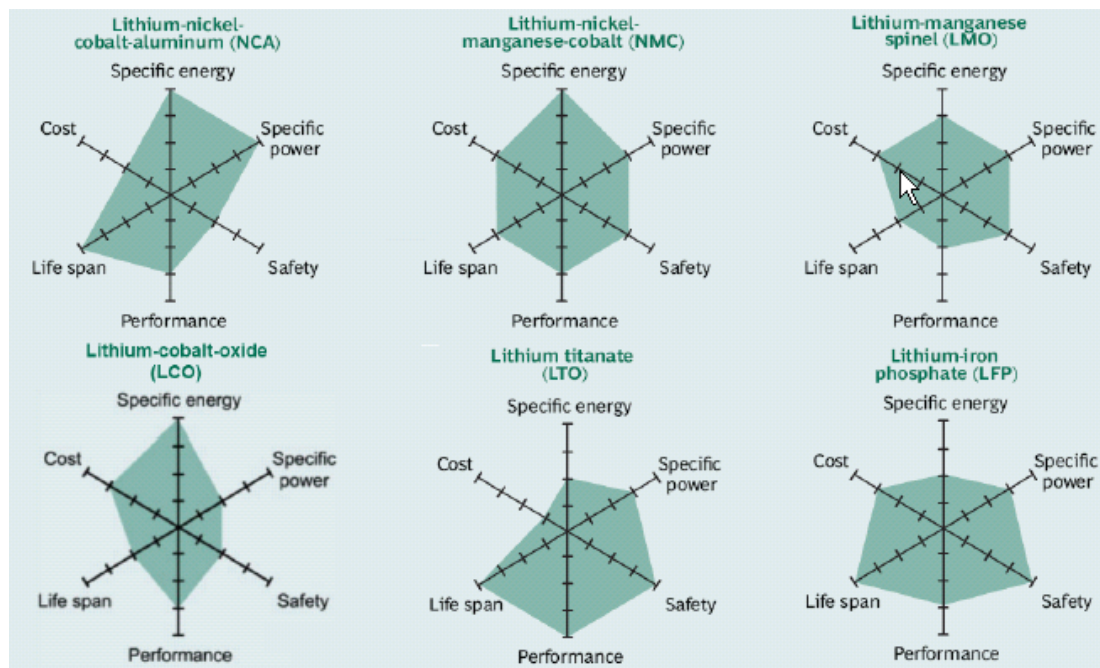


Figure 2: Spider diagram of the characteristics of NCA cathode, NMC cathode, LMO cathode, LCO cathode, LTO anode and LFP cathode [11].

1.1.1.2 Aging Behaviour

Lithium ion batteries age and suffer a fade on its working performance capability. This fade of performance is usually related uniquely with the dischargeable capacity fade [16][17][18], but there are more aspects of the performance of a lithium ion battery that change due to the aging, such as the ohmic resistance [19][20], the faradic resistance [21], the thermal entropy [22], the mechanical behaviour [23][24]. Nonetheless, the main two health indicators of a lithium ion battery are the dischargeable capacity and the pure ohmic resistance because they are linked directly with the storable energy and the power at which the energy can be stored and distributed [25].

This aging occurs whether the battery is inactive (calendar aging) or active (cycling aging) due to several aging mechanisms. Those ageing processes can be defined as changes in the structure of the components and materials of the battery. They are affected by many different elements: the operation conditions, the type of active materials used in the electrodes, the manufacturing process of the whole battery, the load conditioning and the design of the system (cell, battery, module, pack) [26].

The aging process of a lithium ion battery (in a heuristic point of view) is expected to have a complex and non-linear behaviour. The aging of a lithium ion technology battery can be generated by different aging mechanisms that have different effects on the battery behaviour. It must be considered that the performance decay could come from contributions of a predominant mode accompanied with an array of possible subsidiary modes (one might be much less prominent or hidden) [27]. Dubarry et al. [28] presented all the possible degradation mechanisms reported until 2016, see Figure 3.

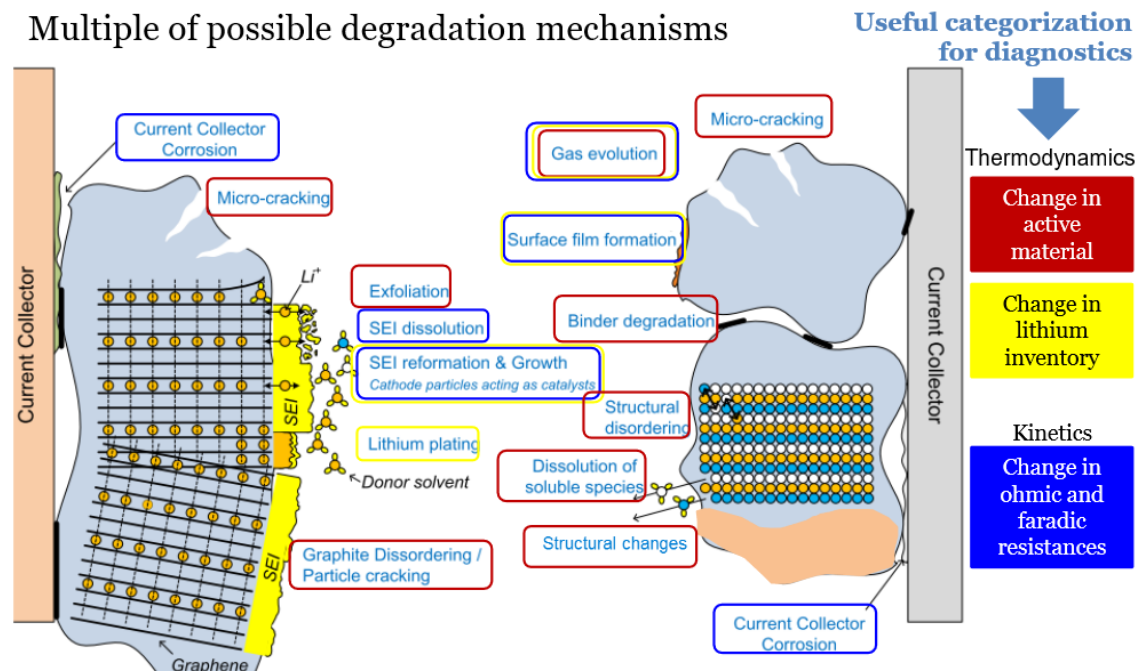


Figure 3: Possible degradation mechanisms [28].

The degradation mechanisms displayed in Figure 3 can be categorized depending on the effect that those mechanisms has on the battery behaviour [29][28]. Firstly, there are those aging mechanisms that affect the thermodynamic behaviour of the battery due to a change in active material or/and lithium inventory. And secondly, there are those aging mechanisms that affect the kinetics of the reactions on the cell caused by a change in ohmic and faradic resistance.

Thanks to this categorization of the aging mechanisms, a unified understanding of those degradation mechanisms of lithium ion technology batteries was achieved. All the aging mechanisms were catalogued in 3 unified and common used aging modes or deterioration processes: Loss of Active Material (LAM), Loss of Lithium Inventory (LLI) and change in ohmic and faradic resistances (kinetic deterioration).

The post-mortem analysis used in [30] indicates that the capacity fade in the tested NMC cathode and graphite anode cells due to the calendar aging is mostly due to LLI. Changes in porosity and weight of the samples reveal the evolution of deposition products in the porous structure of the anode, indicating electrolyte decomposition. Besides, inductively coupled plasma optical emission spectroscopy showed that most of the lithium lost in the cathode was deposited during aging on the anode.

The post-mortem analysis made on the tested LFP batteries by Sarasketa [11] due to the cycling aging showed that the main cause of aging was the non-uniform decomposition of the electrolyte and the resulting evolution of the Solid Electrolyte Interface (SEI) layer due to the deposition of decomposition products over the graphite anode surface.

- **Loss of Lithium Inventory**

A lithium ion battery experiences Loss of Lithium Inventory (LLI) when the lithium ions are consumed by parasitic reactions or side reactions such as surface film formation (e.g. SEI growth), decomposition reactions, lithium plating, etc. The lithium ions are no longer available for cycling between the negative electrode and the positive electrode. The reduction of lithium ions is mainly observed as capacity fade [31]. Thus, the stoichiometric value at charged state of the negative electrode (anode) decreases (the anode is less charged) and the stoichiometric value at discharged state of the positive electrode (cathode) increases. In addition, the decrease of the stoichiometric value at discharged state of the positive electrode (cathode) originates from less cathode active material intercalated at charge state (there are not enough lithium ions available in the cell to intercalate the cathode fully back to the fresh state) which generates an increase of cell impedance [32].

There are different explanations of the degradation mechanism behind LLI in the literature, for example, Grolleau et al. [33] pointed to a cell imbalance the reason behind the LLI. This cell imbalance happens due to different lithium consumption rate at the negative electrode (as consequence of reduction of electrolyte) and lithium oxidation at the anode surface. Sarasketa [11] agrees with the idea of LLI being mainly arisen from the reduction of electrolyte at anode surface that forms the Solid Electrolyte Interphase (SEI) layer, but it also was considered the generation of LLI from Solid Permeable Interface (SPI) formation and from organic solvents oxidation, both happening on cathode surface. According to Pastor et al. [34] the aging mechanism behind LLI is indeed electrolyte decomposition, but also lithium plating and formation of lithium ion grains. Birkl et al. [31] supported the idea of the formation of lithium ion grains as a degradation mechanism that generate LLI because lithium ions can also be lost if they are trapped inside electrically isolated particles of the active materials. Schuster et al. [29] evaluate the isolation effect on active material of the passive layers at extreme operation conditions (high SOC or high T°). However, Schuster et al. [29] found that the evolution of passive layers takes a key role on the aging of lithium ion batteries. It has been found that after the SEI formation, this same SEI prevents any further reduction of the electrolyte at the anode and that the SPI oxidizes continuously the electrolyte at the cathode due to SPI's incapability of full passivation. Those discoveries lead Schuster et al. [29] to conclude that the thickening and reconstruction of passive layers consume active lithium, and that there is a direct correlation between passive layers behaviour and capacity loss. In accordance to this, Schuster et al. [29] also conclude that the reduction of the electrolyte is more relevant in the generation of LLI rather than the other causes.

In this line, several authors such as Sarasketa [11] links the degradation of the lithium ion technology cells (from an heuristic point of view) with just the creation of interface layers on the surface of the electrodes and the LLI generated by those interface layers.

- **Loss of Active Material**

The Loss of active material (LAM) is mainly a result of structural damage and material loss related to dendrite formation that may increase self-discharge (short circuit risk), particle isolation, crystal growth (reduction of the effective area), changes on the volume of the electrodes and electrode delamination [11]. According to Pastor et al. [34] LAM can also be a consequence of material

dissolution, oxidation of the electrolyte (growth of interphase layers at the electrodes), electrode decomposition, intercalation gradient strains in the active particles and crystal structure disorder. Birkl et al. [31] added particle cracking and loss of electrical contact (or blocking of active sites by resistive surface layers) to the causes of generating LAM. To sum up, LAM is related to structural transformations in the active material and electrolyte decomposition which can generate capacity and power fade [31].

According to Dubarry et al. [35], some degree of LAM may be masked for up to 30% of capacity fade if the LAM occurs on the electrode which is not limiting the cell performance. This phenomenon is referred as hidden aging. Eventually, this degradation catches up with that of the limiting electrode and shifts the role in the capacity limiting mechanism over aging. 'Alawa toolbox (created by Dubarry et al. [27]) suggests that LFP cathode and graphite anode cells should not exhibit any initial capacity or power fade due to LAM of the positive electrode as well as of the negative electrode at a delithiation state until those LAM mechanisms reaches a massive capacity fade, see Figure 4. This idea is supported by the fact that LAM may follow a power-law or exponential dependency.

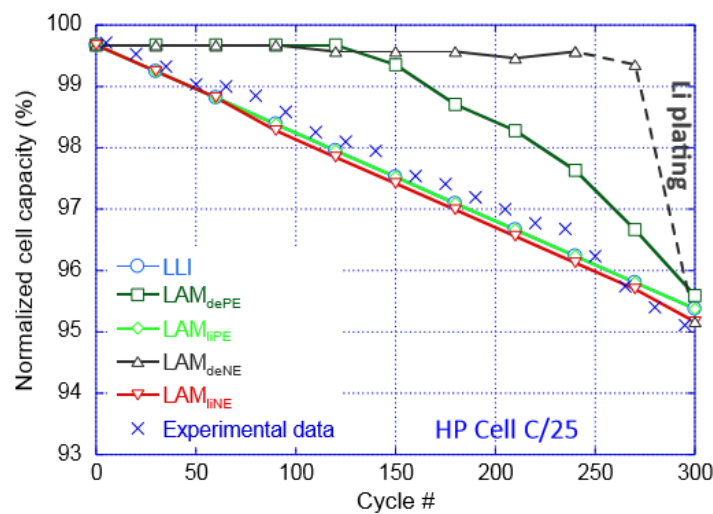


Figure 4: Trends in the capacity fading as a function of cycle number for the five degradation modes: 4.5% LLI, 4.5% LAM at lithiated positive electrode, 16.5% LAM at delithiated positive electrode, 27.0% LAM at delithiated negative electrode, and 4.0% LAM at lithiated negative electrode, respectively, as predicted for C/25, in comparison with test data. All simulations are based on 5% capacity fade in a High-Power LFP/graphite cell using the 'Alawa model [27].

When the LAM controls the capacity fade, the stoichiometric value at charged state (at full lithiation) of the negative electrode (anode) increases [32]. In this case, LAM should lead to a less amount of active material involved in cycling. As a consequence, there is less amount of intercalable active material for the same amount of lithium ions (artificial "enrichment" of Li concentration in the reaction). This forces the remaining active grains to retain a higher end of charge SOC to keep the cell voltage in the voltage plateau [36]. Consequently, the anode is charged to higher SOC values [32].

Under severe LAM of the negative electrode, the phenomenon called lithium plating is expected. Lithium plating refers to the lithium ions deposit as metallic lithium on the negative electrode during charge [37]. The predisposition or susceptibility of a specific lithium ion cell for creating lithium deposition is determined by some factors that affect the anode polarization and lithium intercalation kinetics such as the nature of electrolyte or the capacity ration between anode and cathode. There are also several cell design aspects that will accentuate the propensity towards lithium plating [15]. The ratio of anode capacity to cathode capacity is a critical parameter. The anode is required to be larger in capacity and in area (larger in dimensions) in order to avoid anode's edges reactions (the lithium plating is more susceptible to happen in anode's edges). The electrolyte also plays a strong role in defining the interfacial conditions at the anode and in determining the SEI on the anode's

surface. The nature of the electrolyte affects the intercalation kinetics, and therefore, it affects the plating behaviour. A good “low temperature” electrolyte should minimize or eliminate the problem of lithium plating even in low charging temperatures [15].

Among the different anode materials, it is known that graphite is prone to lithium plating due to the proximity of its reversible potential to that of lithium [15]. Under nominal operation conditions, there is no presence of metallic lithium in the cell. However, under exhausting charge conditions (high charge rates combined with low charge temperature); the graphite voltage may drop below 0 V vs Li. On this scenario, the lithium cannot be intercalated and it is plated between active material and the SEI [29]. This happens due to a reduction in the intercalation kinetics at the anode [29] or loss of graphite active material [15].

The lithium plating appears as a specific voltage plateau at the beginning of the voltage profile in the discharge Open Circuit Voltage (OCV) curve (Figure 5). The high voltage plateau in the discharge OCV curve is a semi-quantitative indication of the lithium plating that would have occurred in the preceding charge. The width of the plateau is proportional to the amount of metallic lithium and it increases after successive charges at low temperatures [15]. The result obtained by Ma et al. [38] showed that a sharp peak is expected to appear in the Incremental Capacity of the discharge if there is lithium plating, which supports the existence of a high voltage plateau in the discharge OCV curve after lithium plating happens.

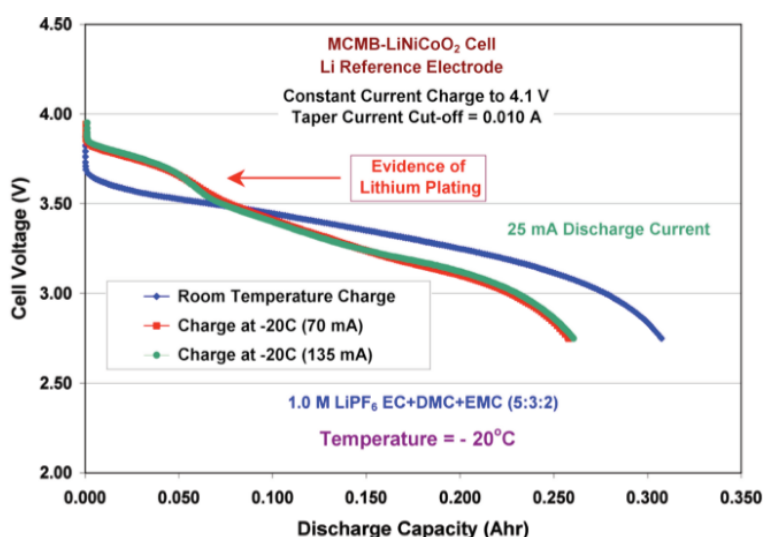


Figure 5: Lithium plating evidences on the OCV profile on discharge [15].

Theoretically, plated lithium is removed in the subsequent discharge because lithium oxidizes at a lower potential than the potential of deintercalation (about 100 mV vs. Li.). Due to that, the plated lithium is considered largely reversible and it is assumed to oxidize at potentials about 100 mV higher than the lithium de-intercalation potentials as long as a conductive connection to the anode material exists [29]. This process of re-oxidation of the plated lithium is called stripping of plated lithium. However, during stripping of plated lithium, it is assumed that porous structures are formed and both, chemical intercalation processes and the plated lithium lose the conductive connection to the anode material, isolating lithium ions and generating an irreversible capacity fade [29]. In consequence, the lithium plating effects do not disappear entirely during subsequent discharge as theoretically considered [15]. Furthermore, isolated plated lithium generated by stripping of plated lithium may further promote SEI growth which again deteriorates the anode's ionic kinetics. In the same time, low ionic kinetics promotes the occurrence of lithium plating, generating a vicious loop and multiplying the degradation rate [29].

Lithium plating may cause problems in terms of performance, reliability and safety since lithium plating is known to be dendritic and it often induces internal shorts [15] and due to that behaviour

lithium plating is considered a phenomenon that deteriorates radically cell performance [11]. Besides, the occurrence of aging induced lithium plating leads to the turning point from linear to nonlinear aging characteristics [15].

- **Kinetics deterioration**

The primary effect of degradation on the cell's kinetics is the increase of the internal resistance or impedance, also referred as polarization resistance (measured by the voltage drop in an operation condition or by an Electrochemical Impedance Spectroscopy (EIS) in steady state), mainly caused by the slowing down of the charge transfer, by the reduction of electrode contact or by the reduction of electrolyte conductivity [38]. The increase of the internal resistance leads to the decrease, in discharge, of nominal voltage at a defined SOC along the cell life [39] which also leads to reaching the end of discharge cut-off voltage earlier (a decrease of dischargeable capacity appears) [31].

In contrast to this, an improvement of electrode kinetics could also occur during the useful life of the lithium ion battery. This improvement on reaction kinetics could come through electrode morphology changes generated in cycle aging or from an improvement on charge transfer kinetics at the electrode-electrolyte interface. Dubarry et al. [27] found that the charge transfer rate improves in the cells that show increasing capacity with discharging rates. This fact was supported with the results obtained in [27], which showed a reduction of the cell ohmic resistance with the progression of cycle aging derived from the initial internal resistance voltage drop upon polarization. This improvement in reaction kinetics was linked to the capacity recovery phenomena.

1.1.2 Remaining useful life

The Remaining Useful life (RUL) of a system is defined as the length from the current time to the end of the useful life [40] where the end of that useful lifetime is described as an event of interest based on the end of life (EOL) criteria. Prognostics deals with fault propagation (or degradation) and predicts how soon a system (or component) will fail or reach a level that cannot guarantee satisfactory performance (the RUL) [8].

The RUL depends on the current age of the asset, the operation environment, the observed health information or condition monitoring data (referred as health indicators in this thesis) [41] and the failure and fault information (event data) [42]. In practice there are always some faults and failures which are not predictable (prognostics cannot completely replace diagnostics or pattern recognition of fault spaces (or event data)), so event data is an important source of information (prediction based on both event and condition data has been considered in the literature [43]). In some cases nonetheless, critical assets are not allowed to run to failure and the data may be scarce, so condition monitoring data gets more important in those cases. Anyway, in both cases, in order to do RUL prognosis, knowledge (or data) on the fault propagation process and knowledge (or data) on the failure mechanism must be available [42].

In RUL prognosis of lithium ion batteries, it is difficult to predict the RUL and the degradation with certainty [40] firstly, because it is nearly impossible to observe the battery internal electrochemical process since the aging of a lithium ion battery is a non-linear and time variant system with the consequent non affordable computational cost in on-board applications with current technologies [44] and secondly, because environmental uncertainties also affect the production and the performance of these lithium ion batteries (dynamic environments induce changes in the physics of failure [40]). Based on this, it could be claimed that a reasonable and appropriate degradation model applied in a RUL prognosis method has to take into account uncertainty of battery behaviour and internal characteristics as well as safety assurance [44]. In this context, the failure event of interest can be seen as the result of a stochastic degradation process crossing a threshold level where the hitting time of the degradation is modelled as a time-dependent stochastic process [40]. However, a point prediction of the RUL is relatively inaccurate and may not be very useful since the variability of the RUL is relatively large [41]. Since RUL is a random variable, the distribution of RUL is of interest for full understanding of the RUL [42].

In order to make the RUL estimation of lithium ion batteries, researchers have used different tools. Overall, those tools are divided in two main groups: methods based on mechanism analysis (models) and methods based on data mining or data-driven analysis (data). However, in most cases, studies have mixed both methods in order to strengthen each methods' weaknesses [45][46].

The RUL prognosis tools have many different characteristics which makes them more appropriate or less appropriate to use them in a particular case, but all of them have to be done from the application and user point of view (customer orientation) [26].

1.1.2.1 Prognosis Method based on models

Model based methods (based on mechanism analysis) uses domain expertise (specific knowledge and theory relevant to the monitored system [42]) to build mathematical models [47]. Among the available options, first principle electrochemical and equivalent circuit models are used to model spatial differences and temporal changes [26]. Methods of RUL estimation of lithium ion batteries based on spectroscopies and on human electrochemical interpretation which gives a deeper insight into important phenomena such as the SEI formation [48]. However, the complexity of a given system continues to increase together with the diversity and uncertainty of its operating environments, which results in extreme difficulties in constructing physical models that capture the system behaviour [40].

Another strategy found in the literature for lithium ion batteries RUL prognosis problem considers semi-empirical based models [49] which describe the aging evolution observed during experimentation. This strategy employs a simplified and generic physical model adjusted to some observations. This type of model is able to describe the evolution of the tracked health indicators under a certain operation window delimited by the gathered observations.

1.1.2.2 Prognosis Method based on data

The methods based purely on data (or data driven methods) are based upon statistical and learning techniques which come from the theory of pattern recognition. These approaches can be developed from multivariate statistical methods or black box methods [50]. Basically, what data driven techniques do is learn from historical data and then wisely suggest a decision [44]. On this process, it is assumed that the data condition and regime remains constant until the failure of the system. In other words, these methods focus on extracting effective information about the observed performance of the system until certain time-instant to build the degradation model and to predict the RUL. This way, inherent relationships and degradation trends based on data are established [51] and since lifetime data is usually correlated with the underlying physical degradation process, unexpected failures and accurate lifetime estimations of the gradually degraded system can be obtained [40].

Data-driven methods have become an effective avenue to evaluate reliability and estimate RUL, specially for vital systems with high reliability and long lifetime [40] such as the lithium ion batteries. Thanks to those algorithms, the behaviour of the battery is learnt based on monitored data of the application while those methods don't demand battery chemical modelling or knowledge [44]. Besides, these algorithms are relatively easy to implement since they employ basic mathematical expressions [43]. However, at the same time, they show some important limitations. These algorithms implicitly assume that there is some underlying stability in the monitored system that may not exist. In addition, they rely on past patterns of degradation to project future degradation (it can lead to inaccurate forecasts) [43].

Amongst the different data driven methods available in the literature to predict the RUL of lithium ion batteries, there are two main generic type of methods: artificial intelligence algorithms [19][52] that are used to model the evolution of the health indicators as a black box; and stochastic algorithms [45][46][53][54] used to predict the RUL and its distribution on on-board applications (they require a minimum amount of observations of the evaluated use case).

1.2 Objectives and scope

The main objective of this thesis consists on determining accurately the most profitable size of an Energy Storage System based on lithium ion batteries satisfying application and lifetime

specifications. Specifically, the sizing exercise is focused on the two most relevant lithium ion battery applications: the electric vehicle and the energy balancing (stationary) application.

The most profitable size of the battery solution is believed to come from integrating the prediction of the lifespan on that sizing exercise. In that context, the next four sub-objectives have been established in order to attain that main objective:

- [O1] Determine the End of Life condition of the battery solution.
- [O2] Track the aging behaviour of the battery solution.
- [O3] Quantify the cost of the project all along the project lifespan.
- [O4] Get reliable results by improving the accuracy of the constructed elements if necessary.

The lifespan of a battery solution requires knowledge about the event that determines the End of Life itself and about the evolution of the performance until that End of Life event. These would be related with the first two sub-objectives. Moreover, based on the believe behind the most profitable sizing, the costs related to each sizing option needs to be quantified taking into account all the costs generated all along the lifespan of the project (the warranty period of an Electric Vehicle or the exploitation period of a stationary application). This would be related with the third sub-objective. Furthermore, the given most profitable sizing value needs to be accurate. For that, the results given by all the constructed elements inside the proposal need to be accurate and reliable. This is why lastly, additional tools aimed at increasing the accuracy of the detected low accurate elements are proposed. This would be the fourth and last sub-objective.

1.3 Methodology and structure of the thesis

In order to meet these objectives, this thesis presents the development of all the necessary elements on a simulation environment where the levelized costs of a set of size values are calculated. The proposed methodology is shown in Figure 7. The outline of the followed structure to complete this methodology is shown in Figure 6.

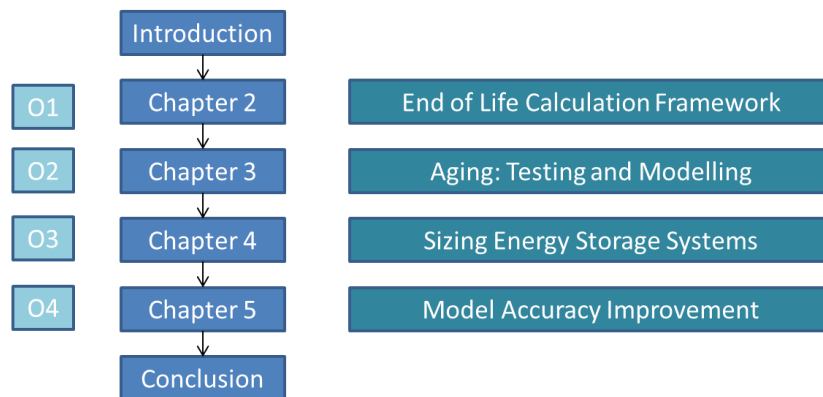


Figure 6: Structure of the thesis.

Firstly, the End of Life state of the battery is determined (chapter 2). The End of Life is calculated as a combined threshold of all the health indicators of interest. Its calculation requires the implementation of an electro-thermal model in a simulation environment defined by the end of life criteria specified by the application requirements. The correctness of the proposal is validated by experimentally testing the application end of life criteria on batteries at different state of health values. In addition, it is proved that the OCV does not change significantly all along the aging, that the resistance is increased uniformly on the entire SOC range and that the resistance increase due to the temperature increase does not change the voltage response significantly.

Secondly, the health indicators of interest are modelled based on the most relevant stress factors (chapter 3). The methodology to acquire the aging data and the construction of the posterior empirical models are presented. The validation of the constructed models based on the acquired data is performed based on three aspects: the accuracy describing the observed cases, the

correctness of interpolations and the real life applicability. In addition, it has been validated that the cycling aging and the calendar aging can be linearly added.

Thirdly, the simulation environment for sizing exercises of lithium ion battery energy storage systems is developed (chapter 4). The simulation environment is set to a generic electric vehicle application and to a generic stationary application with which the levelized cost of different battery solution is calculated. The simulation environment integrates the developed electro-thermal model, end of life map and aging models. The developed simulation environment for a generic Electric Vehicle is applied on a High-Energy electric bus application as well as on a High-Power one. The developed simulation environment for a generic stationary application is applied on an Energy balancing application inside a Micro-grid. In addition, it is validated that the damaged generated by different operation modes can be added in a cumulative way (cumulative damage model). Additionally, it is validated that rest times below 3h do not generate any degradation, except at 100% SOC (at 100% SOC any rest time deteriorates the battery).

Fourthly, the errors in the developed models are minimized (chapter 5). In this case, the critical elements in terms of accuracy are the constructed aging models. The error of the aging models is minimized by focusing on the errors made when extrapolating in time and facing odd events. On one hand, there are cases that the estimation error increases drastically when the generated aging models are extrapolated in time. Our proposal consists on lengthening the data of origin thanks to half-data analysis to afterwards construct again the aging model. In this way, the extrapolations in time turn into interpolations in time, avoiding like this the increase of the estimation error due to extrapolations in time. This step is considered as a pre-processing of the data on the top view methodology and it is not shown in Figure 7. On the other hand, a prognosis stochastic algorithm is selected and employed with real life data to deal with the effect that odd events have on the evolution of the health indicators. In this case, it is necessary to have real life data. This step is considered to be applied to on-board applications (cannot be integrated on the sizing exercise).

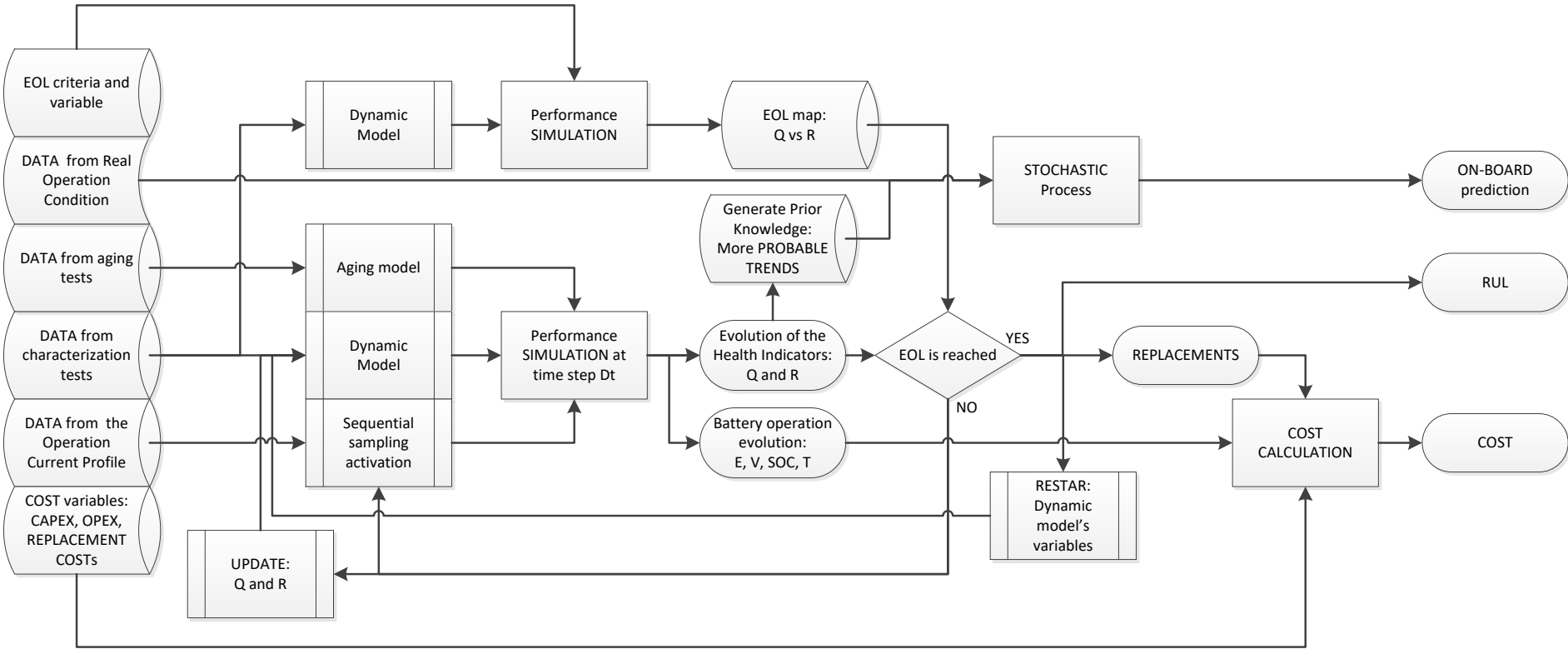


Figure 7: The black-box diagram of the methodology on a top view

1.4 Scientific Contributions

During this thesis, a simulation environment has been developed to determine the most profitable size option. Here, a brief overview of the proposed scientific advances as well as the conference contributions and journal publications are presented:

Proposed scientific advances

- A methodology to calculate the End of Life of a battery solution based on the application requirements. The quantity and entity of the applied Health Indicators on the proposed methodology is not restricted. The End of Life calculation can contain all the Health Indicators that the user of the methodology is interested on.
- A methodology to construct an empirical aging model that covers the aging test matrix design and the final validation. The modelling considerations and performance limits observed on the validation are reflected on the aging test matrix design. It is a closed loop that covers the whole aging modelling process.
- The levelized cost quantification of the battery solution on a complex application such as the evaluated Micro-grid.
- The simulation environment that integrates all the required elements to select the most profitable sizing option of a lithium ion battery Energy Storage System. The simulation environment is built firstly for a generic Electric Vehicle application and secondly to a generic stationary application.
- A unified evaluation framework for prognosis algorithms. Thanks to this, further improvements of these algorithms can be obtained including the selection of the algorithm depending on the application characteristics.
- The comparison of a certain Particle Filter configuration, a certain Gaussian Process configuration, the Extended Kalman Filter and the Unscented Kalman Filter with a common evaluation methodology.
- An artificial data generation tool that can be used to fill uncompleted aging data sets. The proposal introduces a new use of half-cell data. This data is used to increase significantly the accuracy of empirical aging models.

Conference contributions

- (1) M. Arrinda, M. Oyarbide, H. Macicior, and E. Muxika, "Prognosis of the remaining useful life of a Lithium Battery based on a data-driven method and Gaussian processes," in *Electric Vehicle Symposium & Exhibition 30*, 2017, pp. 1–12.
- (2) M. Arrinda, M. Oyarbide, H. Macicior, and E. Muxika, "Comparison of Stochastic capacity estimation tools applied on remaining useful life prognosis of Lithium ion batteries," *PHM Soc. Eur. Conf.*, vol. 4, no. 1, Jul. 2018.
- (3) M. Arrinda, M. Berceibar, M. Oyarbide, H. Macicior, E. Muxika, and M. Messagie, "Using a Second-Life Battery to Optimize the Levelized Cost of Electricity in CO2 Neutral Microgrid," in *Electric Vehicle Symposium & Exhibition 32*, 2019, pp. 1–14.
- (4) H. Popp, G. Glanz, R. Hamid, N. Zhang, M. Arrinda, S. Ritz, I. Cendoya, "BENCHMARK, AGEING AND ANTE-MORTEM OF SOTA CYLINDRICAL LITHIUM-ION CELLS" in *Eco-Mobility 2019 - 14th International A3PS Conference*.
- (5) M. Arrinda, A. Bermúdez, D. Gómez, M. Oyarbide, and P. Venegas, "State of charge estimation of batteries using Preisach hysteresis model", in *SCEE 2020 Schedule of Conference Eindhoven*, February 16-20, 2020.
- (6) M. Arrinda, M. Oyarbide, H. Macicior, and E. Muxika, "Improved SOC and SOH estimators by considering the effect of rest periods analyzed with half-cell data", in *Batterietagung 2020*.

Journal publications

- (1) M. Arrinda, M. Oyarbide, H. Macicior, and E. Muxika, "Unified Evaluation Framework for Stochastic Algorithms Applied to Remaining Useful Life Prognosis Problems" (sent to International Journal of Prognostics and Health Management, ISSN 2153-2648).
- (2) M. Arrinda, M. Bercibar, M. Oyarbide, H. Macicior, E. Muxika, and M. Messagie, "Levelized Cost of Electricity Calculation of the Energy Generation Plant of a CO2 Neutral Micro-grid" (sent to Energy, ISSN: 0360-5442).
- (3) M. Oyarbide, D. Sanchez, M. Arrinda, H. Macicior, O. Miguel, "Capacity and impedance estimation by analysing and modelling in real time incremental capacity curves" (sent to Journal of Energy Storage, ISSN: 2352-152X).
- (4) P. Venegas, M. Arrinda, A. Bermúdez, D. Gómez, M. Oyarbide, "Kalman filter and classical Preisach hysteresis model applied to the state of charge battery estimation" (On process, it will be sent to Journal of Power sources, ISSN: 0378-7753).

CHAPTER 2:

2 End of Life Calculation Framework

This chapter responds to the objective of finding the life state condition of the chosen energy storage system where the defined End of Life (EOL) criterion is reached. For that, a methodology that determines how to calculate the EOL threshold is presented. Here, it is hypothesized that the EOL is application dependent and not a fixed threshold value. In order to validate this hypothesis, the methodology is tested and validated under two lithium ion battery use cases: a High-Energy application and a High-Power application. The contribution of this chapter consist on firstly, the proposed methodology itself; and secondly, the validation of the proposed methodology with real data.

2.1 Introduction

In global terms, the End of Life (EOL) aspect is related to the concept of failure, which can be defined as the fact of something not working, or stopping working as well as it should. The concept of failure can be judged by criteria such as performance (performing at unsatisfactory level), functionality (incapable of conducting specific function) and availability (machine breaks down) [8].

Generally, lithium ion batteries are considered to reach their EOL when their dischargeable capacity fades to 80% of its initial value [11] [48] independent to their function. This threshold is a good enough criterion to observe which design performs better from an electrochemical design point of view, but from the application point of view, a more complex criterion is needed. According to Wenzl et al. [26], combining all effects of the life time prediction into one figure of merit (the EOL) is a must when facing lithium ion batteries EOL estimation. For this purpose, it was proposed to establish clear and unambiguous quantitative definitions for EOL while considering that the EOL depends on the nature of application and design parameters of the battery. In this line, Yingzhi et al. [55] defined the EOL of a lithium ion battery as the time point when the selected lithium ion batteries can no longer provide enough power or energy to accomplish its intended function. Yingzhi et al. [55] estimated the EOL by employing as EOL criterion the incapability of fulfilling a 30% Depth of Discharge (DOD) without reaching the End of Discharge Voltage of the battery. They displayed the End of Discharge Voltage vs cycle trend evolution of (1) full cycles and of (2) 30% DOD cycles so as to calculate the cross point between both lines, defining the cross point as the EOL. However, the proposed EOL estimation approach only addresses an application under specific use conditions (30% DOD at a certain current and at a certain temperature). It still remains notoriously difficult to accurately predict the EOL under environmental and load conditions different from the training data set [56].

In a global sense, it can be defined that assets fail when their level of degradation or condition variable reach a specified failure threshold (the functionality requirement is no longer fulfilled) [50]. Methods depending on setting a critical level (a threshold called “X”) for the condition variable show two difficulties: firstly, relating the unobserved condition to the Condition Monitoring variables; and secondly, estimating the X when the selected condition variable is unobservable [41].

In addition, according to Gorjian et al. [50], even the raw concepts of what threshold should be and how it should be specified are not clear. The fact is that lithium ion batteries are complex electrochemical systems with nonlinear degradation behaviours, which depend on various intrinsic features and external conditions, making the EOL estimation a challenge [20]. In this scenario, this chapter proposes a methodology that defines a functional mapping of the EOL threshold that approximates the simulation to the EOL for given input conditions [57]. Firstly, the methodology of estimating the EOL threshold is presented. Secondly, the typical unobserved condition variables (health indicators) are introduced. Here, the link between Health Indicators and Condition Monitoring variables (behavioural variables) are correlated. Thirdly, possible application requirements are treated. Two examples of use are introduced (a High-Energy application and a High-Power application). Fourthly, the simulation environment is introduced where EOL threshold is mapped by simulating the battery performance on a range of operation conditions. Fifthly, the results of the proposed two examples of use are presented. Sixthly, some hypotheses done on this approach as well as the verification of the obtained results in one of the proposed examples of use are validated. Finally, the discussion of the obtained results and the conclusions are presented.

2.2 Methodology

The proposed approach focuses on an “M” dimensional EOL threshold mapping, where M represents the chosen amount of Health Indicators. For that, an algorithm that searches the combinational value of the selected Health Indicators at which the battery stops fulfilling the requirements defined by the application is done. For that, the proposed approach is divided in five different steps:

1. Select the Health Indicators of interest.
2. Detect the behavioural variable (electric, thermal, physical, etc.) where the effects of the chosen Health Indicators can be appreciated.

3. Define the EOL criteria by addressing the link between the effect of each of the Health Indicators of interest on the behavioural variables and all the application requirements: generate the Testing Inputs.
4. Define the value vector of the chosen Health Indicators that will be evaluated except for one. Generate the evaluation grid composed with the combination of those vectors.
5. Find the combinational value of the Health Indicators where the battery stops fulfilling the EOL criteria using the last Health Indicator under evaluation as a free variable.

The first two steps consist on the use Health Indicators. There are many different Health Indicators and depending on the aim and resources of the study, it will be more interesting to use one or another. It is also important to detect properly the measurable variables that have an effect on each Health Indicator. Once those variables are detected, the link of the Health Indicators with the restrictions imposed by the application on the battery performance will be allowed.

The third and fourth steps consist on merging the chosen Health Indicators on the application environment in order to generate the Testing Inputs and to delimit the simulation grid. These Testing Inputs will feed up the battery model which is set up to map the EOL thresholds. Firstly, the application requirements are translated into battery performance restrictions related to the detected behavioural variables on the step two (the ones where the effects of the selected Health Indicators can be appreciated). In this way, the EOL criteria and the Health Indicators are mixed. Next, the Testing Inputs that respond to each EOL criteria are defined. These Testing Inputs are composed by the initialization parameters and the operation of the battery. The operation can be a current profile that describes the application or a functional procedure that defines a range of operations. Once this is done, the case study is properly delimited to allow the posterior simulations. For this, $M - 1$ numbers of vectors are determined. Each vector has the values that each Health Indicator but one will take on the simulations. Then the evaluation grid is generated based on the combinations of those vectors. The procedure of deducting each value vectors but one is the same in all the cases:

- Define the limits of interest of the HIs under study. For that, find the increase or decrease of each of those Health Indicators that leads to the non-fulfilment of the application requirements at the Beginning of Life.
- Define the intercalation between the limits by considering the balance between accuracy level and computational resources.

This is done with all the Health Indicators except one. The last health indicator of interest is used to find the exact conditions where the battery stops fulfilling the application requirements on the simulations. For that, the electric-thermal behaviour of the battery with the chosen Health Indicators as input is simulated. Thanks to this, an M dimensional EOL threshold map that takes into account M Health Indicators of interest is calculated. The development of the algorithm that introduces the threshold mapping is the fifth step (Algorithm 1)

$$\{EoL_{TH}^{(i)}\}_{i=1}^{\rho} = EOL_{ThresholdMapping} \left(\{HI^{(j)}\}_{j=1}^M, \{EOL_{criteria}^{(u)}, TI^{(u)}\}_{u=1}^L \right)$$

1: $\{\vartheta_E^{(i)}\}_{i=1}^{\rho} = GRID(HI^{(1)}, \dots, HI^{(M-1)})$

2: **for** $i = 1$ **to** ρ **do**

3: **for** $u = 1$ **to** L **do**

4: $EoL_{TH_temp}^{(j)} = BATT_MODEL(EOL_{criteria}^{(u)}, \vartheta_E^{(i)}, HI^{(M)}, TI^{(u)})$

5: **end for**

6: $EoL_{TH}^{(j)} = MIN(EoL_{TH_temp})$

7: **end for**

Where

ρ = The number of threshold points or evaluation points on the EOL map.

$\vartheta_E^{(i)}$ = (i) evaluation point or combination of the Health Indicator values under evaluation.

$EoL_{TH}^{(i)}$ = The End of Life threshold value at (i) evaluation point.

$HI^{(j)}$ = Value vector of (j) Health Indicator.

$GRID$ = Generator of the evaluated numerical grid.

$BATT_MODEL$ = Battery electric-thermal model adapted to the EOL criteria and the Health Indicators.

$EOL_{criteria}^{(u)}$ = The (u) End of Life criterion imposed by the application requirements.

M = Amount of Health Indicators.

L = Amount of End of Life criteria.

TI = The test input of the model that allows the test of each EOL criterion.

Algorithm 1: Top view algorithm of the proposed EOL mapping approach.

2.3 Health Indicators

In a first instance, the Health Indicators that fit our interest need to be selected. The Health Indicators represent in a resumed way the State of Health (SOH) of a battery. Each of the Health Indicators has its own characteristics. The most common health indicators are the next ones:

- The decrease rate on the dischargeable capacity (relative value to the dischargeable capacity measured at the Beginning of Life of the battery in study).
- The increase rate on the pure ohmic resistance response of the battery (relative value to the pure ohmic resistance measured at the Beginning of Life of the battery in study).

The relative value of the dischargeable capacity of the battery is often used as the main Health Indicator and labelled as the SOH itself. It is a direct representation of the energy the battery is able to dispose. A decrease of the dischargeable capacity leads to faster voltage evolution of the battery under the same current profile. Because of this, the battery reaches faster the End of Discharge voltage which can mean the end of the fulfilment of a requirement of the application under study.

The relative value of the inner pure ohmic resistance of the battery appears in many studies since it limits the applicable power at certain voltage levels, which conditions highly the charging time of fast charging and slightly the dischargeable capacity. The increase of the pure resistive value of the battery leads to a higher reduction of the voltage and due to this, there could be cases where the End of Discharge voltage limit is reached.

These two health indicators are relatively easy to measure, and the effects these two health indicators show on the performance decrease of the battery can be linearly addressed to application requirements (the increase of the pure ohmic resistance as well as the decrease of the dischargeable capacity affects the voltage response of the battery). Nonetheless, these two Health Indicators are not the only ones that can be used to determine the SOH of the battery. There are some other Health Indicators that can be added on the proposed EOL mapping such as:

- Decrease on the End of Discharge voltage on repetitive operation conditions [55].
- The drift of the Open Circuit Voltage (OCV) of the electrodes [55].
- The increase of the time constant of the transitory response of the battery [26].
- The decrease on the thermal conductivity of the inner components of the battery [26].
- The increase of the effect of the reversible part on the whole thermal heat generation [26].
- The Loss of Lithium Ion Inventory (LLI) [27].
- The Loss of Active Material (LAM) on the electrodes [27].
- The organic reduction on the electrolyte or the pressure inside the battery [26].

However, it is not common to find them in other works. Some of them represent variables with low observability (LLI, LAM or the organic concentration of the electrolyte cannot be measured, need to be guessed under several assumptions), some other represent variables with no records on typical Aging Check-up Tests (thermal performance variations are typically dismissed), and a few represent variables with a lower study interest level respect to the commonly used Health Indicators (for example, since the increase of the pure ohmic resistance is the most representative element on the increase of the impedance of the battery on the aging process, the rest components of the impedance, such as the transitory time constant, are often dismissed).

Based on this, the proposed approach focuses on the two most common Health Indicators: the decrease rate on the dischargeable capacity and the increase rate on the pure ohmic resistance response of the battery.

2.4 Application requirements

The proposed EOL mapping is application directed. This means that the application becomes the main element on the EOL definition criterion. Among the typical applications (low power electronic devices, stationary energy storage systems, electric vehicles), these are the most common restricting requirements:

- A minimum time of operation.
- A maximum charging time.
- A maximum heat generation.
- An assurance of a catastrophic event not happening (safety margin).

In this study, two applications are evaluated in an electric mobility scenario. Firstly, an application with a high-energy requirement is evaluated; and secondly with an application with a high-power requirement.

2.4.1 High-Energy application

The high-energy application consists on a battery integrated on an electric public bus with the next restrictions:

1. The Battery Energy Storage System (BESS) integrated on the full electric bus has to supply the energy to be working 17 hours non-stop (a minimum autonomy restriction).
2. The rest time of the bus at night of 7 hours is employed to do the charging of the BESS (a charging time restriction).

For that, a High-Energy NMC-C pouch battery has been chosen. The battery characteristics are shown in Table 3.

Item	Specification
Nominal Capacity	54 [Ah]
Maximum voltage	4.2 [V]
Minimum voltage	2.5 [V]
Standard charge current	54 [A]
Standard discharge current	54 [A]
Maximum temperature	45 [°C]

Table 3: High-Energy battery specifications

The Test Input that fits the charge time restriction is a Constant Current-Constant Voltage (CC-CV) standard charge at 1C. In this case, the charge time of 7h is assumed to be long enough to charge the battery to the desired SOC (100% in this case) in any SOH. Therefore, this EOL criterion is ignored on the EOL mapping.

The Test Input that fits the minimum autonomy restriction consists on the operation profile of the application (starting from a 100% SOC). This profile has been generated in terms of the orography of a selected route (the generation of the current use profile is out of the scope of this study) and tested on the battery level in a climatic chamber at 25°C at CIDETEC (see voltage response and SOC evolution in Figure 8).

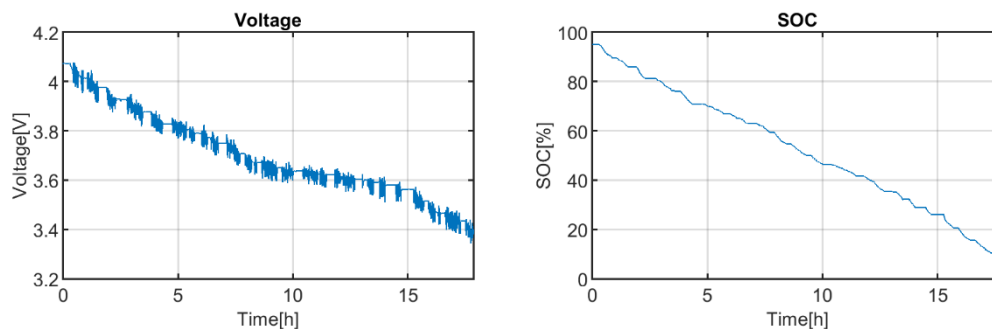


Figure 8: Application profile: voltage response and the SOC evolution of the battery.

According to the observed response of the battery under the operation conditions, the vector with the capacity decrease values that will be studied is defined. The range of that vector is selected based on the reached SOC value at the end of the discharge at Figure 8. The SOC value at the end of the discharge is 12.17% if the battery starts the discharge at a fully charged state, at least at the Beginning of Life. Taking this into account, the range of the capacity decrease has been limited from 0% to 20%. The jump between points is decided in terms of the desired accuracy level and computational resources. In this case, a jump of 0.1% has been chosen.

Once the values that the first health indicator on the study will take are defined, the following next health indicators need to be deducted until reaching the last one. In this case, the next health indicator is the last one, so there is no need to define more vectors for the mapping of the EOL.

2.4.2 High-Power application

The high-power application consists on a battery integrated on an electric public bus with the next restrictions:

- The BESS integrated on the full electric bus has to supply enough energy to do at least once the predefined route after each fast charging stops (a minimum autonomy restriction).
- The bus will be resting 7 minutes at both ends of the route, where a fast charging will be applied (a fast charging time restriction).
- The bus needs to be working 16 hours without any charge out of the schedule (a second autonomy restriction).
- The rest time of the bus at night of 8 hours is employed to do a slow charging of the BESS (a second charging time restriction).

For that, a High-Power NMC-LTO prismatic battery has been selected. The battery characteristics are shown in Table 4.

Item	Specification
Nominal Capacity	23 [Ah]
Maximum voltage	2.7 [V]
Minimum voltage	1.5 [V]
Fast charge current	115 [A]
Fast discharge current	115 [A]
Maximum temperature	55 [°C]

Table 4: High-Power battery specifications

The Testing Input that fits the second charge time restriction is a CC-CV standard charge at 1C. In this case, the charge time of 8h is assumed to be long enough to charge the battery to the desired SOC (100% in this case) in any SOH. Therefore, this EOL criterion is ignored on the EOL mapping.

The Testing Input that fits the first minimum autonomy restriction consists on the operation profile of the application. This profile has been generated in terms of the orography of a selected route (the generation of the current use profile is out of the scope of this study) and tested on battery level on a climatic chamber at 25°C at CIDETEC (see voltage response and SOC evolution in Figure 9). This EOL criterion checks only the fulfilment of the use profile on idle condition (initial SOC set to 100%).

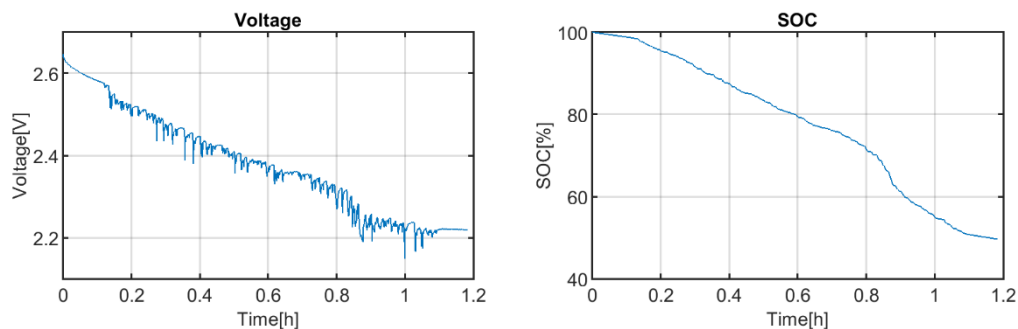


Figure 9: Voltage and SOC response of the battery under the first Testing Input.

The Testing Input that fits the first charge time restriction is a CC fast charge of 7 min at 4C that could change to a CC-CV depending on the initial SOC and the resistance of the battery. In this case, firstly the fulfilment of a fast charge plus a use case discharge would be evaluated after the first use case discharge, however, the fulfilment of the second minimum autonomy restriction implies that this first charge time restriction is fulfilled. This Testing Input is not tested; instead, the tested one is the Testing Input that fits the second minimum autonomy restriction.

The second minimum autonomy restriction consists on the repetition of the first charge time restriction and the first minimum autonomy restriction along the 16 hours of working, which leads to the repetition of both Testing Inputs along the working period of the bus. This Testing Input has been tested on the battery level in a climatic chamber at 25°C at CIDETEC (see voltage response and SOC evolution in Figure 10).

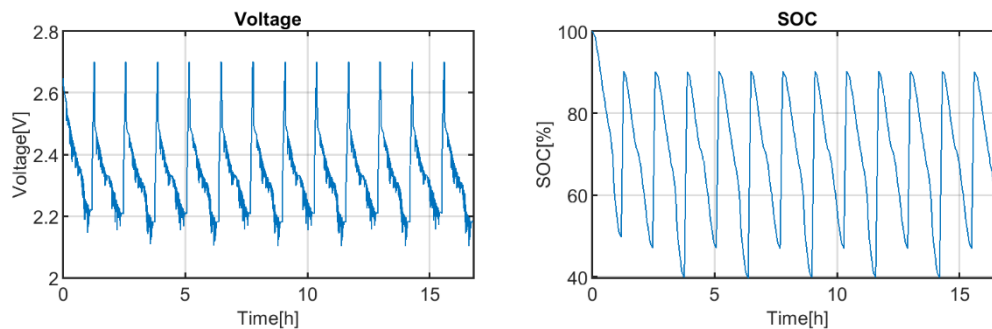


Figure 10: Voltage and SOC response of the battery under the second Testing Input.

According to the observed response of the battery under the firstly defined Testing Input, the vector with the capacity decrease values that will be studied is defined. The range of that vector is selected based on the reached SOC value at the end of the discharge at the Testing Input more restrictive, in this case the second Testing Input, see Figure 10. The minimum SOC value that the battery reaches among all the discharges is 39.79% if the battery starts the first discharge at a fully charged state, at least at the Beginning of Life. Taking this into account, the range of the capacity decrease has been limited from 0% to 45%. The jump between points is decided in terms of the desired accuracy level and computational resources. In this case, a jump of 0.1% has been chosen.

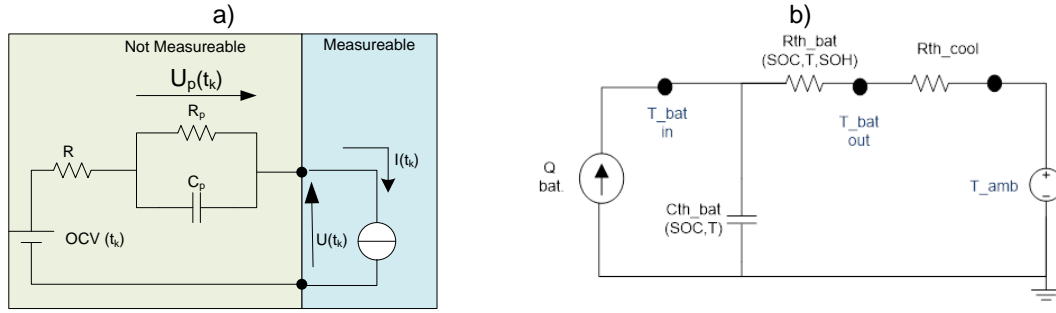
Again in this case, once the values that the first health indicator on the study will take are defined, the following Health Indicators need to be deducted until reaching the last one. In this case, the next health indicator is the last one, so there is no need to define more vectors for the mapping of the EOL.

2.5 Simulation

Once defined all the variables on the EOL mapping approach are properly defined, the actual EOL values need to be calculated. For that, the electric and thermal behaviour of the selected battery is modelled where the Health Indicators are defined as free variables (variables that can be modified from the outside). With this, the EOL mapping algorithm is applied and the EOL “M” dimensional threshold is calculated.

2.5.1 Battery model

The applied battery model describes the electric and thermal behaviour of the chosen battery. It is assumed that the scale up from the battery level to the BESS is trivial and that the interactions between batteries are negligible. The developed electric model [58] and thermal model [59] are shown in Figure 11. The knowledge behind these models are based on the theses of M. Oyarbide [58] and G. Vertiz [59].


Figure 11: a) Equivalent electric model; b) Equivalent thermal model.

The proposed electric model is a first order RC equivalent electric circuit that employs the thermodynamically stable open circuit voltage as the OCV, the ohmic resistance of the battery as the R and the polarization of the battery caused by transfer, diffusion and other factors as the $R_p C_p$ network, see Eq. (1) and (2) [60].

$$I(t_k) = C_p \frac{dU_p(t_k)}{dt} + \frac{U_p(t_k)}{R_p} \quad (1)$$

$$U(t_k) = OCV(t_k) - I(t_k)R - U_p(t_k) \quad (2)$$

Parameter	Description
I	The current delivered by the battery.
U_t, U_p	The terminal voltage and the voltage across the $R_p C_p$ respectively.
OCV	The Open Circuit Voltage.

Table 5: The first order RC equivalent circuit model [60]

This electric circuit is one of the most common equivalent circuit models applied on battery modelling [61], which includes an OCV, a resistor and a RC network in series to forecast battery response at a particular SOC [62]. However, since in real applications (in Lithium ion battery applications) all parameters vary as functions of working conditions (temperature, current rate) and battery usage history (degradation) [62], multi-value parameters are usually applied such as in this case. For that, an array of the values of the parameters at different conditions are saved allowing a posterior look up from a table, finding the appropriate value for each parameter interpolating them at different conditions. For the parametrization of the resistor and the RC network, a pulse characterization test is performed at six different current rates (2C, 1C and 0.5C at charge and discharge) as well as at three different temperatures (10°C, 25°C and 45°C), see Table 6. The OCV values were also taken at those three different temperatures profiting the rest times between different pulses of the applied pulse characterization test.

Step	Action 1	Mode	Conditions	Comments	Current	Temp.
1	Rest	-	1h			T
2	Charge	CC-CV	Vmax@0.05C		C-rate	
3	Rest	-	1h			
4	Discharge	CC-CV	Vmin@0.05C	Capacity measurement ¹	C-rate	
5	Rest	-	1h			
6	Start cycle			Pulse test, charge, start		
7	Rest	-	1h	Take OCV ²		
8	Charge	-	60s@not 100% SoC	Charge Pulse ⁴	C-rate	
9	Rest	-	10min			
10	Charge	-	10%SOC	Set SOC: 10,20,...,80,90		
11	End cycle					
12	Charge	CC-CV	Vmax@0.05C		C-rate	
13	Start cycle			Pulse test, discharge, start		
14	Rest	-	1h	Take OCV ²		
15	Discharge	-	60s@not 0% SOC	Discharge Pulse ³	C-rate	
16	Rest	-	10min			
17	Discharge	-	10%SOC	Set SOC: 90,80,...,20,10		
18	End cycle					

19	Discharge	CC-CV	Vmin@0.05C		C-rate
20	Rest	-	1h		
21	Charge	-	30%SOC	Charge to 30%	C-rate

Table 6: Pulse characterization test used on the parametrization of the equivalent electric circuit

The proposed thermal model is a 1D RCR equivalent thermal circuit that employs the thermal behaviour of the battery as a first order impedance (R_{th_bat}, C_{th_bat}) [63] and the cooling as a thermal resistance (R_{th_cool}) (Eq. (3), Eq. (4) and Eq. (5)). Inside the thermal behaviour of the battery, the capacitive response (C_{th_bat}) is linked to the specific heat generation of the battery and the resistive response (R_{th_bat}) is linked to the inner thermal conductivity of the battery. This model is built under next assumptions:

- The heat is generated in just one point (1D).
- The thermal properties of the battery are completely homogeneous all along the battery.
- The thermal system of the battery is isotherm.
- The physical properties of the battery are independent to the temperature.
- The battery experiences only a convection cooling.

$$Q_{cool}(t_k) = \frac{T_{bat}(t_{k-1}) - T_{amb}(t_k)}{R_{th_bat} + R_{th_cool}} \quad (3)$$

$$Q_{bat}(t_k) = I(t_k)^2 \cdot R + I(t_k) \cdot T_{bat}(t_{k-1}) \cdot \frac{dOCV}{dT} \quad (4)$$

$$T_{bat}(t_k) = T_{bat}(t_{k-1}) + \Delta t \cdot \frac{Q_{bat}(t_k) - Q_{cool}(t_k)}{C_{th_bat}} \quad (5)$$

$$C_{th_bat} = \frac{Q}{m \cdot \frac{dT}{dt}} \quad (6)$$

Parameter	Description
Q_{cool}	The heat exchange from the battery to the exterior.
$T_{bat}(t_k)$	The battery inner temperature at the time instant t_k .
T_{amb}	The room temperature.
Q_{bat}	The heat generation of the battery.
$\frac{dOCV}{dT}$	The entropic factor of the battery.
Q	The applied heat [W].
m	Mass of the element [Kg].
$\frac{dT}{dt}$	The temperature variation rate [$^{\circ}$ K/s].

Table 7: The second order RC equivalent circuit model [59]

The parameters of the model are calculated by applying three specific thermal tests. Firstly, the specific heat capacity is calculated using the energy conservation Eq. (6) on the THT heat capacity protocol defined in Table 8. Then, the entropic factor of the battery, which represents the evolution of the OCV at different temperatures considering different SOC, is modelled with the test described in Table 9. Finally, the remaining thermal variables of the equivalent thermal circuit are obtained by fitting the equivalent thermal circuit equations on any performance test. In this case, the first part of the Hybrid Peak Pulse Characterization test is taken: the 1C charge discharge.

Step	Comments
1	Calibration of the ARC calorimeter according to mass and battery volume
2	Joint assembly of sandwich type analysis (battery-thermal blanket-battery)
3	Heat generation according to THT (5-10mW/gr and 7.75W/m2 max.)
4	Adiabatic environment generation (Heaters ARC)
5	Measuring dT / dt stable area (30°C and 50°C)

Table 8: Specific heat capacity test

Step	Action	Value	End Conditions	Comments
1	Discharge	1C	Vmin	[*initial 24h pause at 0% and 100% SOC. The rest SOC rest 2h]
2	Charge	1C	% SOC desired	
3	Pause	-	*24/2 hours	
4	Set Temp	-20°C	-	
5	Pause	-	2 hours	
6	Set Temp	-10°C	-	
7	Pause	-	2 hours	
8	Set Temp	0°C	-	
9	Pause	-	2 hours	
10	Set Temp	10°C	-	
11	Pause	-	2 hours	
12	Set Temp	20°C	-	
13	Pause	-	2 hours	
14	Set Temp	30°C	-	
15	Pause	-	2 hours	
16	Set Temp	40°C	-	
17	Pause	-	2 hours	
18	Set Temp	50°C	-	
19	Pause	-	2 hours	
20	Set Temp	60°C	-	
21	Pause	-	2 hours	

Table 9: Entropic factor tests

2.5.2 End of Life mapping algorithm

The proposed EOL mapping algorithm is presented in Algorithm 1. It consists on searching the values of each of the selected Health Indicator at which the EOL criteria is fulfilled. For that, the described electric thermal model is simulated under certain use conditions related to the EOL criteria (under certain Testing Input).

2.5.2.1 High-Energy application

The EOL criterion on this case is composed by only one criterion, a minimum autonomy restriction where the current input profile needs to be fulfilled without crossing the minimum voltage threshold.

The two Health Indicators under evaluation are the dischargeable capacity decrease and the pure ohmic resistance increase. The capacity decrease has been already defined (a vector value from 0 to 20 with a step of 0.1). The algorithm performs the evaluation loop N times. N is the length of the capacity decrease value vector ($N = 200$). Next, the value of the second and last Health Indicator is calculated (the resistance increase). This Health Indicator is taken as a free parameter which can take any value. So as to simplify the problem, some assumptions are taken:

- The polarization voltage and OCV do not change with the increase of the pure ohmic resistance.
- The resistance is increased uniformly at the whole SOC range.
- The change on the heating of the cell due to the resistance increase doesn't affect the voltage response of the cell.

Considering these three assumptions, the required resistance increase (ΔR) that leads to overcome the minimum voltage threshold (U_{EOD}) is calculated at each loop iteration, see Eq. (7).

$$\Delta R = \min\left(\frac{U_t - U_{EOD}}{IR}\right) * 100, \quad \Delta R \in \mathbb{R}^+ \quad (7)$$

Parameter	Description
ΔR	The resistance increase.
U_t	The simulated battery voltage response.
U_{EOD}	The safety end of discharge voltage.
I	The current.
R	The pure ohmic resistance.

Table 10: The calculation of the EOL threshold pure ohmic resistance increase

Since there is only one EOL criterion, the obtained values at this loop are the final values of the EOL threshold map.

2.5.2.2 High-Power application

The EOL criterion on this case is composed by two criteria: two minimum autonomy restrictions where the current input profile needs to be fulfilled without crossing the minimum voltage threshold. The first criterion is defined by the operation of the system while the second is composed by the repetition of the operation described on the first criterion along with fast charges.

In both criteria, the two Health Indicators under evaluation are the dischargeable capacity decrease and the pure ohmic resistance increase. The capacity decrease has been already defined (a vector value between 0 and 60 with a step of 1) which takes into account both criteria EOL. The algorithm performs the evaluation loop N times. N is the length of the capacity decrease value vector ($N = 600$). Next, the value of the second and last Health Indicator is calculated (the resistance increase). This Health Indicator is taken as a free parameter which can take any value. So as to simplify the problem, some assumptions are taken:

- The polarization voltage and OCV do not change with the increase of the pure ohmic resistance.
- The resistance is increased uniformly at the whole SOC range.
- The change on the heating of the cell due to the resistance increase doesn't affect the voltage response of the cell.

Considering these three assumptions, the required resistance increase (ΔR) that leads to overcome the minimum voltage threshold (U_{EOD}) is calculated at each loop iteration, see Eq. (7).

The obtained value defines the minimum resistance increase with which the battery stops fulfilling the discharge requirements. For the first criterion, where there are only regenerative charges, the obtained value is enough to have a relative accurate EOL threshold (as accurate as the model itself). However, the use profile on the second EOL criterion considers fast charges. It cannot be assumed that the resistance increase of the battery does not affect the response of the battery on those fast charges. In this scenario, firstly, a Constant Voltage (CV) charge need to be simulated, and secondly, a way of finding iteratively the real EOL threshold need to be generated when integrating those fast charges.

For the first issue, a Proportional Integral (PI) controller that simulates the charge at CV is implemented, see Algorithm 2. The PI controller's parameters are adjusted manually, where the integral controller's parameter is left dependent to the resistance increase ($K_{pe} = 20, K_{ie} = 500/\Delta R$). The previous integral value (I_{c0}) on the first iteration is made equal to Eq. (8).

$$I_{c0} = -\frac{I_{CHA} - (error \cdot K_{pe})}{k_{ie}} \quad (8)$$

Parameter	Description
I_{c0}	The initial current integration before applying the PI controller.
I_{CHA}	The current consign.
$error$	The difference in voltage between the measurement and the end of charge voltage.
K_{pe}	The proportional gain on the PI controller.
k_{ie}	The integral gain on the PI controller.

Table 11: The initialization of the CV controller

$$I_{CHA} = CVcontroller(I_{c0}, I_{CHA,N}, U_{EOC}, U_{est}, K_{ie}, K_{pe})$$

- 1: $error = U_{EOC} - U_{est}$
- 2: $I_c = I_{c0} + error$
- 3: $I_{CHA} = -\left((error \cdot K_{pe}) + (I_c \cdot K_{ie})\right)$
- 4: if $I_{CHA} < I_{CHA,N}$
- 5: $I_{CHA} = I_{CHA,N}$

```

6: else if  $I_{CHA} > 0$ 
7:    $I_{CHA} = 0$ 
8: end if

```

Where

$I_{CHA,N}$ = The charge current at Constant Current (CC) phase.
 U_{EOC} = The end of charge voltage, which is also the consign voltage.
 U_{est} = The estimated voltage with the model.
 K_{ie} = Integral controller's gain.
 K_{pe} = Proportional controller's gain.
 I_{CHA} = Charging current consign.
 $error$ = The voltage difference between the estimated and the consign voltages.

Algorithm 2: PI controller algorithm used to control the CV phase on the fast charging process.

For the second issue, a bisection method is applied with a limit of iterations ($N_{BM} = 5$), see Algorithm 3. It is assumed that the real resistance increase (ΔR) is below the first calculated resistance increase (ΔR_0). As a result, the limit value that makes overcome the EOL criterion is achieved.

$\Delta R = \text{BisectionMethod}(\Delta R_0, I, K_{ie}, K_{pe})$

```

1:  $Study_{range} = \left[ \frac{\Delta R}{2}, \Delta R \right]$ 
2: for  $i = 1$  to  $N_{BM}$  do
3:    $\Delta R_{test} = \text{mean}(Study_{range})$ 
4:    $SOC_{test} = \text{BATT\_MODEL\_PI}(\Delta R_{test}, I, K_{ie}, K_{pe})$ 
5:   if  $SOC_{test} < 0$ 
6:      $Study_{range} = \left[ \frac{\Delta R}{2}, \Delta R_{test} \right]$ 
7:   else
8:      $Study_{range} = [\Delta R_{test}, \Delta R]$ 
9:   end if
11: end for
12:  $\Delta R = Study_{range}(1)$ 

```

Where

N_{BM} = The number of iterations on the bisection method.
 ΔR_{test} = The resistance increase value under study.
 SOC_{test} = The obtained SOC response of the battery under the I current profile.

Algorithm 3: Bisection method used on the Resistance increase calculation with fast charges.

Finally, the obtained thresholds on both criteria are compared and the more restrictive threshold is selected as the real one.

2.6 Results

The EOL mapping algorithm has been applied to both examples of use. The EOL map for the application with a high-energy requirement is displayed in Figure 12 and the EOL map for the application with a high-power requirement is displayed in Figure 13.

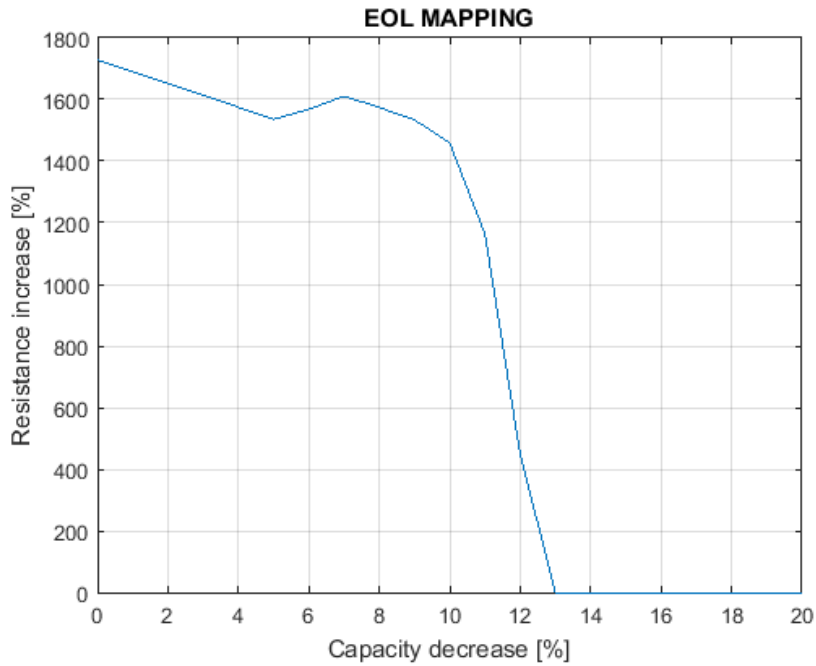


Figure 12: The obtained EOL map in terms of the resistance increase and the capacity decrease on the High-Energy example of use.

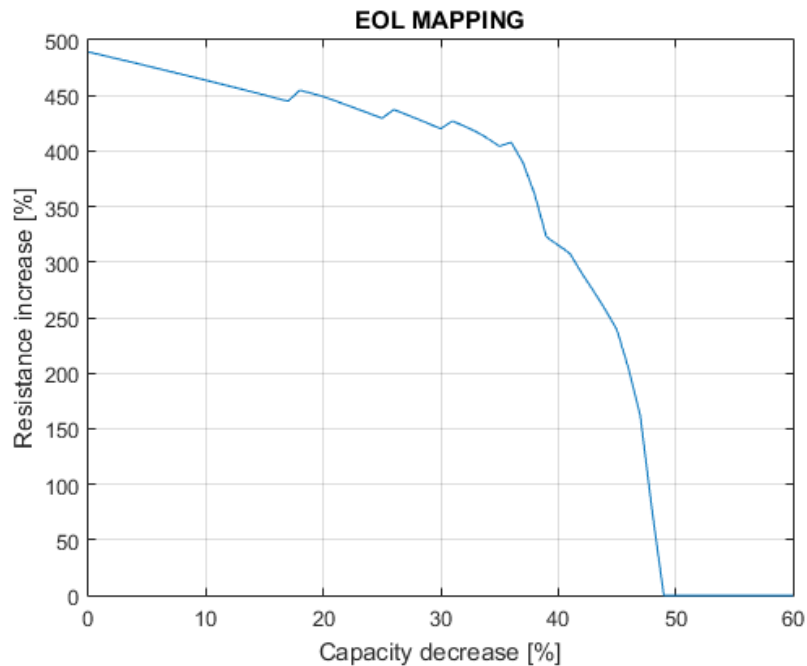


Figure 13: The obtained EOL map in terms of the resistance increase and the capacity decrease on the High-Power example of use.

2.7 Validation

The obtained results have been obtained under certain hypothesis, which are analysed and validated here. The first hypothesis states that the polarization voltage and OCV do not change with the increase of the pure ohmic resistance. To validate this:

- Firstly, the OCV of a fresh and aged cell has been compared (Figure 14). It can be seen how the aged and fresh cell have practically an identical OCV profile.
- Secondly, the RC parameters have been displayed (Figure 15). It can be seen that the fresh and aged RC parameters have values on the same order.

- Thirdly, the correctness of the proposed model representing the behaviour of an aged battery is tested, see Figure 16. The proposed model represents with similar accuracy both batteries, the fresh one and the aged one, so it can be said that this hypothesis is correct.

This hypothesis has been validated only with the data of the High-Energy battery because there is not data of deeply degraded High-Power batteries, therefore, it cannot be validated on those batteries.

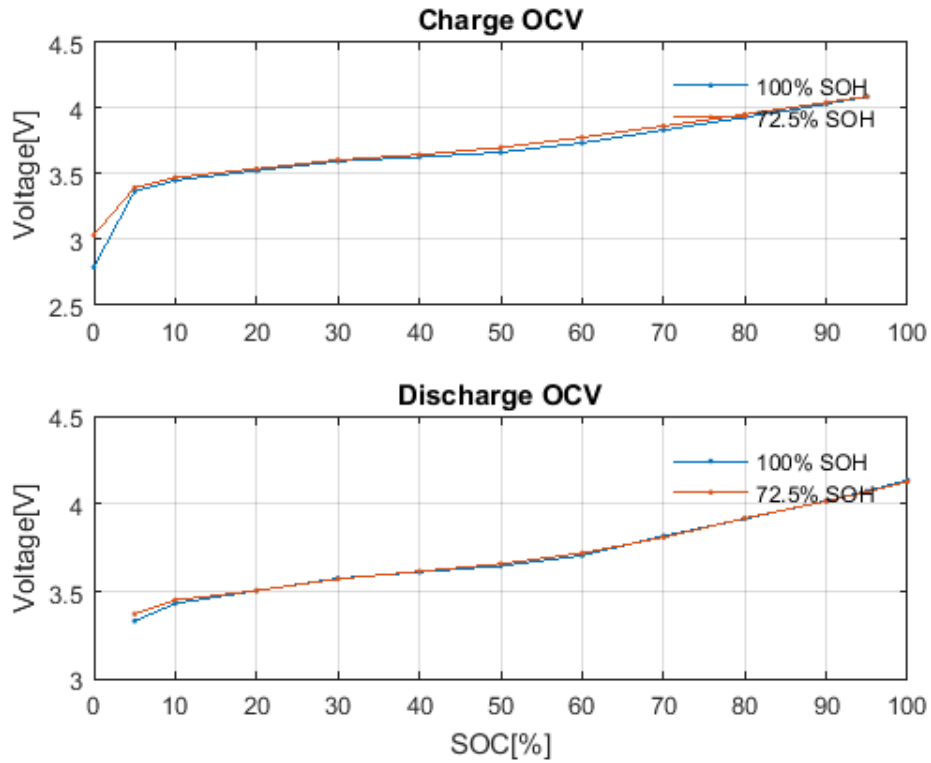


Figure 14: The OCV values at fresh state and aged state of the High-Energy battery.

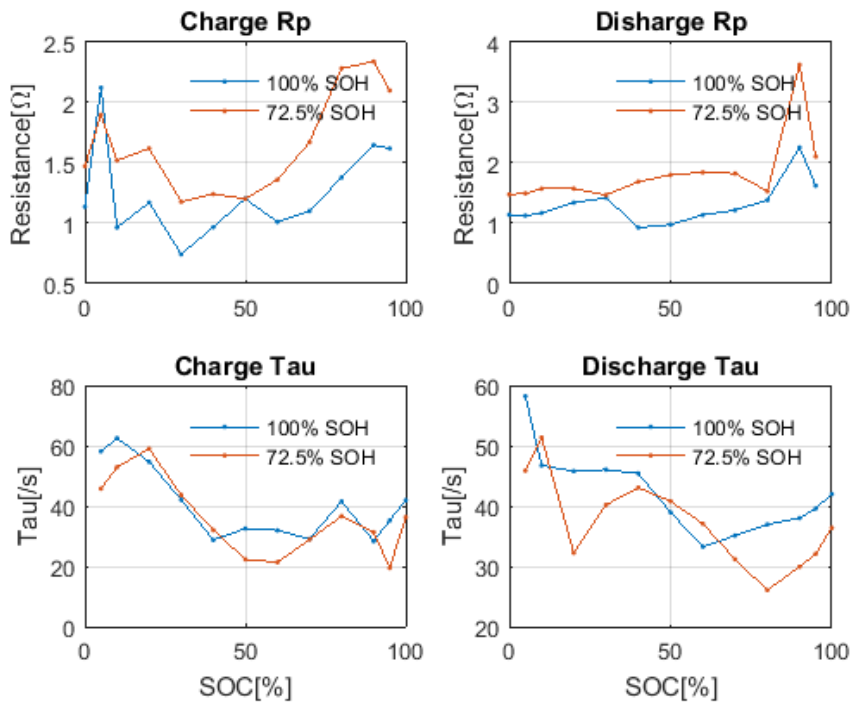


Figure 15: Charge transfer impedance at fresh state and aged state of the High-Energy battery.

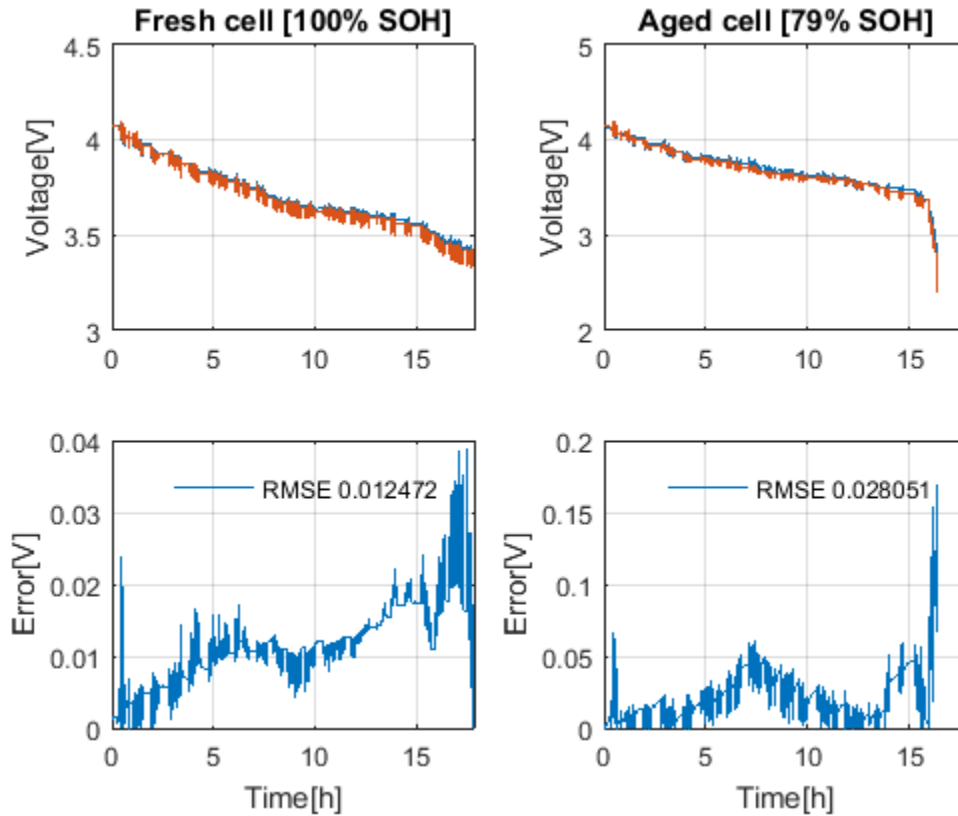


Figure 16: Difference between the estimated voltage and the measured one at fresh state and aged state of the High-Energy battery.

The second hypothesis states that the resistance is increased uniformly at the whole SOC range. This hypothesis is done to simplify the mapping and the simulation. The obtained impedance increase is the required minimum increase to overcome the EOL criteria at the most critical SOC. In this hypothesis, the difference between the increase on the most critical SOC values (below 20% SOC) and the SOC at where the actual resistance is calculated (50% SOC) is evaluated. The results of 4 tested batteries on the proposed aging test matrix on the High-Energy application are shown in Table 12. It can be highlighted three aspects of the results:

- The decrease of the resistance due to the aging (the negative values on cell n° 16).
- A maximum difference on the pure ohmic resistance increase of 15.55% at the cell n° 54 (the one with higher degradation) given between the resistance increase values at 5% SOC and at 50% SOC.
- A common behaviour of increasing the resistive behaviour when the degradation increases.

The decrease of the impedance at a 4% SOH decrease and the difference on the resistive behaviour increase on different SOC can be given by the fact of estimating the pure resistive behaviour of the battery by fitting a 60s current pulse profile with a simplified equivalent electric circuit. The estimation method introduces an error that should be added to the estimated values, which has not been done. In addition to this, the physic behind the estimated parameter itself tells us that the resistive behaviour of the battery is not a stable parameter. The pure ohmic resistive behaviour of a lithium ion battery is composed by many different components inside the battery (the dissolved lithium rate on the electrolyte, the organic rate on the electrolyte, the thickness of the Solid Electrolyte Interphase (SEI) layer, etc.) which depend on many other aspects (temperature, current rate on the active material, etc.). This is why the uncertain margin should be even greater than the one gotten by the estimation method. However, a common trend on the whole SOC range can be seen, at least on the most degraded cells, which support partly this second hypothesis. We propose to tackle this uncertainty by adding a confidence range of 20% to the estimated EOL resistance increase.

Cell	Δ SOH	Δ R at 5% SOC	Δ R at 10% SOC	Δ R at 20% SOC	Δ R at 50% SOC
N° 16	4 %	0.94 %	-8.34 %	-4.54 %	-0.18 %
N° 48	18 %	22.34 %	25.63 %	30.25 %	33.49 %
N° 54	21 %	24.48 %	25.81 %	33.17 %	40.03 %
N° 55	11 %	18.38 %	7.74 %	11.47 %	15.84 %

Table 12: Pure ohmic resistance homogeneity at different SOH of the High-Energy battery

The third hypothesis states that the change on the heating of the cell due to the increase of the resistance increase doesn't affect the voltage response of the cell. This hypothesis is tested by repeating the simulations with the obtained resistance increase, see Figure 17. It is validated that even though the temperature increases due to the increase on the resistance almost 5°C, the voltage response of the battery remains practically the same. The results show that this hypothesis is correct since there is only a maximum drift of 52mV between them.

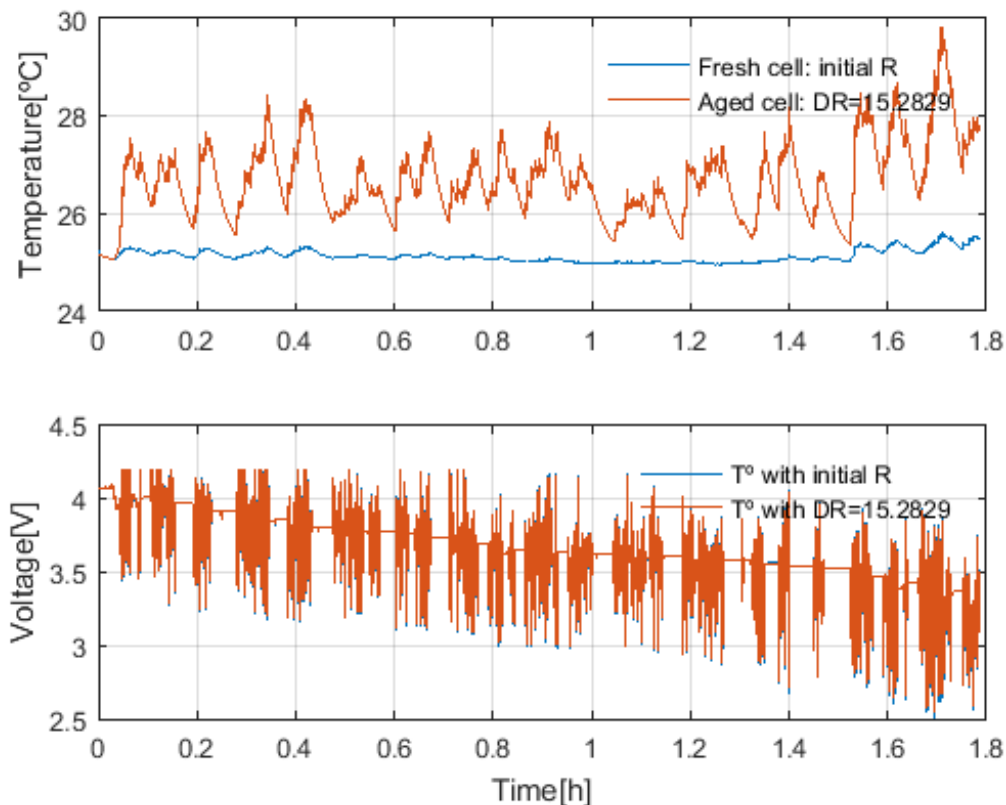


Figure 17: Temperature profile with initial resistance and with the resistance of EOL applied on the electric model set up with the resistance of EOL of the proposed High-Energy application.

After proving that the simulation environment has solid hypothesis behind it, the results of the simulation themselves (the EOL threshold maps) are validated. For that, the use profile defined by the application has been applied to batteries with different capacity decrease and resistance increase levels in a laboratory environment. The fulfilment of the application is represented in the EOL threshold map of the High-Energy application, see Figure 18. In addition, a 20% margin on the resistance increase has been added due to the partial fulfilment of the second hypothesis. In this case, only data of the High-Energy application is available due to the long time required to reach the EOL on the High-Power application (the battery chosen for the High-Power application has been tested at accelerated aging conditions for more than 2 years but there is only a 5% performance decrease on the worst case, which is far from being enough).

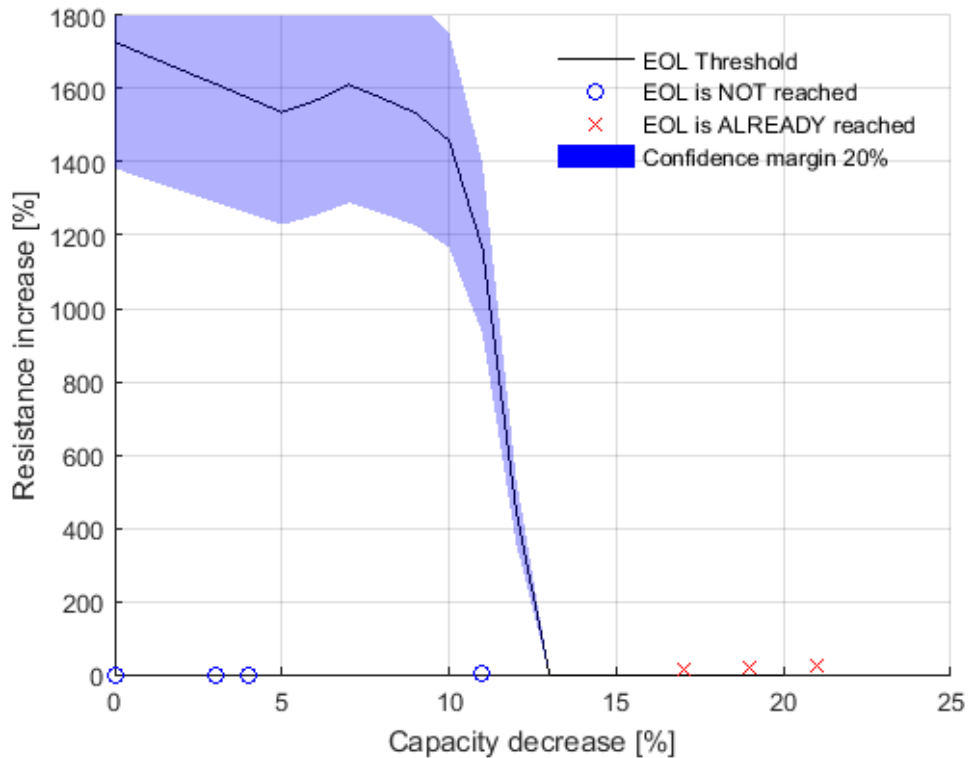


Figure 18: Validation of the EOL mapping of the High-Energy application. The blue circles represent the batteries that have fulfilled the operation profile and the red x symbols are the ones that have not fulfilled the operation profile.

2.8 Conclusions

This chapter has proposed the methodology to design an algorithm that searches the combinational value of some Health Indicators (in this case dischargeable capacity decrease and pure resistance increase) at which the battery stops fulfilling the requirements defined by the application. The methodology has been tested on a High-Power and on a High-energy application. The taken hypotheses along the methodology and the results on the High-Energy application have been validated.

The calculated EOL maps show that the EOL is fully dependent to the battery characteristics as well as to the application requirements. The ranges of resistance increase and capacity decrease that leads to the EOL varies greatly between applications.

We have seen that the hypothesis made along the chapter were correct except for one. The polarization voltage and OCV do not practically experience any change with the increase of the pure ohmic resistance; and that the effect on the voltage response due to the change on the heating with the increase of the resistance increase is negligible. In contrast, the resistance is not increased completely uniformly at the whole SOC range. The resistance on the whole SOC range does increase with the aging but not with the same rate. Due to this, we have considered necessary to add a margin of a 20% of the resistance increase to the EOL map, which will be validated on future works.

Finally, the results obtained on the High-Energy application have been cross-checked in real cases. The application use profile has been applied to batteries with different SOH. It can be seen that the batteries that cannot meet the application requirements and those that do meet them are separated by the calculated EOL threshold.

The batteries used on this validation have resistance increases lower than 100%. The EOL threshold for the chosen batteries for this High-Energy application can be done discarding the Health Indicator

of the resistance increase and leaving only the capacity decrease value. Nonetheless, thanks to the fact that we know the resistance needed to go from meeting the application requirements to not meeting them, we could add the resistance in between the energy consumer and the energy supplier (wires, connections, transformers, etc.) into the EOL determination, which is of great interest on the design step of the application.

CHAPTER 3:

3 Aging: Testing and Modelling

This chapter responds to the objective of finding the aging path of lithium ion batteries under restricted operation profiles. For that, two key concepts are studied: the generation of the aging data itself and the posterior extraction of the aging trends. Firstly, a methodology to design the tests required to generate the aging data is elaborated. Then, the aging models composed by the aging trends that are underneath the obtained data are developed. For that, simple empirical aging models are applied in a quadratic optimization environment. Thanks to this, the stress factors, the resting time, the discharged energy and the observed health indicators are linked. Finally, the proposed methodology and the main hypotheses done along the chapter are validated. The contribution of this chapter consists on firstly, the testing methodology; secondly, the aging model development methodology; thirdly, the actual implementation of the defined aging modelling methodology in two real cases; and fourthly, the validation of the main assumptions done on the construction of the aging model.

3.1 Introduction

The degradation of the lithium ion batteries is caused by several deterioration processes or aging mechanisms that takes place on the normal working state of the battery [26]. The working state of the battery used to be divided in two: firstly, on the resting period that generates the so-called calendar aging; and secondly, on the charging and discharging process that generates the so-called cycling aging.

Calendar aging comprises all aging processes that lead to a degradation of a battery cell independent of charge-discharge cycling. It is an important factor in many applications of lithium ion batteries where the operation periods are substantially shorter than the idle intervals, such as in electric vehicles [64] or in stationary (they may operate 2 times per year).

Aging during storage is widely caused by interactions between electrolyte and active materials interface (side reactions) [11], which affect to the available lithium inventory [30]. This means that a Loss of Lithium Inventory (LLI) is expected [11]. However, if there is a previously generated inhomogeneity of the lithium distribution in the electrodes, the energy content during storage periods could increase instead of decrease (a capacity recovery phenomena); there might be cases that there isn't any aging-related side reaction or LLI in calendar life [64].

Cycling usually causes capacity loss at a greater rate than storage as the aging processes are modified upon cycling on complex operation conditions. At cycle life, the active material changes near the surface of the (both) electrodes [16] and as consequence the initial stoichiometric values for the anode and the cathode ($x_{o,i}$, x_i) change [32]. In addition to this, in the case of the positive electrode (the cathode), the microstructure of its active material is expected to get damaged by runtime operations [16].

After prolonged cycling, Dubarry et al. [27] found that a nonlinear characteristic could appear which increase drastically the capacity fade (LFP cathode and graphite anode cells were used on the tests). In this last stage, lithium ions transport process is apparently blocked in the middle area of the electrode of the tested cells (it can be explained as a rise of the resistance on that middle area, so the lithium ions evade that area). This results in a reduction of lithium intercalation kinetics at the anode (polarization resistance increase) which can provoke irreversible metallic lithium deposition (lithium plating) with additional LLI and Loss of Active Material (LAM) (due to isolated electrode surface). This phenomenon supports the often-made assumption that the sudden acceleration on the capacity fade comes from kinetic degradation accompanied with LAM [35].

With fundamental understanding of failure mechanisms and knowledge of sources of variability, it is possible to develop models that describe the aging behaviour of a lithium ion battery based on physical principles [65]. However, there is not enough physical knowledge to describe accurately the aging behaviour of a lithium ion battery yet. This is why, the most used models in lithium ion battery applications nowadays are empirical or semi-empirical aging models; models that rely on data.

Lithium ion battery data-based aging models describe the selected lithium ion battery behaviour based on mathematical expressions and data. The data from some tested samples is used to adapt generic mathematical expressions to the case under evaluation. As a result, it is possible to build a model that describes the behaviour of the selected system on the observed operation conditions on the tested samples. These models cover the lack of knowledge on the physical behaviour of the lithium ion battery under evaluation. However, it shows some limitations:

- The accuracy on describing the system's behaviour under the observed operation conditions is dependent to the quality and amount of the obtained data.
- The fitting of generic mathematical expressions with data can lead to an overfitting issue and low accurate interpolations.
- The accuracy of the model under extrapolated operation conditions is likely to be low. These models cannot foresee upcoming new aging trends such as sudden increases of degradation.

In this scenario, firstly, this chapter proposes on section 2 an aging testing methodology that will provide the guidance in the data acquisition and test matrix design process. The proper definition of the testing cases and testing methodology will lead to high quality data that will cover enough cases to avoid extrapolations and obtain accurate interpolations. Secondly, this chapter proposes on section 3 a modelling methodology. The proper selection of the generic mathematical expressions will increase the accuracy on interpolations. Then, on section 4, validation of the proposed methodologies and the main hypotheses done along these methodologies are validated. Here, an aging test matrix has been designed from which data that supports the validation of those main hypotheses has been generated. Finally, on section 5, the conclusions are drawn.

3.2 Aging Testing Methodology

Aging evaluation takes too much time, so accelerated aging test are generally conducted. Accelerated aging method is a set of techniques, procedures or conditions designed in order to deteriorate a battery or a cell by enhancing the rate of degradation processes compared to normal operation conditions [66]. The typical accelerated aging test (AAT) in the literature consists on storing cells at different detrimental conditions (calendar ageing) or using different loads in cycling operation mode (cycling ageing) [11].

The accelerated ageing method includes the characterization of the performance level of the cell at different aged states (at different State of Health (SOH)) [66], also called Aging Characterization Tests (ACT). The AATs are not supposed to give significant data (their only aim is to accelerate the deterioration), this is why the ACTs are required to get this significant data of the SOH of the cell [65].

Nonetheless, before an accelerated aging test (AAT) can be performed, the experts on the application field (the engineers) need to know the number of items to test, the sample time and the values of the accelerating factors. The proper selection of these mentioned characteristics will provide estimations with high precision [67].

We propose a methodology that assists researchers on designing the AAT matrix as well as the ACT. The proposed methodology is applied on two real application cases.

3.2.1 Accelerated Aging Tests

Accelerate aging tests (AAT) contain a series of steps to accelerate the ageing of a system by applying ageing stressors [66]. In other words, the aim of the AATs is making "time" (on whatever scale is used to measure device or component life) go more quickly, so that reliability information can be obtained more rapidly. There are different methods of accelerating a reliability test. An option is to increase the use rate of the product (appropriate for products that are ordinarily not in continuous use), a second option is to increase the intensity of the exposure to radiation (various types of radiation can lead to material degradation and product failure), and a third option is to increase the aging rate of the product or the level of stress (amplitude in temperature cycling, voltage or pressure) under which test units operate [65].

In addition to this, there are some key aspects to be considered: testing time, testing cost and modelling accuracy. Firstly, a reasonable accelerated testing time need to be agreed in order to avoid too lengthy experiments [66]. Secondly, the quantity of tests need to be delimited since the fact is that the AATs are costly approaches [50]. Thirdly, the tests are done at accelerated conditions, but estimates are needed at use conditions; all AATs needs to extrapolate outside the range of available data and such extrapolation requires strong model assumptions [65]. A proper choice of the battery stress factors and stress levels is crucial; the generation of additional aging phenomena that are not present in real operating conditions must be avoided [68] (AATs must generate the same failure mode occurring in the field). Based on these key aspects, AATs are designed.

AATs are designed mainly to minimize the testing cost and time. To do that (the design of the aging test matrix), the balance between the stress factor level, the amount of different operation conditions that are aimed to described by the AAT (quantity of AAT), the duration of each of those AAT and the goal of the AAT matrix (application dependent) is evaluated by optimization methods [69].

3.2.1.1 Accelerating aging tests

The acceleration of the aging tests of lithium ion batteries is done considering that the minimum level of stress still represents an accelerated condition [66] and that the maximum level of stress still causes the same failure mode occurring in the field [65]. In the same way, due to the fact that the stress factor levels have a nonlinear effect on the lifetime of the lithium ion batteries, a minimum of three stress levels for each evaluated stress factor is mandatory in order to be able to obtain the lifetime of the cell for the normal operating stress [68].

The hypothetical influence of the stress factors (in lithium ion applications) is showed in [68] (Figure 19). Among these stress factors, the time-temperature superposition is a well-established method for accelerated testing [16]. If a higher temperature accelerates, but does not alter degradation mechanisms, then the test time can be reduced by testing at higher temperatures. Another commonly used accelerating factor is the increase of voltage stress [65]. Schuster et al. [29] added two load profiles with supplementary constant-voltage (CV) phase in the charging process to provoke an early turning point from linear to nonlinear aging characteristics. In this way, longer periods at high state of charge (SOC) (more time on CV means more time at high SOC) and deeper cycles were achieved. The results showed that the turning point of the test case with constant current and constant voltage (CC-CV) discharging appeared about 34% or 51% earlier referred to the test case with only CC-CV charging or no CV phases at all.

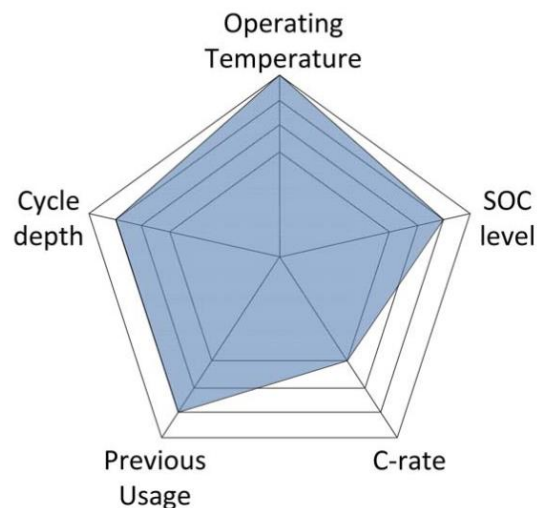


Figure 19: Different stress factors and their hypothetical influence (blue mesh) on lithium ion batteries' aging [68].

Once identified the stress factors, the way of control them need to be evaluated; the way on how these stress factors are reflected on the observable and/or controllable variables need to be addressed:

- The operating temperature is dependent to the room temperature and the heat generation of the battery. It is observed directly from the measurement of the battery temperature. The commonly controllable variable is the room temperature, which is directly given by the thermal management system of the room. The heat generation can be controlled by controlling the current and the SOC, but it is rare to control it based on these variables. Rather, the heat is counteracted with a cooling system to avoid temperature increases.
- The SOC is related to the storage energy and the dischargeable energy of the battery. It cannot be directly observed. The SOC can be tracked with an Ah counting method or it can be estimated with the estimated Open Circuit Voltage (OCV) from the voltage measurement. The controllable variables are the current and the time, which affects directly the storage energy and the voltage.

- The C-rate (the current rate relative to the nominal capacity) is observed directly from the current measurement. It is as itself a controllable variable. Its sign represents the charge or discharge state of the battery.
- The Depth of Discharge (DOD) is related to the discharged energy and the actual dischargeable energy of the battery. It cannot be directly observed. The DOD can be estimated with the estimated SOC evolution. The controllable variables are the current and the time, from which the discharged energy and the voltage are controlled.
- The previous usage is composed by all the operations done by a battery from its Beginning of Life (BOL) to the present day. This stress factor is a key aspect on applications with changeable operation patterns or on “second life” applications. The controllable variables are the current, the room temperature and the time.

In addition to this, increasing the use rate (or frequency) can be an effective method of acceleration in some applications. However, the increased of cycling rate could also generate a heat up or another effect which also affect the degradation [65]. This may not be interesting.

There are also cases where an alteration of a stress factor level is applied dynamically in order to increase the degradation rate. An example is the standard load profile called Dynamic Stress test specified by the United States Advanced Battery Consortium [70]. On the other hand, Sarasketa [11] found just the opposite; she found that the observed cell degradation was lessened under dynamic Depth of Discharge (DOD) conditions (taken the rest stress factors as constant).

Combinations of stress factors to increase the aging rate are also employed. Variables like SOC and temperature can both increase the rate of an electrochemical reaction (thus accelerating the aging rate) and increase stress [65]. The problem of combining stress factors to accelerate even more the test comes from the incapacity of dividing the level of incidence of each stress factor on the deterioration (problems on properly modelling each stress factor).

In resume, the main controllable variables are the current and the room temperature or a derivative of them such as the power. The main observable variables are the current, the voltage and the cell temperature. The combination of these variables leads to generate the AATs that exploit the introduced stress factors.

3.2.1.2 Optimizing AAT matrix

Optimal designs of the AAT matrix reduce the costs of experimentation by allowing statistical models to be estimated with fewer experimental runs [65]. One of the merits of optimizing the AAT program is that optimal designs can accommodate multiple types of factors, such as process, mixture, and discrete factors. Besides, if statistical models are applied, optimal designs allow parameters to be estimated without bias and with minimum variance [65].

One of the optimization methods commonly used is based on constraining the design-space [68]. This consists on reducing the amount of stress factors and limiting their levels of interest. For that, firstly, an evaluation that integrates the knowledge of the product and its environment (the application field details), and the chemical and mechanical aspects of the deterioration is done [65]. Remark that each stress factor might affect differently the lifetime of the considered Lithium ion battery depending of the lithium ion chemistry [68].

Once reducing the design-space based on the product and the application, statistical aspects of the design and analysis of reliability experiments used to be considered. For that, a statistical optimization method can be applied such as Taguchi's method. Taguchi's method is based on statistical and sensitivity analysis for determining the optimal setting of parameters to achieve robust performance. Taguchi method is also based on the fractional factorial experiment (see Figure 20), where the independent variables are divided into controllable factors (those factors that can be used to maintain a desired value) and noise factors (those factors that may not be controlled) [71].

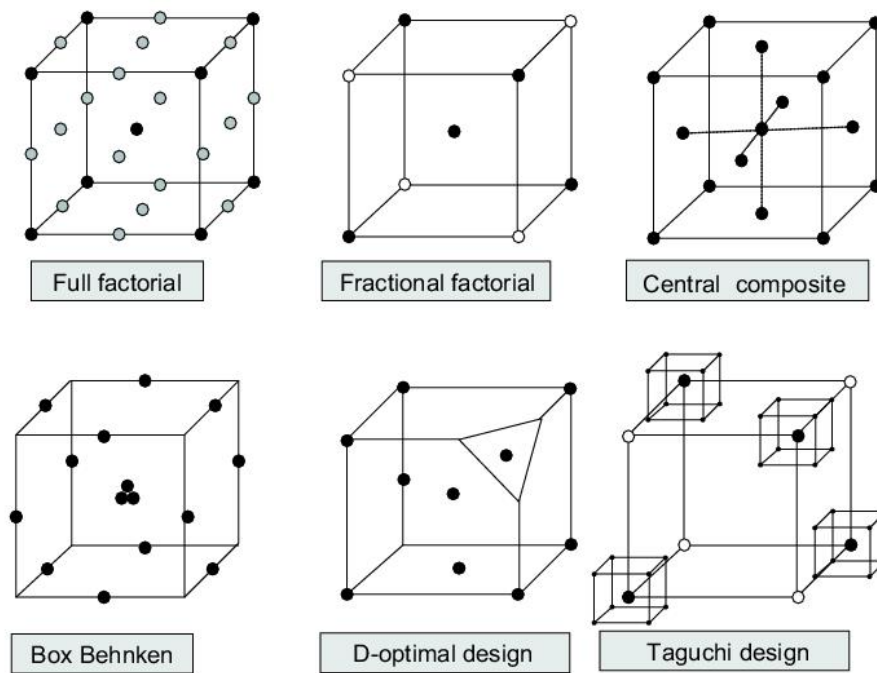


Figure 20: Methods of statistical design of experiments (DOE)[72].

Taguchi’s method involves finding correlation between variables. It uses orthogonal arrays, with the inner array consisting of the mentioned control factors and the outer array consisting of the noise factors. Each inner array is to be run with each outer array.

The steps and procedures of design of experiment using the Taguchi method are identifying the objectives, determining the quality characteristic, selecting the controllable factors and noise factors, selecting an orthogonal array (Orthogonal Arrays are extensively used in parameter design for fractional factorials) and concluding the experiment and analysis. By successfully applying this concept to experimentation, it is possible to achieve the minimum error on the target while minimizing the effect of the chosen noise parameter [71].

3.2.1.3 Proposal of AAT

The proposed AAT design methodology consists on reducing gradually an initial test matrix that can isolate and track the effect of each stress factor except for one on any lithium ion battery chemistry: cycle depth or DOD, SOC level, Operating temperature and current rate or C-rate. The previous usage is discarded as stress factor because it doesn’t have any sense on fresh batteries (there is no previous usage on fresh batteries; this is why they are fresh batteries).

The initial test matrix gathers every possible value each stress factor can take on a lithium ion battery context in CIDETEC’s facilities. The test cases only consider static tests where the stress factors are maintained constant. The defined values for the stress factors have been set by experimental and modelling experience as well as resolution limits on the testing bench. As a result, an initial matrix that contains more than 400 billion tests has been built. This initial test matrix has not been displayed; instead, Table 13 shows the maximum value, the minimum value and the minimum step value of the selected stress factors.

Stress factor	Operating temperature	Current	SOC	DOD
Maximum value	60°C	250A	100%	100%
Minimum value	-20°C	-250A	0%	0%
Minimum step	1°C	0.001A	1%	1%

Table 13: Testing cases possibilities on the initial test matrix

Then, this initial test matrix is reduced by constraining and eliminating testing cases based on the application characteristics and testing resources while maintaining a minimum of testing cases required by the aging model.

Firstly, the stress factors are delimited considering the limitations imposed by the safety operation window of the selected lithium ion battery (application dependent). The limitations are given by the datasheet, which are different from battery to battery. This delimitation cannot be violated since it could bring risks to the testing laboratory.

Secondly, the test matrix is reduced considering the application requirements. Here, the proper understanding of the application is a must as well as comprehending the generic effect of the stress factors on the aging trend, see Table 14.

Stress factor	Generic effect on the aging trend
SOC	High SOC used to increase the deterioration. SOC under or near 0 used to increase the deterioration.
DOD	A 100% DOD used to be the most detrimental DOD range. The higher the DOD, the higher the deterioration.
Current	Current at operation limits used to increase the deterioration.
Operating temperature	The least detrimental condition used to be between 15°C and 25°C. The aging used to increase exponentially when increasing or decreasing the least detrimental temperature. A sudden deterioration increase used to appear at temperatures below 0°C.

Table 14: Comprehending the generic effect of the stress factors on the aging trend

The criterion of eliminating testing cases on this second stage should not be very restrictive. It is recommended to leave a margin for error on the definition of the operation conditions since it is not frequent to have a proper definition of the application before the aging testing activity. This is why it is advisable to consider some more possible operation conditions with a higher operational stress and some others with a lower operational stress than the defined ones with the application requirements. Then, these additional cases should be given a probability value, which would be used as the representative testing cases.

In the same way, it is proposed a colour system that ranks the testing cases in terms of importance. This system allows the proper identification of the fundamental testing cases from those that are not in a user-friendly way. It also determines the level of interest on performing the testing cases that are not fundamental.

- Red: The testing cases linked with the application requirements. From all the possible cases linked directly with the application requirements, only three cases per stress factor will be chosen as red cases: the most stressful case, the least stressful case and the most likely case. If there is not a most likely case, the middle between the most stressful and the least stressful cases will be chosen.
- Orange: The fundamental testing cases that are not red and the testing cases that represents the operation conditions that are very likely to appear (a probability of occurrence of 60% to 90%).
- Yellow: The testing cases that represents the operation conditions that are likely to appear (a probability of occurrence of 30% to 59%).
- White: The testing cases that represents the operation conditions that are not likely to appear (a probability of occurrence lower than 29%).

In case there are few stress factors and testing cases, this could be done in a unique table. However, this is not the case here and an alternative

Thirdly, the remaining testing matrix could be further reduced based on statistical optimization methods. However, these methods can lead to delimiting the posterior applicable aging model. By default, statistical optimization methods design the testing matrix for models with just one free variable per control factor. This is not usually the case on lithium ion batteries [71]. Because of this, advanced knowledge of statistical optimization tools is fundamental, as well as knowing beforehand the mathematical expression that matches the effect of each stress factors on the aging behaviour. The fact is that first, the mathematical expression that matches the effect of each stress factor on each battery chemistry is not completely known until the tests are completed; and second, the

development of new statistical optimization methods is out of the scope of this thesis. Because of this, the statistical optimization methods are discarded on this aging matrix design proposal.

Fourthly, the reduced test matrix on the second stage is further reduced based on the available testing lab resources. The lab will define some limitations to the possible cases that will be tested due to limit resources. This restrictions change on each project since the availability of a lab is not a fixed aspect. In this stage, the cost of testing the batteries is introduced on the testing considerations (cost of samples and cost of occupying the lab resources a specific period of time); this delimitation stage will be the most restrictive one.

The criterion of eliminating testing cases on this fourth stage is focused on at least maintaining the red cases. If it is possible, more cases will be added in terms of the probability of occurrence of the operation condition behind those testing cases. Particular needs or interests will take part as well in the selection of these testing cases such as interest on specific thermal behaviour analysis. Nonetheless, there are times where all the defined red cases will be just too much. If it is not possible to perform all the red cases, firstly, all the orange, yellow and white cases will be discarded and secondly, among the red cases, the cases that have less importance on the description of the application requirements will be nominated to be eliminated. The reduction of red cases will lead to the reduction of the possible mathematical expressions that can be applied on the posterior aging modelling as well as an important increase on the uncertainty on the accuracy of interpolations (interpolations are done with two points instead of three). This is why the final decision of eliminating the nominated cases is done based on the aging modelling experience.

As an advice, when following this process, it would be interesting to generate the red testing case matrix and present it to the lab team before going further. It is very likely to have created too many tests, which means that the orange, yellow and white testing case matrixes are of no use (the time spent doing this can be saved).

Finally, in case there is a customer behind the project, the proposed aging matrix needs to be accepted by this customer before starting running the test matrix. The built aging matrix and the operation cases that the aging model will cover and those which will not are presented to the customer. The aging matrix often suffers modifications due to application definition changes or customer interests. Once discussed the aging matrix and the possible operation cases that the aging model will cover, the aging matrix is presented once again to the lab. If the lab see viable the proposal, the design process of the aging test matrix can be taken as finished. If not, a further discussion with the customer and then with the lab is required until the discussed test matrix agreed by the customer is accepted by the lab.

3.2.2 Aging Characterization Tests

The characterization tests in an accelerated aging method include the measurement of specific metric(s) or Health Indicators to determine the effect of aging (to define the different aged states) [66]. At least, a characterization of the cell is carried out at the beginning and at the end of the whole aging testing process, also called Aging Check-up Test (ACT). An ACT after each periodical AAT (calendar and/or cycling ageing constrained for a defined time or capacity throughout) is usually done [11].

Several techniques are commonly applied and reported within the literature to build the ACT [73][74][75]. These techniques are often classified into in-situ and ex-situ techniques. In-situ methods are not invasive characterisation techniques. Ex-situ methods consist on applying physicochemical and electrochemical invasive techniques to study the cells internally. The ex-situ methods are commonly categorised as post mortem analysis. Since the ex-situ requires the destruction of the cell and the end of the AAT, these techniques cannot be applied in between periodical AATs but only at the end.

There are also techniques that assist the better interpretation of the aging behaviour, such as the Incremental Capacity analysis and the Differential Voltage analysis [36]. For that, specific characterization tests are required.

3.2.2.1 Aging metrics

All aging mechanisms depend on the cell potential (the equilibrium OCV) [29]. The changes on the OCV curves represent the changes in the thermodynamic behaviour. Therefore, tracking the OCV of the positive and negative electrode facilitates to identify the prevalent degradation mechanisms acting on each electrode as well as the degradation path of the whole system (the battery) [31]. For example, Keil et al. [64] derived the characteristics of anodic and cathodic side reactions from the varying end of discharge point slippage for different storage SOCs and temperatures. However, OCV curves tend to be flat with small changes all along its operative life. The changes on OCV values need some interpretation techniques. For that, techniques such as the Incremental Capacity Analysis or the Differential Voltage Analysis are used. These two techniques maximize the slight changes that appear on the OCV profile due to the deterioration of the cell.

Even though being the OCV so relevant on the aging behaviour, the metrics most widely used on lithium ion battery aging analysis are the rate of the capacity fade (decrease on the storable energy) and the increase of the polarization resistance (pure ohmic resistance) [11]. On one hand, the capacity fade defines the reduction of storable energy respect to the beginning of life. On the other hand, the polarization resistance defines the limits of the maximum current rate that the battery can deliver or receive at each SOC. Both metrics can be related directly with safety and operation requirements, which is why they are both the most popular metrics.

Apart from these three metrics, there are some other aging metrics that can be observed from the sub-tests developed on an ACTs:

- The increase of the time constant of the transitory response of the battery [26].
- The increase of entropic heat generation [76].
- The increase of the passive layer and charge transfer resistance (thought to be suitable to predict the appearance of nonlinear aging characteristics upon prolonged cycling) [77].

3.2.2.2 Not invasive characterisation techniques

The common in-situ test used in the aging characterization tests are the capacity characterization, the OCV characterization and the Resistance characterization tests. For example, Sarasketa [11] proposed an ACT composed by the capacity measurement, close to equilibrium OCV measurement, internal resistance measurement by Hybrid Pulse Peak Characterization (HPPC) and impedance change evaluation by Electrochemical Impedance Spectroscopy (EIS). Wang et al. [49] proposed quite similar ACT but instead of calculating the OCV from close to equilibrium OCV measurements, they used the relaxation test.

▪ Capacity characterization test

Thanks to this Characterization test, the analysis of several aspects of the lithium ion batteries can be observed:

- Voltage profiles of charge and discharge.
- Energy (Ah and Wh) used in charge and discharge.
- Discharged energy round trip efficiency at each full cycle.
- Coulombic efficiency.
- Constant Voltage (CV) charging Time.

The capacity could be calculated by the ratio of the accumulated charge to the SOC variation within a period. Selecting two moments with large SOC difference, the capacity is calculated according to the Eq. (9) and the SOH estimation can be successfully accomplish [60].

$$C_{\alpha,\beta} = \frac{\Delta Ah}{\Delta SOC} = \frac{\int_{t_\alpha}^{t_\beta} I_{cell}(t) dt}{SOC(t_\alpha) - SOC(t_\beta)} \quad (9)$$

Parameters	Description
$C_{\alpha,\beta}$	The dischargeable capacity between the chosen two time instants t_α and t_β .
ΔAh	The discharged capacity between time instants t_α and t_β represented in Ah.
ΔSOC	The difference of SOC on the discharged capacity represented in units [0-1 range].
$I_{cell}(t)$	The current measured on the battery terminals.
$SOC(t)$	The State of Charge at time instant t [0-1 range]
t_α, t_β	The time instants that define the operation window used to calculate the capacity.

Table 15: Dischargeable capacity calculation [11]

For capacity characterization, Sarasketa [11] proposed 3 full charge and discharge cycles at the nominal C-rate with 30 min rest period in between charge and discharge, where the average value of the total capacity (in Ah) discharged in the last 2 cycles is considered as the actual nominal capacity. These cycles are run with Constant Current-Constant Voltage (CC-CV) until 0.05 times of the nominal C-rate was reached, see Figure 21.

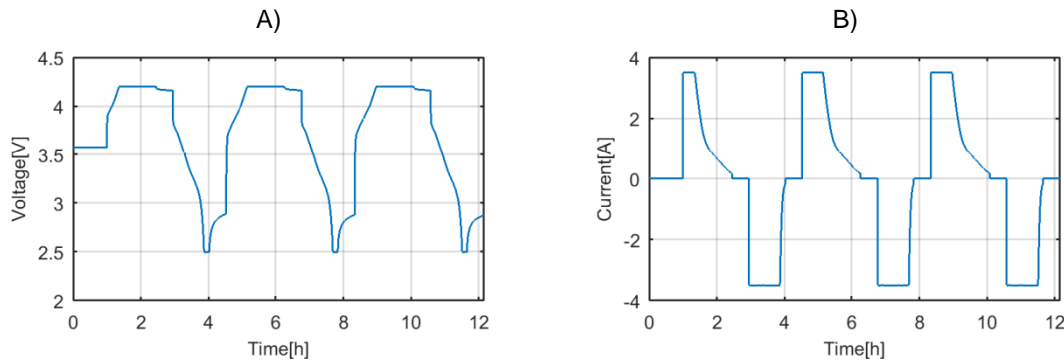


Figure 21: Capacity characterization test applied on a SAMSUNG INR 21700 48G lithium ion cell. A) Voltage profile and B) Current profile.

It should be pointed that the CV phase in the discharging process served to eliminate the influence of impedance in the CC phase by a continuous depletion of polarization. Thanks to this, a better inference of the active lithium in the cell is possible [29].

▪ OCV characterization test

A battery undergoing charge or discharge experiences kinetic effects such as mass transport [78], an effect that impedes the measurement of the OCV. Furthermore, the battery needs to be disconnected from any load enough time to reach the so call internal equilibrium [79]. In this context, OCV measurement requires measuring the voltage after a long relaxation period at SOC levels that span the entire range (relaxation test). The OCV is also commonly calculated by fully charging or discharging the battery at low rate (close to equilibrium OCV measurement).

For the relaxation test, a fully charged cell is discharged for a period (for example for 24min) at certain current C-rate (for example at C/2) followed by a 2h rest period before the subsequent discharge. The test is complete when the discharge voltage reached the end of charge cut-off voltage value [49], see Figure 22.

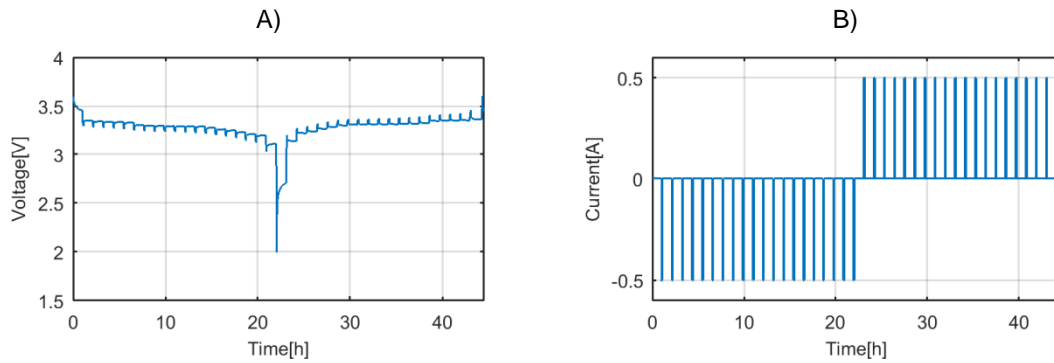


Figure 22: A relaxation test applied on an A123 SYSTEMS APR 18650 M1 lithium ion cell. A) Voltage profile and B) Current profile.

In close to equilibrium OCV measurement test, the measured voltage doing a full cycle at low C-rates is taken as the OCV. It is assumed that the voltage drop on the polarization impedance is negligible due to the low currents. Dubarry et al. [36] claimed that testing at a C-rate of C/25 is the best compromise between time and accuracy in order to measure close to equilibrium OCV. This compromise helps to derive the SOC versus Ah relationship with minimal polarization effects (see Figure 23).

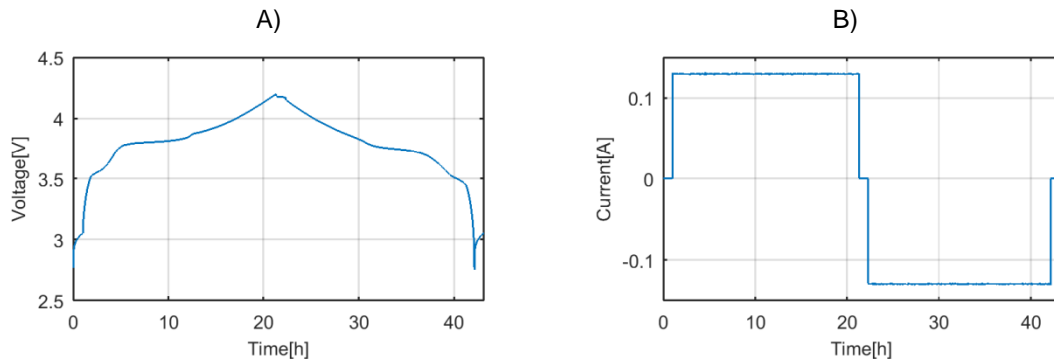


Figure 23: Open Circuit Voltage characterization test at a continuous low current applied on a SAMSUNG ICR 18650 26F lithium ion cell. A) Voltage profile and B) Current profile.

Thanks to these two tests the OCV of most of lithium ion cells can be characterized. However, there are some specific battery chemistries that experience a difference on the OCV; there are batteries that have a hysteresis effect.

The hysteresis can be described by the internal impedance in an Equivalent electric circuit model plus the OCV value. However, the huge hysteresis effect that the OCV suffers in some battery chemistries cannot be explained by RC equivalent circuits and it must be taken into account separately (Figure 24) [80]. On those cases, a hysteresis characterization test is added to the OCV characterization test. It consists on doing the relaxation test in short SOC ranges (also called minor loops) that can characterize the whole OCV evolution under real cycle profiles; under changes on charge-discharge stages. Figure 24 shows an example with the following minor loops:

- Discharge from 100% SOC to 10% SOC; charge to 40% SOC; and discharge to 10% SOC.
- Discharge from 100% SOC to 20% SOC; charge to 50% SOC; and discharge to 20% SOC.
- Discharge from 100% SOC to 30% SOC; charge to 60% SOC; and discharge to 30% SOC.
- Discharge from 100% SOC to 40% SOC; charge to 70% SOC; and discharge to 40% SOC.
- Discharge from 100% SOC to 50% SOC; charge to 80% SOC; and discharge to 50% SOC.
- Discharge from 100% SOC to 60% SOC; charge to 90% SOC; and discharge to 60% SOC.
- Discharge from 100% SOC to 10% SOC; charge to 20% SOC; and discharge to 10% SOC.
- Discharge from 100% SOC to 20% SOC; charge to 30% SOC; and discharge to 20% SOC.
- Discharge from 100% SOC to 30% SOC; charge to 40% SOC; and discharge to 30% SOC.
- Discharge from 100% SOC to 40% SOC; charge to 50% SOC; and discharge to 40% SOC.

- Discharge from 100% SOC to 50% SOC; charge to 60% SOC; and discharge to 50% SOC.
- Discharge from 100% SOC to 60% SOC; charge to 70% SOC; and discharge to 60% SOC.

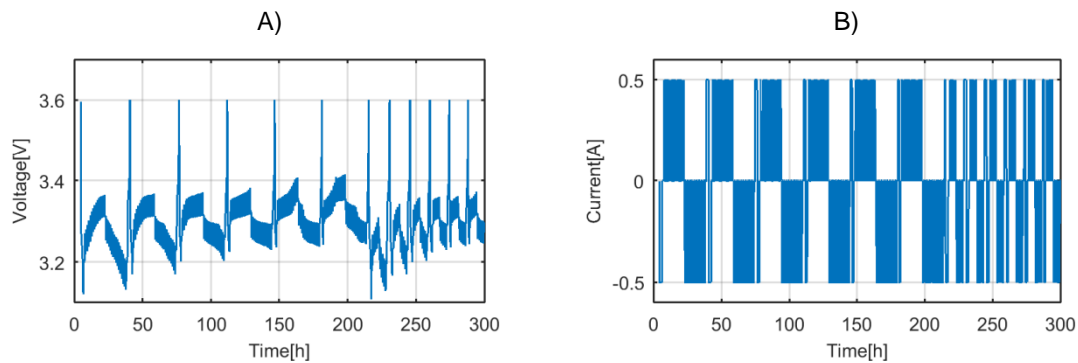


Figure 24: A hysteresis characterization test applied on an A123 SYSTEMS APR 18650 M1 lithium ion cell. A) Voltage profile and B) Current profile.

▪ **Impedance characterization test**

The most common test on the impedance characterization is the current pulse method. The current pulse method consists on applying current pulses to the cell so as to measure the resulting voltage drop (see Figure 25).

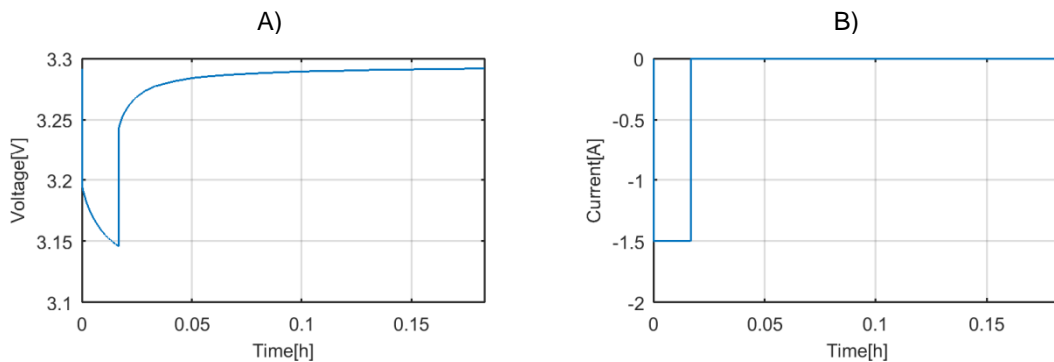


Figure 25: Pulse current test applied on an A123 SYSTEMS APR 18650 M1 lithium ion cell. A) Voltage profile and B) Current profile.

The observed voltage drop can be divided by the current in order to calculate the pure ohmic resistance of the battery. Another way of calculating this resistance comes from the fitting of a pre-defined equivalent circuit with the data gathered from the pulse test. This second calculation method allows us to estimate at the same time the additional impedance values defined on the pre-defined equivalent circuit model.

The duration of the current pulse must be selected differently for different batteries and different battery conditions (temperature, aging state) while considering the frequency behaviour of the battery [21]. We have seen that a 60s pulse with a rest time of 10min is enough to get accurate values of the impedance of the cell at each SOC, see Figure 25.

Another most common test on the impedance characterization is the Electrochemical Impedance Spectroscopy (EIS). The EIS is based on generating and imposing small sinusoidal current signal at a given frequency to the tested lithium ion battery [21]. The voltage response measured at the battery is an approximately sinusoidal signal as well. The magnitude and phase of the impedance for each frequency is calculated considering the relation between voltage and current waveforms. The whole impedance spectrum of the battery is obtained by performing the measurement described above for many frequencies in a given frequency range. This data is usually represented by a Nyquist plot, where the imaginary and the real part of the impedance are plotted on the ordinate (y axis) and abscissa (x axis), respectively [34] (Figure 26).

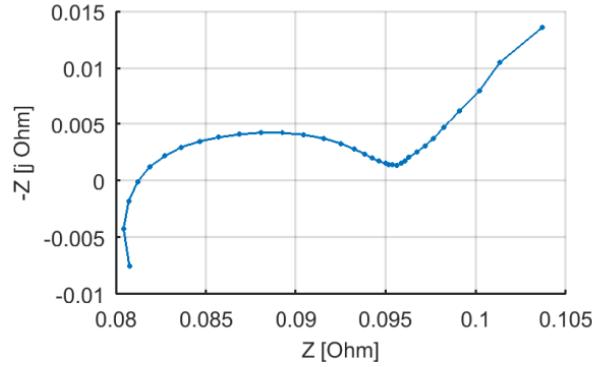


Figure 26: Electrochemical Impedance Spectroscopy applied on a SAMSUNG ICR 18650 26F lithium ion cell.

The imposed sinusoidal current signal amplitude has been experimentally tested on a SAMSUNG ICR 18650 26F lithium ion cell with 2600mAh of nominal capacity. It has been seen that a C/10 and a C/100 sinusoidal gives very similar results and that the higher the current is the smaller the noise is, see Figure 27.

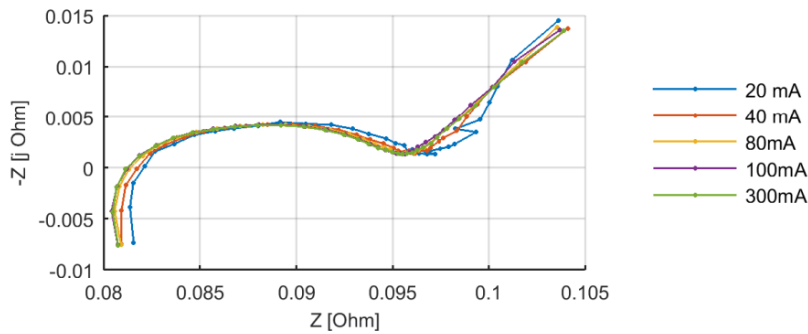


Figure 27: EIS test run with different sinusoidal currents.

Furthermore, the representative Nyquist plot of EIS data (Figure 28) divides the scanned battery into migration, charge transfer and diffusion depending on the frequency of the imposed small sinusoidal current signal. Migration derived at high frequency (on the left of Figure 28) provides resistive characteristics of a battery; the charge transfer (in the middle of Figure 28) forms a semi-circle that represents the kinetics of the battery; and the low frequency part (on the right of Figure 28) represents diffusion [14].

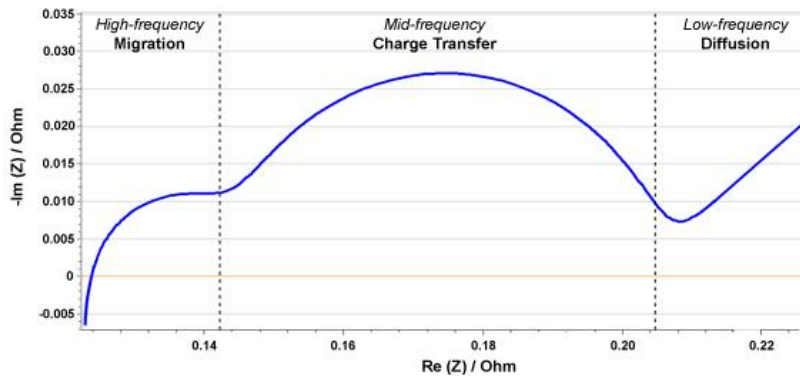


Figure 28: The Nyquist plot is divided into high, mid and low frequency sections [14].

Among all the available data points in the Nyquist plot, there are three points with relevance significance. Firstly, the value of the impedance at the point where $\text{Im}\{\bar{z}(f)\} = 0$ is considered the ohmic resistance of the battery. However, the ohmic resistance measured by the EIS is not exactly

the same as the ohmic resistance measured by the current pulse. The battery has entirely capacitive or inductive behaviour at different frequencies. As a result, the impedance spectrum crosses the x-axis at the frequency at which the inductive behaviour of some battery parts is completely compensated by the capacitive behaviour of the other parts. As a result, the value of the battery impedance at this point is a pure ohmic resistance with some additional resistances [21].

Secondly, the frequency at which the negative imaginary part of the impedance spectrum reaches its local maximum, or the corresponding time constant, defines the dynamic of the battery voltage response by current changes. The lower this frequency is (or the higher the time constant), the slower the voltage change at fast current changes is [21].

Generally, the impedance spectra of new and aged cells remain its basic form at all conditions. However, especially for aged cells at lower temperatures (Figure 29), an additional high frequency semicircle can be distinguished while the other semicircle (related to the charge transfer) increases and shifts towards lower frequencies. This shift correlates to an increasing time constant (τ) over time due to aging and to the third point of relevance on the Nyquist plot. In addition, the SEI growth due to aging causes an increase of the second semicircle. Both effects result in this change of the form of the impedance spectrum [21].

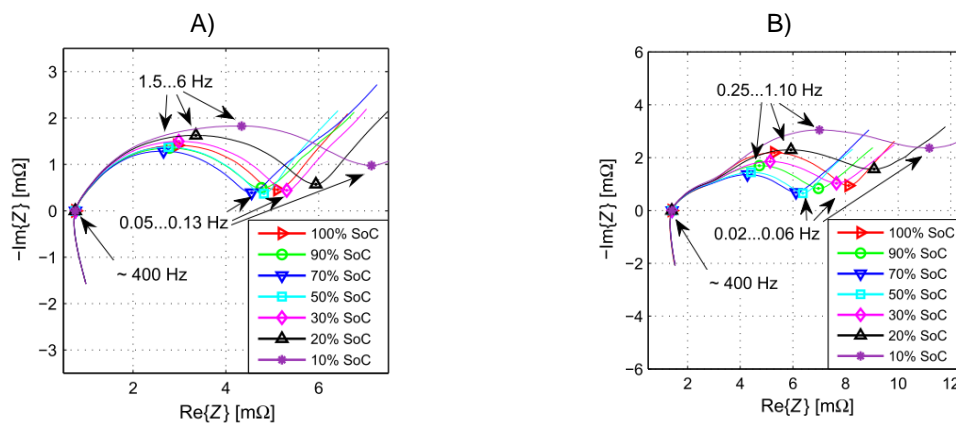


Figure 29: Impedance spectra at 0°C at different SOC of A) a new cell and B) an aged cell [21].

Wang et al. [49] performed the EIS at 40% SOC which was defined as 72min of discharge at C/2 rate of a fully charged cell. The EIS measurement was carried out in a frequency range between 0.01 and 100 kHz and AC amplitude of 5mV. A period of 4h rest was allowed prior to performing each EIS test. This rest period avoided changes in the internal impedance after exciting the cells. It is also worth mentioning the importance of proper connection of the cells to the EIS test system as inaccurate EIS measurements can easily result from poor connections, especially for frequency ranges above 10Khz [34].

The third most common impedance characterization test is the Hybrid Pulse Power Characterization test (HPPC). HPPC is based on pulse trains of charge and discharge intercalating rest period at the end of each cycle. Basically, it is a combination of current pulses defined by a standard (Figure 30). The charge and discharge pulses are set one after the other, where the charge pulse needs to be 0.75 times the discharge pulse. A defined DOD is applied between the cycle and the rest time.

Thanks to the HPPC, the analysis of several aspects of the lithium ion batteries can be observed [11]:

- Voltage profiles as a function of open circuit voltage (OCV) and SOC.
- Electrical performance as a function of OCV and SOC.
- Charge and discharge internal resistance.
- Discharge power density.
- Peak charge power capability.
- The operation window.

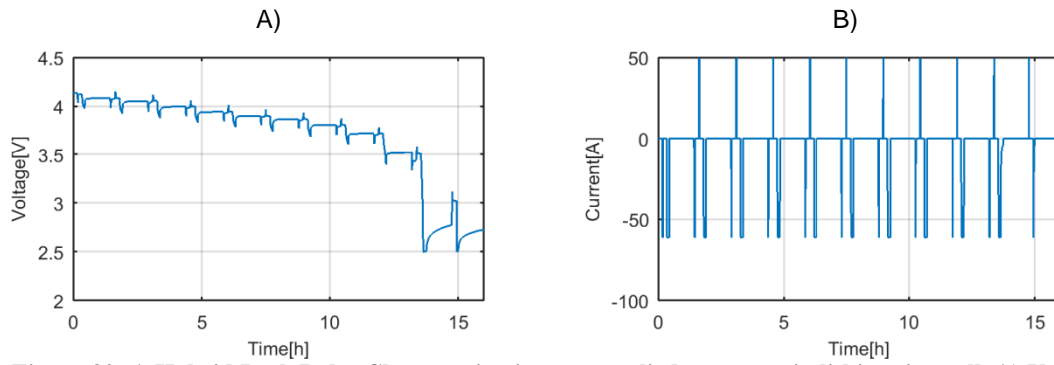


Figure 30: A Hybrid Peak Pulse Characterization test applied on a certain lithium ion cell. A) Voltage profile and B) Current profile.

3.2.2.3 Proposal of ACT

The proposed ACT has two different tests. Firstly, a long ACT for the Beginning of Life (BOL) and End of Life (EOL) is set. The long ACT gathers information for the aging modelling and for the validation of the assumed hypothesis. Secondly, a short ACT is set that focuses uniquely on gathering information for the aging modelling while affecting the minimum the aging itself.

The short ACT focuses on measuring the selected Health Indicators of interest on each SOH on between the AATs while reducing the testing time to the minimum. The proposal is design selecting the most common used health indicators: the dischargeable capacity decrease and the pure ohmic resistance increase. For that, the dischargeable capacity is measured with the “Capacity Characterization Test” (see Table 6) and the pure ohmic resistance is measured with an “Impedance Characterization Test”, in concrete with a discharge pulse test at 50% SOC and at nominal current rate (see Table 17).

Step	Action 1	Mode	Conditions	Comments	Current	Temp.
1	Rest	-	1h			T
2	Charge	CC-CV	Vmax@0.05C		C-rate	
3	Rest	-	1h			
4	Discharge	CC-CV	Vmin@0.05C	Capacity measurement.	C-rate	
5	Rest	-	1h			
6	Charge	CC-CV	Vmax@0.05C		C-rate	
7	Rest	-	1h			
8	Discharge	CC-CV	Vmin@0.05C	Capacity measurement.	C-rate	
9	Rest	-	1h			
10	Charge	CC-CV	Vmax@0.05C		C-rate	
11	Rest	-	1h			
12	Discharge	CC-CV	Vmin@0.05C	Capacity measurement. Save it as Cnom.	C-rate	
13	Rest	-	1h			

Table 16: Proposed Capacity characterization test

Step	Action 1	Mode	Conditions	Comments	Current	Temp.
1	Rest	-	1h			T
2	Charge	CC	50% SOC	SOC relative to the capacity measurement Cnom	C-rate	
3	Rest	-	1h			
4	Discharge	CC	60s	Impedance measurement.	C-rate	
5	Rest	-	1h			
6	Charge	CC	60s	Impedance measurement.	C-rate	
7	Rest	-	1h			

Table 17: Proposed Impedance characterization test

The short ACT should be reduced or increased in terms of the selected Health Indicators. However, the proposed short ACT fits the requirements of most of the aging behaviour studies and modelling works available on the literature [11][30][33] [81][82][83]. Besides, thanks to the simplicity of the

designed ACT and the low testing time (below 24h), the effect of the ACT on the deterioration of the battery has been reduced to its minimum.

On the other hand, the long ACT focuses on retrieving as much information as needed, without worrying on the testing time. The long ACT used to be designed based on the required tests for modelling the electro-thermal behaviour of the cell. In this context, the long ACT changes according to the electro-thermal model complexity and accuracy. As a generic electro-thermal modelling activity in CIDETEC, the long ACT should contain the following tests:

- A Capacity characterization test at different temperatures.
- An OCV characterization test based on continuous low current (C/20) at different temperatures.
- A hysteresis test at the reference temperature if there is a hysteresis effect (not common).
- A full Impedance characterization test (the impedance is tested at the whole operation SOC range) at different C-rates and at different temperatures.

However, the fact is that these tests used to be only run at the reference temperature (it is usually 25°C). Even though the time is not a concern at BOL and EOL, the lab resources are limited. The lab can be overloaded depending on the number of tested cells, so only particular cases are tested at temperatures higher or lower than the reference one. As results, a generic long ACT can be obtained, see Table 18. The given generic proposal does not contain the hysteresis characterization test since it is believed to be unusual in lithium-ion cells [84].

Step	Action 1	Mode	Conditions	Comments	Current	Temp.
START Capacity Characterization test						
1	Rest	-	1h			T
2	Charge	CC-CV	Vmax@0.05C		C-rate	
3	Rest	-	1h			
4	Discharge	CC-CV	Vmin@0.05C	Capacity measurement	C-rate	
5	Rest	-	1h			
6	Charge	CC-CV	Vmax@0.05C		C-rate	
7	Rest	-	1h			
8	Discharge	CC-CV	Vmin@0.05C	Capacity measurement.	C-rate	
9	Rest	-	1h			
10	Charge	CC-CV	Vmax@0.05C		C-rate	
11	Rest	-	1h			
12	Discharge	CC-CV	Vmin@0.05C	Capacity measurement.	C-rate	
13	Rest	-	1h			
END Capacity Characterization test // START OCV Characterization test						
14	Charge	CC	Vmax		C-rate	T
15	Rest	-	1h			
16	Discharge	CC	Vmin	Capacity measurement.	C-rate	
17	Rest	-	1h			
END OCV Characterization test // START Impedance Characterization test						
18	Start cycle			Pulse test, charge, start		T
19	Rest	-	1h	Take OCV		
20	Charge	-	60s@not 100% SOC	Charge Pulse	C-rate	
21	Rest	-	10min			
22	Charge	-	10%SOC	Set SOC: 10,20,...,80,90		
23	End cycle					
24	Charge	CC-CV	Vmax@0.05C		C-rate	
25	Start cycle			Pulse test, discharge, start		
26	Rest	-	1h	Take OCV		
27	Discharge	-	60s@not 0% SOC	Discharge Pulse	C-rate	
28	Rest	-	10min			
29	Discharge	-	10%SOC	Set SOC: 90,80,...,20,10		
30	End cycle					
END Impedance Characterization test						

Table 18: Proposed long Aging Check-up Test

3.3 Aging model

The aging models describe the behaviour of the health indicators along the lifespan. The evolutions of these health indicators or aging metrics are observed on the ACTs of the aging testing process. Generally, information of tests at high levels of one or more accelerating variables (use rate, temperature, voltage) from that aging testing process is extrapolated, through a physically reasonable statistical model, to obtain estimates of life or long-term performance at lower, normal levels of the accelerating variable(s) [65]. With fundamental understanding of failure mechanisms and knowledge of sources of variability, it is possible to develop failure time distributions and electro-chemical aging models. However, there may not be enough physical knowledge to provide an adequate electro-chemical model for acceleration test data (and its extrapolation) when the effect of an accelerating variable is complex [65], such as the effect that have the stress factors on the aging of lithium-ion batteries.

In lithium-ion battery applications, the aging trends are evaluated and general laws for an operation window are built on a modelling environment. The empirical or semi-empirical aging models are the most used aging models on the literature [85] due to the complexity of the aging mechanisms. Besides, it is quite typical to divide the calendar aging effects and the cycling aging effects in two independent aging models in order to simply even more the modelling exercise [11].

The semi-empirical aging models are designed based on physical laws that describe the aging behaviour generated by a physic phenomenon. The most typical variable used on these cases is the temperature. The operation temperature of an electrochemical energy storage system can be linked to an exponential deterioration process expressed by the Arrhenius or the Eyring theory. Then, the general expression of this exponential deterioration process is adapted to the system under evaluation thanks to the observed health indicators (thanks to the data).

The empirical aging models are designed purely on the data and mathematical expressions. The degradation behaviour lacks on physical knowledge and the aging model is built on the mathematical expression that fits the best the observed trends of the health indicators under specific operation conditions.

A sub-objective of the thesis is to generate a universal aging model that can be used on any lithium ion battery. However, any change on each element of the lithium ion battery can generate huge changes on the behaviour of the lithium ion battery. In consequence, the physic or electrochemical models that are built with specific features for each battery element composition are discarded as an option to generate the desired universal aging model. Besides, there is another research team that is working on this kind of models in CIDETEC. Therefore, the efforts are directed on more generic aging models: empirical and semi-empirical aging models.

Nevertheless, even though many of the underlying physical model assumptions, concepts and practices are the same for the different type of responses achieved to build these data based aging models, the actual models fitted to the data and methods of analysis differ because of the different types of responses of each battery chemistry [65]. In this scenario, rather than a universal model (which is thought as not viable), a common methodology to construct the aging model is introduced. But before that, the semi-empirical and empirical aging models available on the literature are studied.

3.3.1 Study of the State of the Art

The modelling of the aging behaviour of lithium ion batteries is trendy nowadays society and a proper look onto the already available knowledge is fundamental in order to propose any kind of aging modelling solution. In this scenario, a state of the art of the available aging models is done as well as its critical evaluation.

3.3.1.1 State of the Art

According to Sarasketa [11], the damage of cycle and calendar aging may all be superimposed. The model developed by Sarasketa [11] (Eq. (10)) uses stress factors in time-domain (calendar aging model, Eq. (11)) and in Ah-throughput domain (cycle aging model, Eq. (13)). The effect of SOC and

temperature is assumed to be the same during storage and operation, so it is taken into account in the calendar ageing model. This way, cycle ageing can be also predicted under different temperature and SOC conditions. As the model was parametrized by the results obtained on static cycle continuous tests, an adjustment coefficient k was added to the proposed cycling aging model when both models (the cycling and calendar aging models) were tested together [11].

$$A_{total} = A_{calendar} + A_{cycling} \quad (10)$$

$$A_{calendar} = f(SoC, T^{\circ}, t) \quad (11)$$

$$Q_{loss_cal}[\%] = \alpha_1 \exp(\beta_1 T^{-1}) \alpha_2 \exp(\beta_2 SOC) t^{0.5} \quad (12)$$

$$A_{cycling} = f(DoD, C\ rate, Ah\ throughput) \quad (13)$$

$$Q_{loss_cyc}[\%] = (\gamma_1 DOD^2 + \gamma_2 DOD + \gamma_3) k Ah^{0.87} \quad (14)$$

$$Q_{loss_cyc}[\%] = (\alpha_3 \exp(\beta_3 DOD) + \alpha_4 \exp(\beta_4 DOD)) k Ah^{0.87} \quad (15)$$

Parameters	Description
$Q_{loss_cyc}[\%]$	The relative capacity loss due to cycling aging respect to the BOL capacity.
$Q_{loss_cal}[\%]$	The relative capacity loss due to calendar aging respect to the BOL capacity.
DOD	The Depth of Discharge.
$\gamma_1, \gamma_2, \gamma_3$	Constants relative to the 10%-50% DOD range.
k	The adjustment coefficient of dynamic operation conditions.
Ah	The charged and discharged capacity along the lifetime in Ah.
α_3, α_4	Pre-exponential constant relative to the 0%-10% and 50%-100% DOD range.
β_3, β_4	Exponential constant relative to the 0%-10% and 50%-100% DOD range.

Table 19: The parameters of the aging model proposed by Sarasketa [11]

Xu [83] proposed an aging model derived from crack propagation theory and Arrhenius relationship, where Millner's crack propagation aging model was taken as reference [86]. Xu [83] made 3 important modifications on Millner's model: firstly, a Rainflow cycle counting algorithm is introduced for the counting of cycles, secondly, calendar aging and cycle aging are decoupled to model separately (Eq. (16)) and thirdly, a two exponential degradation model is introduced to model SEI film formation's impact on degradation rate so as to reflect the strong nonlinearity in the early cycles (Eq. (23)).

It was taken some assumptions:

- (1) The normal degradation rate is proportional to the lithium ion left in active form. Developing this idea, Xu [83] reach to the Eq. (17) that describes the battery aging life over the entire operation period.
- (2) A certain portion of battery's lithium (Eq. (18)) is consumed in the non-steady stage of SEI film formation. The formation rate is inversely proportional to the SEI film already formed and stops when a stable SEI is formed (Eq. (19)). Developing this idea, Xu [83] modelled the degradation as the sum of two exponential function (Eq. (20)).
- (3) The ratio between the linearized SEI degradation rate and the linearized normal degradation rate is a fixed (Eq. (21)). Xu [83] reach to the Eq. (22) introducing the SEI degradation constant ration in the Eq. (20).

Once the assumptions were made, the degradation was written as a functional equation ($y = f(x)$, Eq. (23)). Then, Xu [83] made a linearization of the obtained functional equation (Eq. (24)) using a degradation rate (d) (Eq. (25)) which allows to divide the effect of the cycling aging and the calendar aging (Eq. (16)).

The model developed by Xu [83] has some limitations. The model cannot describe the nonlinearity and sudden increase of capacity fade (the model doesn't take into account lithium plating).

$$f_d(DOD, SOC, C, T, n, N, t) = f_{cyc}(DOD, SOC, C, T, n, N) + f_{cal}(t, SOC_{avg}, T_{avg}) \quad (16)$$

$$L = 1 - e^{-f_{cycle}(SOC, DOD, T, t_{cycle})N} \quad (17)$$

$$p_{SEI} = \frac{Q_{SEI}}{Q_n} \quad (18)$$

$$Q_n = Q_{SEI} + Q_{normal} \quad (19)$$

$$L = 1 - (p_{SEI}e^{-f_{d,SEI}} + (1 - p_{SEI})e^{-f_d}) \quad (20)$$

$$r_{SEI} = \frac{f_{d,SEI}}{f_d} \quad (21)$$

$$L = 1 - (p_{SEI}e^{-r_{SEI}f_d} + (1 - p_{SEI})e^{-f_d}) \quad (22)$$

$$y = 1 - L, \quad a = p_{SEI}, \quad c = 1 - p_{SEI} \\ y = ae^{-bx} + ce^{-dx} \quad (23)$$

$$y' = dx \quad (24)$$

$$d = f_d(DOD, SOC, C, T, n, N, t) \quad (25)$$

Parameters	Description
L	Battery aging life indicator, where 0 correspond to a new battery.
f_{cycle}	The increment of capacity aging life over one cycle.
N	Cycle number.
t_{cycle}	The time period of one cycle.
Q_n	The nominal capacity of the battery.
Q_{SEI}	The part of battery's lithium that is consumed in SEI formation.
Q_{normal}	The rest of lithium that fades with normal aging rate.
p_{SEI}	The portion of lithium consumed in SEI formation.
f_d	The linearized degradation function due to normal operation.
$f_{d,SEI}$	The linearized degradation function due to SEI film formation.
r_{SEI}	The constant SEI degradation ratio.
y	The remaining capacity.
a, b, c, d	Fitting coefficients.
d	Linearized degradation rate per cycle.

Table 20: The parameters of the aging model proposed by Xu [83]

The aging in storage operation conditions of several lithium ion cells have been described and quantified by many authors in the literature using different types of models.

Sarasketa [11] proposed a stress factor based model for calendar aging, Eq. (26). The proposed method is an accumulative aging method where the residual capacity is used as reference point for further predictions. It considers the effect of State of Charge (SOC) and temperature on the capacity fade during calendar aging, Eq. (27).

$$A_{calendar} = f(SoC, T^o, t) \quad (26)$$

$$Q_{loss}[\%] = \alpha_1 \exp(\beta_1 T^{-1}) \alpha_2 \exp(\beta_2 SOC) t^{0.5} \quad (27)$$

Parameters	Description
$Q_{loss}[\%]$	The relative capacity loss respect of the Beginning of Life (BOL) capacity in %.
α_1, α_2	Pre-exponential constants.
β_1, β_2	Exponential constants.
T	The absolute temperature.
SOC	The storage SOC in %
t	The storage time.

Table 21: The parameters if the calendar aging model proposed by Sarasketa [11]

Wang et al. [87] proposed a semi-empirical aging model based on the assumption that calendar life performance is a direct representation of irreversible self-discharge capacity loss, which is mainly

generated by Loss of Lithium Inventory (LLI) during Solid Electrolyte Interphase (SEI) formation at the graphite negative electrode. Wang et al. [87] assumed that the SEI growth is a diffusion limited process with a time^{1/2} relationship and that is a thermally activated process that can be simulated with an Arrhenius law temperature dependence, Eq. (28).

$$Q_{loss,\%} = A \exp\left(\frac{-E_a}{RT}\right) t^{0.5} \quad (28)$$

Parameters	Description
A	The pre-exponential factor.
E_a	The activation energy in J mol^{-1} .
R	The gas constant in $\text{J mol}^{-1}\text{K}^{-1}$.
T	The absolute temperature in K.
t	The life time in days.

Table 22: The parameters of the calendar aging model proposed by Wang et al. [87]

Grolleau et al. [33] proposed a simple empirical expression for predicting capacity fade for the tested LFP cathode and graphite cells at temperatures above 0°C (Eq. (30)) based on firstly, the kinetic dependence of the capacity fade evolution with temperature and SOC (Eq. (29).[1]), secondly, the diffusion limitation of solvent molecule inside the SEI layer (Eq. (29).[2]) and thirdly, the Arrhenius equation (Eq. (29).[3]).

The values of the relation rate between aging time and LLI at a given temperature ($\alpha(T)$) were estimated using robust non-linear regression of aging data. Once $\alpha(T)$ defined for each storage temperature, the kinetic dependence of the capacity fade evolution with temperature and SOC is estimated. According to the results in [33], capacity fade evolution follows a linear dependence with SOC (Eq. (31)) whereas it increases exponentially with temperature (Arrhenius law, Eq. (32)).

$$[1] \quad k(T, SOC), \quad [2] \quad \left(1 + \frac{Q_{loss}(t)}{C_{nom}}\right)^{-\alpha(T)}, \quad [3] \quad k e^{\left(\frac{E_0}{RT}\right)} \quad (29)$$

$$\frac{dQ_{loss}}{dt} = k(T, SOC) \left(1 + \frac{Q_{loss}(t)}{C_{nom}}\right)^{-\alpha(T)} \quad (30)$$

$$k(T, SOC) = A(T)SOC + B(T) \quad (31)$$

$$A(T) = k_A e^{\left\{\frac{E_{0A}}{R} \left(\frac{1}{T} - \frac{1}{T_{ref}}\right)\right\}}, \quad B(T) = k_B e^{\left\{\frac{E_{0B}}{R} \left(\frac{1}{T} - \frac{1}{T_{ref}}\right)\right\}} \quad (32)$$

Parameters	Description
$\frac{dQ_{loss}}{dt}$	The fractional capacity loss at aging time t.
$k(T, SOC)$	the kinetic dependence of the capacity fade evolution with temperature and SOC.
$\alpha(T)$	The relation rate between aging time and LLI at a given temperature.
C_{nom}	The nominal current value (1C).
$A(T)$	The incremental factor of the kinetic dependence of the capacity fade evolution with SOC.
$B(T)$	The kinetic dependence of the capacity fade evolution with temperature.
k_A, k_B	Pre-exponential coefficients.
E_{0A}, E_{0B}	Activation energy.
R	The gas constant.
T	The temperature in kelvin.
T_{ref}	A temperature reference (fixed to 298 K in [33]).

Table 23: Parameters of the calendar aging model proposed by Grolleau et al. [33]

Xu [83] proposed a linearized degradation calendar model based on the effect of stress factors on calendar life (SOC, temperature and time, Eq. (33)). The proposal is composed by a linearized degradation model (Eq. (33)) and two nonlinear stress models (Eq. (36) and (37)). The linearized degradation rate (d) is obtained as a function of SOC and temperature. The stress model for temperature is derived from Arrhenius equation (Eq. (36)) and the stress model for SOC is derived from the Tafel relationship (Eq. (37)). The time stress coefficient (Eq. (40)) is calculated once the other 2 stress factors (Eq. (38) and (39)) are calculated.

This model describes the calendar aging just with one parameter (d), but it has some limitations. Firstly, the proposed temperature stress model is recommended to cover only cases above 15°C and secondly, the inducing effect of low SOC is not modelled [83].

$$y' = dx, \quad y' = f_{cal}(SOC, T, t) \quad (33)$$

$$d = k_t f_{SOC}(SOC) f_T(T) \quad (34)$$

$$x = t \quad (35)$$

$$f_T(T) = e^{k_T(T-T_{ref})\frac{T_{ref}}{T}} \quad (36)$$

$$f_{SOC}(SOC) = e^{k_{SOC}(SOC-SOC_{ref})} \quad (37)$$

$$k_T = \frac{\sum_{i=1}^{N_T} k_T^{T_i}}{N_T}, \quad k_T^{T_i} = \frac{T_i}{T_{ref}(T_i - T_{ref})} \ln\left(\frac{d^{T_i}}{d^{T_{ref}}}\right) \quad (38)$$

$$k_{SOC} = \frac{\sum_{j=1}^{N_{SOC_j}} \sum_{i=1}^{N_{SOC_i}} k_{SOC}^{i,j}}{N_{SOC}}, \quad k_{SOC}^{i,j} = \frac{\ln\left(\frac{d^{SOC_i}}{d^{SOC_j}}\right)}{(SOC_i - SOC_j)} \quad (39)$$

$$k_t = \frac{\sum_{j=1}^{N_{T_j}} \sum_{i=1}^{N_{SOC_i}} k_t^{SOC_i, T_j}}{N_t}, \quad k_t^{SOC_i, T_j} = \frac{d^{SOC_i, T_j}}{f_{SOC}(SOC_i) f_T(T_j)} \quad (40)$$

Parameters	Description
y'	The capacity fade rate in calendar aging.
d	The linearized degradation per time.
x	The time (t) in a chosen unit of time.
k_t	The time stress coefficient for a certain time scale.
$f_{SOC}(SOC)$	The linearized aging model of the SOC stress factor at a given SOC.
$f_T(T)$	The linearized aging model of the temperature stress factor at a given temperature.
T_{ref}, SOC_{ref}	The reference parameters (SOC [50%] and temperature [293 k (25°C)]).
T_i, SOC_i, SOC_j	The value of the stress factors at a specific moment.
$d^{T_i}, d^{SOC_i}, d^{SOC_i, T_j}$	The linearized degradation value extracted from the empirical data.
N_T, N_{SOC}, N_t	The amount of data points on the test data array of each stress factor.
$k_{SOC}^{i,j}$	The SOC stress coefficient calculated from 2 SOC data points.
$k_T^{T_i}$	The temperature stress coefficient at a given temperature (T_i).
$k_t^{SOC_i, T_j}$	The time stress coefficient at a given SOC (SOC_i) and temperature (T_j).

Table 24: Parameters of the calendar aging model proposed by Xu [83]

In cycle aging models there are much more stress factors than in calendar aging models. Due to the complexity of the aging mechanisms, typical proposed cycling aging models are empirical models, which are supported only by experimental data.

Wang et al. [87] proposed a cycle life model for NMC cathode and graphite anode cell taking into account cycling at a constant 50% Depth of Discharge (DOD) (Eq. (41)). The effect of the temperature is used on the fitting of pre-exponential (B_1) and exponential (B_2) factors on the Eq. (43). The equation is updated using the trend showed at the fitting of those factors (Eq. (42)).

$$A_{cycling} = f(DoD, C \text{ rate}, Ah \text{ throughput}) \quad (41)$$

$$Q_{loss, \%} = B_1 \exp^{(B_2 C_{rate})} Ah_{throughput} \quad (42)$$

$$Q_{loss, \%} = (aT^2 + bT + c) \exp^{[(dT+e)C_{rate}]} Ah_{throughput} \quad (43)$$

Parameters	Description
$Q_{loss, \%}$	The relative capacity loss respect of the BOL capacity in %.
a, b, c	Pre-exponential constant.
d, e	Exponential constants.
T	The temperature absolute in °K.

C_{rate}	The C-rate.
$Ah_{throughput}$	The charged and discharged capacity along the lifetime in Ah.

Table 25: The parameters of the cycling aging model proposed by Wang et al. [87]

Sarasketa [11] looked into the influence of DOD, C-rate and Ah-throughput in cycle aging (at both static and dynamic operation schemes). The cycling model is restricted to normal operation conditions of C-rates defined by the manufacturer of the cell. At the same time, the proposed model uses the Ah-throughput instead of time as a parameter of cycle life modelling. The model was proposed in two DOD ranges: the first DOD range was defined between 10%-50% DOD (Eq. (44)) and the second DOD range was defined between 0%-10% and 50%-100% DOD (Eq. (45)).

$$Q_{loss_cyc}[\%] = (\gamma_1 DOD^2 + \gamma_2 DOD + \gamma_3) Ah^{0.87} \quad (44)$$

$$Q_{loss_cyc}[\%] = (\alpha_3 \exp(\beta_3 DOD) + \alpha_4 \exp(\beta_4 DOD)) Ah^{0.87} \quad (45)$$

Parameters	Description
$Q_{loss_cyc}[\%]$	The relative capacity loss respect of the BOL capacity in %.
DOD	The DOD in %.
$\gamma_1, \gamma_2, \gamma_3$	Constants relative to the 10%-50% DOD range.
Ah	The charged and discharged capacity along the lifetime in Ah.
α_3, α_4	Pre-exponential constant relative to the 0%-10% and 50%-100% DOD range.
β_3, β_4	Exponential constant relative to the 0%-10% and 50%-100% DOD range.

Table 26: The parameters of the cycling aging model proposed by Sarasketa [11]

Käbitz et al. [30] proposed an approach of the voltage dependency through complex operation conditions by a weighted average SOC cycle life model, Eq. (46). The model gets an average cycling SOC which correspond to the SOC of a calendar life test at constant voltage (CV), taking into account the same grade of aging (the aging rate of calendar and cycling aging are considered equal). This approximation is not supposed to take into account the effect of capacity increase at low SOC so the multiplying factor $a(SOC)$ is set to one from 20% SOC to 50% SOC.

$$SOC_{avf,weighted} = \frac{\sum_i a(SOC) SOC_i t_i}{\sum_i a(SOC) t_i} \quad (46)$$

Parameters	Description
$SOC_{avf,weighted}$	The average cycling SOC which correspond to the SOC of a calendar life test.
$a(SOC)$	Taking as reference the capacity fade from 50% SOC and 40°C, the multiplying factor at the given SOC_i and temperature.
SOC_i	The mean SOC at cycling aging.
t_i	The period of time at SOC_i .

Table 27: The parameters of the cycling aging model proposed by Käbitz et al. [30]

Wang et al. [49] proposed a cycle life model for LFP cathode and graphite anode cell, establishing a mathematical relationship between capacity loss, discharge C-rate, temperature and charge throughput. The relationship is limited to a defined temperature range (from 15°C to 60°C) and DOD range (from 0% to 90%) for C-rates up to 10C. The capacity fade model is based on the Arrhenius equation and a power law trend, Eq. (47).

The results obtained in [49] showed that a general trend for the pre-exponent factor B exists. B decreases with increasing C-rate. However, it is difficult to quantitatively describe this relationship by using a simple mathematical correlation. Instead, B was found for each C-rate. At the same time, it was found that the C-rate affects the activation energy (Eq. (48)) so the effect of the C-rate has been quantified on the capacity fade model parametrization (similar to the Eyring model, Eq. (49)).

$$Q_{loss} = B \exp\left[-\frac{E_a}{RT}\right] Ah^z \quad (47)$$

$$E_a = D - FC_{rate} \quad (48)$$

$$Q_{loss} = B \exp\left[\frac{-D+FC_{rate}}{RT}\right] Ah^z \quad (49)$$

Parameters	Description
Q_{loss}	The percentage of capacity loss respect to the capacity at BOL.
B	The pre-exponential factor.
D, F	Fitting coefficients of the relationship of the activation energy and the C-rate.
E_a	The activation energy in $J \text{ mol}^{-1}$.
T	The absolute temperature.
R	The gas constant.
Ah	The charge and discharged capacity in Ah.
z	The power law factor.
C_{rate}	The C-rate.

Table 28: The parameters of the cycling aging model proposed by Wang et al. [49]

Xu [83] proposed a linearized degradation cycling model based on the effect of stress factors on cycling life (DOD, SOC, temperature, time and C-rate), where the cycling stress given by the SOC, temperature and time is introduced as calendar stress and thus, considered only on the calendar aging model. The stress model for DOD is derived from gathered supplier's data on cycling life (Eq. (50)) and the stress model for C-rate is designed using the exponential stress model (Eq. (51)). The coefficient of the C-rate stress model (Eq. (52)) is calculated in the same way as the coefficient of the SOC stress factor (Eq. (39)). The coefficient of the DOD is calculated by a fitting process of the data.

$$f_{DOD}(DOD) = \frac{1}{k_{DOD1}DOD + k_{DOD2}DOD^2 + k_{DOD3}DOD^3} \quad (50)$$

$$f_C(C) = e^{k_C(C-C_{ref})} \quad (51)$$

$$k_C = \frac{\sum_{j=1}^{N_{C_j}} \sum_{i=1}^{N_{C_i}} k_C^{i,j}}{N_C}, \quad k_C^{i,j} = \frac{\ln\left(\frac{d^{C_i}}{d^{C_j}}\right)}{(C_i - C_j)} \quad (52)$$

$$N_{EOL}(DOD) = \frac{L_{EOL}}{f_{DOD}(DOD)} \quad (53)$$

Parameters	Description
$f_{DOD}(DOD)$	The linearized aging model of the DOD stress factor at a given DOD.
$k_{DOD1}, k_{DOD2}, k_{DOD3}$	The average DOD stress coefficients.
$N_{EOL}(DOD)$	The number of cycles that can be operated before reaching EOL.
L_{EOL}	The EOL criteria.
$f_C(C)$	The linearized aging model of the C-rate stress factor at a given C-rate.
k_C	The average C-rate stress coefficient.
C_i, C_j, DOD	The value of the stress factor (C-rate and DOD).
C_{ref}	The reference parameter of C-rate.
$k_C^{i,j}$	The C-rate stress coefficient calculated from 2 C-rate data points.
N_C	The amount of data points on the test data array of C-rate stress factor.
d^{C_i}, d^{C_j}	The linearized degradation value extracted from the empirical data.

Table 29: The parameters of the cycling aging model proposed by Xu [83]

3.3.1.2 Critical evaluation

The review on the aging models available on the literature shows that there is not only one way of describing the aging behaviour of a lithium-ion battery and that there is not a clear reference for this aim yet. It is true that the exponential model introduced by the Arrhenius model or the Eyring model is quite common [88]. These two models describe the effect of the temperature on a generic electrochemical system, such as the lithium-ion batteries. Moreover, in the case of the Eyring model, the effect of the temperature is linked with the current in a double exponential mathematical expression (it explains two stress factors with a physical understanding of the aging behaviour of the system). Nevertheless, the rest of the stress factors, the SOC and the DOD, are not completely linked with a specific phenomenon. There are many studies reported on the literature that try to capture the effect of these stress factors with randomly optimized mathematical expressions. Sarasketa [11] uses a second order polynomial and an exponential to describe the effect of the DOD depending on the cycled DOD; Xu [83] proposes an exponential mathematical expression to describe the effect of the

SOC; Käbitz et al. [30] develops a linear model in terms of the mean SOC to describe the effect of the SOC. All these authors propose a mathematical expression that is able to describe the effect of the stress factor of interest without any justification on why they use the model they are using and not some other model. It can be understood that they have tried several different mathematical expressions and they are presenting the one that has shown the best performance rates. There is not any generic model to describe the aging of lithium ion battery, and therefore, this thesis focuses on defining a common methodology to find the best aging model.

3.3.2 Proposal of Modelling Methodology

The proposal modelling methodology defines the steps to develop an empirical aging model on any lithium ion battery chemistry. The proposed methodology has two main phases where firstly, the main trend of the selected health indicator is captured and secondly, the effect of the stress factors have on that captured main trend of the selected health indicator is modelled. As a result, a combined model that is able to describe the selected health indicator evolution in terms of the stress factors (operation conditions) is obtained. But for that, the proposal takes some important assumptions:

- The calendar aging and the cycling aging are independent.
- The calendar and cycling aging can be added linearly to express the cumulative aging.
- There is no capacity recovery effect (the aging trends are monotonic).
- The mean value of a stress factor of a real life cycle profile generates the same deterioration as the deterioration generated with that mean stress factor value at static operation conditions.
- The effect of each stress factor is independent to the other.
- The tested cells experience the same aging mechanisms.

On the first phase, the mathematical expression that fits the best the trends of the observed health indicators is selected. Here, the behaviour of the health indicator itself is modelled. The literature is an interesting support in this task. It can be found a mathematical expression for almost any battery chemistry available on the market, see Table 30.

Chemistry	Linear	Exponential	Logarithmical	Power type	Polynomial
LCO-C				[89]	[90]
LMO-C		[91]			
NCA-C		[92] [93]			
LFP-C				[94][88]	
NMC-C		[95]	[96]	[73]	
NMC-LTO	[97]	[95]			

Table 30: Mathematical expressions for different lithium ion chemistries reported on the literature

In case a new chemistry is evaluated or a mayor doubt about the correctness of the mathematical expression reported on the literature is presented, the mathematical expression selection process would be like this:

- 1- Fit the equations and the data with a quadratic optimization tool such as the “lsqcurvefit” function of MATLAB software.
- 2- Calculate the root mean square error on each testing case and with each mathematical expression.
- 3- Select the mathematical expression that has the minimum root mean square error values.

If there is no a clear difference on the calculated root mean square error values, the use of the simplest mathematical expression of the candidates is recommended.

On the second phase, the variables of the chosen mathematical expression on the first phase are expressed in function of the stress factors. Here, the effect of the stress factors on the health indicator behaviour is modelled. The effect of each stress factor is considered independent and therefore, the mathematical expressions of each stress factor are added linearly (Eq. (54)).

$$var_i = f_1 + f_2 + \dots + f_N \quad (54)$$

Parameters	Description
var_i	The variable i th of the mathematical expression defined on the first phase.
f_j	The mathematical expression that represent the effect of the stress factor j .

Table 31: The parameters that gather the effect of all the stress factors

The available mathematical expressions for this second phase would be the same as in the first phase (Table 30). However, in this case, the literature will not be of any help. There is not knowledge about how the stress factors affect the mathematical expressions that can describe the trend of the selected health indicator. Therefore, we shouldn't discard any mathematical expression; they all should be tested and evaluated.

Evaluating each mathematical expression that could fit the data leads to a huge testing and evaluation matrix, but in reality, the amount of tested levels of each stress factor will delimit the possible applicable mathematical expressions:

- The tested levels of each stress factor delimits the complexity of the model that can be used on describing the effect that that stress factor has on the evaluated health indicator trend (if it has been tested 2 levels, the options are those with as maximum 2 variables to be fitted).

Similarly, there is an aspect of the fitting that we need to be aware of: the relation between the number of variables to be fitted and the length of the output. MATLAB's "lsqcurvefit" function will require that the number of available data points must be greater than the number of variables to find. If the obtained variables on the first phase are used as outputs, reduced aging test matrixes delimit greatly the applicable mathematical expression combinations. This issue can be overcome by joining both phases in one: the variables of the equations that describe the effect of each stress factors has on the trend of the selected health indicator are fitted using the whole data from the observed trends of that same health indicator as output (the second phase is fitted with the data from the first). In this way, the output length is increased as many times as the length of the smaller output vector of the first phase.

The mathematical expression selection process would be same as in the first phase but more complex. Firstly, there are not just 5 mathematical expressions, but the combination of them (exponential increase of possibilities). Secondly, there is not clear knowledge about which mathematical expression should be the selected one and which shouldn't (uncertainty on the performance of the models outside the tested cases). In this scenario, a logic based discrimination process is proposed as an additional aid when a mayor doubt is generated or when clear difference on the values doesn't appear.

The logical discrimination process consists on these two states:

- The simplest mathematical expression is always the best.
- The increase of the effect of the stress factor will always increase the deterioration rate of the health indicator.

Once fulfilled these two modelling phases, the aging model would be completed, see Eq. (55).

$$HI_{trend} = f_{cal}(f(SF_{cal\ 1}), \dots, f(SF_{cal\ M})) + f_{cyc}(f(SF_{cyc\ 1}), \dots, f(SF_{cyc\ N})) \quad (55)$$

Parameters	Description
HI_{trend}	The degradation trend of the selected Health Indicator.
f_{cal}	The mathematical expression of the calendar aging.
f_{cyc}	The mathematical expression of the cycling aging.
$f(SF_{cal\ i})$	The mathematical expression of the effect of the i th stress factor on calendar aging.
$f(SF_{cyc\ i})$	The mathematical expression of the effect of the i th stress factor on cycling aging.
N, M	The amount of evaluated stress factors on cycling and calendar aging respectively.

Table 32: The parameters that describes the evolution of a selected health indicator

3.4 Validation

The proposed aging testing and modelling methodology are put into practice with two different common applications which use battery based energy storage systems: a High-Energy type application and a High-Power type application. The defined requirements are divided on requirements relative to rest periods (calendar aging) and to operating periods (cycling aging). In each application a specific battery is used that matches the application requirements. After a proper evaluation of the application requirements, an aging test matrix for each application has been generated. After that, the test matrix has been implemented on CIDETEC's lab. With the obtained data, an aging model for each application has been built. At the end, the constructed aging model is evaluated in terms of the fitting accuracy of the available data, the interpolation potential and the real life applicability on a validation context. In addition to this, two relevant hypotheses done along the proposed methodologies are analysed and discussed.

3.4.1 Methodology validation on a High-Energy Application

The high-energy application consists on a battery integrated on an electric public bus. For that, a High-Energy NMC-C pouch battery has been chosen. The battery characteristics are shown in Table 3.

Item	Specification
Nominal Capacity	54 [Ah]
Standard charge current	54 [A]
Standard discharge current	54 [A]
Maximum temperature	45 [°C]
Minimum temperature	-20 [°C]

Table 33: High-Energy battery specifications

3.4.1.1 Aging Testing Definition

Following the aging testing methodology, firstly the possible testing cases are reduced based on the delimitation imposed by the battery, see Table 34.

Stress factor	Operating temperature	Current	SOC	DOD
Maximum value	45[°C]	54[A]	100[%]	100[%]
Minimum value	-20[°C]	-54[A]	0[%]	0[%]
Minimum step	1[°C]	0.001[A]	1[%]	1[%]

Table 34: Testing cases possibilities on the first stage of the aging test matrix design on a High-Energy application

Secondly, the obtained aging test matrix is further reduced based on the application characteristics. The application consists on a bus that makes a daily route 320 days of a year. The daily tour consists on 17h of work (the bus is moving) with 7 hours of charging at a constant current rate with a constant voltage stage when the end of charge voltage is reached. The 17h route is translated to a mean use profile of the battery (it is out of the scope of this thesis the way of getting this current profile). The mean current profile and the resultant energy evolution of the battery are shown in Figure 31.

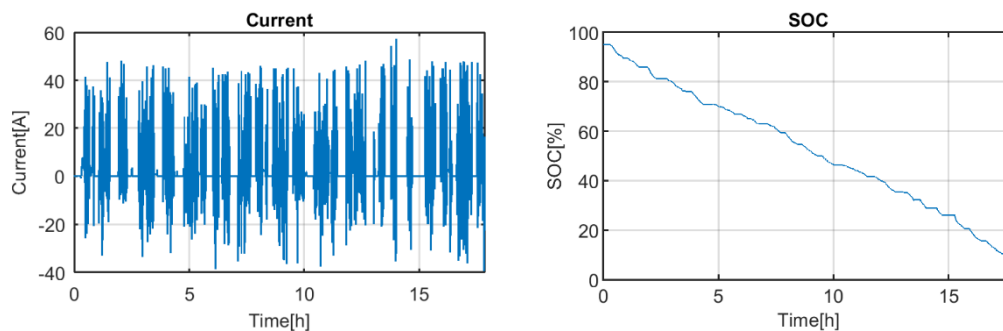


Figure 31: The current profile and the SOC evolution of the battery at BOL. The positive current values represent the discharge while the negative values represent the charge.

After a proper evaluation, several key aspects about the mean application have been resumed:

- The battery will be on cycling mode 320 days per year (mostly, the aging will come from cycling aging).
- The mean discharge current is below 0.1C.
- There are many excursions to peak currents above C/2.
- The use profile reduces the energy of the battery 88% of the nominal one (the DOD of the application is almost 90%).
- The possible initial SOC value before initiating the route goes from 100% to 88%.
- The possible SOC after finishing the route goes from 12% to 0%.
- The temperature of operation will be $25 \pm 10^\circ\text{C}$.
- The charge current is 1C.
- The batteries will be at a rest mode 45 days per year.
- The rest period can be done at end of charge or end of discharge condition (at SOC values from 100% to 88% and values from 12% to 0%), but the most probable scenario is leaving the bus charged at constant current before the beginning of this rest period (around 95%).
- The temperature on rest periods is the temperature at the garage, which is not controlled at holidays. The limit is placed on the temperature limits defined by the weather of the place of the application at the rest period season (summer): $35 \pm 10^\circ\text{C}$.

Alternatives to the defined most probable operation condition would be:

- The current profile is reduced by increasing the number of batteries on the application. This is unlikely based on application expertise (probability below 29%). It is placed the limit to a mean current of 0.05C with a DOD of 70%. This affects the rest time period conditions: SOC values from 100% to 70% and values from 30% to 0%.
- The current profile is increased by reducing the number of batteries on the application. This is not recommendable because it will increase the DOD (probability between 30% and 59%). The current is increased to C/5 with a DOD of 100%.
- The operation temperature range can be increased by simplifying the thermal management system. This is likely to happen (probability between 30% and 59%). The limit is placed on the temperature limits defined by the weather of the place of the application: $25^{+20}_{-25}^\circ\text{C}$.
- The charge current is decreased to C/2. It is very likely (probability between 60% and 90%).
- The charge current is reduced to C/3. It is very likely to happen (probability between 60% and 90%).
- The amount of days on operation is likely to change. It doesn't affect the aging test matrix.

Operation mode		Operation temperature	Charge current	Discharge current	DOD	SOC range	Average SOC
Resting	MIN	25[°C]					0[%]
	MAX	45[°C]					100[%]
	STEP	1[°C]					1[%]
Cycling	MIN	0[°C]	-54[A]	0[A]	70[%]	70[%]-0[%] /.../ 100[%]-30[%]	
	MAX	45[°C]	0[A]	54[A]	100[%]	100[%]-0[%]	
	STEP	1[°C]	0.001[A]	0.001[A]	1[%]	1[%]	

Table 35: Stress factors of calendar and cycling aging

Once the application characteristics are properly evaluated, the possible testing cases that fits the application requirements are generated, see Table 35. For that, firstly, the testing cases are divided in the operation modes that appear on the application: cycling and resting (this makes reference to the cycling aging and calendar aging respectively). Then, the stress factors of interest on each operation mode are redefined. In this application, there are two changes from the defined generic stress factors: the current and the SOC. The effect of the current is divided in terms of the sign of the current and the effect of the SOC is presented as an average value or as a range of values. The current is divided in two in order to properly define the effect of negative currents on one hand (the charging process) and the positive current on the other hand (the discharging process). The SOC is

presented in average value for resting periods, since there is no SOC change in this operation mode. Nonetheless, the cycling operation mode generates a change on the SOC; this is why the range of SOC values is presented instead of the average used on the resting period.

Before the last stage of restraining the aging test matrix, the importance of the testing cases needs to be expressed in a user-friendly way. In this context, the concept of the proposed colour system is applied. Firstly, a matrix containing the red testing cases has been built, see Table 36. Here, the condition that describes better the application requirements is highlighted (the levels of the stress factors that describe this operation condition are turned red). In total, we get 9 testing cases to describe the calendar aging behaviour and 189 testing cases to describe the cycling aging behaviour.

Operation mode	Level	Operation temperature	Charge current	Discharge current	DOD	SOC range	Average SOC
Resting	1	25[°C]					0[%]
	2	35[°C]					95[%]
	3	45[°C]					100[%]
Cycling	1	15[°C]	-54[A]	54[A]	100[%]	100[%]-0[%]	
	2.1	25[°C]	-40[A]	30[A]	90[%]	100[%]-10[%]	
	2.2					95[%]-5[%]	
	2.3					90[%]-0[%]	
	3.1	35[°C]	-27[A]	5.4[A]	80[%]	100[%]-20[%]	
	3.2					90[%]-10[%]	
	3.3					80[%]-0[%]	

Table 36: The Red testing cases. The levels of the stress factors that are in red describe the most probable operation condition defined on the application requirements

Following the advice done at the end of the methodology, the generated test matrix is presented to CIDETEC's lab. First of all, the viability of testing the proposed operations conditions is evaluated. The actual lab availability has forced the following changes on the stress factor levels:

- The absolute value of the current must be above 14A (C/3) since it supposes to occupy the lab resources more than the acceptable project time.
- The temperatures available on cycling operation mode are 10°C, 25°C and 45°C.

Operation mode	Level	Operation temperature	Charge current	Discharge current	DOD	SOC range	Average SOC
Resting	1	25[°C]					0[%]
	2	35[°C]					95[%]
	3	45[°C]					100[%]
Cycling	1	10[°C]	-54[A]	54[A]	100[%]	100[%]-0[%]	
	2.1	25[°C]	-40[A]	30[A]	90[%]	100[%]-10[%]	
	2.2					95[%]-5[%]	
	2.3					90[%]-0[%]	
	3.1	45[°C]	-27[A]	14[A]	80[%]	100[%]-20[%]	
	3.2					90[%]-10[%]	
	3.3					80[%]-10[%]	

Table 37: The Red testing cases after a first iteration with the lab. The levels of the stress factors that are in red describe the most probable operation condition defined on the application requirements. The blue values are the ones modified after the first iteration with the lab

As a result, firstly, the values of the tested temperature on the cycling operation mode are changed; and secondly, the testing case that describes better the application disappears from the testing cases, see Table 37. The change on the temperature values does not affect too much the obtainable result. The restrictions have increased the upper and lower values but all the values of interest are still inside the tested operation window, so it is considered acceptable. However, the restriction on the current leaves the case of interest outside the tested window (the lower tested value is higher than the one of interest), so assumptions on modelling level are required:

- The aging effect due to discharge currents below C/3 is assumed to be the same as the one generated with a C/3 current. The difference that could be is considered negligible.

After that, the numbers of cases that can be tested are discussed. After a proper evaluation of the importance of the project, the cost of samples and the availability of resources, the maximum testing cases have been set on 5 on resting operation mode and 8 on testing the cycling operation mode. Since the red testing case matrix needs to be reduced, there is no sense on developing the orange, yellow and white testing case matrixes.

In other to reduce the calendar aging testing cases from 9 to 5, we need at least discard 2 levels of the defined 6. In this case, the 0% SOC has been directly nominated since it was unlikely to happen. This level was added to improve the calendar aging behaviour description at low SOC. For the temperature, the middle value of the temperature has been nominated according to the following hypothesis:

- The effect of the temperature in between 25°C and 45°C is linear.

As result, a new calendar aging test matrix of 4 testing cases (below the restriction imposed by the lab of 5) can be generated. So as to complete the testing cases the lab is offering, an additional testing case is added. The proposed one is to test the calendar aging at 30% SOC at 25°C. The batteries are used to be distributed at this same SOC (30%) and the most probable temperature in cycling and resting operation modes is this temperature (25°C). The final calendar aging test matrix proposal is shown in Table 38.

Test n°	Temperature [°C]	SOC [%]
1	25	100
2	25	95
3	25	30
4	45	100
5	45	95

Table 38: Aging test matrix to characterize the calendar aging

In other to reduce the cycling aging testing cases from 189 to 8, we need to reduce the levels and combinations of stress factors to the minimum. First of all, the levels need to be reduced to a minimum acceptable for the posterior modelling. The process in this application is as follow:

- DOD: The most likely DOD values are above 90%, so the 80% DOD is nominated.
- SOC range: The most likely operation consists on charging completely the battery (SOC ranges up to 100%) and discharging to values above 5% (values below 0% would generate safety problems), so the SOC range between 90% and 0% is nominated.
- Charge current: The middle charge current is nominated (40A).
- Discharge current: The maximum discharge current could be nominated since the application is very unlikely to work around this value. However, since the effect of the discharge current on the health indicators is expected to be almost the same for currents below C/3, more than 2 points is needed. It is not nominated any of the values on the discharge current stress factor.
- Operation temperature: The effect of the temperature is expected to suffer an increase at low temperatures and high temperatures, so a minimum of 3 points is required. It is not nominated any of the values on the temperature stress factor.

As a result of the nominations, a reduced test matrix can be generated, see Table 39. In this table the SOC range is defined by the upper SOC of this same SOC range.

Operation temperature	Charge current	Discharge current	DOD	Upper SOC
10[°C]	-54[A]	54[A]	100[%]	100[%]
25[°C]	-27[A]	30[A]	90[%]	95[%]
45[°C]	-	14[A]	-	-

Table 39: The reduced testing cases on the cycling operation mode

The new proposed matrix generates a total of 54 testing cases, which are still way above the defined 8 testing cases. However, the levels of the stress factors cannot be reduced further. In this scenario, the combinations between the levels are gradually restricted.

Firstly, the tested temperature combinations are restricted. The three values of the temperature stress factor are only applied on the most probable operation condition: a 1C charge with a C/3 discharge with a 90% DOD and with a SOC range of 100% to 10%. Then, the combinations of the rest stress factors (current, DOD and SOC) are done all at 25°C. However, a modelling assumption is required:

- The effect of the temperature on the cycling aging is independent to the current, DOD or SOC ranges if working on the safety window.

As a result, the total testing cases are reduced from 54 to 20, see Table 40. In this point, the combination between the DOD, SOC range and currents need to be reduced to 6. One of the 6 testing cases is already defined and cannot be changed: a 1C charge with a C/3 discharge with a 90% DOD and with a SOC range of 100% to 10% at 25°C. The rest are selected based on the experience while maintaining some conditions:

- All the defined levels of every stress factor need to appear on the selected conditions.
- The most probable levels of the stress factors will be the ones with more presence on the selected testing cases.
- The more disperse the operation conditions of the testing cases are, the better the covered tested dimension will be.

The selected 8 cases are put on red in Table 40.

Test nº	Temperature [°C]	Upper SOC [%]	DOD [%]	Charge C-rate [%]	Discharge C-rate [%]
1	10	100	90	1	0.3
2	45	100	90	1	0.3
3	25	100	90	1	0.3
4	25	100	90	1	0.5
5	25	100	90	1	1
6	25	100	90	0.5	0.3
7	25	100	90	0.5	0.5
8	25	100	90	0.5	1
9	25	100	100	1	0.3
10	25	100	100	1	0.5
11	25	100	100	0.5	1
12	25	100	100	0.5	0.3
13	25	100	100	0.5	0.5
14	25	100	100	1	1
15	25	95	90	1	0.3
16	25	95	90	1	0.5
17	25	95	90	0.5	1
18	25	95	90	0.5	0.3
19	25	95	90	0.5	0.5
20	25	95	90	1	1

Table 40: The Aging test matrix to characterize the cycling aging with 26 testing cases. The cases that are in red are the selected ones as the final ones

In this point, the customer was consulted and a discussion was started. The calendar aging test matrix was accepted. However, the cycling aging test matrix generated some disagreements. Due to interests of future application of the selected battery, a particular evaluation of the aging generated with lower charging current was demanded. On the same hand, the reduction of the testing time was asked, so an agreement of increasing the minimum discharging current to C/2 and the most probable current to 1C was taken. This reformulation of the testing case levels was done by assuming that:

- The aging effect due to discharge currents below C/2 is assumed to be the same as the one generated with a C/2 current. The difference that could be is considered negligible.

- The effect of the current on the aging trend of the selected health indicator between 1C and C/2 is linear.

In this scenario, the amount of levels of the charging current stress factor is increased to 3 and the amount of levels of the discharging current stress factor is reduced to 2. The final cycling aging matrix is shown in Table 41.

Test n°	Temperature [°C]	Upper SOC [%]	DOD [%]	Charge C-rate [%]	Discharge C-rate [%]
1	25	100	90	1	0.5
2	25	95	90	1	1
3	25	95	90	0.5	1
4	10	100	90	0.3	1
5	45	100	90	0.3	1
6	25	100	90	0.3	1
7	25	100	90	0.5	0.5
8	25	100	100	0.5	1

Table 41: Aging test matrix to characterize the cycling aging

The proposal of the cycling aging test matrix was accepted by the lab and the tests defined on Table 38 and Table 41 were scheduled to run for 2 years, but before starting the tests, the ACT was designed. The long ACTs used at BOL and EOL contain a capacity, an OCV and an impedance characterization test. The selected OCV characterization test is done with a continuous small C-rate. The selected impedance characterization test is done with repeated charge and discharge pulse test on the whole operation SOC range with a step of 10% SOC. The short ACT contains the suggested capacity and impedance characterization test.

3.4.1.2 Aging Model Construction

After finishing the 2 years of testing period, the performed ACTs have been treated and the health indicators of interest have been obtained:

- Dischargeable capacity (see Figure 32 and Figure 33).
- Pure ohmic resistance (see Figure 34 and Figure 35).

The comparison of the obtained results is done in terms of days in the case of calendar aging and in terms of energy throughput or equivalent cycles in the case of cycling aging. The days make reference to the total time in days elapsed in between aging measurements. The energy throughput or equivalent cycles make reference to the total energy discharged in between aging evaluations. The energy throughput is directly the Wh discharged and the equivalent cycle is the Wh discharged divide by the nominal energy in Wh.

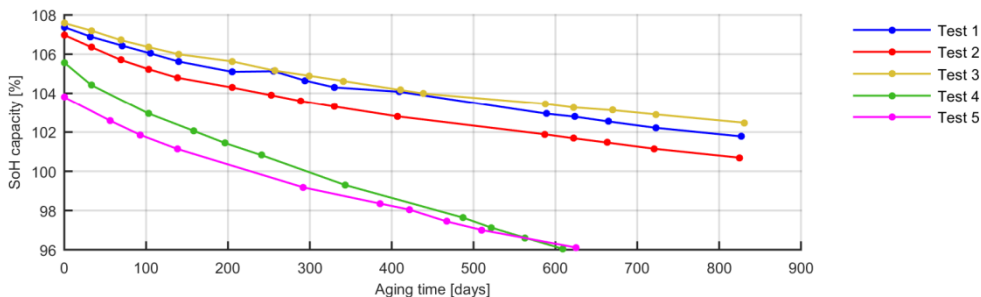


Figure 32: Relative dischargeable capacity values of the tested batteries under the calendar aging test matrix.

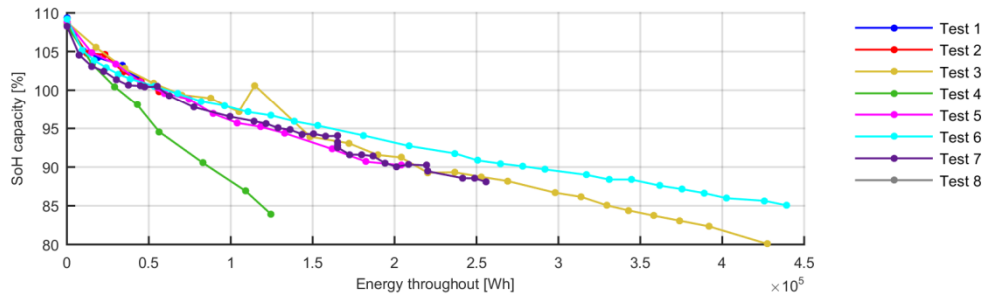


Figure 33: Relative dischargeable capacity values of the tested batteries under the cycling aging matrix.

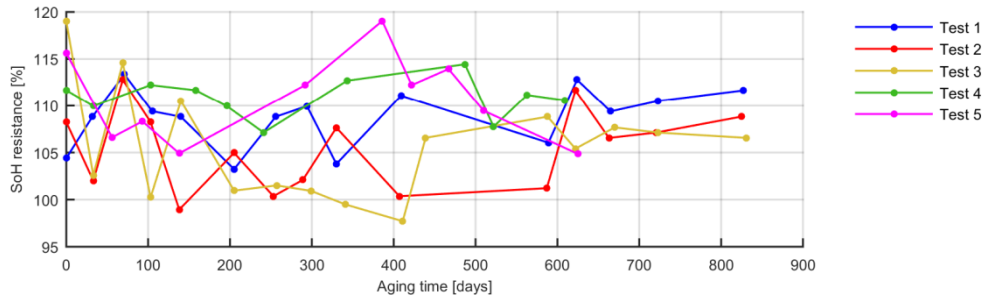


Figure 34: Relative pure ohmic resistance values of the tested batteries at 50% SOC under the calendar aging matrix.

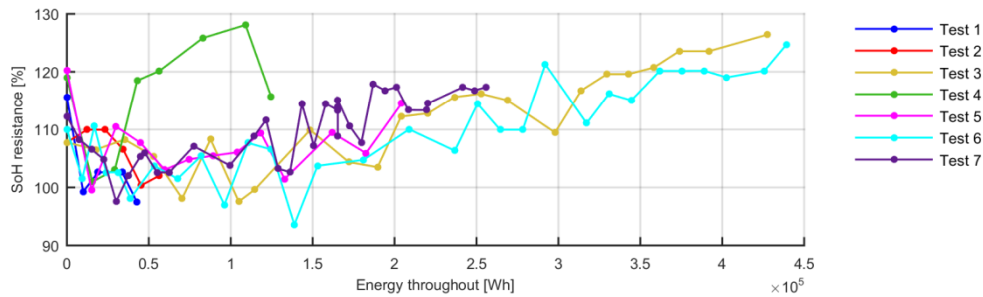


Figure 35: Relative pure ohmic resistance values of the tested batteries at 50% SOC under the cycling aging matrix.

Afterwards, the obtained data has been analysed. In a first glance, it has been detected a problem with the test 8. The impedance data of the test 8 has been corrupted and has been discarded. As a consequence, there are 7 testing cases to develop the aging model that describes the pure ohmic resistance increase due to cycling aging. Then, the proposed modelling methodology has been followed.

The first stage of the proposed modelling methodology consists on choosing the mathematical expression that fits better the selected health indicators (dischargeable capacity and the pure ohmic resistance). The literature tells us that both, the calendar aging model and the cycle aging model of the selected health indicators are likely to have an exponential decay tendency [95] [98]. Nevertheless, all the proposed 5 simple mathematical expressions are tested. The tested mathematical expressions are shown in Table 42.

Aging	Linear	Exponential	Logarithmic	Power type	2 nd order polynomial
Calendar	x	x	x	x	x
Cycling	x	x	x	x	x

Table 42: Applicable mathematical expressions to the obtained data from the aging test matrix

The fitting accuracy is measured with the Root Mean Square Error (RMSE) metric between the measurements and the estimation done with the fitted mathematical expression. This metric has been calculated on each test of both aging test matrix for the two selected health indicators. The mean of the obtained RMSE values on all the tests of the run aging test matrix is added as well, see Table 43, Table 44, Table 45 and Table 46.

	Linear	Exponential	Logarithmic	Power type	2 nd order polynomial
Test 1	0,00867	0,00228	0,01067	0,00006	0,00867
Test 2	0,00777	0,00294	0,01725	0,00147	0,00777
Test 3	0,01879	0,02492	0,07387	0,01873	0,01871
Test 4	0,00806	0,01806	0,06533	0,00780	0,00806
Test 5	0,01303	0,01035	0,03754	0,00323	0,01303
Test 6	0,01413	0,01349	0,05026	0,00282	0,01413
Test 7	0,02353	0,01770	0,06235	0,00903	0,02353
Test 8	0,00812	0,01734	0,07585	0,00801	0,00750
Mean RMSE	0,01276	0,01338	0,04914	0,00640	0,01268

Table 43: Fitting RMSE of the dischargeable capacity evolution data with the proposed cycling aging models

	Linear	Exponential	Logarithmic	Power type	2 nd order polynomial
Test 1	0,04501	0,04501	0,04501	0,04501	0,04501
Test 2	0,06649	0,06649	0,06649	0,06649	0,06649
Test 3	0,04751	0,03631	0,09513	0,03496	0,03592
Test 4	0,07983	0,07257	0,10424	0,07670	0,07724
Test 5	0,04318	0,03793	0,05256	0,03807	0,03960
Test 6	0,03265	0,02998	0,05637	0,03020	0,03025
Test 7	0,04743	0,05063	0,09778	0,04736	0,04729
Mean RMSE	0,05173	0,04842	0,07394	0,04840	0,04883

Table 44: Fitting RMSE of the pure ohmic resistance evolution data with the proposed cycling aging models

	Linear	Exponential	Logarithmic	Power type	2 nd order polynomial
Test 1	0,00240	0,00296	0,01374	0,00137	0,00240
Test 2	0,00373	0,00288	0,01434	0,00086	0,00373
Test 3	0,00299	0,00212	0,01235	0,00091	0,00299
Test 4	0,00190	0,00408	0,02745	0,00060	0,00190
Test 5	0,00365	0,00441	0,02378	0,00045	0,00365
Mean RMSE	0,00293	0,00329	0,01833	0,00084	0,00293

Table 45: Fitting RMSE of the dischargeable capacity evolution data with the proposed calendar aging models

	Linear	Exponential	Logarithmic	Power type	2 nd order polynomial
Test 1	0,03330	0,03086	0,03079	0,03078	0,03330
Test 2	0,04079	0,04084	0,04084	0,03801	0,03954
Test 3	0,04575	0,04575	0,04575	0,04575	0,04575
Test 4	0,01903	0,01583	0,02251	0,01640	0,01714
Test 5	0,01867	0,01866	0,01867	0,01867	0,01867
Mean RMSE	0,03151	0,03039	0,03171	0,02992	0,03088

Table 46: Fitting RMSE of the pure ohmic resistance evolution data with the proposed calendar aging models

The fitting of the dischargeable capacity data on both operation conditions (cycling and resting operation conditions) shows that the model that fits better the data is the power type model. This difference of the power type model with the rest models is almost 10 times on the best case (test 5 of resting operation) and at least 2 times on the worst case (test 1 of cycling operation) with an average improvement of at least 100%. This difference is relevant enough to select this power type model against the others. On the other hand, the fitting of the pure ohmic resistance data shows that there is not a clear winner. The biggest improvement respect to the simplest model is below 50% on all the cases. The difference cannot be defined as relevant. Therefore, the simplest model (linear model) is selected.

Next stage consists on linking the variables of the selected mathematical expressions and the stress factors. The applicable mathematical expressions for that aim are shown in Table 47 and Table 62. Here, the complexity of the available mathematical expression depends on the tested levels and the assumed hypotheses on the aging test matrix design. In this case, the temperature effect on the calendar aging model is considered linear since it is only modelled the temperature effect on high temperatures. In cycling mode, however, both the effect of low temperatures and the effect of high temperatures is tested and therefore, modelled. For this a non-linear mathematical expression based on two linear equations is formulated to model linearly on one hand the effect of low temperatures and on the other hand the effect of high temperatures. The upper SOC and the discharge current effect are evaluated with 2 levels each, so a linear model is only applicable. The effect of DOD is also tested with 2 levels, so a linear model is only applicable, at least on the dischargeable capacity health indicator modelling. Due to loss of data, it cannot be modelled the DOD effect on the pure ohmic resistance health indicator (tested only 1 level). In contrast, the mean SOC and the charge current effect is evaluated with 3 levels, so some more mathematical expressions are evaluated, see Table 47 and Table 62 respectively.

Stress factor	Linear	Exponential	Logarithmic	Power type	2 nd order polynomial
Mean SOC	x	x	x	x	x
Temperature	x				

Table 47: The applicable mathematical expressions to link the stress factors and the free variables designed on the calendar aging model

Stress factor	Linear	Exponential	Logarithmic	Power type	2 nd order polynomial	Double Linear
Upper SOC	x					
Temperature						x
DOD	x					
Charge C-rate	x	x	x	x	x	
Discharge C-rate	x					

Table 48: The applicable mathematical expressions to link the stress factors and the free variables designed on the cycling aging model.

The possible combinations of these mathematical expressions are a total of:

- 25 for the calendar aging model that describes the dischargeable capacity evolution.
- 5 for the calendar aging model that describes the pure ohmic resistance evolution.
- 25 for the cycling aging model that describes the dischargeable capacity evolution.
- 25 for the cycling aging model that describes the pure ohmic resistance evolution.

The RMSE on each possible combination has been calculated, see Table 49.

Combination	Calendar aging		Cycling aging	
	Dischargeable capacity	Pure ohmic resistance	Dischargeable capacity	Pure ohmic resistance
1	0.13064	4.94e-06	6.29038	6.36e-05
2	182.928	7.12e-06	51.3022	0.06393
3	9.43133	9.65e-06	51.3022	0.06395
4	13.6691	7.12e-06	51.3022	0.06393
5	8.59503	4.94e-06	52627866	0.06120
6	2.66485		8.90e+21	
7	52.7651		Inf	
8	3.79468		Inf	
9	4.30601		Inf	
10	52.7651		51.3022	
11	2.69993		8.80e+21	
12	52.7651		Inf	
13	3.82311		Inf	
14	4.34067		Inf	
15	52.7651		51.3022	
16	2.68350		8.90e+21	

17	52.7651		Inf	
18	3.80923		Inf	
19	4.32379		Inf	
20	52.7651		51.3022	
21	Inf		2.37e+22	
22	4795858		Inf	
23	52.76511		Inf	
24	5924139		Inf	
25	Inf		51.3022	

Table 49: The mean RMSE values of each combination of the proposed mathematical expressions

The combination that gets the minimum RMSE among the evaluated ones are the first case for the dischargeable capacity on both calendar aging model (Eq. (56)) and cycling aging model (Eq. (58)), and for the pure ohmic resistance on the cycling aging model (Eq. (59)). In the case of the pure ohmic resistance of the calendar aging model, the first combination gets the same value as the fifth combination. In case of doubt, the simplest model is chosen. In this case, the simplest model is the first combination (two linear models, Eq. (57)).

The obtained calendar aging model of the selected two health indicators, the dischargeable capacity and the pure ohmic resistance, are shown in Figure 36 and Figure 37 respectively. The obtained cycling aging model of the selected two health indicators, the dischargeable capacity and the pure ohmic resistance, are shown in Figure 38 and Figure 39 respectively.

$$Q_{calendar} = Q_{ini} - var_1 \cdot t^{var_2} \quad (56)$$

$$var_1 = (-2.22e^{-5}) \cdot T + (9.53e^{-6}) \cdot SOC$$

$$var_2 = (0.0104) \cdot T + (-0.0022) \cdot SOC$$

Parameters	Description
$Q_{calendar}$	The dischargeable capacity evolution due to calendar aging.
Q_{ini}	The dischargeable capacity value at Beginning of life (initial value).
t	The resting time related to calendar aging in days.
var_1	The pre-power law variable.
var_2	The power law variable.
T	The cell temperature at resting mode.
SOC	The mean SOC at resting mode.

Table 50: Parameters of the calendar aging model of the dischargeable capacity evolution

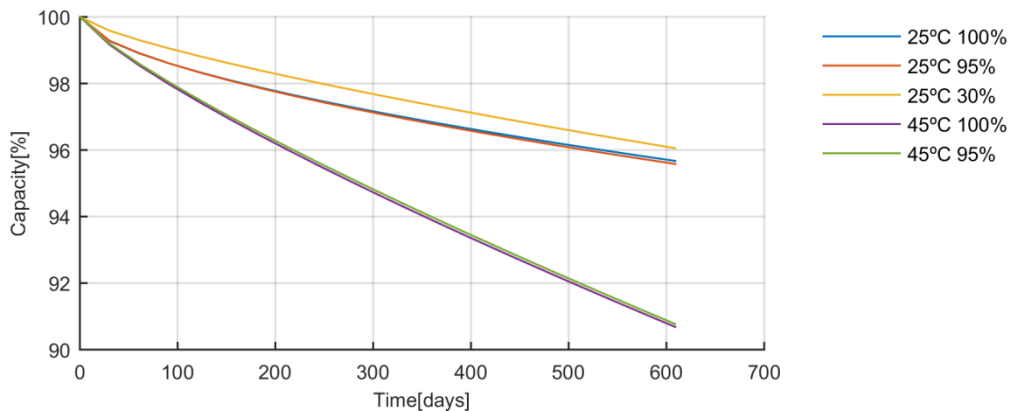


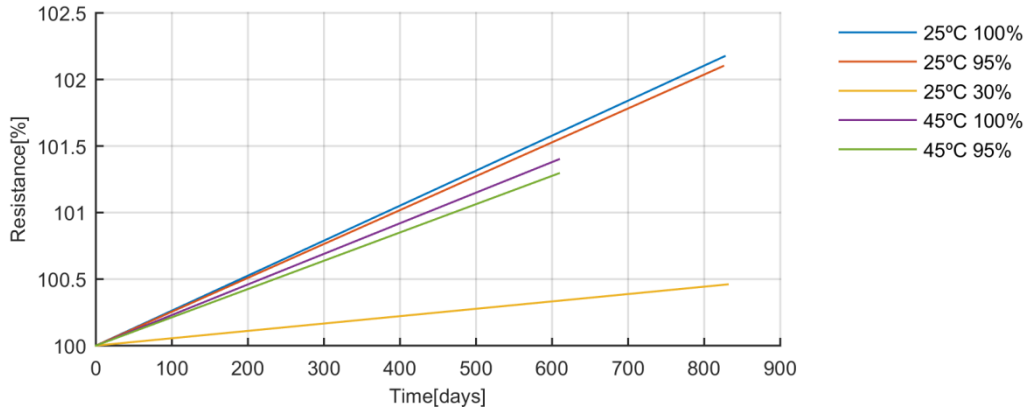
Figure 36: Aging trends of the dischargeable capacity decrease at different calendar conditions.

$$R_{calendar} = R_{ini} + var_1 \cdot t \quad (57)$$

$$var_1 = (-1.39e^{-7}) \cdot T + (2.96e^{-7}) \cdot SOC$$

Parameters	Description
$R_{calendar}$	The pure ohmic resistance evolution due to calendar aging.
R_{ini}	The pure ohmic resistance value at Beginning of life (initial value).
t	The resting time related to calendar aging in days.
var_1	The slope of the linear model.

T	The cell temperature at resting mode.
SOC	The mean SOC at resting mode.

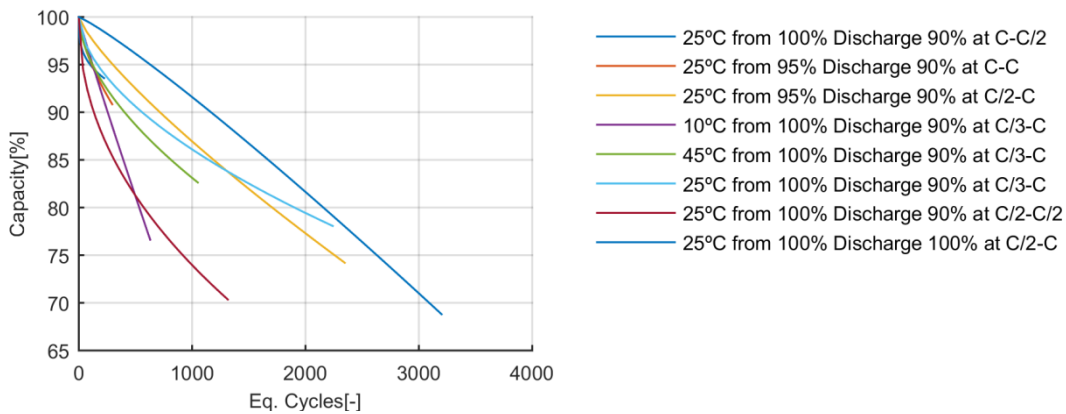
Table 51: Parameters of the calendar aging model of the pure ohmic resistance evolution

Figure 37: Aging trends of the pure ohmic resistance increase at different calendar conditions.

$$Q_{cycling} = Q_{ini} - var_1 \cdot cyc^{var_2} \quad (58)$$

$$\begin{cases} T < 25^\circ C & var_1 = (-1.96e^{-4}) \cdot T + (6.37e^{-4}) \cdot SOC + (-3.70e^{-4}) \cdot DOD \\ & \quad + (7.90e^{-5}) \cdot I_{cha} + (-2.58e^{-4}) \cdot I_{dch} \\ T \geq 25^\circ C & var_1 = (1.91e^{-5}) \cdot T + (6.37e^{-4}) \cdot SOC + (-3.70e^{-4}) \cdot DOD \\ & \quad + (7.90e^{-5}) \cdot I_{cha} + (-2.58e^{-4}) \cdot I_{dch} \end{cases}$$

$$\begin{cases} T < 25^\circ C & var_2 = (-3.89e^{-2}) \cdot T + (-5.73e^{-2}) \cdot SOC + (6.15e^{-2}) \cdot DOD \\ & \quad + (6.01e^{-3}) \cdot I_{cha} + (1.37e^{-3}) \cdot I_{dch} \\ T \geq 25^\circ C & var_2 = (5.91e^{-4}) \cdot T + (-5.73e^{-2}) \cdot SOC + (6.15e^{-2}) \cdot DOD \\ & \quad + (-6.01e^{-3}) \cdot I_{cha} + (-1.37e^{-3}) \cdot I_{dch} \end{cases}$$

Parameters	Description
$Q_{cycling}$	The dischargeable capacity evolution due to cycling aging.
Q_{ini}	The dischargeable capacity value at Beginning of life (initial value).
cyc	The equivalent cycles done at cycling operation mode.
var_1	The pre-power law variable.
var_2	The power law variable
T	The operation temperature.
SOC	The upper SOC on cycling operation mode.
DOD	The DOD.
I_{cha}	The charge current.
I_{dch}	The discharged current.

Table 52: Parameters of the cycling aging model of the dischargeable capacity evolution

Figure 38: Aging trends of the dischargeable capacity decrease at different cycling conditions.

$$R_{cycling} = R_{ini} + var_1 \cdot cyc \quad (59)$$

$$\begin{cases} T < 25^\circ C & var_1 = (1.48e^{-6}) \cdot T + (-2.17e^{-5}) \cdot SOC \\ & + (-5.99e^{-6}) \cdot I_{cha} + (-8.39e^{-6}) \cdot I_{dch} \\ T \geq 25^\circ C & var_1 = (2.82e^{-5}) \cdot T + (-2.17e^{-5}) \cdot SOC \\ & + (-5.99e^{-6}) \cdot I_{cha} + (-8.39e^{-6}) \cdot I_{dch} \end{cases}$$

Parameters	Description
$R_{cycling}$	The pure ohmic resistance evolution due to cycling aging.
R_{ini}	The pure ohmic resistance value at Beginning of life (initial value).
cyc	The equivalent cycles done at cycling operation mode.
var_1	The slope of the linear model.
T	The operation temperature.
SOC	The upper SOC on cycling operation mode.
I_{cha}	The charge current.
I_{dch}	The discharged current.

Table 53: Parameters of the cycling aging model of the pure ohmic resistance evolution

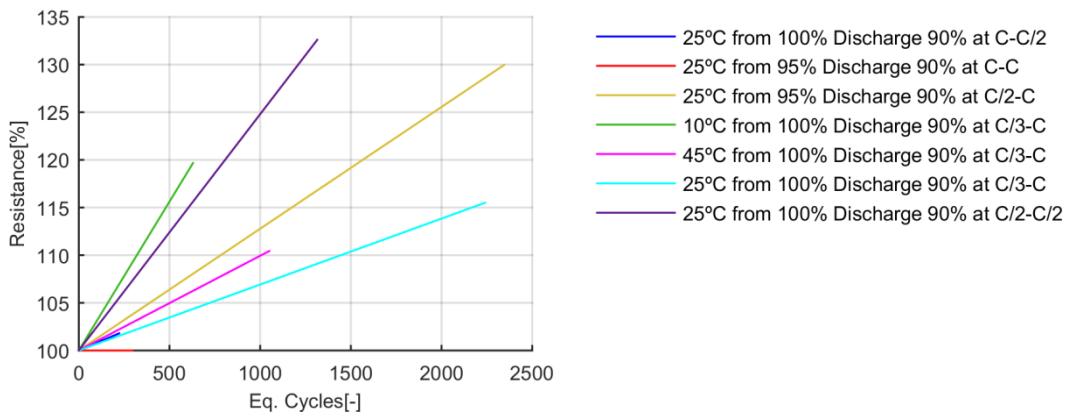


Figure 39: Aging trends of the pure ohmic resistance increase at different cycling conditions.

3.4.1.3 Aging Model Validation

The constructed aging models are validated in terms of the accuracy describing the observed cases, the correctness of interpolations and the real life applicability. For that, firstly, the response of the generated model and the data used on the construction of the model is evaluated with the Root Mean Square Error metric in Table 54.

	Calendar Aging Model		Cycling Aging Model	
	Dischargeable capacity [%]	Pure ohmic resistance [%]	Dischargeable capacity [%]	Pure ohmic resistance [%]
Test 1	0,36314	5,97195	0,34911	9,55325
Test 2	0,23575	8,47539	0,19305	15,1384
Test 3	0,16147	12,7900	3,16271	12,1440
Test 4	0,17353	2,29398	1,08660	15,6313
Test 5	0,21350	2,38823	0,33227	8,66537
Test 6			0,88194	10,7840
Test 7			1,09674	8,03807
Test 8			1,16814	

Table 54: RMSE between the response of the model and the data used to construct the model

The results show that the constructed model that describes the dischargeable capacity evolution has a maximum average fitting error of 3.2% and a fitting error below 1% on most of the tested cases (9 from 13). Based on this, the constructed aging model to describe the dischargeable capacity evolution is considered highly accurate on the observed cases. In contrast, the constructed model that describes the pure ohmic resistance evolution has a minimum fitting error above 2% and a maximum fitting error of 15%. In this case, the accuracy is low even on the observed cases. This happens due to the noise level on the resistance measurements, which is something that cannot be solved once the tests have been finished.

Secondly, the generated models are tested under a wide range non-variable operation conditions that are always inside the tested operation conditions. Basically, the operation conditions are interpolated in order to see if the model gives non-logical values. The results from the constructed aging models need to keep the logic of the expected aging trend:

- The dischargeable capacity will decrease with the rest and the cycling operation.
- The pure ohmic resistance will increase with the rest and the cycling operation.

The interpolated ranges are described in Table 55, taking into account that due to data limitations, the cycling aging model that describes the pure ohmic resistance evolution has 4 stress factors instead of 5; the DOD has not been modelled, so the interpolation of this stress factor is not done when evaluating the evolution of this health indicator. The results are shown in 3D figures; see Figure 40, Figure 41, Figure 42 and Figure 43. The z axis represents the health indicator value, the y axis represents the comparison variable on each operation mode (the calendar aging is related to the time elapsed in between measurements and the cycling aging is related to the discharged energy in terms of equivalent cycles) and the x axis represents all the stress factors all together in a synthesized manner, being the indexing values of each combination of these stress factors the ones displayed on the x axis ("Validation Test [-]").

Stress factor	Calendar aging		Cycling Aging				
	Operating temperature	Mean SOC	Operating temperature	Upper SOC	DOD	Charge current	Discharge current
Maximum value	45[°C]	100[%]	45[°C]	100[%]	100[%]	54[A]	54[A]
Minimum value	25[°C]	30[%]	10[°C]	95[%]	90[%]	18[A]	27[A]
Step	1[°C]	1[%]	2[°C]	1[%]	1[%]	2[A]	2[A]

Table 55: Interpolation cases possibilities on the aging model validation process of a High-Energy application

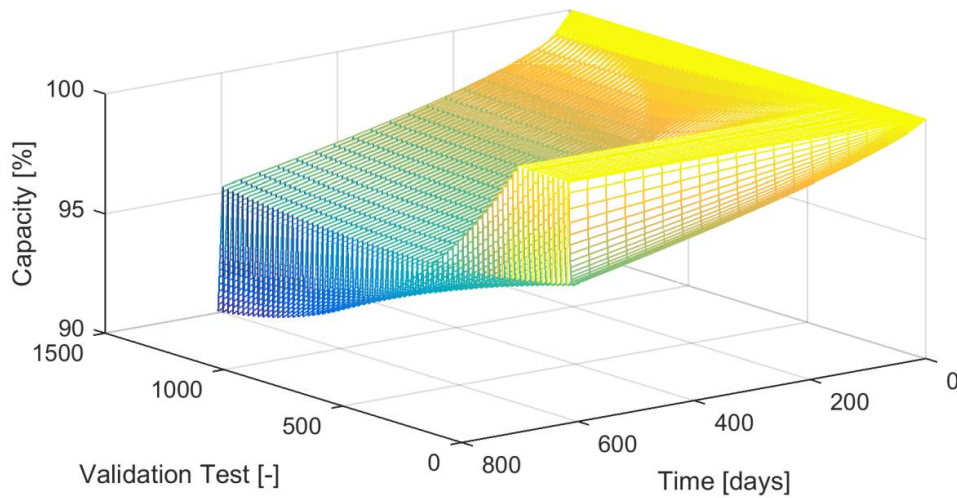


Figure 40: The dischargeable capacity map based on Calendar aging model interpolations.

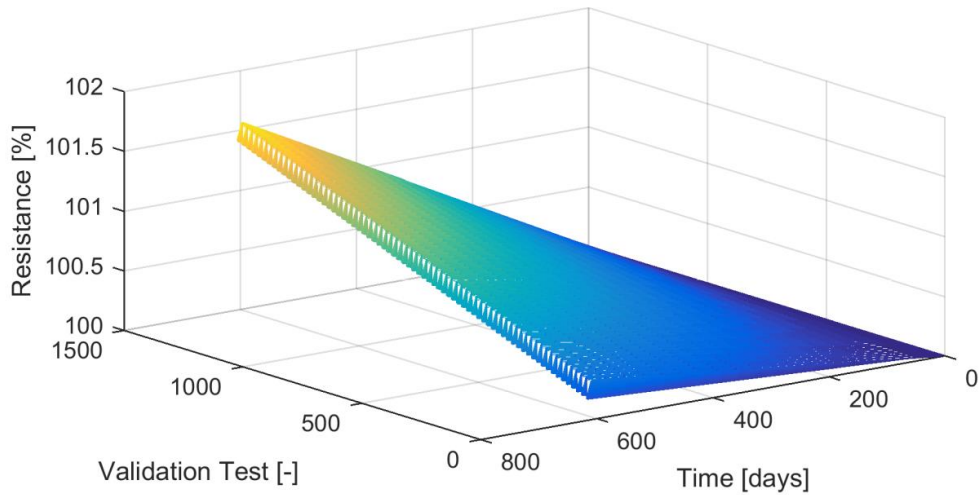


Figure 41: The pure ohmic resistance map based on calendar aging model interpolations.

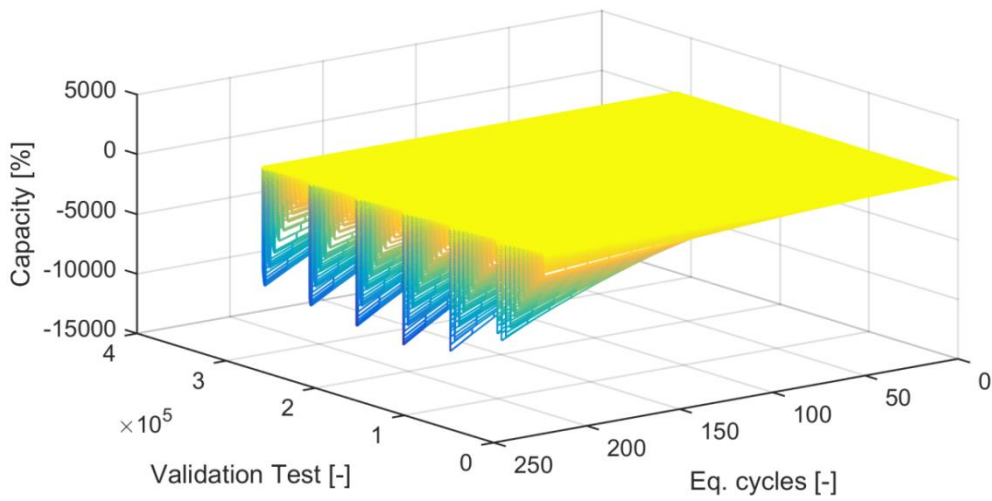


Figure 42: The dischargeable capacity map based on cycling aging model interpolations.

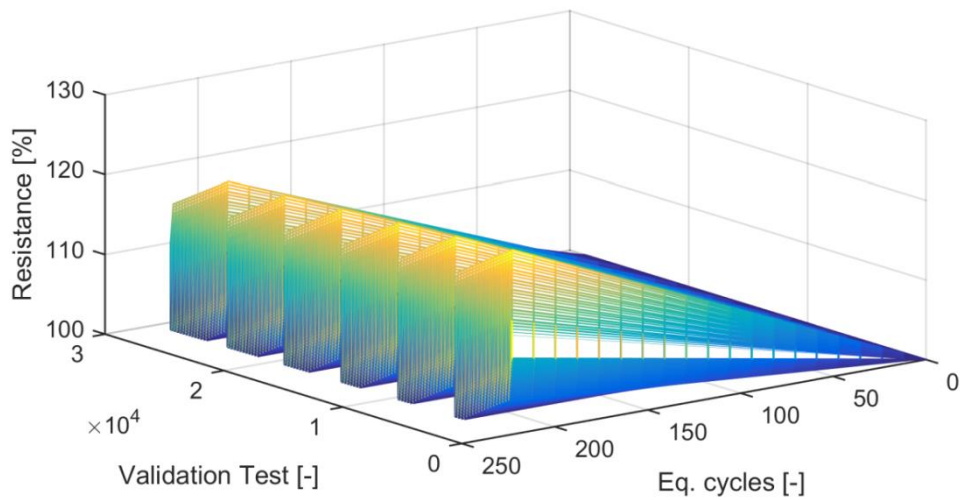


Figure 43: The pure ohmic resistance map based on cycling aging model interpolations.

The results show that the calendar aging model of the dischargeable capacity and the pure ohmic resistance give logical values for interpolated operation conditions (respect to the tested ones). The obtained dischargeable capacity evolution trends are delimited by the observed ones at the tested

cells. The same can be said on the cycling aging model of the pure ohmic resistance. Nonetheless, the cycling aging model of the dischargeable capacity shows more extreme trends inside interpolations, which means that the proposed model cannot describe properly operation conditions that are not tested beforehand. This is thought to be due to the huge amount of stress factors (5) and the sensibility of the proposed model (an exponential model generates huge changes on the final result with slight changes of the exponential variable).

The proposed model needs to be rebuilt from the scratch. For that, the Table 45 need to be reviewed. Among the other possibilities, the one that can be considered more simple than the exponential model would be the linear model. Besides, there is no a clear winner among the rest, which means that the linear model would be the most interesting one.

The stress factor modelling activity needs to be repeated with the selected linear model. The possible combinations of the mathematical expressions to describe the effect of the stress factors on the linear model that describes the dischargeable capacity evolution are a total of 5. The RMSE on each possible combination has been calculated, see Table 56.

Combination	Cycling aging
	Dischargeable capacity
1	6,16994
2	17,5313
3	20,3699
4	17,5313
5	75,2502

Table 56: The mean RMSE values of each combination of the proposed mathematical expressions ones rebuilt the model from scratch

The combination that gets the minimum RMSE among the evaluated ones is the first case (Eq. (60)). The obtained cycling aging model of the dischargeable capacity is shown in Figure 48.

$$Q_{cycling} = Q_{ini} - var_1 \cdot cyc \tag{60}$$

$$\begin{cases} T < 25^{\circ}C & var_1 = (3.95e^{-5}) \cdot T + (4.10e^{-6}) \cdot SOC + (-4.39e^{-6}) \cdot DOD \\ & + (5.94e^{-6}) \cdot I_{cha} + (-2.10e^{-6}) \cdot I_{dch} \\ T \geq 25^{\circ}C & var_1 = (3.60e^{-6}) \cdot T + (4.10e^{-6}) \cdot SOC + (-4.39e^{-6}) \cdot DOD \\ & + (5.94e^{-6}) \cdot I_{cha} + (-2.10e^{-6}) \cdot I_{dch} \end{cases}$$

Parameters	Description
$Q_{cycling}$	The dischargeable capacity evolution due to cycling aging.
Q_{ini}	The dischargeable capacity value at Beginning of life (initial value).
cyc	The equivalent cycles done at cycling operation mode.
var_1	The slope of the linear model.
T	The operation temperature.
SOC	The upper SOC on cycling operation mode.
DOD	The DOD.
I_{cha}	The charge current.
I_{dch}	The discharged current.

Table 57: Parameters of the corrected dischargeable capacity evolution cycling aging model

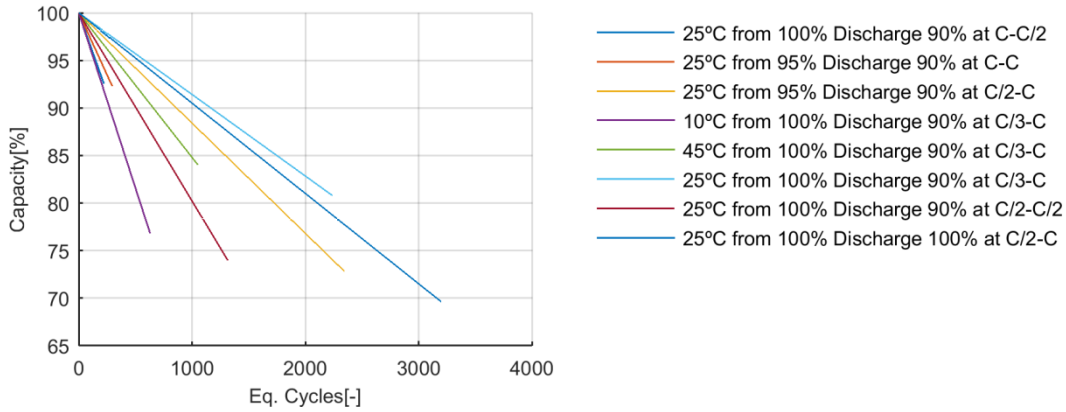


Figure 44: Aging trends of the dischargeable capacity decrease at different cycling conditions ones rebuilt the model from scratch.

The validation process is repeated once again. Firstly, the response of the generated model and the data used on the construction of the model is evaluated with the Root Mean Square Error metric in Table 58. Secondly, the validation of its capacity of interpolation is repeated and displayed in Figure 45

	Cycling Aging Model	
	Dischargeable capacity [%]	
Test 1	1,16748	
Test 2	1,89892	
Test 3	3,70878	
Test 4	1,45956	
Test 5	3,59956	
Test 6	5,77849	
Test 7	8,35217	
Test 8	0,92578	

Table 58: RMSE between the response of the model and the data used to construct the linear model

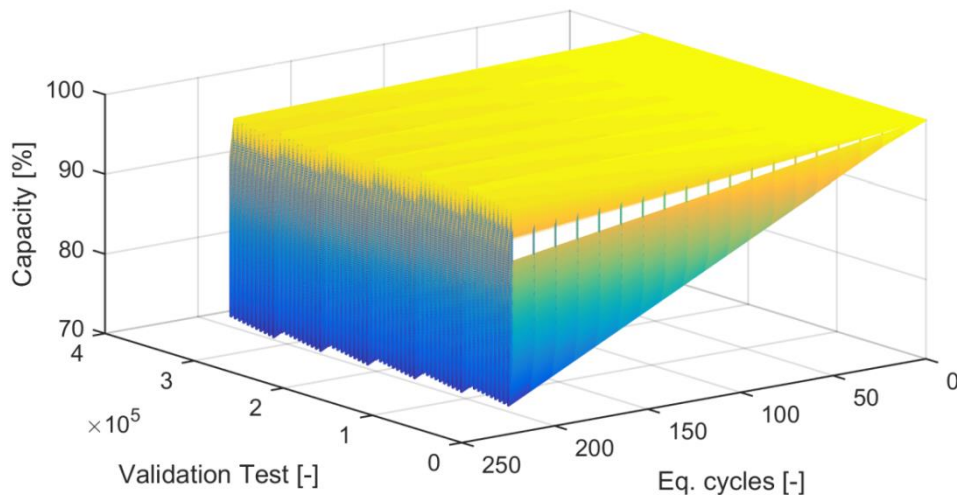


Figure 45: The dischargeable capacity map based on cycling aging model interpolations ones rebuilt the model from scratch.

The results show that the rebuilt model has a minimum fitting error of 1% and a maximum fitting error of 8%. The constructed linear model has much greater fitting errors than the previous power type model. However, it can be seen that the rebuilt model gives logical interpolated values now. This rebuilt cycling aging model that describes the dischargeable capacity evolution has a correct interpolation capacity in contrast with the previous one.

Thirdly, the applicability to real life application is tested. For that, the respond of the constructed aging model is evaluated with aging data obtained with real life cycles. In total, three tests with a real life cycle have been tested in parallel to the designed aging test matrix the 2 years of the project. These three tests consist on running the most probable operation use case profile at 10°C, 25°C and 45°C. The aging data has been obtained with the proposed ACT in the previous Aging Testing Definition section, from which the dischargeable capacity and the pure ohmic resistance evolution are subtracted (Figure 46 and Figure 47 respectively).

In order to apply the constructed aging model along with the obtained real life cycle aging data, the real life cycle need to be expressed with static stress factors. For that, the following assumptions are made:

- The mean values of the dynamic stress factors are representative of the generated aging with those dynamic stress factors.
- The effect of values of stress factors out of the range of the tested ones is considered the same as the nearest tested value.

After analysing the real life cycle profile based on these three assumptions, the static stress factors that represent the use profile of the High-Power application have been generated, see Table 59.

Upper SOC	DOD	Charge current	Discharge current
95[%]	88[%]→90[%]	54[A]	5.4[A]→27[A]

Table 59: The mean stress factor values that represent the operation condition of the proposed High-Power application use case

The constructed models of the dischargeable capacity and the pure ohmic resistance have been run with the representative values of the stress factors shown in Table 85. The results from the aging model and the gathered data of the selected health indicators, the dischargeable capacity and the pure ohmic resistance, are shown in Figure 46 and Figure 47 respectively. The error between measurement and estimation can be seen in Table 60.

	Real cycle at 25°C	Real cycle at 45°C	Real cycle at 10°C
Capacity RMSE [Ah]	1,20961	1,38364	1,22963
Resistance RMSE [Ω]	1.29e-4	1.07e-4	8.88e-5

Table 60: Root Mean Square Error between the measured and estimated values of the real life cycle aging health indicators (dischargeable capacity and pure ohmic resistance)

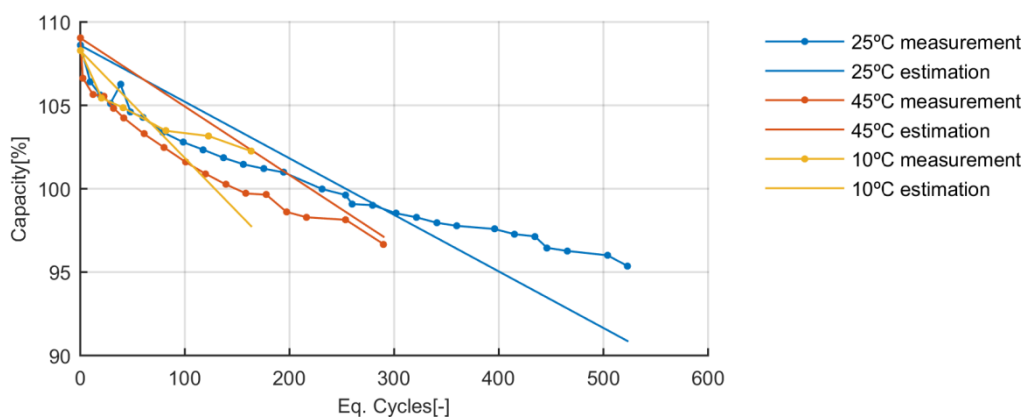


Figure 46: Dischargeable capacity evolution of the real High-Energy application use profile tested at three different temperatures: 10°C, 25°C and 45°C.

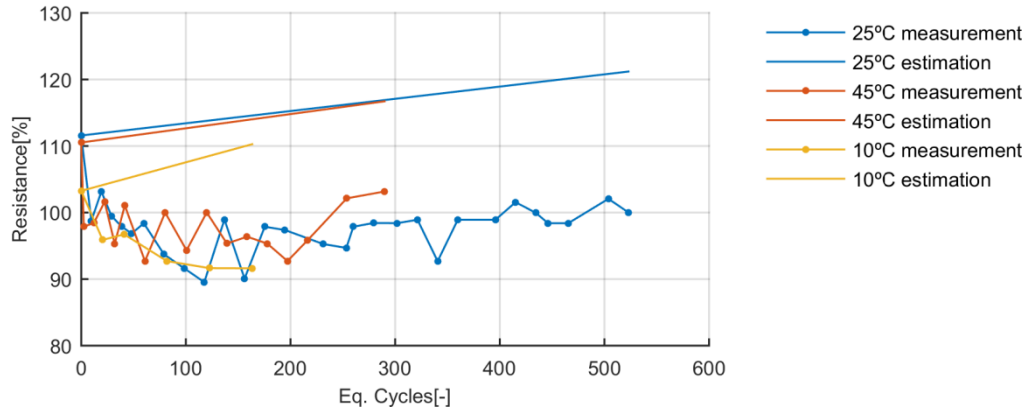


Figure 47: Pure ohmic resistance evolution of the real High-Energy application use profile tested at three different temperatures: 10°C, 25°C and 45°C.

The results show that the proposed models have low accuracy. The proposed dischargeable capacity decrease model does not capture the actual trend of this health indicator evolution. In this case, the initial results have shown that the power based mathematical expression fits the dischargeable capacity fade much better than the rest models. However, because of the not fulfilment of the interpolation validation (due to the sensibility of the parameter used on the power based mathematical expression and the high number of stress factors involved in the modelling), the linear model has been selected instead of the power based mathematical expression. Besides, it can be seen that the behaviour of the test at 10°C does not fit with the expected degradation rate. In Figure 33, the most harmful operation condition is done at 10°C with a huge difference. In contrast, the degradation rate experienced on the test at 10°C on Figure 46 shows less harmful effect than the tests at 25°C or at 45°C. This can mean two things, first, that the testing time has not been long enough to observe properly the degradation on those operation conditions; and second, it is not correct the assumption that the effect of the temperature is independent to the effect of the rest stress factors. Since the project was already finished, it has not been possible to generate more aging data. Therefore, it was not possible to check this issue. Besides, it is not possible to improve the model to describe the behaviour at 10°C. Therefore, it is validated that the constructed model is not able to describe the behaviour of the dischargeable capacity evolutions under temperatures below 25°C.

On the other hand, the pure ohmic resistance evolution is overestimated. This health indicator is expected to increase with aging but instead, it decreases. This phenomenon is observed on the results from the aging tests run at cycling operation mode in Figure 35. Firstly, the measured pure ohmic resistance is higher than the nominal one. After several ACTs, the resistance decreases to its nominal value and then starts increasing. In Figure 47, we can just see the first decrease to its nominal value. This is why there are huge errors in between the measurements and estimations. The project is already finished and it is not possible to lengthen the tests and get more data, so the model that describes the pure ohmic resistance evolution cannot be validated in terms of real life applicability.

To sum up, the interpolation capacity of the models has forced us to change the dischargeable capacity model at cycling operation mode (the rest have been validated). It has been selected a more simple model, which in this case is a linear model. On the other hand, the real life applicability has shown that this dischargeable capacity model at cycling operation mode does not capture correctly the aging trend of this health indicator and has been restricted to work in between temperature ranges from 25°C to 45°C. Moreover, due to lack of data, the pure ohmic resistance model has not been validated in terms of real life applicability.

3.4.2 Methodology validation on a High-Power Application

The high-power application consists on a battery integrated on an electric public bus. For that, a High-Power NMC-LTO prismatic battery has been chosen. The battery characteristics are shown in Table 61.

Item	Specification
Nominal Capacity	23 [Ah]
Fast charge current	115 [A]
Fast discharge current	115 [A]
Maximum temperature	55 [°C]
Minimum temperature	-30 [°C]

Table 61: High-Power battery specifications

3.4.2.1 Aging Testing Definition

Following the aging testing methodology, firstly the possible testing cases are reduced based on the delimitation imposed by the battery, see Table 62.

Stress factor	Operating temperature	Current	SOC	DOD
Maximum value	55[°C]	115[A]	100[%]	100[%]
Minimum value	-33[°C]	-115[A]	0[%]	0[%]
Minimum step	1[°C]	0.001[A]	1[%]	1[%]

Table 62: Testing cases possibilities on the first stage of the aging test matrix design on a High-Power application

Secondly, the obtained aging test matrix is further reduced based on the application characteristics. The application consists on a bus that makes a daily route 320 days of a year. The daily tour consists on repeating 13 times the same route that takes around 1h to fulfil it. Each time the route is finished, the bus is partly charged for 7 min (fast charge) before starting again the route. It takes around 16 hours to fulfil the 13 repetitions. Then, the bus goes to the garage for 8 h. There, the bus is charged at a normal charge current rate (slow charge) with a constant voltage stage when the end of charge voltage is reached. The working 16h is translated to a mean use profile of the battery (it is out of the scope of this thesis the way of getting this current profile). The mean current profile and the resultant energy evolution of the battery are shown in Figure 31.

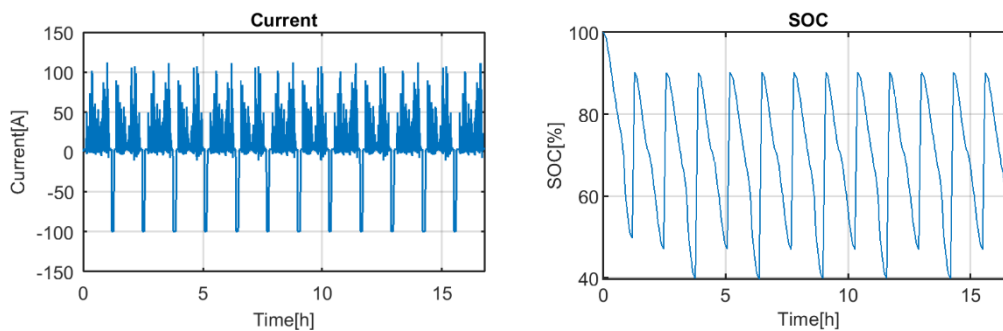


Figure 48: Application profile: current profile and the SOC evolution of the battery under that current profile at BOL. The positive values on the current profile represent the discharge current values while the negative values represent the charge current values.

After a proper evaluation, several key aspects about the mean application have been resumed:

- The battery will be on cycling mode 320 days per year (mostly, the aging will come from cycling aging).
- The mean discharge current is almost C/2.
- There are many excursions to peak currents above 4C.
- The use profile reduces the energy of the battery a 60% of the nominal one (the DOD of the application is 60%).
- The possible initial SOC value before initiating the route goes from 100% to 60%.

- The possible SOC after finishing the route goes from 40% to 0%.
- The temperature of operation will be $25 \pm 10^\circ\text{C}$.
- The fast charge current is 4C.
- The fast charge current is limited to 7min.
- The slow charge current is 1C.
- The batteries will be at a rest mode 45 days per year.
- The rest period can be done at end of charge or end of discharge condition (at SOC values from 100% to 60% and values from 40% to 0%), but the most probable scenario is leaving the bus charged at constant current before the beginning of this rest period (around 90%).
- The temperature on rest periods is the temperature at the garage, which is not controlled at holidays. The limit is placed on the temperature limits defined by the weather of the place of the application at the rest period season (spring and summer): $25^{+17}_{-15}^\circ\text{C}$.

Alternatives to the defined most probable operation condition would be:

- The current profile is reduced by increasing the number of batteries on the application. This is unlikely because it increases the costs (probability below 29%). It is placed the limit to a mean discharge current of C/3 with a DOD of 50%. This affects the rest time period conditions: SOC values from 100% to 0%.
- The current profile is increased by reducing the number of batteries on the application. This is likely to happen only if the application requirements are fulfilled (probability between 30% and 59%). A higher DOD could require a longer fast charge time, which is not acceptable. The limit is placed on a 1C discharge current with a total DOD of 75% keeping the maximum fast charge time of 7min.
- The operation temperature range can be increased by simplifying the thermal management system. This is likely to happen (probability between 30% and 59%). The limit is placed on the temperature limits defined by the weather of the place of the application: $25^{+17}_{-30}^\circ\text{C}$.
- The fast charge current is decreased to 3C. It is very likely to happen (probability between 60% and 90%).
- The slow charge current is reduced to C/3. It is very likely to happen (probability between 60% and 90%).
- The amount of days on operation is likely to change. It doesn't affect the aging test matrix.

Once the application characteristics are properly evaluated, the possible testing cases that fits the application requirements is generated, see Table 63. For that, firstly, the testing cases are divided in the operation modes that appear on the application: cycling and resting (this makes reference to the cycling aging and calendar aging respectively). Then, the stress factors of interest on each operation mode are redefined. In this application, there are two changes from the defined generic stress factors: the current and the SOC. The effect of the current is divided in terms of the sign of the current and the effect of the SOC is presented as an average value or as a range of values. The current is divided in two in order to properly define the effect of negative currents on one hand (the charging process) and the positive current on the other hand (the discharging process). The SOC is presented in average value for resting periods, since there is no SOC change in this operation mode. Nonetheless, the cycling operation mode generates a change on the SOC; this is why the range of SOC values is presented instead of the average used on the resting period.

Operation mode		Operation temperature	Charge current	Discharge current	DOD	SOC range	Average SOC
Resting	MIN	10[°C]					0[%]
	MAX	42[°C]					100[%]
	STEP	1[°C]					1[%]
Cycling	MIN	-5[°C]	-115[A]	0[A]	50[%]	50[%]-0[%] / ... / 100[%]-50[%]	
	MAX	42[°C]	0[A]	115[A]	75[%]	75[%]-0[%] / ... / 100[%]-25[%]	
	STEP	1[°C]	0.001[A]	0.001[A]	1[%]	1[%]	

Table 63: Stress factors of calendar and cycling aging

Before the last stage of restraining the aging test matrix, the importance of the testing cases needs to be expressed in a user-friendly way. In this context, the concept of the proposed colour system is applied. Firstly, a matrix containing the red testing cases has been built, see Table 64. Here, the condition that describes better the application requirements is highlighted (the levels of the stress factors that describe this operation condition are turned red). In total, we get 9 testing cases to describe the calendar aging behaviour and 189 testing cases to describe the cycling aging behaviour.

Operation mode	Level	Operation temperature	Charge current	Discharge current	DOD	SOC range	Average SOC
Resting	1	10[°C]					0[%]
	2	25[°C]					50[%]
	3	42[°C]					100[%]
Cycling	1.1	15[°C]	-92[A]	92[A]	75[%]	100[%]-25[%]	
	1.2					90[%]-15[%]	
	1.3					75 [%]-0[%]	
	2.1	25[°C]	-57[A]	52[A]	60[%]	100[%]-40[%]	
	2.2					80[%]-20[%]	
	2.3					60[%]-0[%]	
	3.1	35[°C]	-23[A]	12[A]	50[%]	100[%]-50[%]	
	3.2					75[%]-25[%]	
	3.3					50[%]-0[%]	

Table 64: The Red testing cases. The levels of the stress factors that are in red describe the most probable operation condition defined on the application requirements

Following the advice done at the end of the methodology, the generated test matrix is presented to CIDETEC’s lab. First of all, the viability of testing the proposed operations conditions is evaluated. CIDETEC’s facilities are able to test the defined conditions; however, there are limit resources that need to be shared with some other projects. This is why the actual lab availability has forced the following changes on the stress factor levels:

- The absolute value of the current must be above 23A (1C) since it supposes to occupy the lab resources more than the acceptable project time.
- The temperatures available on cycling operation mode are 10°C, 25°C and 45°C.

Operation mode	Level	Operation temperature	Charge current	Discharge current	DOD	SOC range	Average SOC
Resting	1	10[°C]					0[%]
	2	25[°C]					50[%]
	3	45[°C]					100[%]
Cycling	1.1	10[°C]	-92[A]	92[A]	75[%]	100[%]-25[%]	
	1.2					90[%]-15[%]	
	1.3					75 [%]-0[%]	
	2.1	25[°C]	-57[A]	52[A]	60[%]	100[%]-40[%]	
	2.2					80[%]-20[%]	
	2.3					60[%]-0[%]	
	3.1	45[°C]	-23[A]	23[A]	50[%]	100[%]-50[%]	
	3.2					75[%]-25[%]	
	3.3					50[%]-0[%]	

Table 65: The Red testing cases after a first iteration with the lab. The levels of the stress factors that are in red describe the most probable operation condition defined on the application requirements. The blue values are the ones modified after the first iteration with the lab

As a result, firstly, the values of the tested temperature on the cycling operation mode and on the resting operation mode are changed; and secondly, the testing case that describes better the application disappears from the testing cases, see Table 65. The change on the temperature values on both operation modes does not affect too much the obtainable result. The restrictions have increased the tested limits but all the values of interest are still inside the tested operation window, so it is considered acceptable. However, the restriction on the current leaves the case of interest outside the tested window (the lower tested value is higher than the one of interest), so assumptions on modelling level are required:

- The aging effect due to discharge currents below 1C is assumed to be the same as the one generated with a C/2 current. The difference that could be is considered negligible.

After that, the numbers of cases that can be tested are discussed. After a proper evaluation of the importance of the project, the cost of samples and the availability of resources, the maximum testing cases have been set on 5 on resting operation mode and 9 on testing the cycling operation mode. Since the red testing case matrix needs to be reduced, there is no sense on developing the orange, yellow and white testing case matrixes.

In other to reduce the calendar aging testing cases from 9 to 5, we need to reduce the levels and combinations of stress factors. In this case, the 0% SOC has been directly nominated since it was unlikely to happen. This level was added to improve the calendar aging behaviour description at low SOC. As result, a new calendar aging test matrix of 6 testing is generated, see Table 66. In this point, a combination between the temperature and the SOC needs to be nominated. For that, the preference and likelihood of the application is evaluated:

- The tested cases at 25°C are the most probable cases (cannot be nominated).
- Among the temperature, the cases with 10°C are the least probable cases since the resting operation mode happens on spring and summer (likely to nominate).
- The most likely SOC is 100% (the 100% SOC shouldn't be nominated).

As a result, the nominated test is the testing case at 10°C and at 50% SOC.

Test nº	Temperature [°C]	SOC [%]
1	10	100
2	10	50
3	25	100
4	25	50
5	45	100
6	45	50

Table 66: The Aging test matrix to characterize the calendar aging with 6 testing cases. The cases that are in red are the selected ones as the final ones

In other to reduce the cycling aging testing cases from 189 to 9, we need to reduce the levels and combinations of stress factors to the minimum. First of all, the levels need to be reduced to a minimum acceptable for the posterior modelling. The process in this application is as follow:

- DOD: The least probable DOD is nominated, which is the 50% DOD (it is unlikely to increase the amount of batteries).
- SOC range: The most likely operation consists on charging completely the battery (SOC ranges up to 100%) so the low limits are nominated. In addition to this, the middle value is put in common; the SOC range of 80% to 20% with a 60% DOD is changed to a SOC range of 90% to 30%.
- Charge current: It appears in two levels along the application, at 1C and at 4C. The three levels are left as they are.
- Discharge current: The maximum discharge current could be nominated since the application is very unlikely to work around this value.
- Operation temperature: The effect of the temperature is expected to suffer an increase at low temperatures and high temperatures, so a minimum of 3 points is required. It is not nominated any of the values on the temperature stress factor.

As a result of the nominations, a reduced test matrix can be generated, see Table 67. In this table the SOC range is defined by the upper SOC of this same SOC range.

Operation temperature	Charge current	Discharge current	DOD	Upper SOC
10[°C]	-92[A]	52[A]	75[%]	100[%]
25[°C]	-57[A]	23[A]	60[%]	90[%]
45[°C]	-23[A]	-	-	-

Table 67: The reduced testing cases on the cycling operation mode

The new proposed matrix generates a total of 72 testing cases, which are still way above the defined 9 testing cases. However, the levels of the stress factors cannot be reduced further. In this scenario, the combinations between the levels are gradually restricted.

Firstly, the tested temperature combinations are restricted. The three values of the temperature stress factor are only applied on the most probable and stressful operation condition: a 4C charge with a 1C discharge with a 60% DOD and with a SOC range of 100% to 40%. Then, the combinations of the rest stress factors (current, DOD and SOC) are done all at 25°C. However, a modelling assumption is required:

- The effect of the temperature on the cycling aging is independent to the current, DOD or SOC ranges if working on the safety window.

As a result, the total testing cases are reduced from 72 to 26, see Table 68. In this point, the combination between the DOD, SOC range and currents need to be reduced to 7. One of the 7 testing cases is already defined and cannot be changed: a 4C charge with a 1C discharge with a 60% DOD and with a SOC range of 100% to 40% at 25°C. Besides, since there are two levels of the charge current on a normal operation, it is imposed another testing case: a 1C charge with a 1C discharge with a 60% DOD and with a SOC range of 100% to 40% at 25°C. The rest 6 cases are selected based on the experience while maintaining some conditions:

- All the defined levels of every stress factor need to appear on the selected conditions.
- The most probable levels of the stress factors will be the ones with more presence on the selected testing cases.
- The more disperse the operation conditions of the testing cases are, the better the covered tested dimension will be.

The selected 9 cases are put on red in Table 68.

Test nº	Temperature [°C]	Upper SOC [%]	DOD [%]	Charge C-rate [%]	Discharge C-rate [%]
1	10	100	60	4	1
2	45	100	60	4	1
3	25	100	60	4	1
4	25	100	60	4	2.3
5	25	100	60	2.5	1
6	25	100	60	2.5	2.3
7	25	100	60	1	1
8	25	100	60	1	2.3
9	25	100	75	4	1
10	25	100	75	4	2.3
11	25	100	75	2.5	1
12	25	100	75	2.5	2.3
13	25	100	75	1	1
14	25	100	75	1	2.3
15	25	90	60	4	1
16	25	90	60	4	2.3
17	25	90	60	2.5	1
18	25	90	60	2.5	2.3
19	25	90	60	1	1
20	25	90	60	1	2.3
21	25	90	75	4	1
22	25	90	75	4	2.3
23	25	90	75	2.5	1
24	25	90	75	2.5	2.3
25	25	90	75	1	1
26	25	90	75	1	2.3

Table 68: The Aging test matrix to characterize the cycling aging with 26 testing cases. The cases that are in red are the selected ones as the final ones

In this point, the customer was consulted and a discussion was started. Firstly, the calendar aging test matrix was evaluated. Here, the customer asked us to introduce a new SOC level. The customer

showed an interest in analysing the effect of operating the bus on resting mode with or without a previous charge. In this scenario, the added level is 30% of SOC because it is inside the operation range and because the suppliers used to send the batteries at this same SOC (considered the least detrimental SOC on resting periods). On the same hand, the customer discarded the 100% SOC level since he claimed that it was very unlikely to reach this value before a rest period. In consequence, the SOC levels were finally modified to 90%, 60% and 30%.

Among the generated 9 new cases, the cases at 90% SOC were kept at the three temperature levels due to the high interest of the customer on this regard. Then, the other two SOC levels were tested at 45°C, since it was expected to have higher probability of occurrence of temperatures of 45°C than temperatures of 10°C (resting mode at spring and summer) and because fast results were demanded (it is expected to have higher degree of deterioration at cells stored at 45°C than at 25°C). The accepted final calendar aging test matrix is shown in Table 69.

Test n°	Temperature [°C]	SOC [%]
1	25	90
2	45	90
3	10	90
4	45	60
5	45	30

Table 69: Aging test matrix to characterize the calendar aging

Secondly, the cycling aging test matrix was discussed. Due to interests of future application of the selected battery, several modifications were introduced:

- The maximum charge current rate was increased to the maximum value (5C).
- The discharge current rate at higher levels was demanded. The maximum discharge current was raised to 3C.
- The testing of a lower level of DOD was asked. The lower DOD was modified to 50%.
- The maximum upper SOC was restricted to 95%. In consequence, the 90% of upper SOC was reduced to have a minimum difference between levels of 10% of SOC in order to increase the case inside the testing conditions.
- The temperature evaluation was modified to an operation condition of 95% upper SOC, 50% DOD, 1C charge current rate and 1C discharge current rate.

Considering all these changes, the final cycling aging test matrix is generated (Table 70).

Test n°	Temperature [°C]	Upper SOC [%]	DOD [%]	Charge C-rate [%]	Discharge C-rate [%]
1	25	100	50	1	1
2	25	100	50	3	1
3	25	100	50	5	1
4	25	100	50	1	3
5	10	100	50	1	1
6	45	100	50	1	1
7	25	100	75	1	1
8	25	90	50	1	1
9	25	90	75	1	1

Table 70: Aging test matrix to characterize the cycling aging

The final proposals of the cycling aging test matrix and the calendar aging test matrix were accepted by the lab and the tests defined on Table 69 and Table 70 were scheduled to run for 3 years, but before starting the tests, the ACT was designed. The long ACTs used at BOL and EOL contain a capacity, an OCV and an impedance characterization test. The selected OCV characterization test is done with a continuous small C-rate. The selected impedance characterization test is done with repeated charge and discharge pulse test on the whole operation SOC range with a step of 10% SOC. The short ACT contains the suggested capacity and impedance characterization test.

3.4.2.2 Aging Model Construction

After finishing the 3 years of testing period, the performed ACTs have been treated and the health indicators of interest have been obtained:

- Dischargeable capacity (see Figure 49 and Figure 50).
- Pure ohmic resistance (see Figure 51 and Figure 52).

The comparison of the obtained results is done in terms of days in the case of calendar aging and in terms of energy throughput or equivalent cycles in the case of cycling aging. The days make reference to the total time in days elapsed in between measurements. The energy throughput or equivalent cycles make reference to the total energy discharged in between measurements. The energy throughput is directly the Wh discharged and the equivalent cycle is the Wh discharged divide by the nominal energy in Wh.

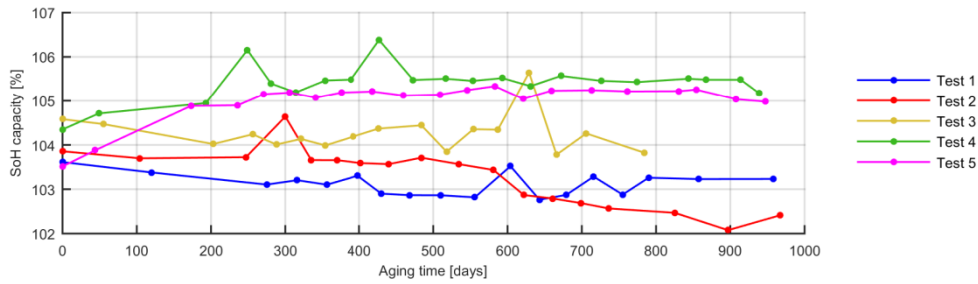


Figure 49: Relative dischargeable capacity values of the tested batteries under the calendar aging test matrix.

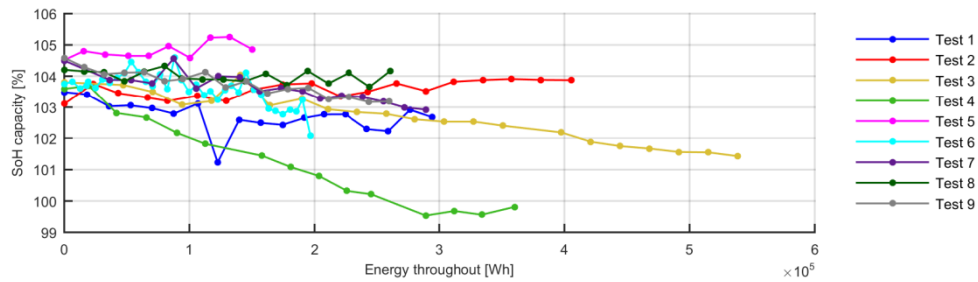


Figure 50: Relative dischargeable capacity values of the tested batteries under the cycling aging matrix.

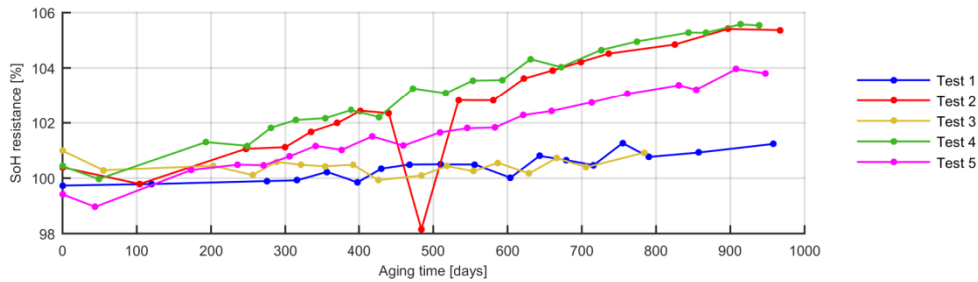


Figure 51: Relative pure ohmic resistance values of the tested batteries at 50% SOC under the calendar aging matrix.

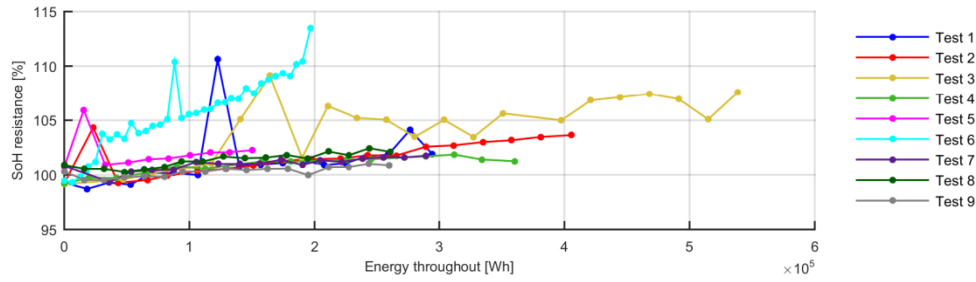


Figure 52: Relative pure ohmic resistance values of the tested batteries at 50% SOC under the cycling aging matrix.

Afterwards, the obtained data has been analysed. In a first glance, it has been seen that the dischargeable capacity on all the tests of the defined calendar and cycling aging test matrixes except one are still above the nominal value given by the datasheet, even though being running for 3 years. We cannot observe properly the decay trend of the dischargeable capacity. However, the project cannot be lengthened anymore.

Then, the proposed modelling methodology has been followed. The first stage of the proposed modelling methodology consists on choosing the mathematical expression that fits better the selected health indicators (dischargeable capacity and the pure ohmic resistance). The tested mathematical expressions are shown in Table 71.

Aging	Linear	Exponential	Logarithmic	Power type	2 nd order polynomial
Calendar	x	x	x	x	x
Cycling	x	x	x	x	x

Table 71: Applicable mathematical expressions to the obtained data from the aging test matrix

The fitting accuracy is measured with the Root Mean Square Error (RMSE) metric between the measurements and the estimation done with the fitted mathematical expression. This metric has been calculated on each test of both aging test matrix for the two selected health indicators. The mean of the obtained RMSE values on all the tests of the run aging test matrix is added as well, see Table 72, Table 73, Table 74 and Table 75.

	Linear	Exponential	Logarithmic	Power type	2 nd order polynomial
Test 1	0,00438	0,00388	0,00412	0,00406	0,00438
Test 2	0,00258	0,00258	0,00258	0,00258	0,00258
Test 3	0,00207	0,00206	0,00568	0,00199	0,00199
Test 4	0,00300	0,00226	0,00864	0,00233	0,00300
Test 5	0,00243	0,00243	0,00243	0,00243	0,00243
Test 6	0,00362	0,00291	0,00454	0,00295	0,00314
Test 7	0,00223	0,00225	0,00327	0,00221	0,00219
Test 8	0,00178	0,00173	0,00181	0,00174	0,00178
Test 9	0,00133	0,00155	0,00319	0,00130	0,00133
Mean RMSE	0,00260	0,00241	0,00403	0,00240	0,00254

Table 72: Fitting RMSE of the dischargeable capacity evolution data with the proposed cycling aging models

	Linear	Exponential	Logarithmic	Power type	2 nd order polynomial
Test 1	0,02397	0,02318	0,02423	0,02365	0,02397
Test 2	0,01073	0,01008	0,01298	0,01024	0,01024
Test 3	0,01923	0,01686	0,02101	0,01790	0,01923
Test 4	0,00357	0,00189	0,00392	0,00233	0,00357
Test 5	0,01402	0,01348	0,01398	0,01398	0,01402
Test 6	0,01211	0,01322	0,01989	0,01153	0,01211
Test 7	0,00334	0,00305	0,00523	0,00332	0,00334
Test 8	0,00265	0,00224	0,00605	0,00259	0,00264
Test 9	0,00265	0,00248	0,00442	0,00260	0,00263
Mean RMSE	0,01025	0,00961	0,01241	0,00979	0,01020

Table 73: Fitting RMSE of the pure ohmic resistance evolution data with the proposed cycling aging models

	Linear	Exponential	Logarithmic	Power type	2 nd order polynomial
Test 1	0,00236	0,00208	0,00214	0,00213	0,00236
Test 2	0,00334	0,00257	0,00613	0,00283	0,00284
Test 3	0,00414	0,00406	0,00407	0,00407	0,00414
Test 4	0,00408	0,00408	0,00408	0,00408	0,00408
Test 5	0,00442	0,00442	0,00442	0,00442	0,00442
Mean RMSE	0,00367	0,00344	0,00417	0,00351	0,00357

Table 74: Fitting RMSE of the dischargeable capacity evolution data with the proposed calendar aging models

	Linear	Exponential	Logarithmic	Power type	2 nd order polynomial
Test 1	0,002217	0,00215	0,00420	0,00214	0,00214
Test 2	0,010746	0,01037	0,01818	0,01034	0,01038
Test 3	0,002738	0,00244	0,00273	0,00273	0,00269
Test 4	0,00233	0,00253	0,01450	0,00232	0,00233
Test 5	0,00192	0,00290	0,01156	0,00192	0,00192
Mean RMSE	0,00399	0,00408	0,01023	0,00389	0,00389

Table 75: Fitting RMSE of the pure ohmic resistance evolution data with the proposed calendar aging models

The fitting of the data of both health indicators show that there is not a clear winner. The biggest improvement respect to the simplest model is below 50% on all the cases. The difference cannot be defined as relevant. Therefore, the simplest model (linear model) is selected.

Next stage consists on linking the variables of the selected mathematical expressions and the stress factors. The applicable mathematical expressions for that aim are shown in Table 47 and Table 62. Here, the complexity of the available mathematical expression depends on the tested levels and the assumed hypotheses on the aging test matrix design. In this case, both the effect of low temperatures and the effect of high temperatures are tested and therefore, modelled on both aging test matrix. For this, a non-linear mathematical expression based on two linear equations is formulated to model linearly on one hand the effect of low temperatures and on the other hand the effect of high temperatures on calendar aging model as well as on the cycling aging model. The upper SOC, DOD and discharge current effect are evaluated with 2 levels each, so a linear model is only applicable. In contrast, the mean SOC and the charge current effect are evaluated with 3 levels, so some more mathematical expressions are evaluated; see Table 47 and Table 62 respectively.

Stress factor	Linear	Exponential	Logarithmic	Power type	2 nd order polynomial	Double Linear
Mean SOC	x	x	x	x	x	
Temperature						x

Table 76: The applicable mathematical expressions to link the stress factors and the free variables designed on the calendar aging model of the High-Power application

Stress factor	Linear	Exponential	Logarithmic	Power type	2 nd order polynomial	Double Linear
Upper SOC	x					
Temperature						x
DOD	x					
Charge C-rate	x	x	x	x	x	
Discharge C-rate	x					

Table 77: The applicable mathematical expressions to link the stress factors and the free variables designed on the cycling aging model of the High-Energy application

The possible combinations of these mathematical expressions are a total of:

- 5 for the calendar aging model that describes the dischargeable capacity evolution.
- 5 for the calendar aging model that describes the pure ohmic resistance evolution.
- 5 for the cycling aging model that describes the dischargeable capacity evolution.
- 5 for the cycling aging model that describes the pure ohmic resistance evolution.

The RMSE on each possible combination has been calculated, see Table 78.

Combination	Calendar aging		Cycling aging	
	Dischargeable capacity	Pure ohmic resistance	Dischargeable capacity	Pure ohmic resistance
1	0.10389	1,39e-05	0,25893	3,34e-05
2	0.13880	1,75e-05	20,9965	0,00399
3	0.16611	1,95e-05	21,0173	0,00399
4	0.13880	1,75e-05	20,9965	0,00399
5	0.10389	1,39e-05	39,8590	0,00452

Table 78: The mean RMSE values of each combination of the proposed mathematical expressions

The combination that gets the minimum RMSE among the evaluated ones are the first case for both health indicators, the dischargeable capacity and the pure resistance increase, on the cycling aging model (Eq. (61) and Eq. (62)) In the case of both health indicators on the calendar aging model, the first combination gets the same value as the fifth combination. In case of doubt, the simplest model is chosen. In this case, the simplest model is the first combination (two linear models, Eq. (63) and Eq. (64)).

The obtained calendar aging model of the selected two health indicators, the dischargeable capacity and the pure ohmic resistance, are shown in Figure 53 and Figure 54 respectively. The obtained cycling aging model of the selected two health indicators, the dischargeable capacity and the pure ohmic resistance, are shown in Figure 55 and Figure 56 respectively.

$$Q_{calendar} = Q_{ini} - var_1 \cdot t \quad (61)$$

$$\begin{cases} T < 25^{\circ}C & var_1 = (-2.94e^{-7}) \cdot T + (1.01e^{-7}) \cdot SOC \\ T \geq 25^{\circ}C & var_1 = (-7.69e^{-8}) \cdot T + (1.01e^{-7}) \cdot SOC \end{cases}$$

Parameters	Description
$Q_{calendar}$	The dischargeable capacity evolution due to calendar aging.
Q_{ini}	The dischargeable capacity value at Beginning of life (initial value).
t	The resting time related to calendar aging in days.
var_1	The pre-power law variable.
var_2	The power law variable.
T	The cell temperature at resting mode.
SOC	The mean SOC at resting mode.

Table 79: Parameters of the calendar aging model of the dischargeable capacity evolution

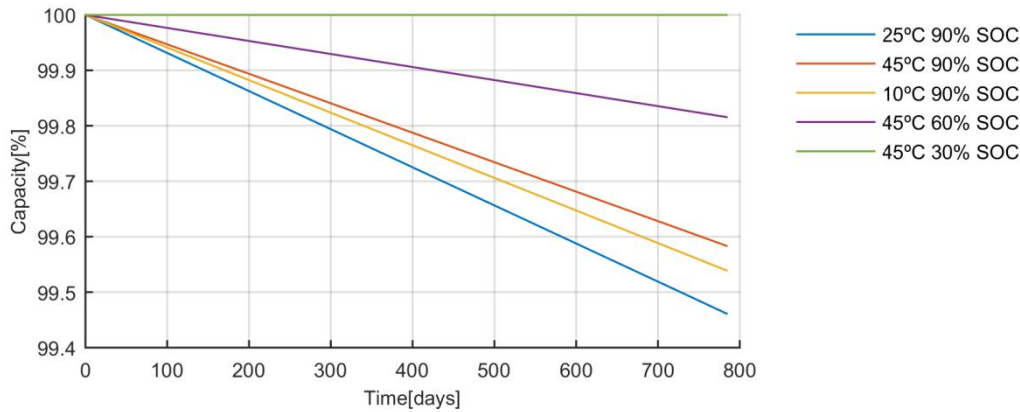


Figure 53: Aging trends of the dischargeable capacity decrease at different calendar conditions.

$$R_{calendar} = R_{ini} - var_1 \cdot t \quad (62)$$

$$\begin{cases} T < 25^{\circ}C & var_1 = (-1.50e^{-6}) \cdot T + (1.07e^{-7}) \cdot SOC \\ T \geq 25^{\circ}C & var_1 = (-1.17e^{-6}) \cdot T + (1.07e^{-7}) \cdot SOC \end{cases}$$

Parameters	Description
$R_{calendar}$	The pure ohmic resistance evolution due to calendar aging.
R_{ini}	The pure ohmic resistance value at Beginning of life (initial value).
t	The resting time related to calendar aging in days.

var_1	The pre-power law variable.
var_2	The power law variable.
T	The cell temperature at resting mode.
SOC	The mean SOC at resting mode.

Table 80: Parameters of the calendar aging model of the pure ohmic resistance evolution

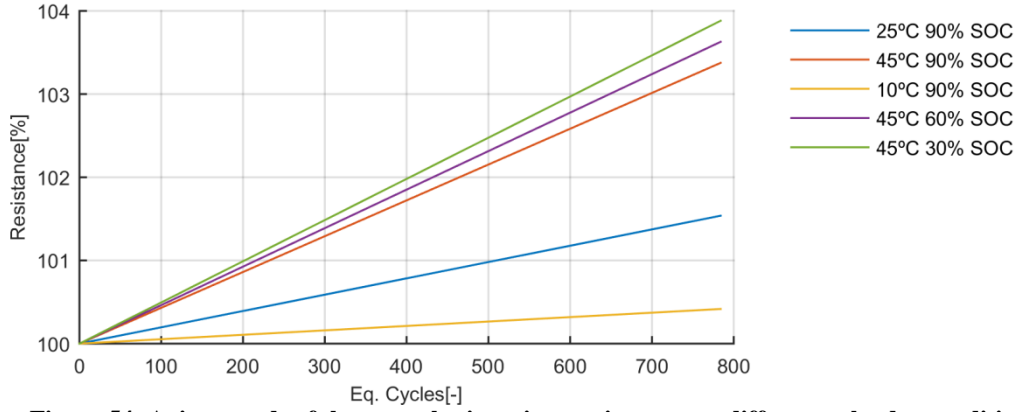


Figure 54: Aging trends of the pure ohmic resistance increase at different calendar conditions.

$$Q_{cycling} = Q_{ini} - var_1 \cdot cyc \quad (63)$$

$$\begin{cases} T < 25^\circ C & var_1 = (3.15e^{-7}) \cdot T + (-1.76e^{-8}) \cdot SOC + (8.66e^{-8}) \cdot DOD \\ & + (2.04e^{-8}) \cdot I_{cha} + (1.33e^{-7}) \cdot I_{dch} \\ T \geq 25^\circ C & var_1 = (1.35e^{-7}) \cdot T + (-1.76e^{-8}) \cdot SOC + (8.66e^{-8}) \cdot DOD \\ & + (2.04e^{-8}) \cdot I_{cha} + (1.33e^{-7}) \cdot I_{dch} \end{cases}$$

Parameters	Description
$Q_{cycling}$	The dischargeable capacity evolution due to cycling aging.
Q_{ini}	The dischargeable capacity value at Beginning of life (initial value).
cyc	The equivalent cycles done at cycling operation mode.
var_1	The slope of the linear model.
T	The operation temperature.
SOC	The upper SOC on cycling operation mode.
DOD	The DOD.
I_{cha}	The charge current.
I_{dch}	The discharged current.

Table 81: Parameters of the cycling aging model of the dischargeable capacity evolution

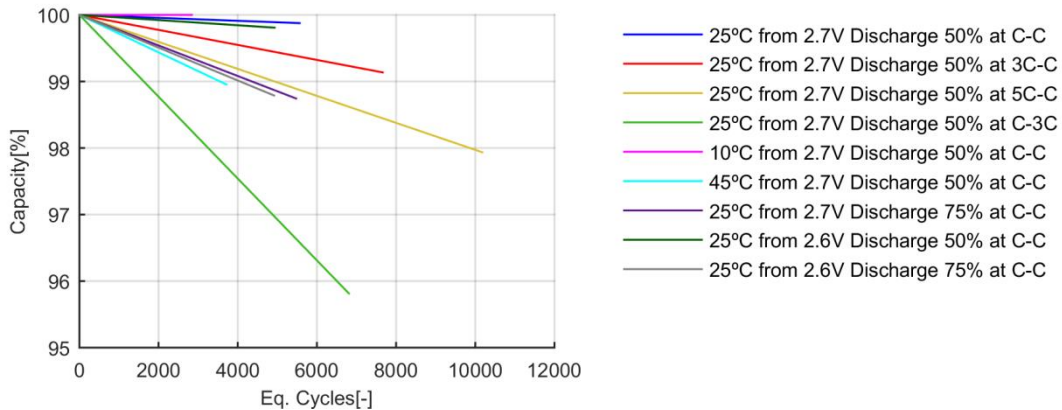


Figure 55: Aging trends of the dischargeable capacity decrease at different cycling conditions.

$$R_{cycling} = R_{ini} + var_1 \cdot cyc \quad (64)$$

$$\begin{cases} T < 25^{\circ}\text{C} & var_1 = (2.48e^{-6}) \cdot T + (7.32e^{-8}) \cdot SOC + (-6.38e^{-8}) \cdot DOD \\ & \quad + (2.08e^{-8}) \cdot I_{cha} + (-3.09e^{-7}) \cdot I_{dch} \\ T \geq 25^{\circ}\text{C} & var_1 = (1.17e^{-6}) \cdot T + (7.32e^{-8}) \cdot SOC + (-6.38e^{-8}) \cdot DOD \\ & \quad + (2.08e^{-8}) \cdot I_{cha} + (-3.09e^{-7}) \cdot I_{dch} \end{cases}$$

Parameters	Description
$R_{cycling}$	The pure ohmic resistance evolution due to cycling aging.
R_{ini}	The pure ohmic resistance value at Beginning of life (initial value).
cyc	The equivalent cycles done at cycling operation mode.
var_1	The slope of the linear model.
T	The operation temperature.
SOC	The upper SOC on cycling operation mode.
DOD	The DOD.
I_{cha}	The charge current.
I_{dch}	The discharged current.

Table 82: Parameters of the cycling aging model of the pure ohmic resistance evolution

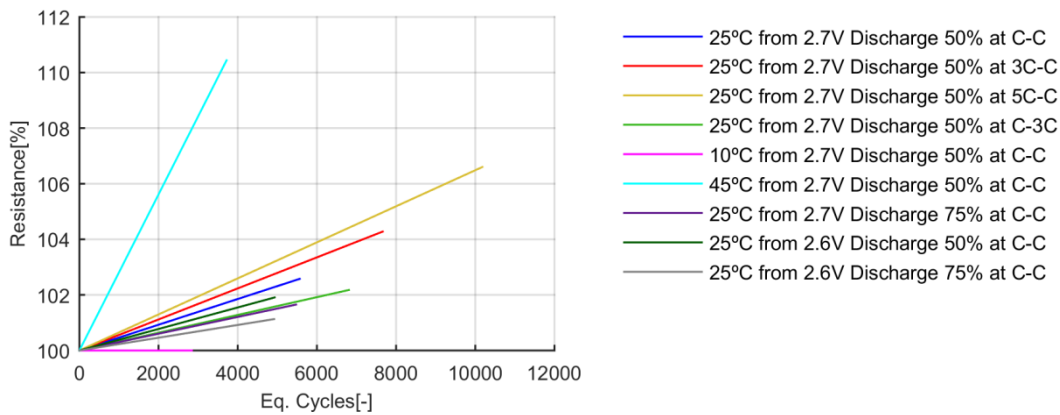


Figure 56: Aging trends of the pure ohmic resistance increase at different cycling conditions.

3.4.2.3 Aging Model Validation

The constructed aging models are validated in terms of the accuracy describing the observed cases, the correctness of interpolations and the real life applicability. For that, firstly, the response of the generated model and the data used on the construction of the model is evaluated with the Root Mean Square Error metric in Table 83.

	Calendar Aging Model		Cycling Aging Model	
	Dischargeable capacity [%]	Pure ohmic resistance [%]	Dischargeable capacity [%]	Pure ohmic resistance [%]
Test 1	0,28469	0,42434	0,84678	2,40938
Test 2	0,60584	1,19068	1,03068	1,33488
Test 3	0,43300	0,84270	0,23540	5,28276
Test 4	1,25762	0,59201	0,35958	1,48808
Test 5	1,52367	0,29520	0,38704	1,67186
Test 6			0,52278	1,34346
Test 7			0,27298	2,00911
Test 8			0,20735	1,21311
Test 9			0,23034	1,71074

Table 83: RMSE between the response of the model and the data used to construct the model

The results show that the constructed model that describes the dischargeable capacity evolution has a maximum fitting error of 1.5% and an error below 0.5% on most of the tested cases (8 from 14); and that the constructed model that describes the pure ohmic resistance evolution has a maximum fitting error of 5.2% and an error below 1.5% on most of the tested cases (8 from 14). Based on this, the constructed two aging models are considered highly accurate on the observed cases. The accuracy of the model that describes the pure ohmic resistance evolution is lower than the accuracy level obtained with the model that describes the dischargeable capacity evolution due to the noise level on the measurements, but it is still low enough to be considered highly accurate.

Secondly, the generated models are tested under a wide range non-variable operation conditions that are always inside the tested operation conditions. Basically, we interpolate the operation conditions in order to see if the model gives non-logical values. The results from the constructed aging models need to keep the logic of the expected aging trend:

- The dischargeable capacity will decrease with the rest and the cycling operation.
- The pure ohmic resistance will increase with the rest and the cycling operation.

The interpolated ranges are described in Table 84. The results are shown in 3D figures; see Figure 40, Figure 41, Figure 42 and Figure 43. The z axis represents the health indicator value, the y axis represents the comparison variable on each operation mode (the calendar aging is related to the time elapsed in between measurements and the cycling aging is related to the discharged energy in terms of equivalent cycles) and the x axis represents all the stress factors all together in a synthesized manner, being the indexing values of each combination of these stress factors the ones displayed on the x axis ("Validation Test [-]").

Stress factor	Calendar aging		Cycling Aging				
	Operating temperature	Mean SOC	Operating temperature	Upper SOC	DOD	Charge current	Discharge current
Maximum value	45[°C]	90 [%]	45[°C]	100[%]	75[%]	115[A]	69[A]
Minimum value	10[°C]	30[%]	10[°C]	90[%]	50[%]	23[A]	23[A]
Step	1[°C]	1[%]	2[°C]	1[%]	5[%]	5[A]	5[A]

Table 84: Interpolation cases possibilities on the validation process of a High-Energy application

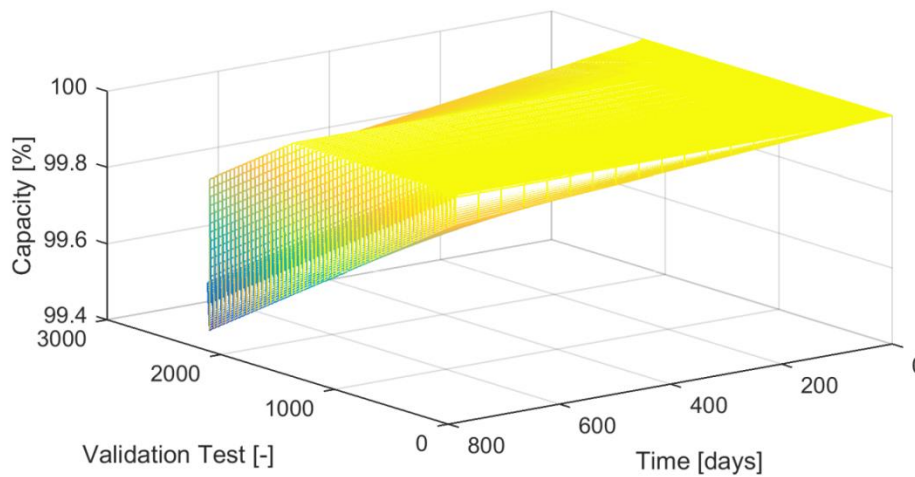


Figure 57: The dischargeable capacity map based on Calendar aging model interpolations.

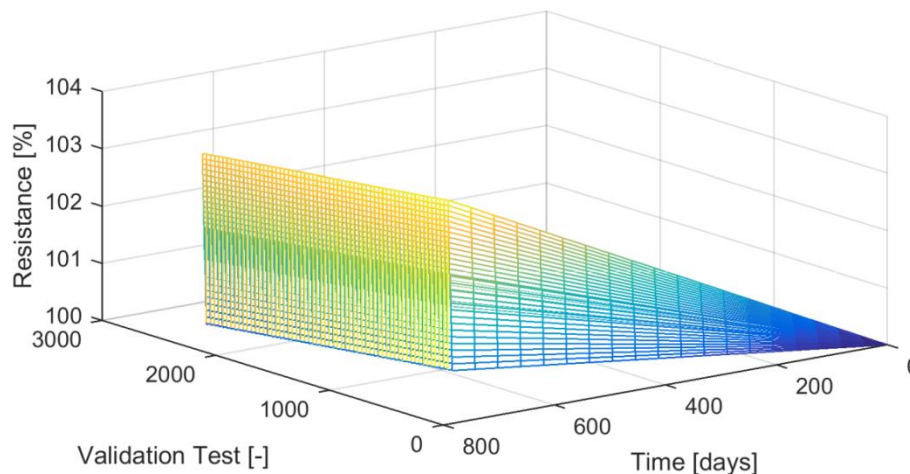


Figure 58: The pure ohmic resistance map based on calendar aging model interpolations.

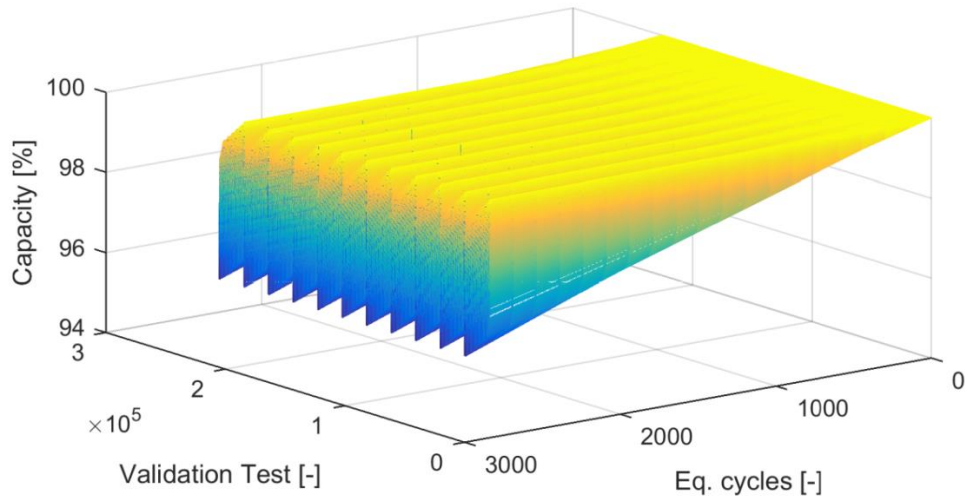


Figure 59: The dischargeable capacity map based on cycling aging model interpolations.

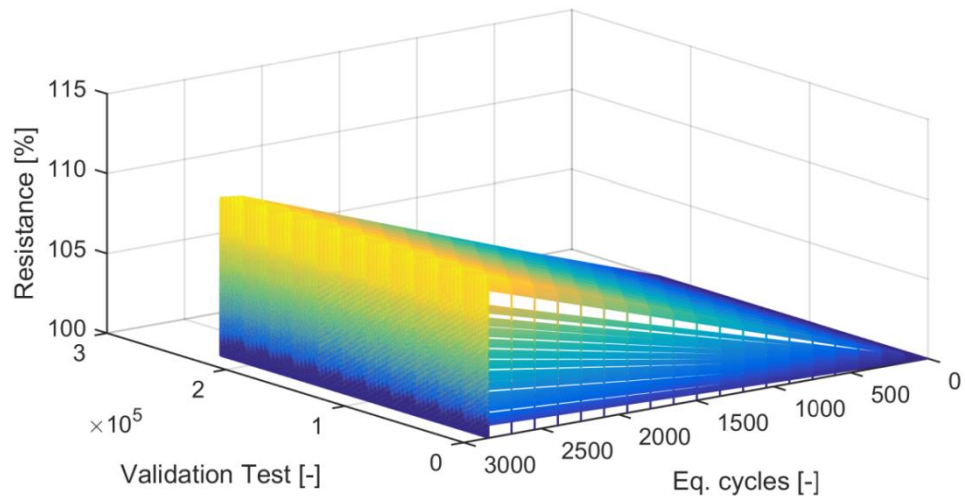


Figure 60: The pure ohmic resistance map based on cycling aging model interpolations.

The results show that the constructed calendar and cycling aging models of the dischargeable capacity and the pure ohmic resistance give logical values for interpolated operation conditions (respect to the tested ones). The obtained dischargeable capacity evolution trends and pure ohmic resistance evolution trends are delimited by the observed ones. It can be claimed that the proposed models interpolate correctly.

Thirdly, the applicability to real life application is tested. For that, the respond of the constructed aging model is evaluated with aging data obtained with real life cycles. In total, three tests with a real life cycle have been tested in parallel to the designed aging test matrix the 3 years of the project. These three tests consist on running the most probable operation use case profile at 10°C, 25°C and 45°C. The aging data has been obtained with the proposed ACT in the previous Aging Testing Definition section, from which the dischargeable capacity and the pure ohmic resistance evolution are subtracted (Figure 61 and Figure 62 respectively).

In order to apply the constructed aging model along with the obtained real life cycle aging data, the real life cycle need to be expressed with static stress factors. For that, the following assumptions are made:

- The slow charging does not accelerate the aging in comparison with the slow charge. Therefore, the static current charge value is taken the current value of the fast charge.

- The effect of values of stress factors out of the range of the tested ones is considered the same as the nearest tested value.
- The mean values of the dynamic stress factors are representative of the generated aging with those dynamic stress factors.

After analysing the real life cycle profile based on these three assumptions, the static stress factors that represent the use profile of the High-Power application have been generated, see Table 85.

Upper SOC	DOD	Charge current	Discharge current
100[%]→95[%]	60[%]	92[A]	12[A]→23[A]

Table 85: The mean stress factor values that represent the operation condition of the proposed High-Power application use case

The constructed models of the dischargeable capacity and the pure ohmic resistance have been run with the representative values of the stress factors shown in Table 85. The results from the aging model and the gathered data of the selected health indicators, the dischargeable capacity and the pure ohmic resistance, are shown in Figure 61 and Figure 62 respectively. The error between measurement and estimation can be seen in Table 86.

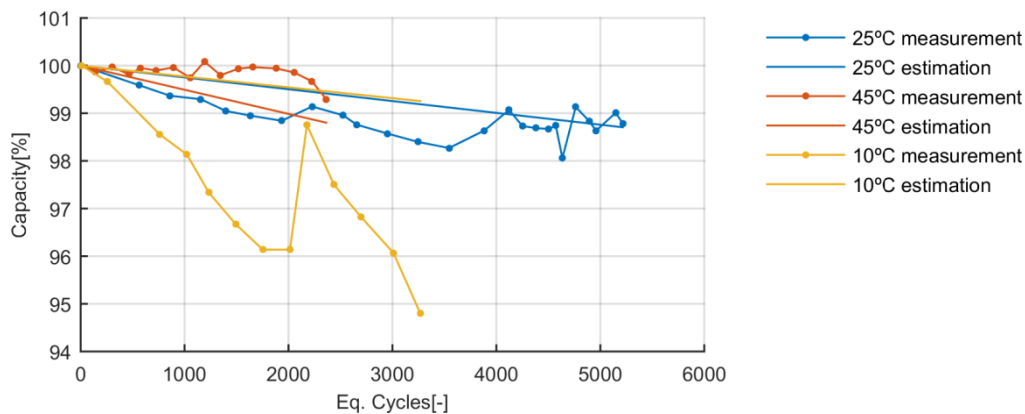


Figure 61: Dischargeable capacity evolution of the real High-Power application use profile tested at three different temperatures: 10°C, 25°C and 45°C.

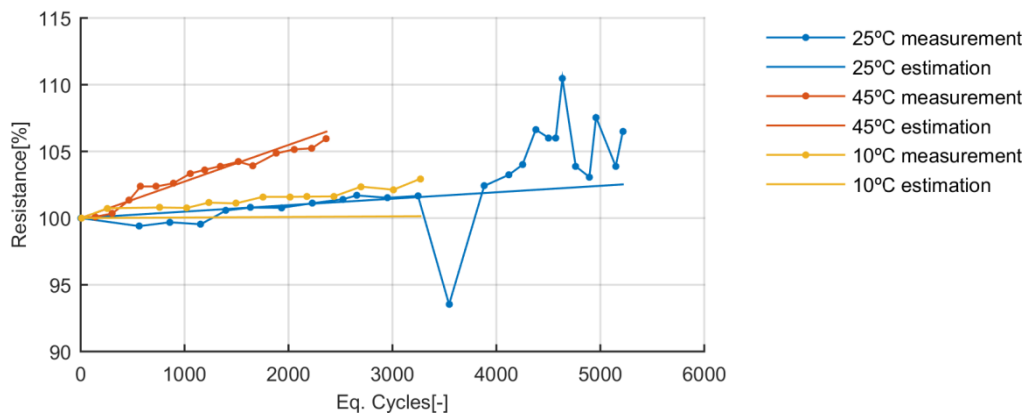


Figure 62: Pure ohmic resistance evolution of the real High-Power application use profile tested at three different temperatures: 10°C, 25°C and 45°C.

	Real cycle at 25°C	Real cycle at 45°C	Real cycle at 10°C
Capacity RMSE [Ah]	0,11037	0,13080	0,60625
Resistance RMSE [Ω]	4,38e-05	7,64e-06	2,15e-05

Table 86: Root Mean Square Error between the measured and estimated values of the real life cycle aging health indicators (dischargeable capacity and pure ohmic resistance)

The results show that the proposed model with the representative stress factors at 25°C and 45°C fits well the trend of both health indicators. The error between the estimated and the measured pure ohmic resistance at 25°C is the highest among the three, but in Figure 62 can be seen that this huge error comes from the noise of the measurements and that it is indeed capturing correctly the trend of this health indicator. Nonetheless, the results from fitting the behaviour of the real life cycle aging trends at 10°C are not acceptable at all. The behaviour of both health indicators at 10°C cannot be described with the proposed model.

The aging data obtained at 10°C is evaluated, see Figure 63. The effect of low temperatures on static operation conditions and on dynamic operation conditions (real life cycle) are not correlated. The low temperature reduces the degradation rate experienced in static operation conditions; in contrast, it increases the degradation rate in dynamic operation conditions. This can mean two things, first, that the testing time has not been long enough to observe properly the degradation on those operation conditions; and second, the assumption that the effect of the temperature is independent to the effect of the rest stress factors is not correct. Since the project was already finished, it has not been possible to generate more aging data. Therefore, it was not possible to check this issue. Besides, it is not possible to improve the model to describe the behaviour at 10°C. Therefore, it is validated that the constructed model is not able to describe the behaviour of both health indicator evolutions under temperatures below 25°C.

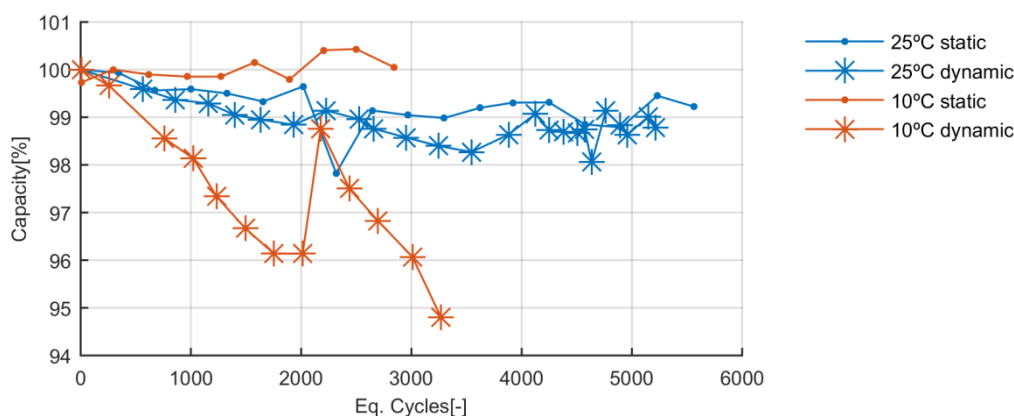


Figure 63: Comparison of the effect of low temperatures on the dischargeable capacity decay under static operation conditions and dynamic operation conditions.

To sum up, the interpolation capacity is validated on all the proposed models; and the applicability of real cases of the proposed models is validated but restricted to work in between temperature ranges from 25°C to 45°C.

3.4.3 Hypothesis validation

The proposed aging test matrix design methodology and aging model construction methodology are consolidated on some strong hypothesis. From all of them, the following ones have been studied in detail:

- The calendar and cycling aging can be added linearly.
- The mean values of the dynamic stress factors are representative of the generated aging with those dynamic stress factors.

Item	Specification
Nominal Capacity	2600 [mAh]
Fast charge current	2600 [mA]
Fast discharge current	5200 [mA]
Maximum temperature	45 [°C]
Minimum temperature	0 [°C]

Table 87: SAMSUNG's ICR18650-26F battery specifications

For that, specific aging tests have been run on certain batteries that have given information about the correctness of these hypotheses. The selected battery is SAMSUNG's ICR18650-26F lithium-ion battery. The characteristics of this battery are shown in Table 87.

The data required to validate the correctness of these hypotheses consist on the dischargeable capacity and pure ohmic resistance evolution under different operation conditions. In order to study the first hypothesis, three types of tests are thought to be needed: a test with only calendar effect, a test with only cycling effect and a test with a mix of both calendar and cycling effect. In order to study the second hypothesis, two types of tests are thought to be needed: a test with a static operation condition equal to the mean value of the stress factors extracted from the second type of test that consist on a real life cycle (see Figure 64).

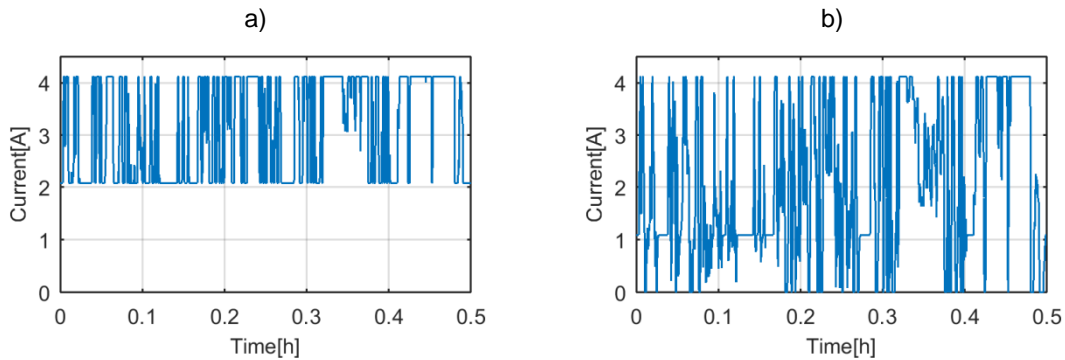


Figure 64: Current profiles of the tested real life cycles. A) has a mean current of 3120 mA and b) has a mean current of 2080 mA.

On the same hand, the design of the test matrix has taken into account all the different validation that have been thought to be necessary on this thesis, which are the next ones:

- A resting time inferior of 3h generates a relaxing effect instead of a calendar aging effect.
- The damage generated on the different operation modes can be added in a cumulative damage model.

Test	Upper SOC	Discharge time	Discharge current	Rest SOC	Rest time	Operation mode
1	-	-	-	20[%]	Inf	Resting
2	-	-	-	40[%]	Inf	Resting
3	-	-	-	60[%]	Inf	Resting
4	-	-	-	100[%]	Inf	Resting
5	100[%]	30[min]	2080[mA]	-	-	Static cycle
6	100[%]	30[min]	3120[mA]	-	-	Static cycle
7	100[%]	30[min]	4160[mA]	-	-	Static cycle
8	100[%]	30[min]	A train of cycles of tests 5, 6 and 7	-	-	Dynamic cycle
9	100[%]	30[min]	A train of cycles of tests 5, 6 and 7	End of charge	1[h]	Dynamic cycle
10	100[%]	30[min]	A train of cycles of tests 5, 6 and 7	End of discharge	1[h]	Dynamic cycle
11	100[%]	30[min]	A train of cycles of tests 5, 6 and 7	End of charge	8[h]	Dynamic cycle
12	100[%]	30[min]	A train of cycles of tests 5, 6 and 7	End of discharge	8[h]	Dynamic cycle
13	100[%]	30[min]	Mean value of 2080[mA]	-	-	Real cycle
14	100[%]	30[min]	Mean value of 3120[mA]	-	-	Real Cycle

Table 88: Aging test matrix design to validate the main hypotheses done on the aging model development

In order to study the third hypothesis, three types of tests are thought to be needed: a test with only calendar effect, a reference test without any resting time, a test with a cycling operation mode that

intercalates rest time smaller than 3h and a test with a cycling operation mode that intercalates rest time bigger than 3h. In order to test the fourth hypothesis, two types of tests are thought to be needed: a test with non-variable or static operation conditions and a test with an operation condition that changes from one static operation to another one, repeating the same static operation conditions in a closed loop way. In addition, the difference of having rest times at the end of the discharge and at the end of charge is also added to the evaluation because of CIDETEC's interests. As a result, the combined aging test matrix shown in Table 88 is designed, from which the tests numbers 4, 5, 6, 7, 8, 11, 13 and 14 are used on the study of the two hypotheses done on this chapter (highlighted in bold letters).

The ACT developed on this study is the same as the one used on the previous validations: a capacity validation test, an OCV characterization test using low C-rate values and an impedance characterization test using charge and discharge pulse tests all along the SOC range.

After the design of all the required tests (the aging test matrix and the ACT), these tests have been run for 6 months in CIDETEC's facilities and the obtained data has been treated with the aim of validating the proposed two hypotheses.

3.4.3.1 First hypothesis validation

Among the tests defined on this new aging test matrix, the test 4 (only resting), the test 8 (only cycling) and the test 11 (mix of resting and cycling) are evaluated to validate the first hypothesis. For that, firstly, the health indicators of interest are extracted from the data obtained from the tests: the dischargeable capacity and pure ohmic resistance, see Figure 65 and Figure 66.

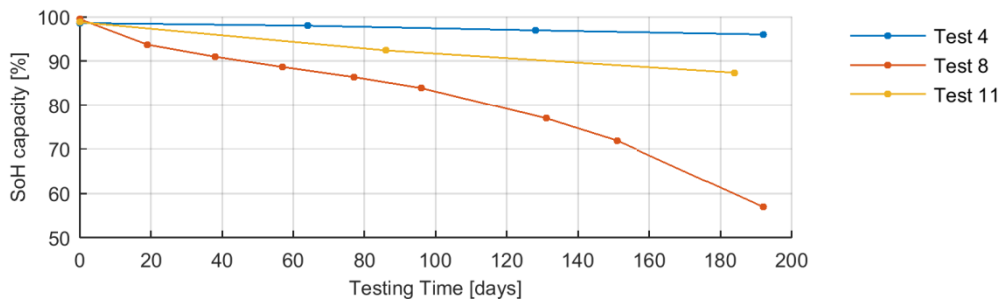


Figure 65: Dischargeable capacity evolution of tests 4, 8 and 11.

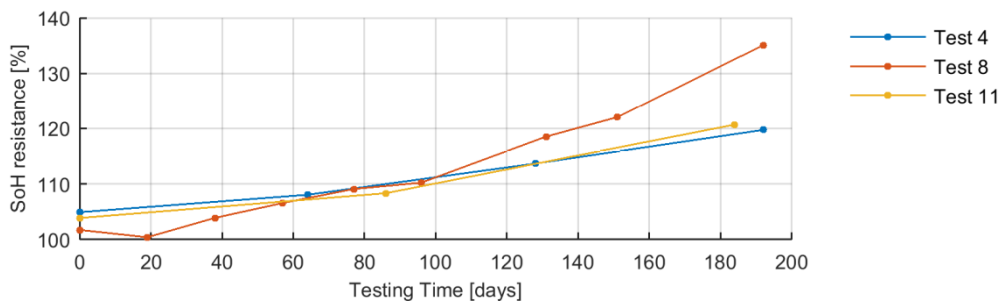


Figure 66: Pure ohmic resistance evolution of tests 4, 8 and 11.

Then, the extracted health indicators are modelled with the aim of correlating the health indicator evolution with the resting time and with the discharged energy. This modelling exercise only requires fitting the observable trends of the health indicators extracted from the tests 4 and 8 with a mathematical expression. The required steps to fulfil this modelling exercise are detailed on the first phase of the proposed aging modelling methodology.

The first phase of the proposed modelling methodology consists on choosing the mathematical expression that fits better the selected health indicators (dischargeable capacity and the pure ohmic resistance). The tested mathematical expressions are shown in Table 89.

Aging	Linear	Exponential	Logarithmic	Power type	2 nd order polynomial
Calendar	x	x	x	x	x
Cycling	x	x	x	x	x

Table 89: Selection of mathematical expressions that can be applied to describe the aging trend of the selected health indicators

The fitting accuracy is measured with the Root Mean Square Error (RMSE) metric between the measurements and the estimation done with the fitted mathematical expression. This metric has been calculated on each test of both aging test matrix for the two selected health indicators. The mean of the obtained RMSE values on all the tests of the run aging test matrix is added, see Table 90 and Table 91.

	Linear	Exponential	Logarithmic	Power type	2 nd order polynomial
Test 4	0,00103	0,00053	0,00666	0,00048	0,00061
Test 8	0,02836	0,02947	0,10794	0,02048	0,01846

Table 90: Fitting RMSE of the dischargeable capacity evolution data extracted from the proposed test number 4 and test number 8

	Linear	Exponential	Logarithmic	Power type	2 nd order polynomial
Test 4	0,00765	0,00441	0,03942	0,00136	0,00228
Test 8	0,06188	0,06224	0,09453	0,06085	0,06072

Table 91: Fitting RMSE of the pure ohmic resistance evolution data extracted from the proposed test number 4 and test number 8

The fitting of the data of both health indicators show that the mathematical expression that fits better the results obtained from the test 4 (the calendar aging) is the power type equation. In contrast, there is not a clear winner among the mathematical expressions that describe the results obtained from the test 8 (the cycling aging). Therefore, the simplest model (linear model) is selected.

The selected calendar and cycling aging models are added linearly in a complete aging model, see Eq. (65) and Eq. (66). for the concrete operation conditions imposed on the test 11 (a train of cycles defined on tests 5, 6 and 7), the aging behaviour on test 11 is estimated by adding both models linearly and compared with the actual health indicators extracted from the test 11, see Figure 67 and Figure 68.

$$Q = Q_{ini} - (4.07e^{-5} \cdot t^{1.23}) - (1.37e^{-4} \cdot cyc) \tag{65}$$

$$R = R_{ini} + (1.21e^{-4} \cdot t^{1.35}) + (8.89e^{-5} \cdot cyc) \tag{66}$$

Parameters	Description
Q	The dischargeable capacity.
Q_{ini}	The dischargeable capacity value at Beginning of life (initial value).
t	The resting time related to calendar aging in days.
cyc	The discharged energy in Ah.
R	The pure ohmic resistance.
R_{ini}	The pure ohmic resistance value at Beginning of life (initial value).

Table 92: Parameters of the complete aging model

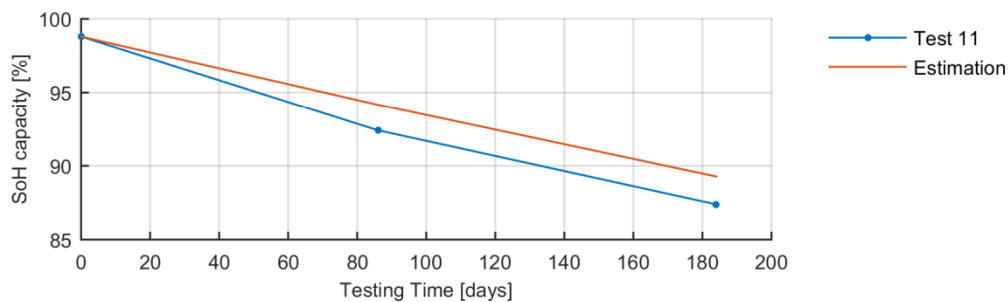


Figure 67: Comparison of the observed dischargeable capacity evolution in the test 11 (blue dotted line) and the estimated dischargeable capacity with the complete aging model (red line).

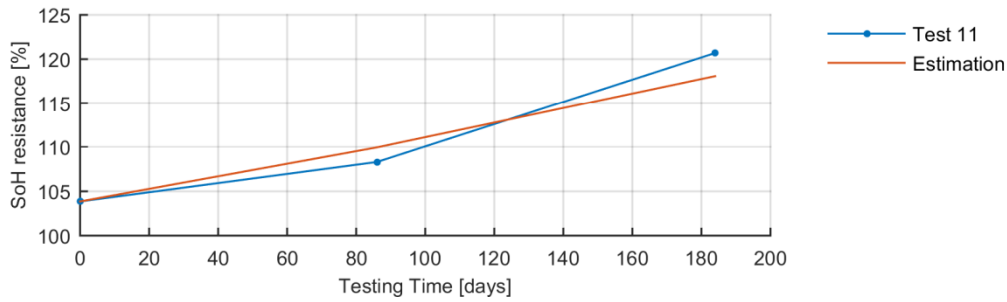


Figure 68: Comparison of the observed pure ohmic resistance evolution in the test 11 (blue dotted line) and the estimated pure ohmic resistance with the complete aging model (red line).

The results show that the complete model is able to capture the trend of the dischargeable capacity and the pure ohmic resistance evolution. Based on this, this first hypothesis is validated at the observed operation conditions.

3.4.3.2 Second hypothesis validation

Among the tests defined on this new aging test matrix, the test 5 (static operation conditions), the test 6 (static operation conditions), the test 7 (static operation conditions), the test 13 (real life operation conditions) and 14 (real life operation conditions) are evaluated to validate the second hypothesis. For that, the health indicators of interest are extracted from the data obtained from the tests: the dischargeable capacity and pure ohmic resistance, see Figure 69 and Figure 70.

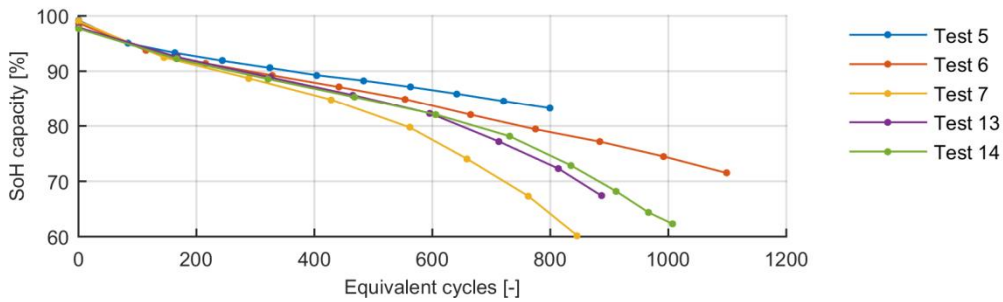


Figure 69: Dischargeable capacity evolution of the tests 5, 6, 7, 13 and 14.

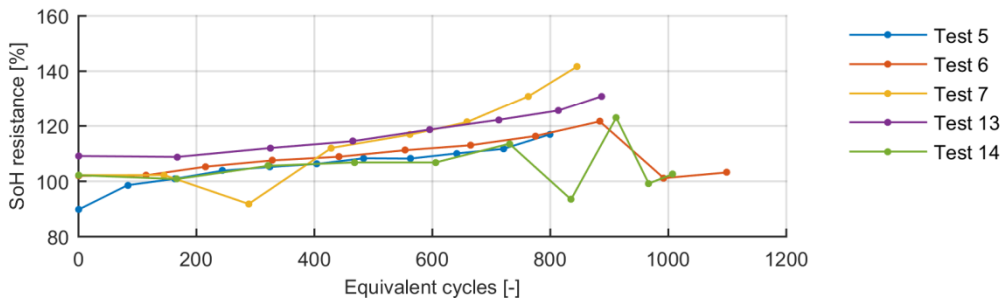


Figure 70: Pure ohmic resistance evolution of the tests 5, 6, 7, 13 and 14.

In this case, the validation of the hypothesis comes from the testing data itself, since the assumed hypothesis states that the aging on the tests 5 and 13 are the same and the aging on the tests 6 and 14 are the same. This hypothesis could be assumed to be true looking at the pure ohmic resistance evolution. The observed trends on the tests 5, 6, 13 and 14 look alike. However, this is not happening on the dischargeable capacity evolution. The cases with real life cycles suffer higher dischargeable capacity decay than the cases with static operation conditions (considering the mean value of the real life cycles as the correlation parameter). Besides, the results show that both tests run with the defined two real cycle current profiles (tests 13 and 14) experience almost the same aging trend, even though having a difference between their mean current value of 1040mA (a 50% higher mean current level).

In this scenario, the data is further analysed. The real applied operation conditions on tests 5, 6, 7, 13 and 14 are evaluated. The most relevant variables are displayed: the average current on each cycle (Figure 71), the average temperature on each cycle (Figure 72), the discharged time on each cycle (Figure 73) and the end of discharge voltage on each cycle (Figure 74).

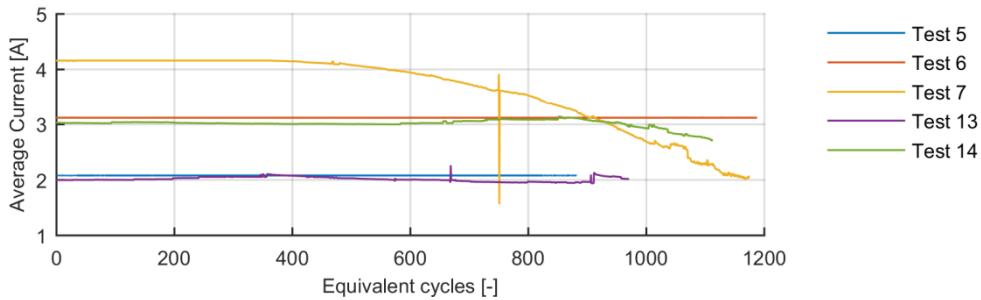


Figure 71: Average current values of each cycle done at tests 5, 6, 7, 13 and 14.

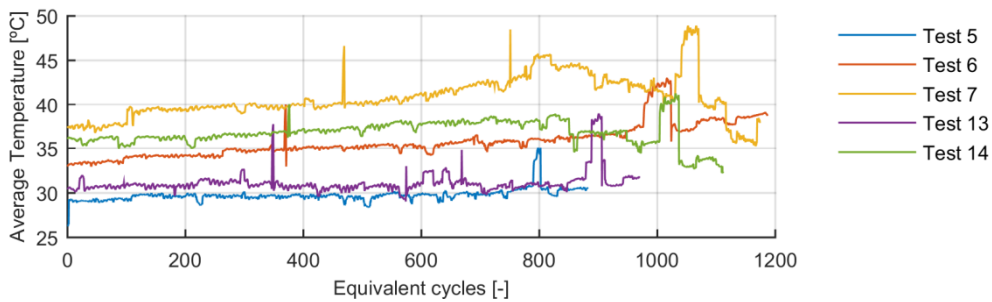


Figure 72: Average temperature values of each cycle done on the tests 5, 6, 7, 13 and 14.

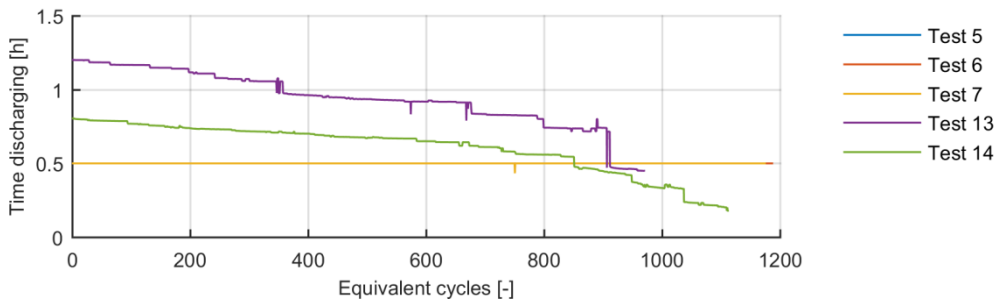


Figure 73: Time of discharge on each cycle done on the tests 5, 6, 7, 13 and 14.

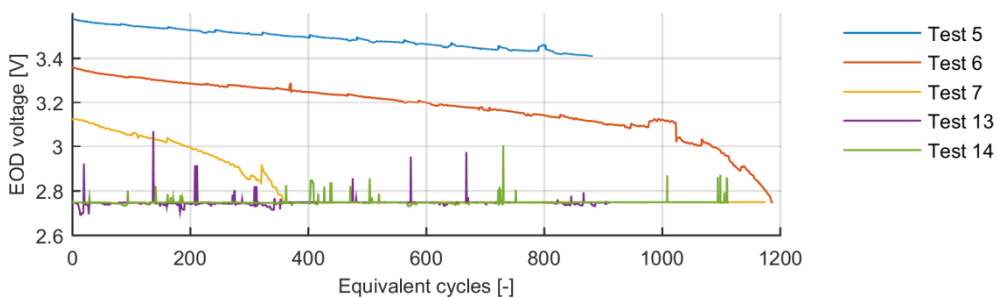


Figure 74: End of Discharge voltage on each cycle done on the tests 5, 6, 7, 13 and 14.

The results show that the mean current values of the tests 5, 6, 13 and 14 are coincident with the expected ones. The test 7 starts to enter the Constant Voltage mode at around 500 equivalent cycles (the mean current reduces) but the rest of the tests keep the mean current imposed on the design of the tests. The temperature measurements show that the temperature on tests 13 and 14 are a bit higher than the temperatures measured on cell 5 and 6, but they have a similar temperature difference between 5-6 and 13-14. Checking on the time of discharge of each cycle and the end of discharge voltage, it has been found that the implementation of the operation conditions of the tests

13 and 14 have not been respected. The tests 13 and 14 have been discharged until the end of discharge voltage every cycle. The discharge time on each cycle has not been restricted to 30 min but rather to the required time to reach the end of discharge voltage. This was not what it was planned. However, it explains why both tests experience similar aging trends since both have a DOD near the 100% (there is no Constant Voltage phase so it changes slightly on each cycle). It is more; it also explains why the test 13 with lower current rates could generate greater degradation. The deeper the DOD is, the greater the deterioration of the battery is expected. Lower currents allow deeper discharge since more energy is discharged before reaching the end of discharge voltage.

The wrong implementation of the tests 13 and 14 makes impossible to completely validate this second hypothesis. However, relevant information about the degradation has been obtained. Firstly, it has been seen that the discharge with constant current and with a real life current profile generates similar mean operation temperatures. This fact points to the correctness of this second hypothesis. Secondly, the most relevant stress factor has been identified on SAMSUNG 18650 26F batteries: the deepness of the discharge or DOD. The tested battery on test 14 is experiencing higher discharge current rates and higher temperatures than the battery on test 13; nevertheless, both batteries are experiencing almost the same deterioration. This means that the effect of deep discharges contributes much greater than the current and temperature to the battery aging at least on the tested ranges (almost 100% DOD, 2-3A and 30-37°C).

3.5 Conclusions

This chapter has proposed the methodology to design the whole aging evaluation exercise: from the design of the aging test matrix to the construction of the aging model. The whole methodology has been tested on a High-Power and on a High-energy application. The constructed aging models have been validated with real life cycle aging data. Some important hypotheses assumed along the proposal have been discussed and validated as well.

The design of the aging testing methodology has shown that a full and deep aging analysis of the operation conditions on a certain application is not realistic. A proper aging analysis contains just too many testing cases where even some of the most relevant ones are doomed to be discarded. Both applications has shown us that the economic restrain (invested lab resources on the project) limits greatly the testing cases, where testing cases out of the most likely operation conditions are automatically discarded and where testing cases with operation conditions with low deterioration rates are modified (increased to couple the expected testing time of the project). All this leads to the need of embracing hypotheses about the aging behaviour such as the done respect to the temperature (it shows a linear effect up –down a certain level) or the discharge current (there is a constant deterioration rate under a certain level). The practice of assuming hypotheses is fundamental but dangerous, since the final results will be conditioned to the assumed hypotheses. In case those are not correct, the constructed aging model will not give accurate results on the operation conditions where those hypotheses are not correct. A clear example is the assumed hypothesis of being the temperature independent from the rest stress factors, at least at temperatures below 25°C (tested at 10°C). The effect of the 10°C operation temperature on the aging behaviour shows a much greater deterioration at the real life cycle test than at the test with static operation conditions. It has been found that there could be a dependency between low temperatures and the rest stress factors. As a result, the constructed model cannot describe the aging behaviour of applications operated at temperatures below 25°C.

In addition to this, it has been seen that the testing matrix design is in continuous change due to changes on the client priorities. The details of the application are often poorly defined at the beginning of the project and the acquired knowledge about it reforms all the requirements. It is found to be interesting to spend time in the proper understanding of the application and in the identification of the most likely deviations from the initial statement of the application requirements.

Besides, specific aging analyses are typically added to the aging modelling exercise, such as an aging-thermal study used for the selection of the thermal management system. Those aging analyses will restrain even more the options that the aging test matrix designer has in case they are

not considered on the proposal design. This is why there should be a fluent communication between the project leader, the lab and the customer.

The aging modelling proposal has shown that the applicable mathematical expressions used on the second phase of the proposed aging modelling methodology are completely dependent to the aging testing matrix. A stress factor that has been tested with 2 levels can only be described by a linear model; there is no sense on using a mathematical expression with a higher dimension if there are available only two points.

On the same hand, it has been seen that the restrains imposed on the aging testing matrix limits greatly the operation window that the obtained model is able to describe. The results show how the constructed model could have only been validated on a smaller operation window than the expected one; the performance of the constructed aging models at low temperatures has shown huge fitting errors.

The modelling activities developed on the evaluated use cases have shown that the quality of the data is a key aspect when constructing the aging model. Firstly, the observed health indicators need to show relevant deteriorations in order to capture and validate the effect of the evaluated stress factors. Low deterioration levels are shown by the observed dischargeable capacity at the High-Power application and by the pure ohmic resistance at the High-Energy application. Shallow degradation rates on the gathered data trammels the identification and/or the validation of the effect of the stress factors. The validation of the dischargeable capacity evolution model constructed for the High-Power application does not shows conclusive results. It looks like the constructed model is able to describe the dischargeable capacity decay experienced under real cycle operation conditions, but in reality, there is just 1% capacity decay. It is not an enough deterioration to state anything around the model itself. The validation of the pure ohmic resistance evolution model constructed for the High-Energy application shows practically the same; there is no significant raise of the pure ohmic resistance on the data used for the validation to state anything around the model itself. Secondly, the obtained data need to be as clear as possible. Noisy data leads to the incapacity of distinguishing good results from bad results on the proposed modelling methodology. The selection of the mathematical expressions is done by measuring and comparing the Root Mean Square Error. Noisy data increases this metric indistinctive to the applied mathematical expression which will decline the selection to the simplest mathematical expression. Besides, noisy data increases the uncertainty and makes less clear the validation of the models, such as in the validation of the pure ohmic resistance model constructed for the High-Energy application.

The first part of the selection of the mathematical expression has shown that the power type mathematical expression is likely to be the one that describes the best the evolution of the dischargeable capacity decay of the selected battery on the High-Energy application. Instead, the linear model is the mathematical expression that is likely to describe the best the pure ohmic resistance increase of the selected battery on the High-Energy application and the evolution of both selected health indicators of the selected battery on the High-Power application.

The second part of the selection process of the mathematical expressions has shown that the mathematical expression that could fit the best all the effects of the stress factors on the proposal is the linear model. In this case, the temperature effect is expected to be exponential [88] but at the same time forced to be linear due to the hypotheses done at the design of the aging test matrixes. The effect of the DOD, the SOC ranges and the discharge current are only tested with 2 levels, therefore, limited to be characterized with a linear model. The charge current is the only stress factor that could have been modelled with a mathematical expression different to the linear model, but finally, the Root Mean Square Errors have determine to be the linear model the most appropriate mathematical expression. This could be interpreted as being the simplest model the best option when there is not enough data to describe properly the behaviour of the system under evaluation.

The validation of the constructed aging models for the defined two applications show different aspects of the constructed models. Firstly, it has been discovered that the proposed aging modelling methodology is able to capture the effect of the stress factors on the trend of the selected health

indicators even though having little data (up to 9 operation conditions to describe 5 stress factors). The models get low fitting errors on most of the cases. It is found that the fitting of the pure ohmic resistance evolution has greater relative fitting errors, which has been addressed to the measurement noise. The noise of the measurements needs to be treated before doing the measurements. This means that there is no other choice but to deal with this noisy data and accept a high fitting error. Secondly, it has been perceived that the interpolation capability of all the linear models get logical results. The constructed power type model that describes the calendar effect on the dischargeable capacity evolution has been validated as well in terms of interpolation capability; nonetheless, the one related with the cycling aging has not been able to be validated. This model returns values of capacity of -1500% on some interpolated cases, which are not realistic. This is thought to be due to the increase of the stress factors. When dealing with a mathematical expression that has a very sensible variable, such as the power type equation (the power variable), the increase of free variables inside the calculation of this sensible variable leads to the inconsistency of the model itself. The fact is that there is too little data; the free variables that describe this sensible variable cannot be adjusted properly. Therefore, it is advisable to use simple models on those cases, such as the rebuilt model, which gets higher fitting errors but that give logic interpolated values. Thirdly, it has been seen that the constructed models by following the proposed modelling methodology are able to describe 2 of the tested 3 cases with real life cycle current profile. It has been seen that the effect of the temperature at temperatures below 25°C is not independent to the rest of the stress factors; one of the main hypotheses done at the model construction is violated. Therefore, the constructed model does not describe the operation window at temperatures below 25°C. The description of this operation window comes from doing additional aging tests.

The validation of two of the most relevant hypotheses have shown that, firstly, the deterioration given on resting periods and the deterioration given on cycling periods can be linearly added. Secondly, the mean values of the dynamic stress factors are likely to be representative of the generated aging with those dynamic stress factors. It has not been possible to prove that a static operation and a real life operation can be linked with the mean value of the stress factors, but hints about its correctness have been given (the generation of temperature is similar). On the same hand, it has been found some details about the deterioration of the SAMSUNG 1865026F battery. Firstly, it has been found that operating this battery at 100% DOD is really harmful. Secondly, It has been found that the operation on some ranges can generate the same deterioration on the battery independent to the changes of some stress factors (the change on current and temperature levels has not had any effect on the degradation path of the tests 13 and 14). This discovery shows that there are predominant stress factors, at least operating within some ranges, which overlap the effect of the rest of the stress factors.

At the same time, this chapter has been able to respond some hypotheses done at the research project definition. It has been seen that it is possible to describe the degradation that experiences the battery on real life application using a model constructed uniquely on data obtained from tests done at lab level with static operation conditions. It has also found that the aging path that the battery has can be totally described by the monitoring of the selected two health indicators: the dischargeable and pure ohmic resistance evolution. In contrast, it was expected that the developed aging testing methodology could reduce the testing cost by reducing the testing cases, which has been impossible to perform. The evaluated applications have had a budget so tight that it has been impossible to really reduce anything. However, the proposed aging testing methodology has served to meet the economic restrains of the project while allowing an aging model able to fit properly the obtained data, interpolate realistically and describe the aging of batteries cycled with real life current profiles, which is a merit by itself.

CHAPTER 4:

4 Sizing Energy Storage Systems

This chapter presents a sizing tool that not only considers the electric and thermal performance of the battery solution, but also the aging and the cost. For that, a decision approach built on a simulation environment is developed. The electric, thermal and aging behaviour of the system are simulated on the application operation conditions for the entire lifespan of the project. Meanwhile, the previously generated End of Life map and the tracked aging health indicators are used to determine the replacements of the batteries. The whole simulation is repeated on a pre-defined sizing range. As a result, the proposed sizing tool shows a cost diagram containing the cost of each tested size from a pre-defined range of sizes and highlights as the optimal size the one with the minimum cost. The tool is presented in two contexts: an e-mobility solution and a stationary solution. In addition to this, the assumption that the aging behaviour can be modelled by a cumulative aging model and the assumption that a rest period below 3h does not generate calendar aging are discussed and validated. The contributions of this chapter consist on firstly, the simulation environment that introduces the three performance aspects of a lithium ion battery: the electric behaviour, the thermal behaviour and the aging behaviour; secondly, the cost determination of a battery solution on an electric vehicle; thirdly, the cost determination of a battery solution on a stationary application; fourthly, the validation of the cumulative behaviour of the aging model; and fifthly, the identification of a relaxation effect at certain rest periods and at certain SOC values.

4.1 Introduction

The sizing exercise of electric components is a key aspect on the design of any machine. The electric components are commonly sized based on the functional requirements of the machine. The machine needs to fulfil certain application requirements and the components of that machine are selected to allow the fulfilment of them all along the lifespan of the machine. Firstly, a size option that assures the correct performance of the machine at the beginning of life of the machine is pre-selected. Then, the typical sizing process considers a performance decay of the evaluated electric components until the end of the guarantee with which the pre-selected sizes are increased to tackle the deterioration.

This process is not optimum. This process tends to oversize the components more than the required to assure the correct performance of the machine all the guarantee period. Besides, it may be more profitable to reduce the size of some evaluated components even though requiring replacement of those components. In this scenario, this thesis proposes to calculate the cost that different sizing options of lithium ion battery energy storage systems have on the most relevant applications of lithium ion batteries: the Electric Vehicle and Stationary storage systems. The cost calculation integrates the simulation of the operation and deterioration of the batteries all along the energy storage system's lifespan with which all the economic costs and incomes are calculated. For that, firstly, a standard simulation environment used to simulate the operation and deterioration of the battery solution is described. Secondly, the proposed standard simulation environment is adapted to calculate the cost of different sizing options of each application. Finally, the proposed adapted simulation environment is tested with real cases and the most significant hypotheses done on the developed simulation environment are discussed and validated.

4.2 Simulation environment

The proposed simulation environment consists on running a certain yearly input current profile N times with the constructed performance models, where N is the lifespan of the project in years. If the simulated performance of the battery reaches the End of Life threshold before the end of the whole simulation, replacement activities are activated. The replacement activity supposes that the operation of the battery is stopped for a certain time period and that aged batteries are replaced by new ones. The replacement of the batteries is represented by resetting the State of the Health-Indicators of the battery. The whole algorithm is described in Algorithm 1.

The input current profile is considered as a given by the application requirements. If the operation conditions are uncertain, the most probable profile is used to determine the most probable optimal size.

The performance models are the electric, thermal and aging models. The electric and thermal models are constructed as defined at the "End of Life Calculation Framework" chapter, see section "Battery model". These two models are directly used to calculate the voltage and temperature responses of the battery. The aging models are constructed as defined at the "Aging: Testing and Modelling" chapter, section "Proposal of Modelling Methodology". These models need to be constructed before using them on this simulation environment.

The electric and thermal performance of the battery is proposed to be simulated with a step time of 15 min. This step time is small enough to get relevant information about the electric and thermal performance evolution of the battery all along the project lifespan but big enough not to saturate the computer. There are cases where a smaller time step is required due to the characteristics the current profile has. On those cases, a subroutine loop is run inside those two models. As a result, the current profile is simulated with full detail and the simulation is not saturated (only the information at each 15 min is saved).

The aging of the batteries is simulated with a discrete time step as well. It is assumed that firstly, the cycling and the calendar deterioration are gradually and discretely accumulating each time step: and secondly, the previous aging path does not affect the actual aging path. The simulation of the aging model in this way means that the simulated aging model is based on cumulative damage theory [50],

which basically justifies the use of discrete samplings and discrete deterioration estimations. The proposed simulation time step is 24h. The dynamic of the aging behaviour is much slower than the dynamic of the electric and thermal behaviour. There will not be a relevant degradation on just a day, but 24h is a short enough time step to simulate a gradual performance decrease.

The End of Life threshold is proposed to be calculated as a map that gathers the information of the tracked health indicators as defined at the “End of Life Calculation Framework” chapter, section “Methodology”. In this thesis, the pure ohmic resistance evolution and the dischargeable capacity evolution are the proposed health indicators with which the EOL map is constructed. The End of Life threshold needs to be calculated before using it on this simulation environment. Besides, it may be necessary to calculate more than one End of Life threshold beforehand if the current profile of the application changes when modifying the size of the battery solution.

*SIZING*_{SimulationEnvironment}(*I, N, Δt, Δs, B, EoL_{TH}*)

```

1: INITIALIZE simulation
2: for i = 1 to N do
3:   for u = 1 to L do
4:     if EoLTH is reached
5:       REPLACEMENT exercise
6:       if  $\Delta u == M$ 
7:         END REPLACEMENT exercise
8:         INITIALIZE performance models
9:       end if
10:    else
11:      [SOC(u), T(u), V(u)] = ELECTRIC_THERMAL_M( $\bar{I}^{(u)}$ ,  $\Delta t$ ,  $\Delta s$ )
12:      if  $\Delta u == B$ 
13:        [Q(u), R(u)] = AGING_M(SOC( $\Delta u$ ), T( $\Delta u$ ),  $\bar{I}^{(\Delta u)}$ ,  $\Delta t_1$ ,  $\Delta s$ , B, Q(u-1), R(u-1))
14:      end if
15:    end if
16:  end for
17: end for

```

Where

I = Yearly current profile.

N = Lifespan of the project.

L = The amount of simulation time steps that contains a year.

M = Amount of step times required on the replacement exercise.

B = The amount of simulation step times that are inside the aging step time.

Δt = Step time of the simulation.

Δs = Input sample time.

EoL_{TH} = The End of Life threshold.

$\bar{I}^{(u)}$ = The input current profile vector at (*u*) simulation time step.

ELECTRIC_THERMAL_M = The electric-thermal model.

AGING_M = The aging model.

SOC^(*u*) = The State of Charge at (*u*) simulation time.

T^(*u*) = The temperature of the cell at (*u*) simulation time.

V^(*u*) = The voltage response of the battery at (*u*) simulation time.

Q^(*u*) = The dischargeable capacity at (*u*) simulation time.

R^(*u*) = The pure ohmic resistance at (*u*) simulation time.

Algorithm 4: Algorithm of the proposed simulation environment.

4.3 Applications

Lithium ion batteries are nowadays integrated on many kinds of applications such as mobile phones, laptops, drones, electric cigarettes etc, but there are two applications that have a much more impact on our society and on the war against the climate change: the electric vehicle application and the stationary application. Besides, the proper sizing of the battery solution on these two applications plays especially a very important role in the business model due to the required huge investments.

4.3.1 Electric vehicle application

The electric vehicle is the alternative that important vehicle OEMs (Original Equipment Manufacturer) are providing to internal-combustion vehicles. Cities all over the world are betting on this type of vehicle to replenish their bus or track fleet. In this scenario, the proper sizing of the battery solution of these vehicles is primordial to reach the final application requirements.

This particular application of lithium ion batteries used to have some sizing common criteria. Firstly, there used to be an electric performance requirement. There is a minimum feasible size. Secondly, there used to be a space limitation. The electric vehicle has a defined size with a limited space for the battery solution (there is a maximum size). Thirdly, there used to be a minimum battery module level. The sizing options are reduce considerably due to modularity limitations of the solution. Fourthly, there used to be a defined route or a routine that needs to be fulfilled. The electric vehicle will need to provide certain performance all along the project lifespan. This criterion is used on the End of Life mapping developed on the chapter “End of Life Calculation Framework”. And fifthly, there used to be a guaranty agreement that needs to be respected. This represents the project lifespan in terms of potential costs (the cost from replacements will be assumed by the OEM).

Once the application is understood, the simulation environment has been adapted to the application characteristics, see Algorithm 5. The cost of each feasible sizing option is quantified based on the battery units that are needed on the lifespan of the project. The simulation environment is set up with the selected size and run with the yearly routine of the application a total of times equal to the lifespan of the project. As a result, the total amount of batteries required on the project is guessed. Thanks to this, a cost value is attached to each feasible sizing option and a cost diagram is generated, from which the optimal size is highlighted (the size option with the smallest cost).

$$\{COST^{(j)}\}_{j=1}^p = SIZING_{ElectricVehicleApp} \left(\{I^{(j)}\}_{j=1}^p, N, \Delta t, \Delta s, B, \{EoL_{TH}^{(j)}\}_{j=1}^p, \{CI^{(j)}\}_{j=1}^p \right)$$

```

1: INITIALIZE simulation
2: for  $i = 1$  to  $N$  do
3:   for  $u = 1$  to  $L$  do
4:     if  $EoL_{TH}^{(j)}$  is reached
5:       REPLACEMENT exercise
6:       if  $\Delta u == M$ 
7:         END REPLACEMENT exercise
8:          $RC(i) = 1$ 
8:         INITIALIZE performance models
9:       end if
10:    else
11:       $[SOC^{(u)}, T^{(u)}, V^{(u)}] = ELECTRIC\_THERMAL\_M(\bar{I}^{(j,u)}, \Delta t, \Delta s)$ 
12:      if  $\Delta u == B$ 
13:         $[Q^{(u)}, R^{(u)}] = AGING\_M(SOC^{(\Delta u)}, T^{(\Delta u)}, \bar{I}^{(j,\Delta u)}, \Delta t, \Delta s, B, Q^{(u-1)}, R^{(u-1)})$ 
14:      end if
15:    end if
16:  end for
17: end for
18:  $COST^{(i)} = COST\_CALCULATION(CI^{(j)}, RC)$ 

```

Where

$I^{(j)}$ = Yearly current profile of the (j) size option.

N = Lifespan of the project.

L = The amount of simulation time steps that contains a year.

M = Amount of step times required on the replacement exercise.

B = The amount of simulation step times that are inside the aging step time.

Δt = Step time of the simulation.

Δs = Input sample time.

$EoL_{TH}^{(j)}$ = The End of Life threshold of the (j) size option.

$\bar{I}^{(j,u)}$ = The input current profile vector of the (j) size option at (u) simulation time step.

$ELECTRIC_THERMAL_M$ = The electric-thermal model.

$AGING_M$ = The aging model.

$SOC^{(u)}$ = The State of Charge at (\mathbf{u}) simulation time.
 $T^{(u)}$ = The temperature of the cell at (\mathbf{u}) simulation time.
 $V^{(u)}$ = The voltage response of the battery at (\mathbf{u}) simulation time.
 $Q^{(u)}$ = The dischargeable capacity at (\mathbf{u}) simulation time.
 $R^{(u)}$ = The pure ohmic resistance at (\mathbf{u}) simulation time.
COST_CALCULATION = The cost calculation equation.
 $CI^{(j)}$ = Initial capital costs of the (j) size option.
RC = Replacements done all along the lifespan of the project.
 $COST^{(j)}$ = Total cost of the (j) size option.

Algorithm 5: Algorithm of the updated simulation environment to an Electric Vehicle application.

The sizing exercise has been applied on two different types of applications of an electric bus fleet: an electric bus fleet that requires a High-Energy battery and an electric bus fleet that requires a High-Power battery. The application scenario has been simplified to only one bus line on each type of application. The sizing activity of the battery solution on the buses of each bus line is repeated, see Table 93. Therefore, the sizing of the battery solution of the bus of one bus line is considered enough to test the proposed methodology under different types of electric vehicle application.

Bus line	Daily current profile	Yearly operation	EOL	Optimal size
1		320 days working. 45 days resting.	90% SOH	20 modular battery units
2		300 days working. 65 days resting.	60% SOH	26 modular battery units
...
N		320 days working. 45 days resting.	83% SOH	58 modular battery units

Table 93: A fictitious example of the sizing activity of an entire bus fleet with N bus lines

4.3.2 Stationary application

The stationary application of lithium ion batteries is a consequence of increasing the rate of solar and wind renewable energy on the grid. This kind of renewable energy cannot be generated in a flexible way; it depends on the weather conditions. Therefore, it requires an energy balancing element. In

this scenario, lithium ion battery based Energy Storage Systems are positioning first in the market [3][4].

This particular application of lithium ion batteries used to have some sizing common criteria. Firstly, there used to be a pre-defined minimum feasible size. Secondly, there used to be a minimum battery module level. The sizing options are reduce due to modularity limitations of the solution. Thirdly, there used to be a limit on the initial investment. The investors have a limited budget that cannot be overcome.

The stationary application has many differences respect to the electric vehicle application that complicates greatly the cost estimation. Firstly, the discharged energy from the battery generates incomes while the charged one generates expenses. Besides, the price for the charged and discharged energy is a variable element. This complicates the cost quantification. Secondly, the batteries are operated as the operator wants. The operation of the battery solution affects the cost-income balance. On one hand, the more the battery solution is used the more income is generated. On the other hand, the more the battery solution is used, the more degradation is generated and the less profitability can be obtained on future uses. Thirdly, the End of Life criteria is not always known. The stationary application may have imposed a minimum performance rate with which define the End of Life criterion or may not. Self-supply applications (at a household level or at energy plant level) are examples of the stationary application that do not have to fulfil a certain electric requirement. The battery solution of those stationary applications can be completely squeezed until the State of Health of the battery reaches the possible lowest value in terms of safety. However, even the battery manufacturers cannot determine the State of Health at which catastrophic events could occur. To solve these two issues, firstly, a techno-economic metric is provided to add the energy incomes-expenses onto the whole cost calculation: the Levelized Cost of Energy (LCOE); secondly, the simplest operation criteria is applied on all the run sizing simulations: the battery is operated to get the maximum efficiency; and thirdly, a conservative State of Health value is used to determine the End of Life.

The Levelized Cost of Energy (LCOE) is the energy price required for a project to exactly meet its operating costs in a year and the share of capital in that year. In other words, the LCOE is the minimum price at which energy must be sold for an energy project to break even [99]. For that, the cost of the whole system and the energy provided all along the lifespan of the project is calculated, Eq. (67).

$$LCOE = \frac{C}{E} \tag{67}$$

Parameters	Description
$LCOE$	The Levelized Cost of Energy.
C	The levelized cost.
E	The levelized provided energy.

Table 94: The Levelized Cost of Energy equation

Once the application is understood, the simulation environment has been adapted to the application characteristics, see Algorithm 6. The simulation environment is set up with the selected size and run with the yearly routine of the application a total of times equal to the lifespan of the project. As a result, the Levelized Cost of Energy (LCOE) provided by the battery solution all along the project lifespan is calculated. Thanks to all this, a cost value is attached to each feasible sizing option and a cost diagram is generated, from which the optimal size is highlighted (the size option with the smallest cost).

$$\{LCOE^{(j)}\}_{j=1}^p =$$

$$SIZING_{StationaryApp} (P_g, P_d, N, \Delta t, \Delta s, B, EoL_{TH}, \{CI^{(j)}\}_{j=1}^p, \{MO^{(j)}\}_{j=1}^p, \{S^{(j)}\}_{j=1}^p, \theta_{losses}, \theta_{\epsilon})$$

- 1: INITIALIZE simulation
- 2: for $i = 1$ to N do
- 3: for $u = 1$ to L do
- 4: if EoL_{TH} is reached

```

5:      REPLACEMENT exercise
6:      if  $\Delta u == M$ 
7:          END REPLACEMENT exercise
8:           $RC(i) = 1$ 
8:      INITIALIZE performance models
9:      end if
10:     else
11:          $[\bar{I}^{(u)}, E^{(u)}] = BATT\_OPERATOR(P_g^{(u)}, P_d^{(u)}, S^{(j)}, SOC^{(u-1)}, V^{(u-1)}, \theta_{losses}, \theta_{\epsilon})$ 
12:          $[SOC^{(u)}, T^{(u)}, V^{(u)}] = ELECTRIC\_THERMAL\_M(\bar{I}^{(u)}, \Delta t, \Delta s)$ 
13:         if  $\Delta u == B$ 
14:              $[Q^{(u)}, R^{(u)}] = AGING\_M(SOC^{(\Delta u)}, T^{(\Delta u)}, \bar{I}^{(\Delta u)}, \Delta t_1, \Delta s, B, Q^{(u-1)}, R^{(u-1)})$ 
15:         end if
16:     end if
17: end for
18: end for
19:  $LCOE^{(i)} = LCOE\_CALCULATION(E, CI^{(j)}, MO^{(j)}, S^{(j)}, RC, \theta_{\epsilon})$ 

```

Where

P_g = Yearly available charge power profile.

P_d = Yearly power demand profile.

BATT_OPERATOR = Decision maker of battery operation.

θ_{losses} = The variables needed to calculate the power losses (inversors etc.).

θ_{ϵ} = Economical variables.

N = Lifespan of the project.

L = The amount of simulation time steps that contains a year.

M = Amount of step times required on the replacement exercise.

B = The amount of simulation step times that are inside the aging step time.

Δt = Step time of the simulation.

Δs = Input sample time.

EoL_{TH} = The End of Life threshold.

$\bar{I}^{(u)}$ = The input current profile vector at (u) simulation time step.

E = The charged-discharged energy evolution.

ELECTRIC_THERMAL_M = The electric-thermal model.

AGING_M = The aging model.

$SOC^{(u)}$ = The State of Charge at (u) simulation time.

$T^{(u)}$ = The temperature of the cell at (u) simulation time.

$V^{(u)}$ = The voltage response of the battery at (u) simulation time.

$Q^{(u)}$ = The dischargeable capacity at (u) simulation time.

$R^{(u)}$ = The pure ohmic resistance at (u) simulation time.

LCOE_CALCULATION = The LCOE calculation equation.

$CI^{(j)}$ = Initial capital costs of the (j) size option.

$MO^{(j)}$ = Maintenance and Operation costs of the (j) size option.

RC = Replacements done all along the lifespan of the project.

$LCOE^{(i)}$ = The levelized cost of energy of the (j) size option.

Algorithm 6: Algorithm of the updated simulation environment to a Stationary application.

4.4 Validation

The proposed sizing simulation environment has been adapted to the most relevant lithium ion battery applications: the Electric Vehicle application and the stationary application. These adapted simulation environments are tested and discussed. For that, a stationary battery solution use case and two electric vehicle use cases are introduced. The work done along this thesis is profited to feed up the simulation environment such as the EOL maps and the performance models (electric, thermal and aging models). Firstly, the application characteristics are deeply analysed. Here, the cost calculation and the simulation outputs are determined. Then, the elements required on the simulation environment are constructed. Next, the elements related with the cost calculation are gathered. Finally, the obtained results are shown and discussed.

In addition to this, two relevant hypotheses done along the proposed simulation environment are analysed and discussed.

4.4.1 High-Energy Electric Vehicle application

This electric vehicle application is sized with the point of view of a bus OEM. The OEM takes responsibility to fulfil the performance and guaranty requirements imposed by the customer. The maintenance of the bus used to be done by the OEM but the operation of the bus is commonly done by a third enterprise or the customer itself.

Most of the characteristics of the High-Energy application have been already described on this thesis. The End of Life criteria has been already defined on the “End of Life Calculation Framework” chapter. Here the End of Life map for the minimum size has been already estimated. The daily current profile for the minimum size as well as the yearly days on operation and on rest is introduced on the “Aging: Testing and Modelling” chapter, with which the yearly current profile is generated. The results from the aging modelling have shown that a charge at C/3 is less harmful than a charge at 1C, so the charge current has been changed to C/3. The resume of these variables are gathered in Table 95.

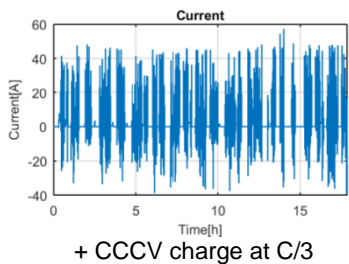
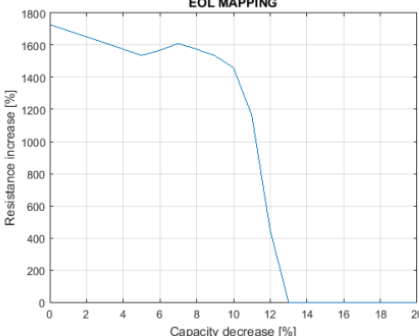
Daily current profile	Yearly operation	EOL
 <p>Current [A]</p> <p>Time [h]</p> <p>+ CCCV charge at C/3</p>	<p>320 days working. 45 days resting.</p>	 <p>EOL MAPPING</p> <p>Resistance increase [%]</p> <p>Capacity decrease [%]</p>

Table 95: Characteristics of the High-Energy minimum sizing option introduced on the sizing activity

The rest characteristics are the following ones:

- The minimum unit of the battery solution is a battery pack.
- The minimum size of the battery solution is 4 battery packs in parallel.
- The maximum size of the battery solution is 8 battery packs.
- The guaranty of the project is 10 years.

The resume of the characteristics leaves us five sizing options: 4 battery packs in 4p1s connexion (4 in parallel and 1 in serial), 5 battery packs in 5p1s, 6 battery packs in 6p1s, 7 battery packs in 7p1s or 8 battery packs in 4p2s. Before running the simulation, the current profiles for each sizing option and the EOL maps are estimated; see Figure 75 and Figure 76 respectively.

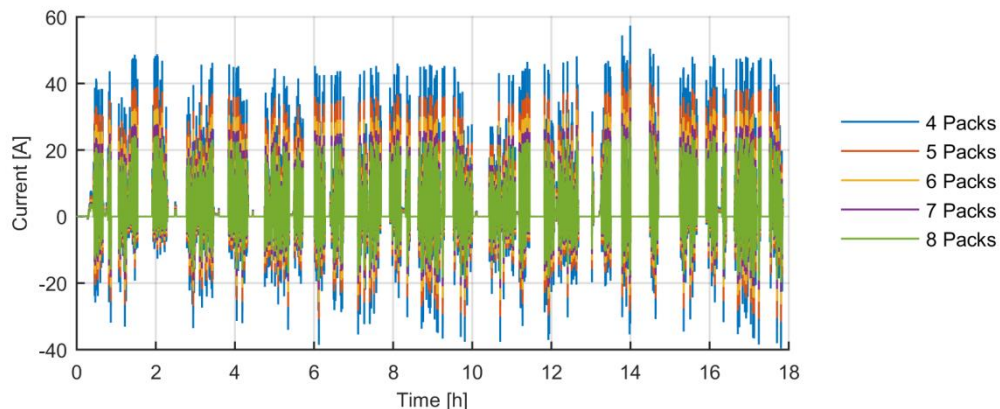


Figure 75: Current profiles of the different sizing options on the High-Energy application.

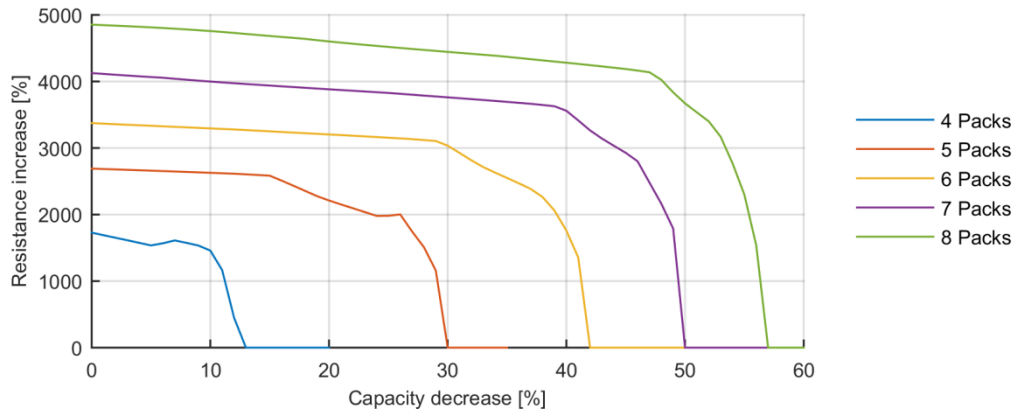


Figure 76: EOL maps of the different sizing options on the High-Energy application.

The cost of the whole battery solution can be divided in an initial capital investment (CI), the maintenance and operation cost (M&O) and the replacement cost (RC).

Firstly, the initial capital investment is calculated. For that, the components that composed the battery solution have been defined:

- The batteries.
- The battery module.
- The battery pack.
- The Battery Management System (BMS).

The cost of the batteries is defined based on nowadays commercial prices (the price of each battery is confidential). For the battery module and pack housing, an approach of the industrial cost has been introduced. For the cost of the BMS, a price of an actual BMS designed by CIDETEC has been added. The results are resumed in Table 104.

Element	CI [€]
Battery (per pack)	10,000
Battery pack and module housing (per pack)	4,000
BMS per pack	1,000

Table 96: Cost values taken into account on BESS CI calculation

Secondly, the maintenance and operation cost is defined. In this case, the maintenance of the bus doesn't depend on the sizing of the battery solution. At the same time, the operation of the bus is not done by the bus manufacturer. Therefore, the maintenance and operation cost is discarded on the cost calculation.

Thirdly, the replacement cost is calculated. The replacement is done when the EOL criteria is reached. In that moment, all the batteries are replaced. The cost of the selected battery is assumed to decrease 2% each year. With this assumption, the replacement cost is calculated at the operation years that a replacement is required.

Finally, the cost related to each sizing option is calculated. In this case, the payment is done in one time. It is not necessary to loan money to the bank. Therefore, the costs are linearly added to calculate the total cost of the battery solution.

The simulation environment is constructed and run for each possible size of the battery solution. The generated replacement events are displayed in Figure 77. The obtained results are displayed in Table 97.

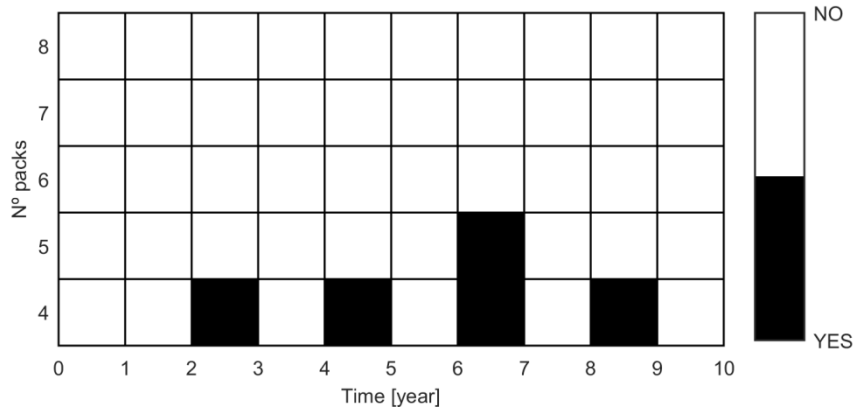


Figure 77: Replacement events on the High-Energy Electric Vehicle application.

Sizes	Initial Investment [€]	Replacement Cost [€]	Total Cost [€]
4 Battery packs	60,000	144,000	204,000
5 Battery packs	75,000	44,000	119,000
6 Battery packs	90,000	0	90,000
7 Battery packs	105,000	0	105,000
8 Battery packs	120,000	0	120,000

Table 97: Sizing simulation results of the High-Energy Electric Vehicle application

It can be seen that the replacement cost makes the smallest two sizing options more expensive than the next bigger sizing option. As a consequence, the optimum sizing is the third sizing option with 6 battery packs.

4.4.2 High-Power Electric Vehicle application

This electric vehicle application is sized with the point of view of a bus OEM. The OEM takes responsibility to fulfil the performance and guaranty requirements imposed by the customer. The maintenance of the bus used to be done by the OEM but the operation of the bus is commonly done by a third enterprise or the customer itself.

Most of the characteristics of the High-Power application have been already described on this thesis. The End of Life criteria has been already defined on the “End of Life Calculation Framework” chapter. Here, the End of Life map for the minimum size has been already estimated. The daily current profile for the minimum size as well as the yearly days on operation and on rest is introduced on the “Aging: Testing and Modelling” chapter, with which the yearly current profile is generated. The resume of these variables are gathered in Table 98.

Daily current profile	Yearly operation	EOL
<p>Current (A) vs Time (h) + CCCV charge at 1C</p>	<p>320 days working. 45 days resting.</p>	<p>EOL MAPPING: Resistance increase (%) vs Capacity decrease (%)</p>

Table 98: Characteristics of the High-Power minimum sizing option introduced on the sizing activity

The rest characteristics are the following ones:

- The minimum unit of the battery solution is a battery pack that contains 200 batteries.
- The minimum size of the battery solution is 4 battery packs.

- The maximum size of the battery solution is 5 battery packs.
- The guaranty is of the project is 15 years.

The resume of the characteristics leaves us two sizing options: 4 battery packs in 4p1s connexion (4 in parallel and 1 in serial) or 5 battery packs in 5p1s. Before running the simulation, the current profiles for each sizing option and the EOL maps are estimated; see Figure 78 and Figure 79 respectively.

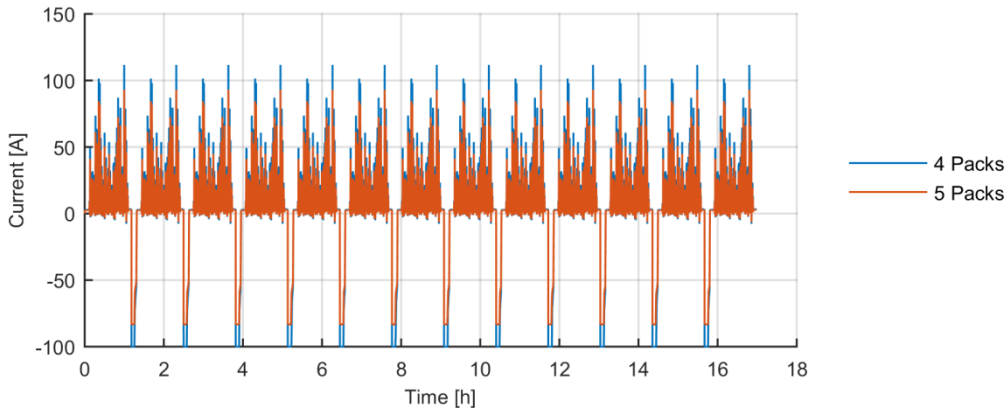


Figure 78: Current profiles of the different sizing options on the High-Power application.

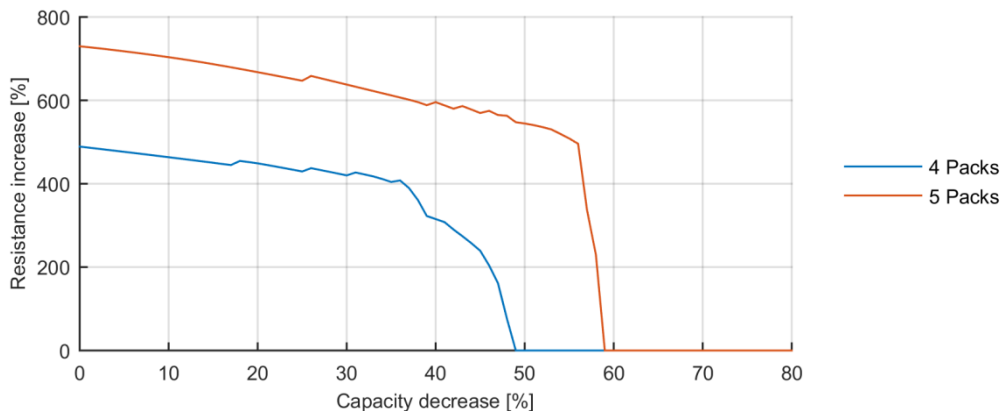


Figure 79: EOL maps of the different sizing options on the High-Power application.

The cost of the whole battery solution can be divided in an initial capital investment (CI), the maintenance and operation cost (M&O) and the replacement cost (RC).

Firstly, the initial capital investment is calculated. For that, the components that composed the battery solution have been defined:

- The batteries.
- The battery module housing.
- The battery pack housing.
- The Battery Management System (BMS).

The cost of the batteries is defined based on nowadays commercial prices (the price of each battery is confidential). For the battery module and pack housing, an approach of the industrial cost has been introduced. For the cost of the BMS, a price of an actual BMS designed by CIDETEC has been added. The results are resumed in Table 104.

Element	CI [€]
Battery (per pack)	22,000
Battery pack and module housing (per pack)	5,000
BMS per pack	1,000

Table 99: Cost values taken into account on BESS CI calculation

Secondly, the maintenance and operation cost is defined. In this case, the maintenance of the bus doesn't depend on the sizing of the battery solution. At the same time, the operation of the bus is not done by the bus manufacturer. Therefore, the maintenance and operation cost is discarded on the cost calculation.

Thirdly, the replacement cost is calculated. The replacement is done when the EOL criteria is reached. In that moment, all the batteries are replaced. The cost of the selected battery is assumed to decrease 2% each year. With this assumption, the replacement cost is calculated at the operation years that a replacement is required.

Finally, the cost related to each sizing option is calculated. In this case, the payment is done in one time. It is not necessary to loan money to the bank. Therefore, the costs are linearly added to calculate the total cost of the battery solution.

The simulation environment is constructed and run for each possible size of the battery solution. The generated replacement events are displayed in Figure 80. The obtained results are displayed in Table 100.

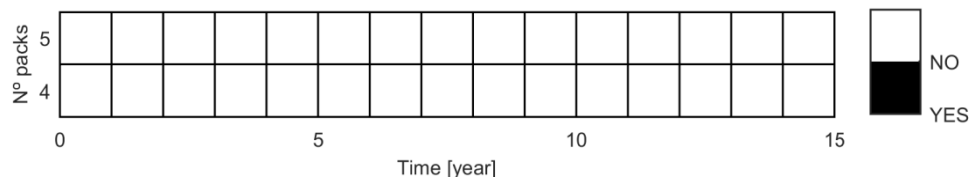


Figure 80: Replacement events on the High-Power Electric Vehicle application.

Sizes	Initial Investment [€]	Replacement Cost [€]	Total Cost [€]
4 Battery packs	112,000	0	112,000
5 Battery packs	140,000	0	140,000

Table 100: Sizing simulation results of the High-Power Electric Vehicle application

In this use case, the optimal sizing option is the smallest sizing option. The used High-Power batteries have high endurance to aging, which means that even the smallest battery solution doesn't need any replacement. As a result, the smallest size that fits the electrical and thermal requirements is also the cheapest sizing option (optimum).

4.4.3 Micro-grid stationary application

The proposed stationary application is contextualized in a CO₂-neutral, self-sufficient micro-grid that switches from island mode to grid connected mode at will (Figure 81). This micro-grid is being constructed in Zellik, Belgium and managed by VUB with the Green Energy Campus project [100]. It will host interconnected prosumers including a large green data center (>1 MW thermal producer), an incubator for start-ups, a large parking lot (150-400 vehicles) with electric charging infrastructure and 72 companies from different sectors. The Green Energy Campus will integrate renewable energy production systems (10MW solar and 13.2MW wind Energy) along with battery energy storage capacity for energy balancing issues to generate part of the demanded energy.

On this context, the battery solution is sized with the point of view of the owner of the energy installation. The owner of the energy installation takes responsibility of constructing, operating and maintaining the whole energy installation. The produced energy is used to cover the energy demand on the micro-grid. Once covered the energy demand of the micro-grid, the energy surplus is sold to Belgium's grid manager or used to charge the batteries. In case the generation cannot cover the whole demand, the batteries are used to fill the energy difference between generation and demand.

The battery system has operational aspects that affect the provided energy to the micro-grid and to Belgium's grid. As a result, the cost estimation of the energy generation elements is affected. This means that the cost estimation of the energy generation elements and the cost estimation of the battery solution cannot be divided. In consequence, the proposed cost estimation integrates the

costs and incomes generated by the energy generation elements as well as the costs and incomes generated by the Battery Energy Storage System (BESS).

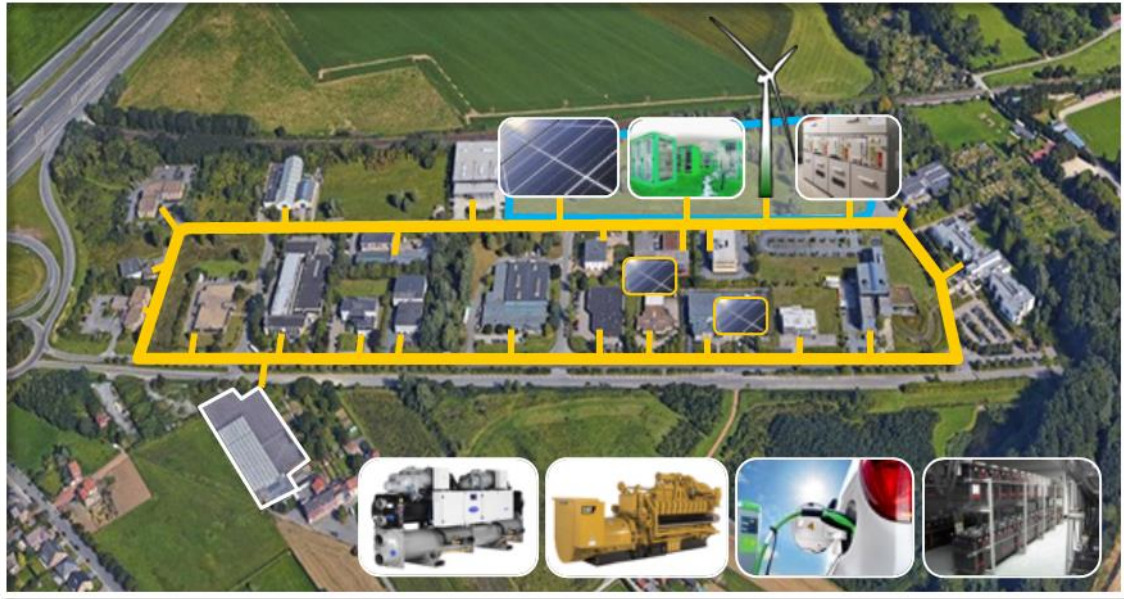


Figure 81: Green Energy Campus's electrical Micro-Grid design [100].

The cost of the energy generation installation is quantified with the LCOE. The proposed LCOE calculation approach takes some assumptions:

- The energy generation installation will have to cover the energy demand of the micro-grid ($E_{solar\&windDirect}$). The energy generation installation cannot use the energy to charge the BESS or to sell it to the grid unless this demand is completely covered.
- The grid will buy the entire energy surplus the energy generation installation has but at a reduced price respect to its cost price ($E_{surplusReduced}$).
- The BESS is only charged with the energy surplus generated by the renewable energy generation elements (the energy surplus obtained from the solar and wind power plants once the demand of the industrial park at Zellik is covered).
- The BESS is taken as an energy generation power plant where the energy used on charging and the energy losses on battery and power electronics are taken as self-consumption (discarded on the LCOE calculation).

Based on these assumptions and based on the works of C. S. Lai et al [101] and M. Bruck et al [102], the equation to calculate the LCOE is developed (Eq. (68)).

$$LCOE_{system} = \frac{\sum_{t=0}^N \frac{C_{solar} + C_{wind} + C_{BESS}}{(1+r)^t}}{\sum_{t=0}^N \frac{E_{solar\&windDirect} + E_{BESS} + E_{surplusReduced}}{(1+r)^t}} \quad (68)$$

Parameters	Description
$LCOE_{system}$	The Levelized Cost of Energy of the whole energy generation plant.
C_{solar}	The yearly cost of the solar power plant.
C_{wind}	The yearly cost of the wind power plant.
C_{BESS}	The yearly cost of the Battery Energy Storage System.
N	The lifespan of the project.
r	The discount rate.
$E_{solar\&windDirect}$	The provided energy to the micro-grid from the solar and wind power plants.
E_{BESS}	The provided energy to the micro-grid from the Battery Energy Storage System.
$E_{surplusReduced}$	The energy surplus sold to the grid

Table 101: The Levelized Cost of Energy equation adapted to the proposed stationary application

This equation introduces the yearly cost of the energy generation installations and the yearly total energy generation. In total, the energy generation plant is scheduled to be operative N years. This N

number is defined by the power plant that has the higher operation expectation. The expected lifetime from the wind and solar installations is 25 years [103], longer than the BESS lifetime. Therefore, the lifespan of the energy generation installation is set to 25 years. Another element added to the formula is the “discount rate” that represents the currency inflation (r). This parameter considers the investment risk as well as some other economic metrics used on economic assessments. As for this work, the assumed discount rate value is taken from the study on [104], that is 8.9%.

The used batteries on this stationary application are the same as the batteries used on the High-Energy Electric Vehicle application. The performance models have been already constructed. The rest characteristics of the simulation are the following ones:

- A minimum BESS of 3MWh.
- The minimum modular element is a battery module of 5kWh.
- The limit of the initial investment is 4,500,000€ (more or less 10MWh).
- The EOL threshold is set up to a 60% relative dischargeable capacity, a 250% relative pure ohmic resistance or to the failure of covering the demand of the micro-grid at least half of the year.
- The BESS is charge and discharged whenever it is possible as long as the safety window is respected.

The resume of the characteristics leaves us 1401 sizing options: from 3MWh to 10MWh with a step of 5kWh. There are too many options with low relevance (3.000MWh and 3.005MWh are practically the same); therefore, it has been decided to increase the step to 1MWh. This leaves us 8 sizing options: 3MWh, 4MWh, 5MWh, 6MWh, 7MWh, 8MWh, 9MWh and 10MWh.

Before running the simulation, the energy generation and demand power profiles are calculated. The required energy (demand) is calculated from the 2017’s energy consumption of the 70 enterprises placed at the Green Campus (Figure 82) and from the thermal management system of the BESS. The selected thermal management system consists on a liquid heating-cooling system that will ensure a constant operation temperature of 25°C. The consumption has been assumed to be proportional with a factor of 1.5 to the cooling power required to keep those constant 25°C, see Figure 83.

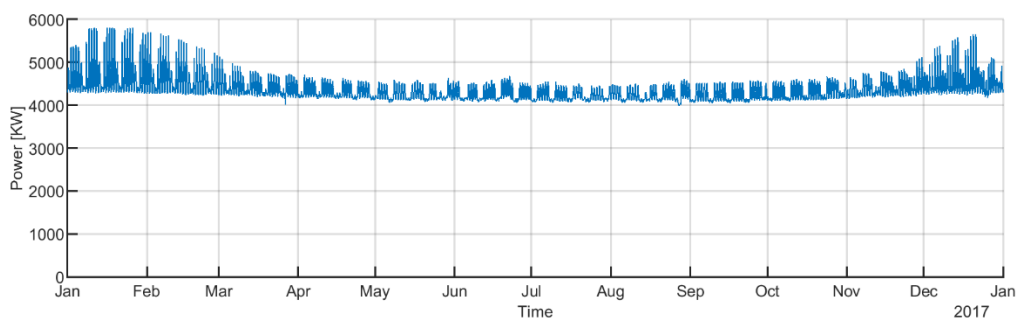


Figure 82: The demand on Zellik on 2017 with an interval of 15 min.

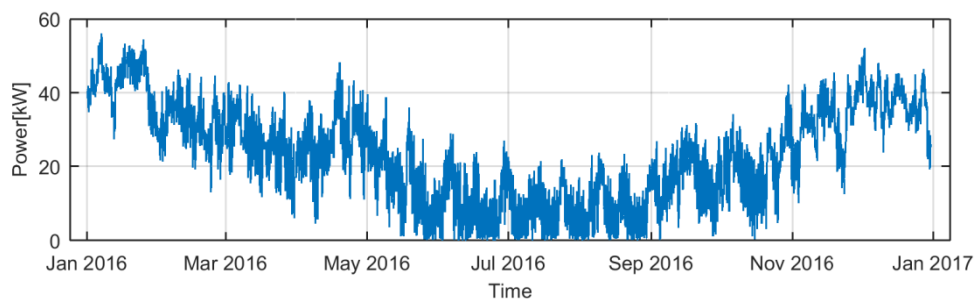


Figure 83: The energy demand from the Thermal Management System.

The energy generation is calculated from the solar and wind energy generation. As for simplifications, due to restrictions on data availability, the yearly solar and wind energy generation is taken as constant (the environmental conditions given on 2017 are repeated every year). The wind power is calculated based on the wind speed measured on Zellik. The wind speed is used on a look up table function where it is related with the power generation of a 3.3 MW wind turbine (Figure 84). In total, 4 wind turbines are installed, making it an installation of 13.2 MW.

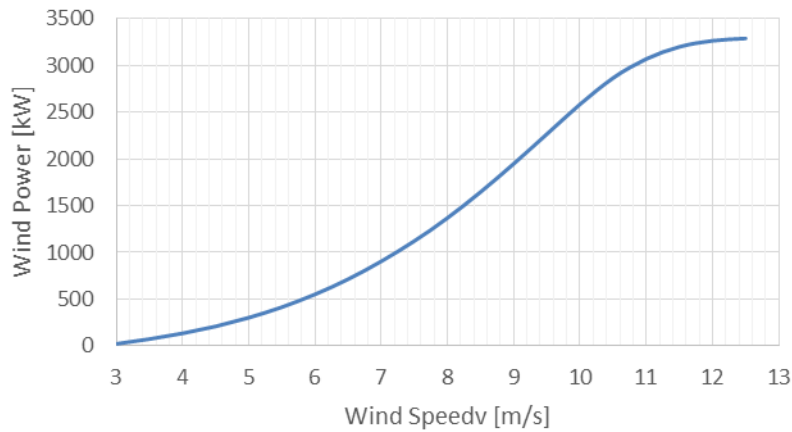


Figure 84: Wind Power generation of a 3,3MW wind turbine.

The chosen solar energy generation is Photovoltaic (PV). The PV energy generation calculus is based on a 816 KW peak power PV generation system that is already installed at Zellik. The power generation and the installed peak power generation are considered to be linearly proportional and the scaling is done dividing the generation data by 816 and multiplying by the installed peak power generation in kW, which in this case is 10 MW.

Once obtained the yearly power profiles of the generation and demand, the simulation is run. To do so, the operation of the BESS along the whole project lifespan is simulated. On the simulation, the battery operator decides how to use the batteries in terms of the defined operation criteria (conservative operation). The battery dynamic behaviour and deterioration are modelled to couple realistically the imbalance between the energy generation and the demand. In addition, the energy losses given by the Joule effect on the BESS and the converter efficiency are quantified. In the case of BESS Joule effect losses, the losses depend on the efficiency of the battery, the increase of the resistance due to the aging and the power the BESS is operated (Eq. (69)).

$$P_{joule}(t_k) = P(t_k) \cdot \eta_{BESS} \cdot \Delta R_{r,0 \text{ to } k} \quad (69)$$

Parameters	Description
$P_{joule}(t_k)$	The power losses due to the Joule effect at time instant t_k .
$P(t_k)$	The power that is demanded to or from the battery solution at time instant t_k .
η_{BESS}	The efficiency of the battery.
$\Delta R_{r,0 \text{ to } k}$	The relative increment of the pure ohmic resistance of the battery (respect to the nominal value) from time instant t_0 to time instant t_k .

Table 102: Joule losses on the BESS

In the case of the converter, each commercial converter has an efficiency curve which can be used to know the losses on the converter (Figure 85). The chosen converter is the SIEMENS sinvert 200 MS [105]. The images of data has been reverse engineered to extract the underlying numerical data available using the WebPlotDigitizer [106].

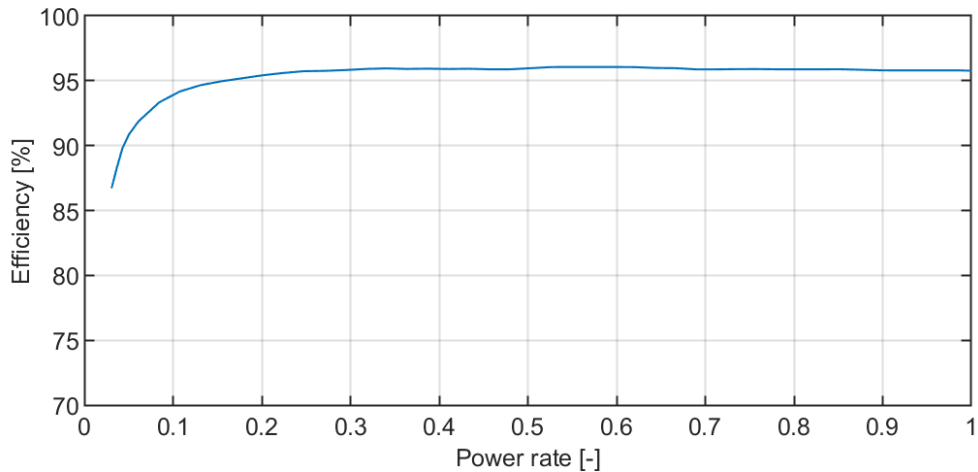


Figure 85: Efficiency of SIEMENS sinvert 200 MS [105].

The simulation is kept without any maintenance event unless the EOL threshold is reached. When the EOL is reached, the replacement exercise is set up and all the battery are replaced. The BESS is disabled for a replacement time and the deterioration of the batteries is reset to the initial values.

After simulating the BESS behaviour for the lifespan of the project, the cost related to its operation are estimated. The cost of the whole installation has been assumed to be the sum of the costs of each energy generation that the micro-grid is composed. This cost comprises the costs of the solar power plant, the wind power plant and the BESS, which are divided in the initial capital investment (CI), the maintenance and operation cost (M&O) and the replacement cost.

The cost of the solar and wind power plants are taken from average cost values calculated by the European Commission [103]. The cost values used on the simulations are shown in Table 103, where in this case, the M&O comprises also the replacement cost. The CI value given by the European Commission and the M&O value given by the Green Campus project is multiplied by the installed MW (13.2 for wind and 10 for solar).

Generation type	CI [€/KW]	M&O [€/MWyear]
Solar PV (ground)	800	34,000
Wind onshore	1,767	50,000

Table 103: Cost values of an average solar and wind power plant on Belgium [103]

In the case of the BESS, the cost has been calculated from the scratch. Firstly, the components of the BESS installation have been defined:

- The batteries.
- The battery module.
- The Battery Management System (BMS).
- The battery container.
- The energy converter.
- The thermal management system.

For the batteries and battery modules, an approach of the industrial cost has been introduced. For the cost of the BMS, a price of an actual BMS designed by CIDETEC has been added. The cost of the battery container considers both, the space to stock all the battery modules (industrial containers) as well as the infrastructure to stack them (shelving for heavy loads). The cost for the energy converter is calculated multiplying the required number of converters with the cost of the chosen commercial converter: SIEMENS sinvert 200 MS. The cost of the proposed thermal management system is calculated based on commercial elements and CIDETEC's expertise. The results are resumed in Table 104.

Element	CI [€]
BESS battery (per module)	1,000
BESS housing (per module)	400
BMS per module	100
Container	13,500
Converter (unit)	50,000
Thermal management system	50,000

Table 104: Cost values taken into account on BESS CI calculation

Secondly, the M&O is calculated. Based on our experience, the yearly maintenance cost of a 1 MW BESS installation is 3,000 €. The operation cost is assumed to be the cost of having a qualified employee hired to operate the BESS (50,000€).

Finally, the replacement cost is calculated. The replacement is done when the EOL criteria is reached. In that moment, all the batteries are replaced. The cost of the selected battery is assumed to decrease 2% each year. With this assumption, the replacement cost is calculated at the operation years that a replacement is required, see Figure 86.

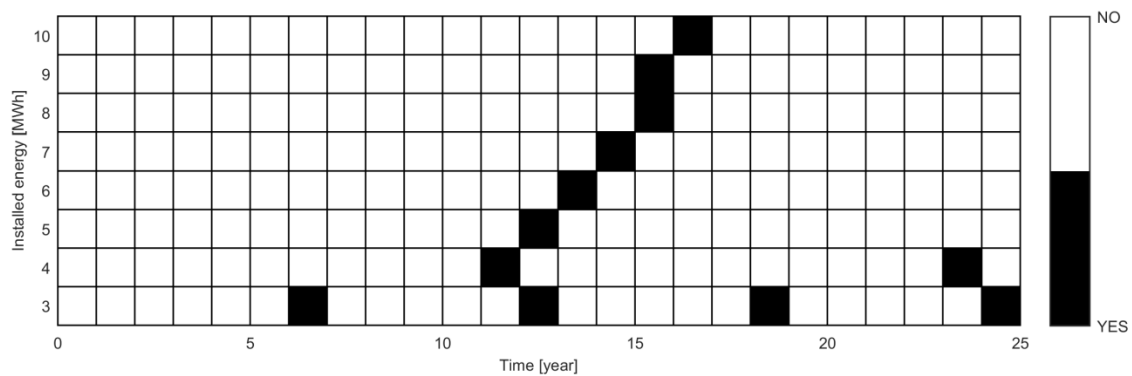


Figure 86: Replacement events on the Micro-grid stationary application.

Once the investment cost is properly defined, the maintenance and operation cost and the replacement cost, the total cost of the whole energy generation plant is calculated. For that, one more assumption is taken: the initial investment is done with a 10-year loan to a bank with an interest of 5% to pay in yearly payments. The calculus of the payment of each year is done with MATLAB's function "payper" [107]. Then, the obtained values along the loan interest for each year are used as the yearly cost on the LCOE calculation (Eq. (68)).

All the calculated LCOE are shown in Table 105 and in Figure 87. In addition, the contribution of each the battery solution to the LCOE value is displayed in Figure 88.

Sizes	LCOE [€/MWh]
3 MWh	130,56
4 MWh	130,90
5 MWh	133,56
6 MWh	136,56
7MWh	139,63
8 MWh	142,79
9 MWh	145,96
10 MWh	149,03

Table 105: LCOE simulation results of the Micro-grid stationary application

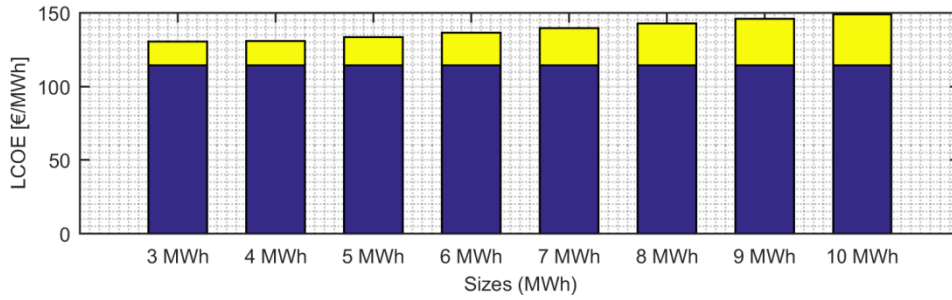


Figure 87: LCOE results. The blue part of each bar represents the LCOE contribution of the solar and wind power plants and the yellow part represents the contribution of the BESS on the selected BESS size.

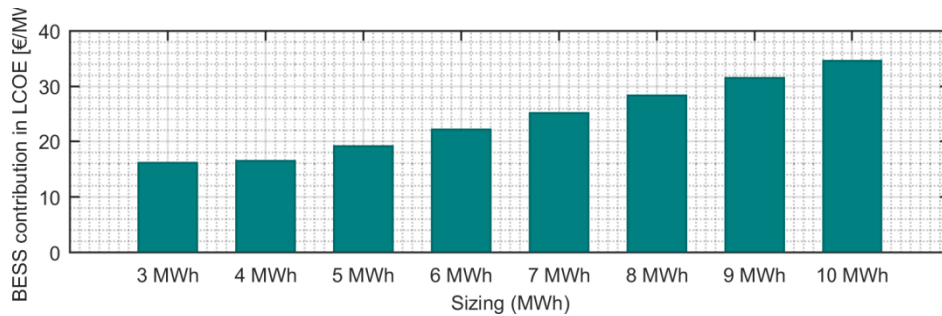


Figure 88: BESS contribution on the LCOE of the whole energy generation plant of the evaluated micro-grid.

The results show that the most profitable sizing is the smallest sizing option (3 MWh). However, there is a small difference between the LCOE obtained with 3MWh and 4MWh (0.34 €/MWh) and there is an important difference on the time the whole micro-grid can work on island mode, see Figure 89. Roominess on the operation of the BESS opens a range of possibilities such as offering additional ancillary services to another grid (additional incomes) or the reduction of the operation conditions (reduction of the replacement costs) [108].

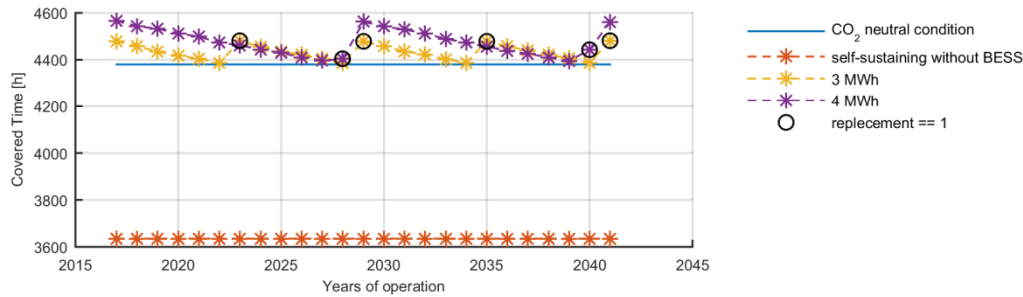


Figure 89: The covered time at island mode by the energy generation plant.

The sizing needs to consider these possibilities if applicable. However, the operation of the proposed battery solution on this Micro-grid stationary application is believed to be restricted to the evaluated case: the BESS is operated in order to maximize the operation time. Supplementary information about the effect of the BESS operation criteria is available in [108].

4.4.4 Hypotheses validation

The proposed sizing methodology is consolidated on some strong hypotheses. From all of them, the following ones have been studied in detail:

- A resting time inferior of 3h generates a relaxing effect instead of a calendar aging effect.
- The damage generated on the different operation modes can be added in a cumulative damage model.

For that, specific aging tests have been run on certain batteries that have given information about the correctness of these hypotheses. The selected battery is SAMSUNG's ICR18650-26F lithium-ion battery. The characteristics of this battery are shown in Table 106.

Item	Specification
Nominal Capacity	2600 [mAh]
Fast charge current	2600 [mA]
Fast discharge current	5200 [mA]
Maximum temperature	45 [°C]
Minimum temperature	0 [°C]

Table 106: SAMSUNG's ICR18650-26F battery specifications

As introduced on "Aging: Testing and Modelling" chapter, in order to study the third hypothesis, two types of tests are thought to be needed: a reference test without any resting time and a test with a cycling operation mode that intercalates rest time smaller than 3h. In order to test the fourth hypothesis, two types of tests are thought to be needed: a test with non-variable or static operation conditions and a test with an operation condition that changes from one static operation to another one, repeating the same static operation conditions in a closed loop way. This can come from only cycling operation conditions or it can come from mixing operation conditions that generate cycling aging as well as calendar aging.

Test	Upper SOC	Discharge time	Discharge current	Rest SOC	Rest time	Operation mode
1	-	-	-	20[%]	Inf	Resting
2	-	-	-	40[%]	Inf	Resting
3	-	-	-	60[%]	Inf	Resting
4	-	-	-	100[%]	Inf	Resting
5	100[%]	30[min]	2080[mA]	-	-	Static cycle
6	100[%]	30[min]	3120[mA]	-	-	Static cycle
7	100[%]	30[min]	4160[mA]	-	-	Static cycle
8	100[%]	30[min]	A train of cycles of tests 5, 6 and 7	-	-	Dynamic cycle
9	100[%]	30[min]	A train of cycles of tests 5, 6 and 7	End of charge	1[h]	Dynamic cycle
10	100[%]	30[min]	A train of cycles of tests 5, 6 and 7	End of discharge	1[h]	Dynamic cycle
11	100[%]	30[min]	A train of cycles of tests 5, 6 and 7	End of charge	8[h]	Dynamic cycle
12	100[%]	30[min]	A train of cycles of tests 5, 6 and 7	End of discharge	8[h]	Dynamic cycle
13	100[%]	30[min]	Mean value of 2080[mA]	-	-	Real cycle
14	100[%]	30[min]	Mean value of 3120[mA]	-	-	Real Cycle

Table 107: Aging test matrix design to validate the main hypotheses done on the aging model development

The ACT developed on this study is the same as the one used on the previous validations: a capacity validation test, an OCV characterization test using low C-rate values and an impedance characterization test using charge and discharge pulse tests all along the SOC range.

After the design of all the required tests (the aging test matrix and the ACT), these tests have been run for 6 months in CIDETEC's facilities and the obtained data has been treated with the aim of validating the proposed two hypotheses.

4.4.4.1 First hypothesis validation

Among the tests defined on Table 88, the test 8 (reference) and the tests 9 and 10 (1h rest period) are evaluated to validate the first hypothesis. For that, the health indicators of interest are extracted from the data obtained from the tests: the dischargeable capacity and pure ohmic resistance, see Figure 69 and Figure 70.

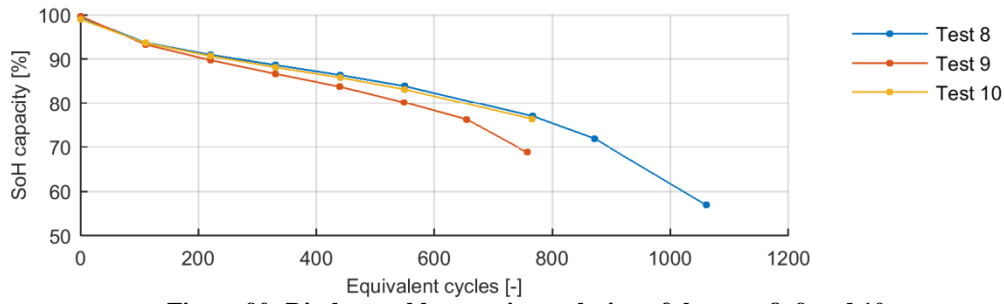


Figure 90: Dischargeable capacity evolution of the tests 8, 9 and 10.

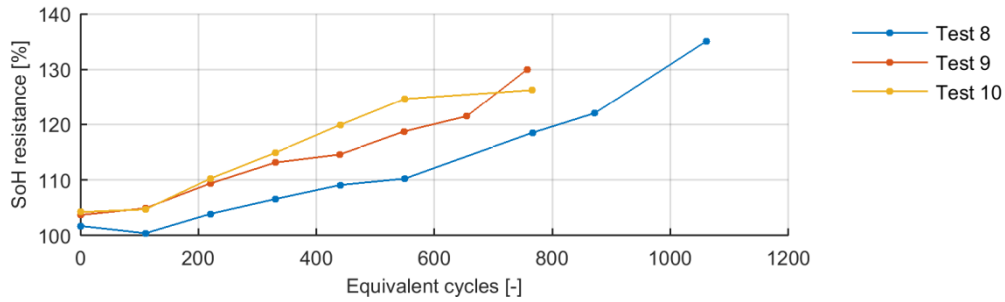


Figure 91: Pure ohmic resistance evolution of the tests 8, 9 and 10.

In this case, the validation of the hypothesis comes from the testing data itself. The assumed hypothesis states that the aging on the test 8 (no rest time) and the aging on the tests 9 and 10 (rest times shorter than 1h) are the same. The observed pure ohmic resistance aging paths have quite similar trends, which supports this hypothesis. The test 8 experiences an unexpected resistance decrease on the second ACT, but the aging paths from this point onwards are almost parallels. On the other hand, the dischargeable capacity evolution shows a contradiction. The dischargeable capacity of test 9 reduces much faster than the tests 8 and 10, but the dischargeable capacity evolution of test 10 and test 8 are practically the same. Surprisingly, the test with rest times at middle SOC values (20%, 40% and 60%) shows a different degradation path than the test with rest times at 100% SOC. This could indicate that there is not a relaxation effect at high SOC; instead, there is calendar aging.

To prove that the increase on the observed aging path’s trend of the test 9 comes from the calendar aging, the addition of both aging is calculated with the developed cycling and calendar aging models at the “Aging: Testing and Modelling” chapter, see Eq. (65) and Eq. (66). The results are displayed in Figure 67 and Figure 68.

$$Q = Q_{ini} - (4.07e^{-5} \cdot t^{1.23}) - (1.37e^{-4} \cdot cyc) \tag{70}$$

$$R = R_{ini} + (1.21e^{-4} \cdot t^{1.35}) + (8.89e^{-5} \cdot cyc) \tag{71}$$

Parameters	Description
Q	The dischargeable capacity.
Q_{ini}	The dischargeable capacity value at Beginning of life (initial value).
t	The resting time related to calendar aging in days.
cyc	The discharged energy in Ah.
R	The pure ohmic resistance.
R_{ini}	The pure ohmic resistance value at Beginning of life (initial value).

Table 108: Parameters of the complete aging model

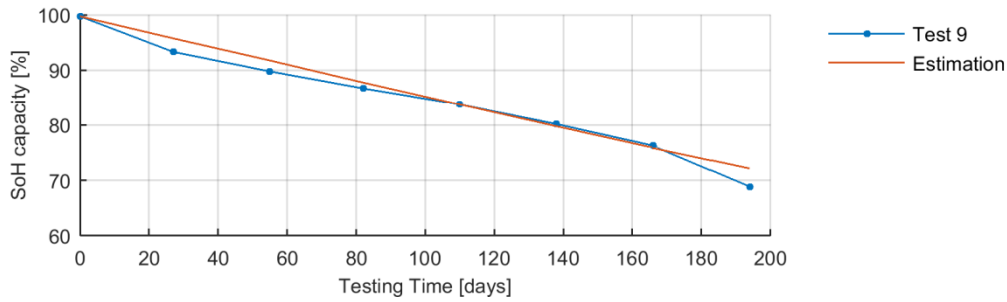


Figure 92: Comparison of the observed dischargeable capacity evolution in the test 9 (blue dotted line) and the estimated dischargeable capacity with the complete aging model (red line).

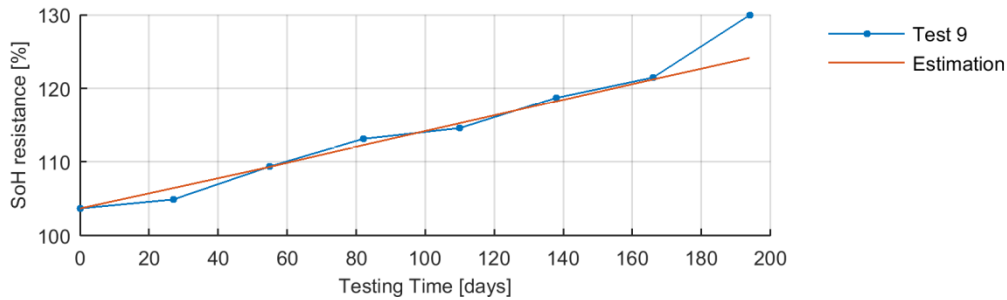


Figure 93: Comparison of the observed pure ohmic resistance evolution in the test 9 (blue dotted line) and the estimated pure ohmic resistance with the complete aging model (red line).

The estimated aging path that considers both calendar and cycling aging contributions matches the aging path generated with rest times of 1h at 100% SOC. The results show that the test 9 has a calendar aging contribution even though having a rest time of just 1h.

To sum up, it has been proved that rest times of 1h at middle SOC does not generate any degradation but that rest times of 8h at those middle SOC does generate it. In contrast, rest times of 1h at 100% SOC generates calendar aging from the start of the rest period.

In this scenario, in order to completely validate that there is a relaxation effect on rest times below 3h, the generation of calendar aging at higher rest times is studied. In this way, the confirmation of having different deterioration behaviour at different rest periods is evaluated. Among the tests defined on Table 88, the test 1, 2 and 3 (only resting), the test 8 (only cycling) and the test 12 (mix of resting and cycling at middle SOC) are evaluated to completely validate the first hypothesis. For that, the health indicators of interest are extracted from the data obtained from the tests: the dischargeable capacity and pure ohmic resistance, see Figure 94 and Figure 95.

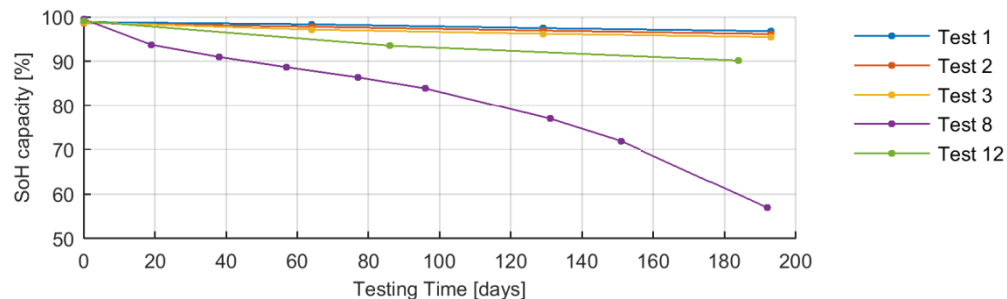


Figure 94: Dischargeable capacity evolution of the tests 1, 2, 3, 8 and 12.

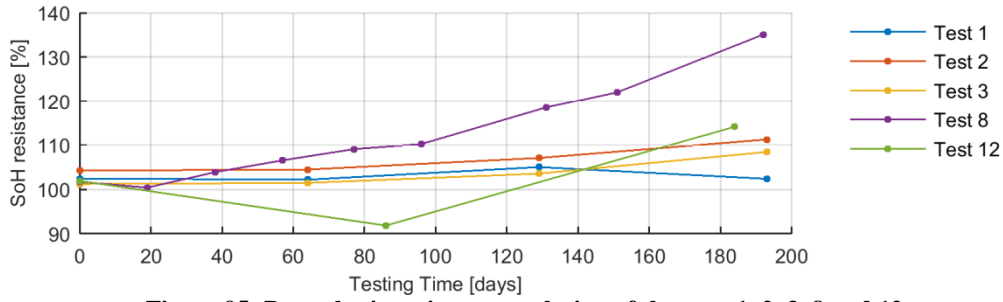


Figure 95: Pure ohmic resistance evolution of the tests 1, 2, 3, 8 and 12.

Then, the extracted health indicators are modelled with the aim of correlating the health indicator evolution with the resting time and with the discharged energy. This modelling exercise only requires fitting the observable trends of the health indicators extracted from the tests 1, 2, 3 and 8 with a mathematical expression. The required steps to fulfil this modelling exercise are detailed on the first phase of the proposed aging modelling methodology section of the “Aging Modelling” chapter. Furthermore, the Health Indicators extracted from the test 8 are already modelled. The efforts need to be done with the calendar aging representation of tests 1, 2 and 3.

The first phase of the proposed modelling methodology consists on choosing the mathematical expression that fits better the selected health indicators (dischargeable capacity and the pure ohmic resistance). The tested mathematical expressions are shown in Table 89.

Aging	Linear	Exponential	Logarithmic	Power type	2 nd order polynomial
Calendar	x	x	x	x	x

Table 109: Selection of mathematical expressions to describe the aging trend

The fitting accuracy is measured with the Root Mean Square Error (RMSE) metric between the measurements and the estimation done with the fitted mathematical expression. This metric has been calculated on tests 1, 2, 3 for the two selected health indicators, see Table 90 and Table 91.

	Linear	Exponential	Logarithmic	Power type	2 nd order polynomial
Test 1	0,00073	0,00031	0,00520	0,00048	0,00057
Test 2	0,00019	0,00072	0,00543	0,00015	0,00019
Test 3	0,00228	0,00082	0,00539	6,414e-05	0,00228

Table 110: Fitting RMSE of the dischargeable capacity evolution data extracted from the proposed test number 1, 2 and 3

	Linear	Exponential	Logarithmic	Power type	2 nd order polynomial
Test 1	0,01132	0,01088	0,01121	0,01112	0,01132
Test 2	0,00989	0,00019	0,02349	0,00139	0,00208
Test 3	0,01464	0,01446	0,01449	0,01446	0,01464

Table 111: Fitting RMSE of the pure ohmic resistance evolution data extracted from the proposed test number 1, 2 and 3

The fitting of the data of both health indicators show that the mathematical expression that fits better the results obtained from the test 1, 2 and 3 is the power type equation or the exponential equation. The work done with the other calendar aging tests (test 4) showed that the mathematical expression that fits better the results is the power type equation. Therefore, the power type equation is selected.

The selected calendar and cycling aging models are added linearly in a complete aging model, see Eq. (72) and Eq. (73). The aging on test 12 is estimated and displayed in Figure 96 and Figure 97.

$$Q = Q_{ini} - (4.51e^{-5} \cdot t_1^{1.16} + 1.48e^{-4} \cdot t_2^{0.97} + 1.10e^{-3} \cdot t_3^{0.64}) - (1.37e^{-4} \cdot cyc) \quad (72)$$

$$R = R_{ini} + (1.30e^{-3} \cdot t_1^{0.37} + 4.21e^{-7} \cdot t_2^{2.28} + 5.40e^{-3} \cdot t_3^{0.00}) + (8.89e^{-5} \cdot cyc) \quad (73)$$

Parameters	Description
Q	The dischargeable capacity.
Q_{ini}	The dischargeable capacity value at Beginning of life (initial value).

t_i	The resting time related to calendar aging in days related to the test i .
cyc	The discharged energy in Ah.
R	The pure ohmic resistance.
R_{ini}	The pure ohmic resistance value at Beginning of life (initial value).

Table 112: Parameters of the complete aging model

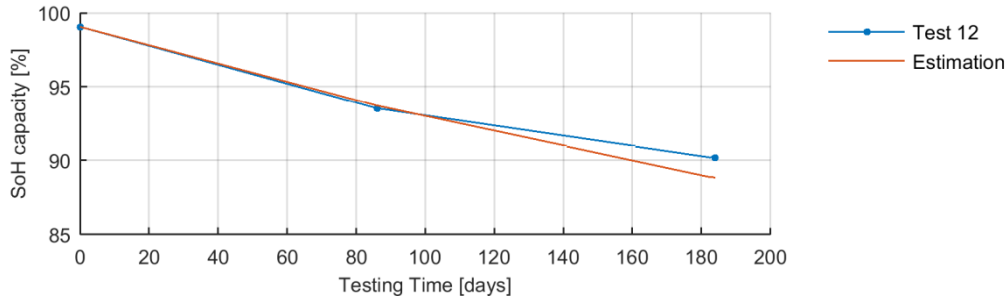


Figure 96: Comparison of the observed dischargeable capacity evolution in the test 12 (blue dotted line) and the estimated dischargeable capacity with the complete aging model (red line).

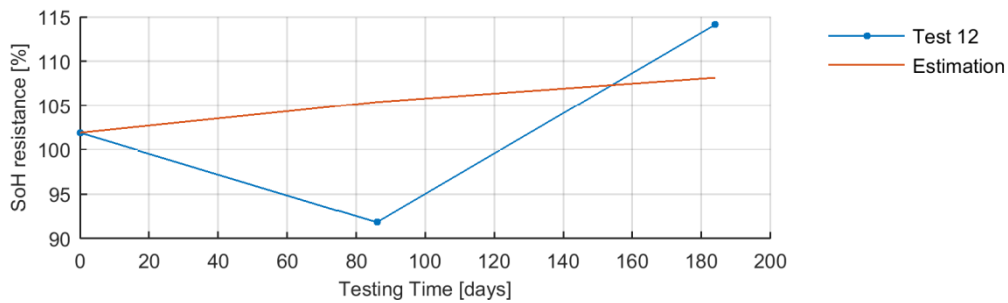


Figure 97: Comparison of the observed pure ohmic resistance evolution in the test 12 (blue dotted line) and the estimated pure ohmic resistance with the complete aging model (red line).

The results show that there is a contribution of calendar aging with rest time of 8h. This supports the hypothesis of having a different behavior depending on the length of the rest period.

4.4.4.2 Second hypothesis validation

A cumulative aging model implies that the aging is independent to its previous state. The damage on the battery is linearly added as time advances independently to its previous use. It has been proved already that the calendar aging and the cycling aging can be added in a cumulative way on “Aging Modelling” chapter, however, it still remains to test if the aging generated at different operation conditions fulfils this hypothesis. Among the tests defined on Table 88, the test 8 with cycling static operation conditions (tests 5, 6 and 7) and that with dynamic operation conditions (tests 8) are evaluated to validate the second hypothesis. For that, the health indicators of interest are extracted from the data obtained from the tests: the dischargeable capacity and pure ohmic resistance, see Figure 98 and Figure 99.

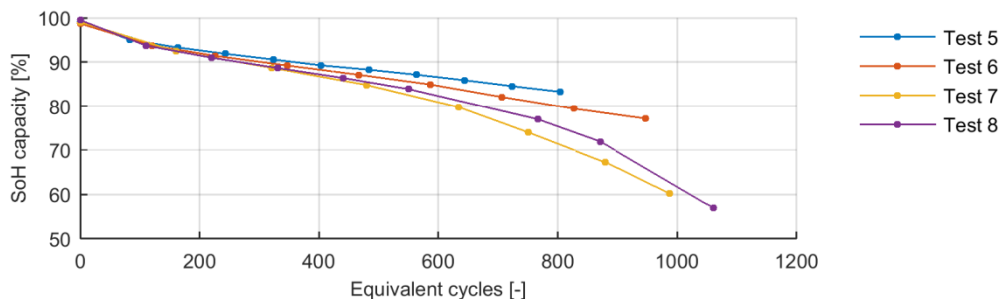


Figure 98: Dischargeable capacity evolution of the tests 5, 6, 7 and 8.

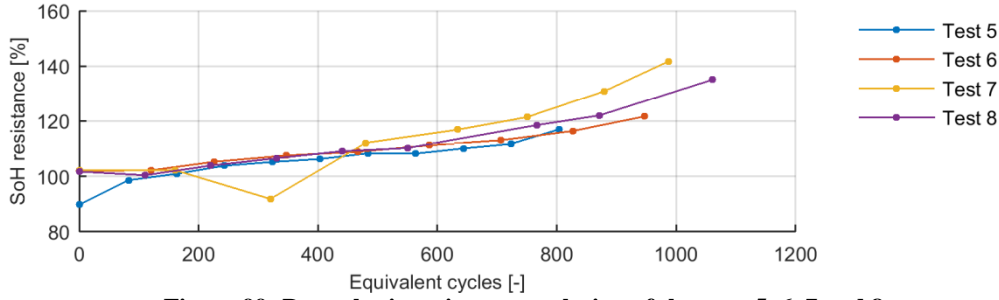


Figure 99: Pure ohmic resistance evolution of the tests 5, 6, 7 and 8.

Then, the extracted health indicators are modelled with the aim of correlating the health indicator evolution with discharged energy. This modelling exercise only requires fitting the observable trends of the health indicators extracted from the tests with static operation conditions (tests 5, 6 and 7) with a mathematical expression. The required steps to fulfil this modelling exercise are detailed on the first phase of the proposed aging modelling methodology.

The first phase of the proposed modelling methodology consists on choosing the mathematical expression that fits better the selected health indicators (dischargeable capacity and the pure ohmic resistance). The tested mathematical expressions are shown in Table 113.

Aging	Linear	Exponential	Logarithmic	Power type	2 nd order polynomial
Cycling	x	x	x	x	x

Table 113: Selection of mathematical expressions to describe the aging trend

The fitting accuracy is measured with the Root Mean Square Error (RMSE) metric between the measurements and the estimation done with the fitted mathematical expression. This metric has been calculated on the tests 5, 6 and 7 for the two selected health indicators, see Table 114 and Table 115.

	Linear	Exponential	Logarithmic	Power type	2 nd order polynomial
Test 5	0,00832	0,01044	0,03140	0,00248	0,00832
Test 6	0,00688	0,01425	0,04755	0,00435	0,00688
Test 7	0,02066	0,02370	0,09606	0,01353	0,01103

Table 114: Fitting RMSE of the dischargeable capacity evolution data extracted from the proposed test number 5, 6 and 7

	Linear	Exponential	Logarithmic	Power type	2 nd order polynomial
Test 5	0,02199	0,02196	0,04287	0,01246	0,02199
Test 6	0,01180	0,01328	0,05247	0,00829	0,00774
Test 7	0,06865	0,04144	0,14216	0,04411	0,04504

Table 115: Fitting RMSE of the pure ohmic resistance evolution data extracted from the proposed test number 5, 6 and 7

The fitting of the data of both health indicators show that the mathematical expression that fits better all the results is the power type equation. The constructed calendar and cycling aging models are added linearly in a complete aging model, see Eq. (74) and Eq. (75). The aging on test 12 is estimated and displayed in Figure 96 and Figure 97.

$$Q = Q_{ini} - (1.13e^{-3} \cdot cyc_1^{0.64} + 3.63e^{-4} \cdot cyc_2^{0.81} + 4.16e^{-6} \cdot cyc_3^{1.44}) \quad (74)$$

$$R = R_{ini} + (5.25e^{-3} \cdot cyc_1^{0.49} + 2.36e^{-6} \cdot cyc_2^{1.44} + 6.31e^{-9} \cdot cyc_3^{2.29}) \quad (75)$$

Parameters	Description
Q	The dischargeable capacity.
Q_{ini}	The dischargeable capacity value at Beginning of life (initial value).
cyc_i	The discharged energy in Ah related to the test $i + 4$.
R	The pure ohmic resistance.
R_{ini}	The pure ohmic resistance value at Beginning of life (initial value).

Table 116: Parameters of the complete aging model

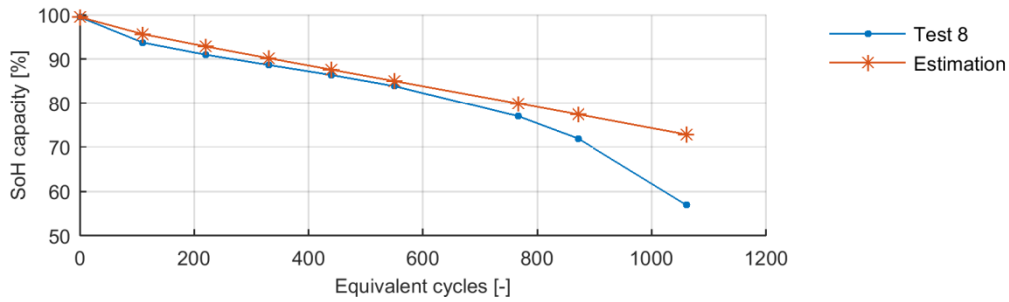


Figure 100: Comparison of the observed dischargeable capacity evolution in the test with dynamic operation conditions (dots) and the estimated one with the complete aging model (stars).

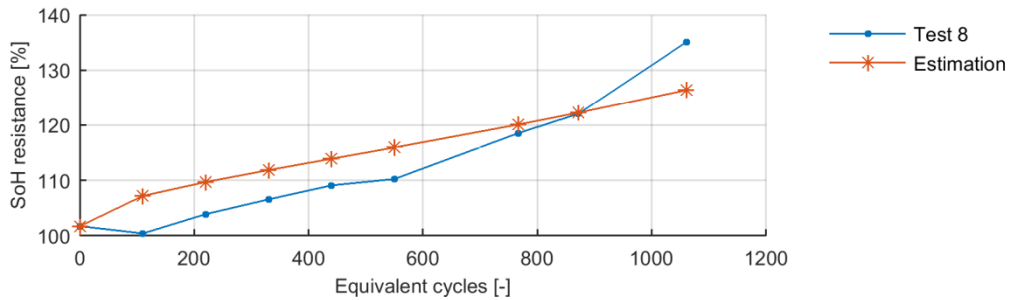


Figure 101: Comparison of the observed pure ohmic resistance evolution in the test with dynamic operation conditions (dots) and the estimated one with the complete aging model (stars).

The results show that the model does not describe the pure ohmic resistance and the dischargeable capacity evolution at the last observed ACTs. Both aging trends at the last ACTs change but the model does not show this change. The reason behind this is attributed to the change on the first derivative of the mathematical expression (also referred as the aging rate). The used power type equation has a derivative value dependent to the discharged energy. This implies that the aging rate is different at different state of health. In this scenario, the direct linear adding of the aging generates a cumulative error that increases with time, having the highest errors at the latest state of health observations.

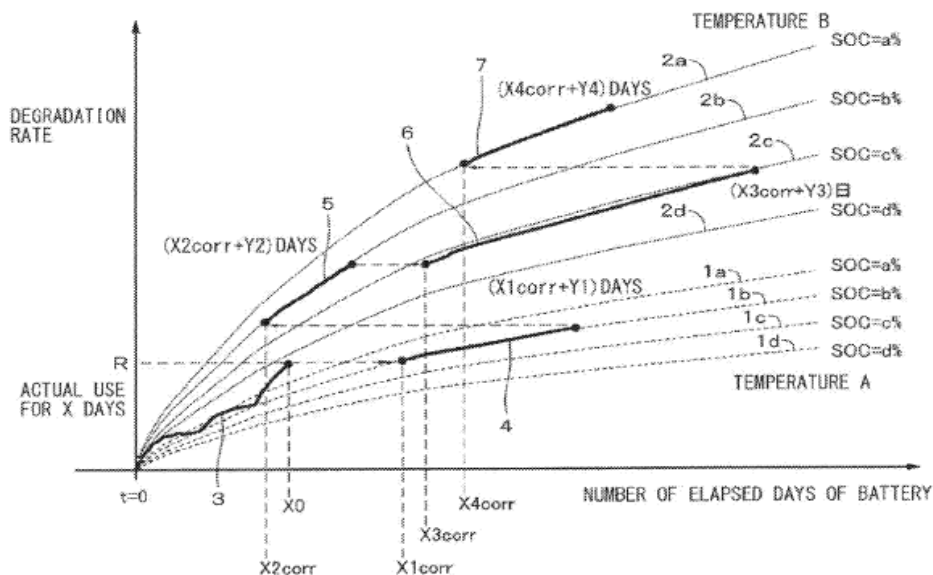


Figure 102: Elapsed concept on cumulative aging model [109].

The solution of the linear addition has been thought to be resolved with the concept of elapsed time (and elapsed discharged energy) used on [109]. Yukio [109] stated that there are some master curves (also referred as aging paths) that correspond to the deterioration at specific operation conditions. The real aging path of the battery can be deduced from this master curves, see Figure

102. Basically, the proposal on [109] requests to determine the elapsed time (or elapsed discharged energy if calculating cycling aging) that is required to reach the actual state of health of the battery at the operation conditions that the battery has been used beyond that actual state of health. For that, the process shown in Figure 102 can be implemented. Nonetheless, it is simpler to deduct the elapsed variable analytically by solving the equation itself (guess the time or discharged energy by knowing the pure ohmic resistance increase or dischargeable capacity decrease).

As a result, the complete model is modified (see Eq. (76) and Eq. (77)) and the dischargeable capacity evolution on test 8 is estimated again, see Figure 103.

$$Q(t_k) = Q(t_{k-1}) - \left((1.13e^{-3} \cdot (ecyc_1 + \Delta cyc_1)^{0.64} - 1.13e^{-3} \cdot ecyc_1^{0.64}) + (3.63e^{-4} \cdot (ecyc_2 + cyc_2)^{0.81} - 3.63e^{-4} \cdot (ecyc_2)^{0.81}) + (4.16e^{-6} \cdot (ecyc_3 + cyc_3)^{1.44} - 4.16e^{-6} \cdot (ecyc_3)^{1.44}) \right) \quad (76)$$

$$R(t_k) = R_{ini}(t_{k-1}) + \left((5.25e^{-3} \cdot (ecyc_1 + cyc_1)^{0.49} - 5.25e^{-3} \cdot (ecyc_1)^{0.49}) + (2.36e^{-6} \cdot (ecyc_2 + cyc_2)^{1.44} - 2.36e^{-6} \cdot (ecyc_2)^{1.44}) + (6.31e^{-9} \cdot (ecyc_3 + cyc_3)^{2.29} - 6.31e^{-9} \cdot (ecyc_3)^{2.29}) \right) \quad (77)$$

Parameters	Description
Q	The dischargeable capacity.
Q_{ini}	The dischargeable capacity value at Beginning of life (initial value).
Δcyc_i	The discharged energy in Ah related to the test $i + 4$ in between the previous sample time instant t_{k-1} and the current sample time instant t_k .
$ecyc_i$	The elapsed discharged energy in Ah required to reach the value of the modelled health indicator in the previous sample time instant t_{k-1} related to the test $i + 4$.
R	The pure ohmic resistance.
R_{ini}	The pure ohmic resistance value at Beginning of life (initial value).

Table 117: Parameters of the corrected complete aging model

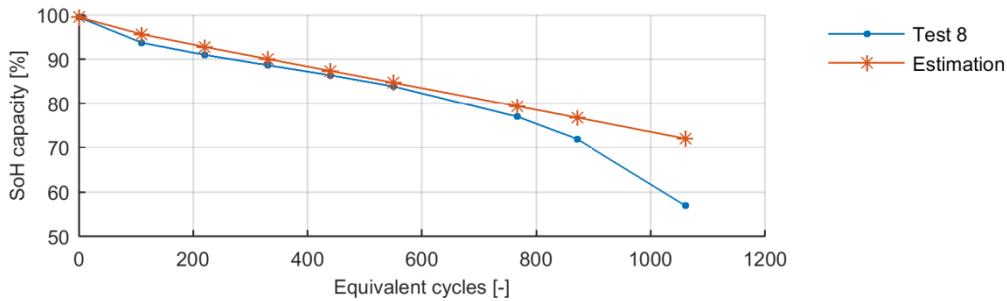


Figure 103: Comparison of the observed dischargeable capacity evolution in the test with dynamic operation conditions (dots) and the estimated one with the corrected complete aging model (stars).

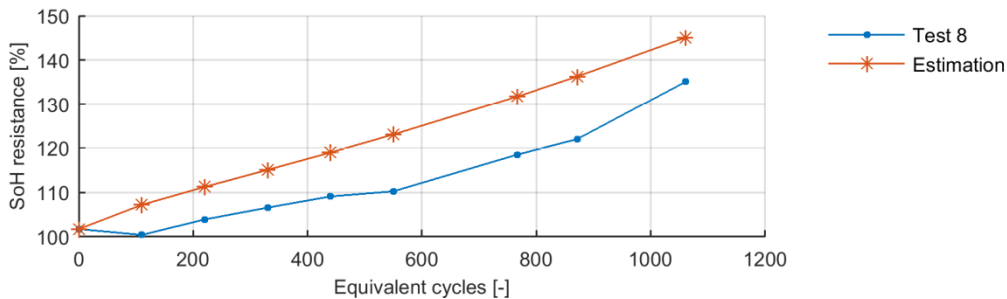


Figure 104: Comparison of the observed pure ohmic resistance evolution in the test with dynamic operation conditions (dots) and the estimated one with the complete aging model (stars).

The results show that there is a high fitting error between the estimated and observed pure ohmic resistance evolution. However, it looks like there is a constant offset between both lines (they are almost parallel). Based on this, the model that uses the elapsed concept is believed to be able to

capture the trend of the pure ohmic resistance evolution. The fitting error is attributed to an odd event rather than to the model. The battery has experienced an unexpected resistance decrease at the second check-up, which is not related to the common aging behaviour (out of this thesis the evaluation of odd events). This can be corrected with few observations and with an in-field prediction algorithm (see next chapter).

On the other hand, the dischargeable capacity evolution has still the same issue at the latest check-ups. In this case, the problem is attributed to the lack of observations on those relative dischargeable capacity values. The tests 5 and 6 have only generated 20% of dischargeable capacity decrease; there is no observation below this value. The constructed model needs to extrapolate the captured trend to further relative dischargeable capacity values, which adds high uncertainty levels to the estimations. In this case, it is especially critical since it is expected a change of the aging rate on those extrapolated cases. This issue is left to the next chapter, which treats the improvement of the errors committed on the aging modelling.

4.5 Conclusions

This chapter has proposed the methodology to select the most profitable sizing option of a lithium ion battery solution integrated on the two most relevant use cases: the Electric Vehicle and the Stationary storage system. The optimization is done based on the levelized cost of the application, which takes into account the initial capital investment, the maintenance costs, the operation costs-benefits and the replacement costs. A simulation environment has been designed to calculate the operation costs-benefits and the replacement costs. The constructed simulation environment has been adapted and tested with real case applications. Some important hypotheses assumed along the proposal have been discussed and validated as well.

The results from the High-Energy Electric Vehicle application show that the smallest sizing option is not the most profitable one. The calculated costs show that the replacement costs related with the first two smallest sizing options make them more expensive than the third smallest sizing option. On the same hand, the fourth and fifth sizing options have higher initial investments than the third option. Consequently, the third sizing option is the most profitable sizing option. It can be concluded that the cost of the energy storage system can be reduced and optimized by a proper sizing that considers the remaining useful life.

The results from the High-Power Electric Vehicle application show that the smallest sizing option is the most profitable one. The selected High-Power battery has a remarkable lifespan and subsequently, there are no replacement costs on any of the evaluated sizing options on the 15 operation years. These results show that the smallest size of the battery solution can also be the most profitable one on some cases, avoiding like this an unnecessary oversizing.

The results from the Micro-grid stationary application show that the defined minimum sizing option is the most profitable one. The calculated values of levelized cost of the electricity from the energy generation plant of the evaluated Micro-grid show that the increase of the sizing increases significantly as well the final cost almost all cases. The exception occurs between the smallest two installations. The difference in cost between the installation of 3 MWh and 4 MWh is only 0.34€/MWh while between the rest there is a constant increase of 3 €/MWh more or less. This could be interpreted as being the supplied energy insufficient to compensate the installation cost on those cases that there is a constant cost raised. The installation of 3 MWh, in contrast, shows higher cost than the expected if applied the observed constant raised of the electricity cost. The cost of the installation of 3 MWh should be 3 €/MWh lower than the cost of the installation of 4 MWh, but it is only 0.34 €/MWh. The difference of cost between these two cases and the rest is believed to come from the replacements cost. The installation of 3 MWh requires 4 replacements while the installation of 4MWh only requires 2 (a half). In this scenario, the aging of the battery would be a key aspect to get higher profitability especially from the installation of 3 MWh. The conservative operation of the battery can decrease the total cost of the installation, see [108]. Nonetheless, the most profitable case should still be the installation of 3 MWh since it has the highest room of improvement (the case with higher replacements with a total of 4). In addition to this, the offering of an ancillary service to

another grid could be considered, which could increase considerably the income [108]. The use of ancillary services can only come from oversized installation and on countries that this service is paid (in Spain it is not paid, but in Belgium there is an ancillary energy market). The installation of 3 MWh couldn't afford this additional service. This means that the installation of 4 MWh could become the most profitable one.

In this chapter, the validation of the proposed sizing methodology comes from analysing the final cost of the evaluated applications at the end of their lifespan, which will not be available before the end of this thesis. Besides, it would require implementing the different sizing options on the real life, which is not viable. Therefore, the obtained results from the developed studies cannot be validated.

The validation of two of the most relevant hypotheses have shown that, firstly, there is not a deterioration due to resting periods of 1h at middle SOC values but resting period of the same length at 100% SOC does generate it. At the same time, it has been checked that resting times of 8h does generate calendar aging indistinctly to the SOC. This has proved that short rest periods cannot be always taken as calendar aging. Secondly, the cumulative behaviour of the model has been studied and confirmed. It has been seen that the constructed model could generate relevant errors on some cases. It has been seen that an odd event could bias all the estimations from that event onwards. It has been also seen that the model is as good as the data available. The constructed model extrapolates the trends observed on the training data; the model cannot estimate unobserved trend changes. This is a huge limitation when dealing with mixed operation condition since the operation conditions that stress little the battery will be certainly limited (time is money), adding like this huge uncertainties to the correctness of the estimations.

CHAPTER 5:

5 Model Accuracy Improvement

This chapter responds to the objective of improving the accuracy of the constructed models, focusing on the aging model. The detected most critical issues on the previous chapter are, on one hand, the raise of the estimation error due to odd events; and on the other hand, the raise of the estimation error when extrapolating in time the observed operation conditions. To solve this, firstly, data-driven prognosis tools are proposed to reduce the committed error due to odd events on describing the aging behaviour, but before that, the performance of some stochastic prognostic tools on a lithium ion battery Remaining Useful Life prognosis problem are evaluated and compared. For that, a universal evaluation framework has been designed. As a result, the most interesting stochastic prognostic tool among the evaluated ones is deduced and applied with aging data with an odd event on a validation framework. Secondly, the extrapolations in time on the observed operation conditions are reduced by generating artificially the posterior aging path of those observed operation conditions thanks to Half-cell data. To do that, the most likely posterior aging path is deduced by inferring the occurrence of a sudden change on the observed aging path. The contributions of this chapter consist on firstly, the universal evaluation framework for stochastic prognosis tools; secondly, the comparison of the different evaluated stochastic prognosis algorithms; thirdly, the Half-Cell data analysis tool; and fourthly, the proposed approach to quantify the likelihood of a sudden change on the observed aging path.

5.1 Introduction

Some of the constructed aging models show limitations on capturing the real form of the aging path of the evaluated health indicators (the dischargeable capacity and the pure ohmic resistance evolution). It has been observed that those limitations can come from different immovable sources: noisy data, too small aging test matrixes, data with shallow degradation, unexpected odd events etc. On those cases, the estimations done with the models are not accurate. This problem cannot be completely dealt with on the modelling exercise. The accuracy needs to be improved by adding external elements. Data-diving algorithms from the machine learning domain are a suitable option.

Data-diving or data-driven algorithms consist on finding patterns on huge data sets. It is not expected to have huge data sets available but rather little field data. Nonetheless, the ability of finding patterns on data sets can be applied to correct the response of the aging model. These algorithms capture the aging behaviour that the model is not able to describe. Thanks to this, the handicap of having noisy, little or not relevant data can be partially compensated.

These algorithms are applied only when field data is available. In those cases, the response of the model is improved with early measurements of the dischargeable capacity and pure ohmic resistance.

Among the available data-diving algorithms, there are plenty of options that can assist on improving the constructed aging models. However, it is not evident how to select one. Each algorithm has its advantages and disadvantages. There is not a single optimal algorithm. There are many aspects that need to be thoughtfully evaluated before choosing one. This chapter provides a unified evaluation framework of this kind of algorithms. In concrete, the evaluation framework is placed on the context of the scheduled continuation of this thesis: the on-field Remaining Useful Life (RUL) prognosis of a lithium ion battery.

The RUL prognosis of a lithium ion battery has been deeply discussed. It is widely believed that a reasonable and appropriate RUL estimator has to take into account the uncertainty of battery behavior [44]. The RUL is a random variable and therefore, a point prediction of the RUL is relatively inaccurate [41]. The distribution of RUL is of interest for full understanding of the RUL [42]. This is why stochastic algorithms are the most appropriate algorithms to increase the accuracy of the RUL estimator.

The most used stochastic algorithms on lithium ion batteries RUL prognosis are evaluated. The obtained results are compared and the most appropriate algorithm is selected. The selected algorithm is tested with the real life cycle data of the evaluated High-Energy and High-Power use cases in a validation environment.

Furthermore, the constructed aging models do not expect any kind of aging path change. The modelling methodology is built on the assumption that the battery experiences the same observed aging trends on future unknown states. This hypothesis is especially uncertain when feeding the model with data with shallow degradation (little observation of the trend evolution). It has been found that sudden performance decays can come from one point onwards, which increases drastically the error committed by the model. The literature points that the sudden change of the aging trend is caused by the lithium plating phenomenon [11].

Lithium plating refers to the lithium ions deposit as metallic lithium on the negative electrode during charge [37]. The occurrence of aging induced by lithium plating leads to the turning point from linear to nonlinear aging characteristics (the sudden change of aging trend) [15]. This means that it is likely that something that happens at an electrode level (the negative electrode) generates that sudden aging trend change.

In this scenario, the state of health of the negative electrode needs to be calculated. For that, the Open Circuit Voltage (OCV) of the full cell is used. The fact is that the OCV always provides a thermodynamic fingerprint of the electrodes at any point in time [31], which is exploited for this issue.

The OCV of each electrode at a fresh state¹ (beginning of life) are convoluted to fit the OCV of the full cell at the observed different state of healths. As a result of the fitting process, the stoichiometric change of the OCV of the negative electrode is calculated. This is used as the health indicator of the negative electrode with which the aging of the negative electrode is tracked and modelled. Then, if a sudden performance decay is likely to happen, the constructed aging model of the negative electrode is used to generate artificially the data of that sudden performance decay in order to correct the aging model of the full cell. This process is applied on two tests with incomplete data sets achieved with the validation aging test matrix.

5.2 On-field Remaining Useful Life Prognosis

Nowadays' industry has increased the demand of prognostic solutions to optimize as much as possible the operation efficiency and the return of the investment. Among the different kind of solutions required by industrial entities that require prognosis, the integration of Remaining Useful Life (RUL) predictions on the solution design step or on decision-making applications is becoming quite popular. For this, data-mining algorithms are the methods that are having more popularity, and among them, the ones that quantify the uncertainty such as the stochastic algorithms are the most popular ones.

Nonetheless, there are many kinds of stochastic algorithms that can be applied on an on-field RUL prognosis and it is not clear which one should be used. The selection of the "optimal" algorithm for the desired application is non-trivial. In this context, it is proposed an evaluation methodology that will assist on clarifying the advantages and disadvantages of every stochastic algorithm. The proposal is applied onto the stochastic algorithms that appear the most on lithium ion battery RUL prognosis studies. The obtained evaluation metrics are compared and discussed in order to guess which of the evaluated algorithms would be the most appropriate.

5.2.1 Evaluation Methodology

There are many studies that compare different kinds of stochastic algorithms [110][111] or that present improved algorithms which overcome deficiencies of the original algorithms [93][112]. However, the comparison between evaluated algorithms in different studies becomes untreatable due to the differences on the evaluation methods taken on each study. The unavailability of validation and verification methods for prognostics [57] leads to each author to perform the evaluation of those algorithms according to his own chosen methods. Besides, due to the lack of consensus on the comparison metrics, in many cases, authors only use evaluation metrics that consist on the fitness of the result respect to the prediction data set [113][92], leaving aside some other important characteristics such as the evaluation of the probability distribution of the estimation [42].

In addition to this, all these algorithms are tested under a certain input constraint (a certain data set and prior knowledge of the system), which influences the performance. In general, each author uses the inputs they have interest on and treat these inputs the way they need to. The fact is that many of the sources of uncertainty on the RUL estimation are "inputs" to the prognostic algorithm and these are rarely taken into account on the tested algorithms [114]. This means that the algorithm could be penalized or accepted according to the fitness of the prediction respect to the ground truth in case the algorithm did not have access to accurate prior knowledge and/or an accurate data of the future conditions of the component/system.

Besides all this, stochastic algorithms themselves have many key design concepts that change completely their performance and that are not always completely described or taken into account. As a general trend, authors don't specify the method used on the parameterization of the algorithm [112][115][116][117][47] even though the chosen parameters have a big influence on the final results [111]. Authors don't either specify the method applied to quantify the uncertainty (the probability distribution) of RUL predictions [118] even though knowing that any prediction would be meaningless for effective decision-making unless uncertainty in prognostic is carefully accounted for [57].

¹ The aging mechanisms that appear on the observed aging trend are assumed not to damage the voltage response inherent to the electrode composition (the OCV profile).

Motivated by this, and aiming at achieving indicators to select the “optimal” algorithm, a unified evaluation framework for stochastic algorithms applied to RUL prognosis problems is presented.

5.2.1.1 Unified evaluation methods

The evaluation methods quantifies (qualitatively and/or quantitatively) the attributes of a test unit in a certain context with a certain goal. Then, the attributes or features are compared with reference features or with features taken from some other units in the same context.

This chapter proposes to measure and quantify the key attributes by the calculation of some specific set of metrics (quantitative evaluation) along with the display of a set of graphs (qualitative evaluation), which can be used as a standardized language with which technology developers and users can share their findings [57]. The context of the proposed evaluation method on this chapter is a RUL prognosis problem (description of the prediction performance) with the goal of developing and implementing robust performance assessment algorithms with desired performance levels as well as implementing the prognostics system within user specifications.

▪ Quantitative method

The proposed quantitative method quantifies two of the three key performance attributes on RUL prognosis problems: the correctness and the timeliness in a prediction; and the computational performance. The correctness makes reference of the accuracy and precision of the algorithm, what is the main evaluation metrics on all algorithms. However, it wouldn't be fair to judge an algorithm's performance based on only a single instant, as it is likely predicting a more general case under uncertainty. This is why timeliness is also evaluated. Besides, the algorithms are often rejected due to final user requirements. This means that the candidates for the optimal will only be the ones that meet the final user requirements. This is why computational performance is also evaluated. To cover all this aspects, we present three set of unified evaluation metrics (Table 118, Table 123 and Table 127).

The third key performance attribute, which is not considered in the proposed quantitative method, would be the confidence. The confidence refers to the level of trust a prediction method's output can have [57]. The reason why the confidence quantification has been discarded on the proposed quantitative method is that the trust on the output has a higher relationship with the trust on the data and the prior knowledge of the system (inputs) rather than the algorithm itself [119]. The confidence remains almost the same when using the same inputs.

Correctness

When searching for an optimal solution, the correctness is what we all think about. Correctness refers to the accuracy and precision of the predicted distributions. The metrics that evaluate the correctness measure the deviation of a prediction output from ground truth and the spread of the distribution at any given time instant that may be of interest to a particular application [57]. For this aim, the proposed metrics to measure the correctness of the obtained output with respect to its desired specification in terms of accuracy are the Root Mean Squared Error of the prediction (*RMSE*), the relative accuracy of the RUL value (*RA*) and the probability of predicting the ground truth; and in terms of precision is the probability distribution width (Table 118).

Metric	Description
Prediction RMSE	Root Mean Squared Error (RMSE) on the prediction data set (prediction fitting error) [113][92].
RA	Relative Accuracy (RA) of the predicted RUL respect to the real RUL [120].
P value	The probability of estimating the ground truth (from a normalized PDF) [114].
PDF width	The relative width of the probability distribution with a 68% confidence range respect to the real RUL [121].

Table 118: Set of metrics that quantifies the correctness

The root mean squared error is one of the most used metrics in evaluation and comparison studies [112][92][122]. In this work, the prediction RMSE is evaluated as an accuracy indicator (Eq. (78)). This metric shows the average differences between ground truth data and predictions, quantifying the accuracy on the tracking of the system's behaviour (the trend under the noise) as well as the

noise. We suggest not basing the accuracy evaluation just on this metric, since the noise is also affecting the value of this metric. However, it is useful to show if there is something off on the tracking of the system's behaviour (accurate predictions usually have low prediction errors), and therefore, on the prediction accuracy of the algorithm.

$$RMSE(t_\lambda) = \sqrt{\frac{\sum_{j=1}^{L+1}(\hat{y}_j - y_j)^2}{L+1}}, \quad y_j = y(t_\lambda), y(t_\lambda + 1), \dots, y(t_\lambda + L) \quad (78)$$

Parameters	Description
$RMSE$	The Root Mean Square Error on the prediction.
t_λ	The time instant that starts the prediction.
L	The amount of estimations.
\hat{y}	The estimation.
y	The measurement.

Table 119: The prediction Root Mean Square Error

Therefore, in order to have more information about the accuracy of the prediction algorithm, another metric is proposed: the Relative Accuracy. This metric quantifies the accuracy on predicting the most probable values of the desired events (the end of life event). This metric is calculated by Eq. (79). The range of values for the Relative Accuracy is $[0, 1]$, where the perfect score is 1 [57].

$$RA(t_\lambda) = 1 - \left| \frac{\widehat{RUL}_\lambda - RUL_\lambda}{RUL_\lambda} \right| \quad (79)$$

Parameters	Description
RA	The Remaining Useful Life prediction Relative Accuracy
t_λ	The time instant that starts the prediction.
\widehat{RUL}	The estimated Remaining Useful Life.
RUL	The measured Remaining Useful Life.

Table 120: The Relative Accuracy

To complete the accuracy evaluation, the accuracy of the predicted distribution is also quantified. This work proposes to calculate the probability of predicting the real RUL (P_{value}), see Eq. (80). The probability value is taken from the normalized probability distribution of the predicted RUL.

$$P_{value}(t_\lambda) = p(RUL_\lambda) \quad (80)$$

Parameters	Description
P_{value}	The probability of predicting the measured Remaining Useful Life.
t_λ	The time instant that starts the prediction.
RUL	The measured Remaining Useful Life.

Table 121: The probability of predicting the real RUL

Besides, thanks to the P_{value} , we can know if the uncertainty has been underestimated or not. When the probability of predicting the real RUL is near 0, the uncertainty can be considered underestimated.

Once the accuracy of the algorithm is properly quantified, the precision (the spread of the predicted distribution) needs to be addressed. Consequently, this work proposes to use the relative probability distribution width (PDF width (P_{width}) [121] or confidence interval [123]) shown in Eq. (81). This metric determines the relative number of time-instants that are in between the time-instants that delimit a certain central mass probability of the estimated RUL probability distribution.

$$P_{width}(t_\lambda) = \left| \frac{\overline{RUL}_\lambda[p_\lambda = (1 - \varepsilon)] - \overline{RUL}_\lambda[p_\lambda = \varepsilon]}{RUL_\lambda} \right|, \quad \varepsilon = 16\% \quad (81)$$

Parameters	Description
P_{width}	The relative probability distribution width.
t_λ	The time instant that starts the prediction.
$\overline{RUL}[p_\lambda = \varepsilon]$	The estimated Remaining Useful Life with a probability p_λ equal to ε .
RUL	The measured Remaining Useful Life.

Table 122: The PDF width

Timeliness

Timeliness refers to the time aspects related to availability and usability of predictions. The metrics that evaluates this attribute measure how quickly a prediction algorithm produces its outputs, in comparison to the effects that it is mitigating [57]. For this aim, the proposed metrics to measure the timeliness are the Prognosis Horizon (PH) and the Convergence of the Relative Accuracy (CRA) (Table 123).

Metric	Description
PH	The Prognosis Horizon (PH) defines from which time-instant of interest the accuracy of the algorithm reaches a certain threshold β (minimum acceptable probability mass) [120].
CRA	The convergence of the relative accuracy (CRA) quantifies the rate at which the RA improves with time [120].

Table 123: Set of metrics that quantifies the timeliness

The PH defines the first time when the prediction satisfies a certain criterion (generally defined by a predefined β threshold, Eq. (82)) and uses this time to calculate the time interval between this event and the event that wants to be predicted (EOL event). Thanks to this, the availability aspect of the timeliness attribute is put under evaluation: the greater the PH is, the better the timeliness performance of the algorithm is (faster availability). To standardize this metric, the relative of this metric is proposed in this work, see Eq. (83).

$$t_e = \min \left\{ t_\lambda : \pi[RUL(t_\lambda)]|_{\alpha_1^\pm} \geq \beta \right\} \quad (82)$$

Parameters	Description
t_e	The first time instant that the prediction satisfies a certain criterion.
t_λ	The time instant that starts the prediction.
π	The probability mass.
RUL	The estimated Remaining Useful Life distribution.
α_1^+	The upper α bound of the Prognosis Horizon criterion
α_1^-	The lower α bound of the Prognosis Horizon criterion
β	The minimum acceptable probability mass.

Table 124: The Prognosis Horizon fulfilment criterion

Where $\pi[RUL(t_\lambda)]|_{\alpha_1^\pm}$ is the probability mass of the prediction PDF within the α bounds that are given by $\alpha_1^+ = (1 + \alpha)RUL(t_1)$ and $\alpha_1^- = (1 - \alpha)RUL(t_1)$, see Figure 105.

$$PH = \frac{t_{EOL} - t_e}{RUL(t_1)} \quad (83)$$

Parameters	Description
PH	The Prognosis Horizon.
t_{EOL}	The time instant of the event that wants to be predicted.
t_e	The first time instant that the prediction satisfies the Prognosis Horizon criterion.
$RUL(t_1)$	The measured Remaining Useful Life at the first prediction time instant.

Table 125: The Prognosis Horizon

Thanks to the PH, the most important aspect of timeliness (the availability of predictions) is properly described. However, another aspect of the timeliness is found to be interesting when evaluating and comparing prognostic algorithms: the improvement rate of accuracy and precision metrics with time (the convergence). The Convergence of the Relative Accuracy measures how quickly the error on the predictions is reduced. For that, the centroid of the area under the curve for the Relative Accuracy is calculated in the same way as in [120], see Eq. (84), (85) and (86).

$$C_{RA} = \sqrt{(x_c - t_1)^2 + y_c^2} \quad (84)$$

$$x_c = \frac{\frac{1}{2} \sum_{\lambda=1}^{EoL-1} (t_{\lambda+1}^2 - t_{\lambda}^2) RA(t_{\lambda})}{\sum_{\lambda=1}^{EoL-1} (t_{\lambda+1} - t_{\lambda}) RA(t_{\lambda})} \quad (85)$$

$$y_c = \frac{\frac{1}{2} \sum_{\lambda=1}^{EoL-1} (t_{\lambda+1} - t_{\lambda}) RA(t_{\lambda})^2}{\sum_{\lambda=1}^{EoL-1} (t_{\lambda+1} - t_{\lambda}) RA(t_{\lambda})} \quad (86)$$

Parameters	Description
C_{RA}	The centroid of the area under the curve for the RA.
x_c, y_c	The centre of the mass of the area under the curve for the RA between t_1 and $t_{E_{\lambda}}$.
t_1	The first time prediction.
EoL	The amount of prediction time instants until the event that wants to be predicted.
RA	The Relative Accuracy of the Remaining Useful Life being the perfect score 0.

Table 126: The Convergence of the Relative Accuracy

Computational performance

Computational performance quantification is required to meet the resource constrains of user application [57]. For this aim, the proposed metric to measure the computational performance is the count of floating-point operations (FLOP) (Table 127). This metric quantifies the amount of numerical operation (both basic and complex) are done when running the algorithm.

Metric	Description
FLOP counts	The number of operations executed in an algorithm computed by Floating-point operations (FLOP) [111].

Table 127: Set of metrics that quantifies the computational performance

- **Qualitative method**

The proposed qualitative method focuses on describing the correctness and timeliness attributes of the prognosis algorithm in a more visual way. For this, a figure that combines an alternative version of the α - λ accuracy [120] and the Prognosis Horizon is displayed. This illustration can represent both attributes in a synthesized manner and give enough clues when discussing the obtained metrics.

In case the discussion needs extra information, a second graphical aid is proposed: the graphical representation of all the estimations done by the algorithm for a specific trial at a specific evaluation time (called trial-instant figure in this work) [119]. This figure shows each and every detail of the performance of the algorithm at the evaluation time instant. However, the lack of synthesis on this representation leads us only to propose the use of this graphical aid when there is a mayor doubt on the understanding of the metrics.

PH and α - λ accuracy

The PH is already defined as a metric itself, which quantifies the timeliness of the prediction algorithm. However, the illustration of PH boundary fulfilment gives information of the correctness of the prediction algorithm as well. The fulfilment of the PH boundary determines that a β mass of the estimated probability distribution is inside the defined precision boundaries α_1^+ and α_1^- (Eq. (87)).

As for the α - λ accuracy boundary fulfilment, the precision boundaries that delimit the acceptable β mass of the estimated probability distribution are α^+ and α^- , Eq. (87) [120].

$$\alpha - \lambda \text{ Accuracy} = \begin{cases} 1 & \text{if } \pi[RUL(t_\lambda)]_{\alpha^-}^{\alpha^+} \geq \beta \\ 0 & \text{otherwise} \end{cases} \quad (87)$$

Parameters	Description
$\alpha - \lambda \text{ Accuracy}$	The binary variable that determines if the α - λ accuracy is fulfilled or not.
t_λ	The time instant that starts the prediction.
π	The probability mass.
RUL	The estimated Remaining Useful Life distribution.
$\alpha +$	The upper α bound of the α - λ accuracy fulfilment criterion
$\alpha -$	The lower α bound of the α - λ accuracy fulfilment criterion
β	The minimum acceptable probability mass.

Table 128: The α - λ accuracy boundary fulfilment criterion

Where $\pi[RUL(t_\lambda)]_{\alpha^-}^{\alpha^+}$ is the probability mass of the prediction PDF within the α bounds that are given by $\alpha^+ = (1 + \alpha)RUL(t_\lambda)$ and $\alpha^- = (1 - \alpha)RUL(t_\lambda)$.

Taking advantage that the output of these two metrics is binary, a colour code on the PH and α - λ accuracy figure is set, Figure 105. The black line represents the ground truth; the red lines represent the α boundaries of PH (α_1^+ and α_1^-); the blue lines represent the α boundaries of the α - λ accuracy (α^+ and α^-); the empty circle represents a prediction with a probability mass within α^+ and α^- lower than β ; the blue point represents a prediction with a probability mass within α^+ and α^- equal or greater than β ; the red point represents a prediction with a probability mass within α^+ and α^- less than β but with a probability mass within α_1^+ and α_1^- equal or greater than β .

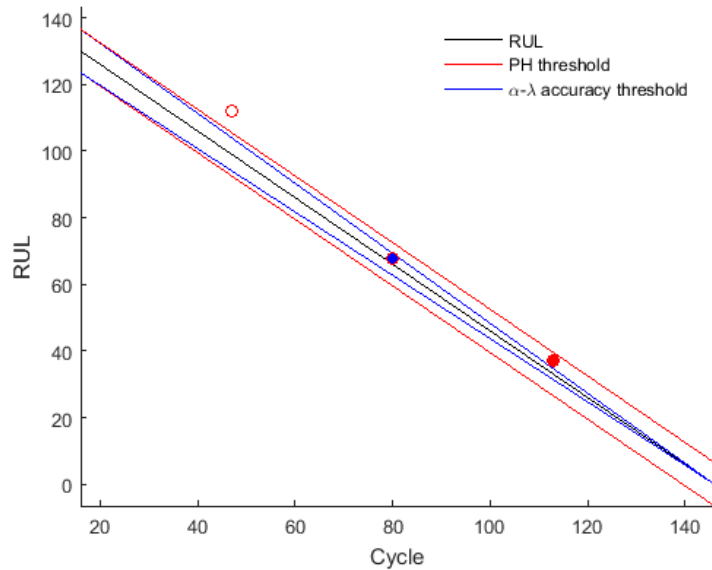


Figure 105: Qualitative response

Trial-instant

The trial-instant figure shows the response of the algorithm on the whole test data set (training and prediction). This figure displays the training, prediction and EOL thresholds, the inputs (data and prior knowledge) and the output (the response of the algorithm on the whole data set and the RUL distribution). Thanks to this, cases where metrics have estranged values can be further evaluated. This will certainly enrich the discussion, see Figure 106. Figure 106 is an example of the trial-instant figure with a training data set of 71 samples from which the last 6 samples compose the validation data set (the vertical green line represents the learning threshold and the blue line represents the validation threshold). The prior knowledge is composed by a linear model (yellow line) and data from the battery B0005 (blue dots). The time-instant of interest is defined by the EOL threshold (the horizontal red line), which is the capacity value at the 146 sample. The prediction probability density

is displayed by the dark blue area called PDF. The algorithm response on the learning data set is the orange line (named “filtered observation” in Figure 106). The purple line represents the prediction given by the algorithm on the rest of the data set.

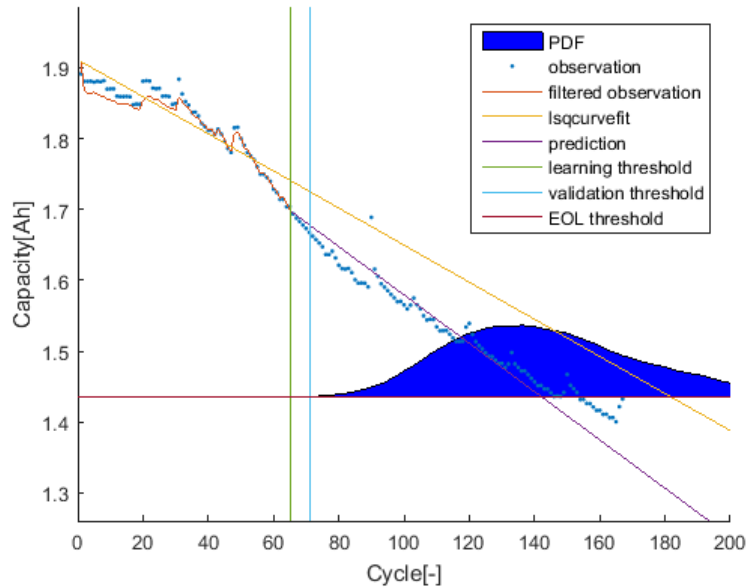


Figure 106: Example of the trial-instant figure

▪ **Reference features**

This work develops a standardized language using a unified set of metrics that describe the key attributes of the algorithm, but in order to find the “best”, the attributes of study need to be ranked. For this, some reference values for the proposed metrics are gathered in Table 129.

Metrics	“Worst”	“Best”
Prediction RMSE	∞	0
RA	0	1
P value	0	1
PDF width	∞ or 0	When it quantifies the true uncertainty of the prediction (should be between 0 and 1).
PH	0	1
CRA	∞	0
FLOP counts	∞	0

Table 129: Reference values of the unified set of metrics

5.2.1.2 Trial matrix design methodology

The design of the trials needs to keep in mind that many of the sources of uncertainty on the RUL estimation are “inputs” to the prognostic algorithm [114]. This uncertainty can penalize the algorithm if the information regarding the “inputs” themselves is incorrect; it would not be reasonable to penalize or accept an algorithm according to the fitness of the prediction respect to the ground truth data in case the algorithm did not have access to accurate prior knowledge and/or an accurate measurement of the future conditions of the component/system. That is why it is necessary to develop a rigorous comparison approach to separate:

- The evaluation of correctness of information regarding these “inputs”.
- The evaluation of the prognostic algorithm itself.

This proposal aims to somehow control the uncertainty of the “inputs” (data and prior knowledge) when designing the trials, which will allow evaluating the prognosis algorithm itself. The idea is to apply cases with different level of uncertainty, leading to the illusive “control” of this uncertainty. Firstly, the trial matrix considers data of at least two systems that have different level of noise contribution; and secondly, the trial matrix considers two prior models describing the behaviour of the system with different level of accuracy. In this way, the correctness of the “inputs” for each algorithm

can be discriminate in a certain degree and the evaluation of the prognostic algorithms themselves is improved. This work proposes a minimum of a 4 cases trial matrix, shown in Table 130.

	Data		Prior knowledge	
	Low uncertainty	High uncertainty	Low accuracy	High accuracy
Algorithm X	Trial 1	Trial 2	Trial 3	Trial 4

Table 130: Proposed trial matrix to separate input uncertainty effect on algorithm's evaluation.

5.2.1.3 Universal parameterization criterion

The performance level of an algorithm is determined by many factors, but the parameterization is one of the key factors. The chosen parameters will define the algorithm's performance level on a given context and goal. However, each algorithm usually has integrated on it its own parametrization method, which does not take into account the context and the goal with which the algorithm needs to work. This leads to evaluate algorithms that are optimized to work on a context different to the interesting one. A universal (applicable to any algorithm) parameterization criterion is proposed corresponding to the context and goals of interest: a RUL prognostic problem context within user specifications with the goal of developing and implementing robust performance assessment algorithms with desired performance levels.

Firstly, the **key** aspect of the context of interest needs to be defined, which would be "*predict a future unknown event*". Next, the parameterization criterion that shares the same key aspect needs to be set. In case of doing a literal interpretation of the **key** aspect, the parameterization must focus on the future event, but this would go against the purpose of the algorithm since that future event needs to be predicted (needs to be unknown).

In this scenario, some assumptions need to be done. It is assumed that accurate predictions come when the algorithm tracks accurately the future behaviour of the system. The **key** aspect of the context of interest is reformulated as "*the tracking of the future behaviour of the system*". Thanks to this, the focus of the **key** aspect that needs to fulfil the algorithm changes from a specific future event data point to future data in general.

This work proposes a parametrization criterion based on quantifying the accuracy of the future behaviour of the system by a cross validation of a part of the training data set. Since a cross validation is implemented, the part designed for cross validation need to be removed from the training data set, reducing the amount of data available for training the algorithm. However, thanks to this criterion, a universal parameterization related with its context is achieved.

The validity of the proposed universal parametrization criterion is supported by the statement that the parameterization depends on the performance of the algorithm doing predictions (the key aspect of the context is prediction) and by the statement that this criterion can be applied to every algorithm designed for RUL prediction.

5.2.1.4 Uncertainty propagation method

The uncertainty management is embedded on the stochastic algorithms, which means that each stochastic algorithm has its own way of taking into account the uncertainty [124]. This intrinsic part of the algorithm will impact the precision level that the algorithm achieves.

The proposed evaluation framework has been built on the context of predicting the RUL of the system. This means that the proposed precision evaluation is quantified from the precision on predicting the RUL. Consequently, the managed uncertainty on the training section needs to be propagated to unknown estimations (to the RUL prediction). However, there are stochastic algorithms that don't have, as an intrinsic characteristic, a way of quantifying the uncertainty on unknown estimations (interpolation or extrapolation), even though being stochastic algorithms (such as stochastic filters). In this scenario, an uncertainty propagation method is proposed in order to cover this deficiency and in order to standardize the uncertainty propagation method under the proposed evaluation framework.

Among the huge variety of uncertainty propagation methods available in the literature [57] [116] [123], the proposed one is a sampling based method called Monte Carlo prediction. In Monte Carlo prediction, samples from the input distributions are drawn randomly and simulated until the desired event (EOL event), making predictions of the RUL of each sample. The resultant predicted RUL values are weighted depending on the prior probability that each sample had on the input distribution, generating like this a statistic distribution of the predicted RUL. The pseudo-code is available in Algorithm 7.

$$\{t_E^{(i)}\}_{i=1}^{\rho} = MC \left(p \left(x(t_p), \theta(t_p | y(t_0: t_p)) \right), p(\Theta_{t_p}), p(U_{t_p}), p(V_{t_p}), \rho \right)$$

```

1: for  $i = 1$  to  $\rho$  do
2:    $(x^{(i)}(t_p), \theta^{(i)}(t_p)) \sim p(x(t_p), \theta(t_p | y(t_0: t_p)))$ 
3:    $\Theta_{t_p}^{(i)} \sim p(\Theta_{t_p})$ 
4:    $U_{t_p}^{(i)} \sim p(U_{t_p})$ 
5:    $V_{t_p}^{(i)} \sim p(V_{t_p})$ 
6:    $t_E^{(i)} \leftarrow F(x^{(i)}(t_p), \Theta_{t_p}^{(i)}, U_{t_p}^{(i)}, V_{t_p}^{(i)})$ 
7: end for

```

Where

ρ = The total number of Monte Carlo samples.

$t_E^{(i)}$ = The event time instant of i th Monte Carlo sample.

$x(t_p)$ = The state at prediction time (t_p).

$\theta(t_p | y(t_0: t_p))$ = The parameter at prediction time knowing the system outputs (y) at $t_0: t_p$.

Θ = Parameter trajectory.

U = Input trajectory.

V = Process noise trajectory.

F = the function to compute t_E .

Algorithm 7: Monte Carlo Prediction [57].

Monte Carlo predictions get exact approaches when the numbers of samples is infinite. This suggests that the higher the number of samples is, the better the approximation will be but the higher the computational burden will be [57]. Therefore, a trade-off between accuracy and computational burden need to be considered when selecting the number of samples.

5.2.2 Stochastic algorithms

The stochastic algorithms that are more frequently applied on lithium ion battery Remaining Useful Life prognosis studies are algorithms based on the Particle Filter [93][92][121][123][125] and algorithms based on the Gaussian Process [126][127][128][129][46]. Nonetheless, there are more stochastic algorithms that could be applied on a lithium ion battery remaining useful life prognostic problem such as the Extended Kalman Filter and the Unscented Kalman Filter.

These four algorithms are analyzed in detail, highlighting the free elements (or variables) that affect the most their performance.

5.2.2.1 Particle Filter

Particle Filter (PF) is a sequential Monte Carlo method [8]. It is based on the idea of Monte Carlo method to solve the integral operation in the Bayes estimators. It estimates the state Probability Density Function (PDF) from a set of "particles" and their associated weights [112]. The use of weight adjusts the state PDF to its most likely form. Thanks to the use of state PDF, an appropriate management of inherent estimation uncertainty is allowed [8]. This provides non-linear projection in forecasting [43].

The particles are inferred recursively by two alternate phases, see Algorithm 8. The first phase is the prediction where the value of each particle for the next step is estimated by previous step information. No measurement or observation is involved in this step. The second phase is the update where the value of each particle estimated in the prediction phase is compared with measurements and updated accordingly [8]. As an initialization step ($k = 1$), the particles are commonly generated

from a Gaussian distribution ($\mathcal{N}(0, \sigma_{ini})$) and the weights are commonly calculated from a uniform distribution ($\mathcal{U}(0, 1/\rho)$) [130].

$$\left[\{x_k^i, w_k^i\}_{i=1}^\rho, \hat{x}_k \right] = \text{PFstep} \left(\{x_{k-1}^i, w_{k-1}^i\}_{i=1}^\rho, \mathbf{u}_{k-1}, \mathbf{v}_k, \mathbf{y}_k \right)$$

- 1: for $i = 1$ to ρ do
- 2: $x_k^i \sim p(x_k | x_{k-1}^i, \mathbf{u}_{k-1})$
- 3: $w_k^i \leftarrow p(y_k | x_k^i, \mathbf{v}_k)$
- 4: end for
- 5: $W \leftarrow \sum_{i=1}^\rho w_k^i$
- 6: for $i = 1$ to ρ do
- 7: $w_k^i \leftarrow w_k^i / W$
- 8: end for
- 9: $\hat{N}_{eff} \leftarrow \frac{\rho}{\sum_{i=1}^\rho (w_k^i)^2}$
- 10: if $\hat{N}_{eff} < N_T$ then
- 11: $\{x_k^i, w_k^i\}_{i=1}^\rho \leftarrow \text{RESAMPLE} \left(\{x_k^i, w_k^i\}_{i=1}^\rho \right)$
- 12: end if
- 13: $\hat{x}_k \leftarrow \sum_{i=1}^\rho x_k^i \cdot w_k^i$

Where

ρ = Amount of particles.

\hat{x}_k = The most probable variables of the defined state space model at k th time.

x_k^i = The variables of the defined state space model of i th particle at k th time.

y_k = The output at k th time.

\mathbf{u}_k = The state space model noise factor at k th time.

\mathbf{v}_k = The measurement noise factor at k th time.

w_k^i = The weight of i th particle at k th time.

W = Cumulative weight.

\hat{N}_{eff} = Effective number of particles.

N_T = User defined threshold of effective number of particles.

Algorithm 8: Sample Importance Resampling Particle Filter [130].

However, PF has two main problems: Particle degradation and sample impoverishment. To tackle these issues, code that improves the prior distribution and the final particles is further developed.

▪ Proposal Distribution Methods

In a standard PF algorithm, lack of information on the latest observation model corrective action can lead to particle degradation [112]. A method that selects a reasonable distribution is an effective method to alleviate this phenomenon of particle degradation, such as the use of an unscented transformation onto the degraded particle distribution.

The Particle Filter algorithm that uses an unscented transformation to generate the proposal distribution is called Unscented Particle Filter (UPF). The Unscented Kalman Filter is typically used to generate this proposal distribution [121]. In this way, the PF's posterior probability is obtained taking into account the latest observation [112], see Algorithm 9. Consequently, the prediction results can better fit the true situation.

$$\left[\{x_k^i, w_k^i\}_{i=1}^\rho, \hat{x}_k \right] = \text{UPFstep} \left(\{x_{k-1}^i, w_{k-1}^i\}_{i=1}^\rho, \hat{x}_{k-1}, \mathbf{P}_{k-1|k-1}, \mathbf{u}_{k-1}, \mathbf{v}_k, \mathbf{y}_k \right)$$

- 1: $\hat{x}_{k|k}, \mathbf{P}_{k|k} \leftarrow \text{UKFStep}(\mathbf{u}_{k-1}, \mathbf{y}_k, \hat{x}_{k-1}, \mathbf{P}_{k-1|k-1})$
 - 2: for $i = 1$ to ρ do
 - 3: $x_k^i \sim p(x_k | \hat{x}_{k|k}, \mathbf{P}_{k|k})$
 - 4: $w_k^i \leftarrow p(y_k | x_k^i, \mathbf{v}_k)$
 - 5: end for
 - 6: $W \leftarrow \sum_{i=1}^\rho w_k^i$
 - 7: for $i = 1$ to ρ do
 - 8: $w_k^i \leftarrow w_k^i / W$
 - 9: end for
 - 10: $\hat{N}_{eff} \leftarrow \frac{\rho}{\sum_{i=1}^\rho (w_k^i)^2}$
-

11: If $\hat{N}_{eff} < N_T$ then
12: $\{x_k^i, w_k^i\}_{i=1}^\rho \leftarrow RESAMPLE(\{x_k^i, w_k^i\}_{i=1}^\rho)$
13: end if
14: $\hat{x}_k \leftarrow \sum_{i=1}^\rho x_k^i \cdot w_k^i$

Where

ρ = Amount of particles.

x_k^i = The variables of the defined state space model of i th particle at k th time.

\hat{x}_k = The most probable variables of the defined state space model at k th time.

y_k = The output at k th time.

u_k = The measurement noise factor at k th time.

w_k^i = The weight of i th particle at k th time.

W = Cumulative weight.

\hat{N}_{eff} = Effective number of particles.

N_T = User defined threshold of effective number of particles.

Algorithm 9: Unscented Particle Filter pseudo-code.

The main merit of the UPF is that it can alleviate the impact of particle degeneration due to the generation of a better proposal distribution. Consequently, the prediction results with the PF can better fit the true situation. However, the UPF cannot solve the problem of sample impoverishment or particle diversity lack caused by the basic resampling process [112].

Zhang et al. [112] proposes an improved unscented particle filter (IUPF) method for Lithium ion Battery Remaining Useful Life (RUL) prediction based on Markov Chain Monte Carlo (MCMC), which uses the MCMC method to maintain the diversity of particles. At the same time, since the IUPF is on the basis of UPF, it can also suppress the particle degradation existing in the standard PF [112].

▪ **Resampling methods**

So as to lessen the impact of particle degradation, system importance resampling of the particles is carried out on certain iterations (the iterations that don't reach the pre-set resampling threshold " N_T "). This helps in maintaining the track of the state vector even under the presence of disruptive effects like un-modelled operational conditions [131].

Among the possibilities on system importance resampling methods, the most basic and used ones are the multinomial, the systematic, the stratified and the residual resampling methods [132]. There are many more resampling methods [133], which are in continuous improvement. Lately, two interesting resampling methods approaches have been developed: the Linear Optimizing Combination Resampling (LOCR) [93] or the Heuristic Kalman Algorithm (HKA) [92].

Basic Resampling methods

The multinomial resampling method is based on the idea of generating independently N random numbers from the uniform distribution. The selected particles for replication are based on the cumulative sum of the normalized weights [115].

The stratified resampling divides the whole particle set into N equal subsets. The random number is drawn independently from each subset where the selected particles for replication are based as well on the cumulative sum of the normalized weights [115].

The systematic resampling is similar to the stratified resampling method. The difference is that samples drawn are no longer independent since only one random number is drawn in the whole resampling step [115], see Algorithm 10.

$\left[\{x_k^j, w_k^j\}_{j=1}^\rho \right] \leftarrow SISTEMATIC_RESAMPLE(\{x_k^i, w_k^i\}_{i=1}^\rho)$

1: $c_1 \leftarrow w_k^1$
2: for $i = 2$ to ρ do
3: $c_i \leftarrow c_{i-1} + w_k^i$
4: end for
5: $i \leftarrow 1$

```

6:  $u_1 \sim \mathcal{U}(0, 1/\rho)$ 
7: for  $j = 1$  to  $\rho$  do
8:    $u \leftarrow u_1 + (j - 1)/\rho$ 
9:   while  $u > c_i$  do
10:     $i \leftarrow i + 1$ 
11:   end while
12:    $x_k^j \leftarrow x_k^i$ 
13:    $w_k^j \leftarrow 1/\rho$ 
14: end for
    
```

Where

x_k^i = The variables of the defined state space model of i th particle at k th time.

w_k^i = The weight of i th particle at k th time.

ρ = Amount of particles.

\mathcal{U} = Uniform distribution.

Algorithm 10: Systematic Resampling [133].

The residual resampling method is an efficient means to decrease the variance due to resampling. It consists of two stages. Firstly, particles weights greater than $1/\rho$ are deterministically replicated without any draws. For these particles, the input weights are reduced by a multiple of $1/\rho$. Secondly, particles are randomly sampled using the remaining of the weights (referred to as residuals) and a random sampling method (it can be one of the described above) [115].

In a previous work [119], it was proved that the developed PF algorithm with the multinomial, the systematic and the residual systematic resampling methods don't have a quantifiable difference when propagating the uncertainty and predicting the Remaining Useful Life (RUL), being $\rho = 500$ and $N_T = 50\%$.

Linear Optimizing Combination Resampling

In systematic resampling, the resampling procedure removes small weight particles and copies large weight particles, which results in the loss of diversity in particles. The Linear Optimizing Combination Resampling (LOCR) method is developed to generate new particles by combining the selected particles and abandoned particles, which partly overcome the loss of diversity in particles, and improves the precision of PF [93]. The linear combination is described in Eq. (88) and (89).

$$x_n = x_s + LK(x_a - x_s) \quad (88)$$

$$L = \left[\frac{1}{Np(x)} \right]^{1/m} = \left[\frac{1}{N\omega} \right]^{1/m} \quad (89)$$

Parameters	Description
x_n	The new sampling particles obtained by linear combination.
x_a	The repeated particles.
x_s	The discarded particles.
K	The step coefficient (adjusted to eliminate the influence of the Euclidean distance).
L	The rational step for the Euclidean distance ($x_a - x_s$).

Table 131: The Linear Optimizing Combination Resampling method

The LOCR algorithm is composed by three stages (see Algorithm 11):

- Classification
- Discard those particles with too small weight.
- Combination resampling.

$$\left[\{x_k^j, w_k^j\}_{j=1}^{\rho} \right] \leftarrow \text{LOCR} \left(\{x_k^i, w_k^i\}_{i=1}^{\rho}, u_k \right)$$

1: $c_1 \leftarrow w_k^1$

2: for $i = 2$ to ρ do

```

3:    $c_i \leftarrow c_{i-1} + w_k^i$ 
4: end for
5:  $i \leftarrow 1$ 
6:  $u_1 \sim \mathcal{U}(0, 1/\rho)$ 
7: for  $j = 1$  to  $\rho$  do

```

Classification

```

8:    $u \leftarrow u_1 + (j - 1)/\rho$ 
9:   while  $u > c_i$  do
10:     $i \leftarrow i + 1$ 
11:  end while
12:   $xa_k^j \leftarrow x_k^i$ 
13:  if  $xa_k^j = xa_k^{j-1}$ 
14:     $xs_k^j \leftarrow x_k^i$ 
15:     $ws_k^j \leftarrow w_k^i$ 
16:  end if

```

Discard those particles with too small weight

```

17: for  $ind_1 = 1$  to  $\rho_s$  do
18:    $w_{th} \leftarrow K/(\rho \cdot nj^{ind_1})$ 
19:   if  $ws_k^{ind_1} > w_{th}$  do
20:     $xsa_k^{ind_2} \leftarrow xs_k^{ind_1}$ 
21:   end if
22: end for

```

Combination resampling

```

23:  $x_k^j \leftarrow xsa_k + (L \cdot K \cdot (xa_k - xsa_k))$ 
24:  $w_k^j \leftarrow p(y_k | x_k^j, u_k)$ 
25: end for

```

Where

x_k^i = The variables of the defined state space model of i th particle at k th time.

w_k^i = The weight of i th particle at k th time.

ρ = Amount of particles.

\mathcal{U} = Uniform distribution.

xa_k = The repeated particles at k th time.

xs_k = The discarded particles at k th time.

ws_k^i = The weight of i th discarded particle at k th time.

w_{th} = The threshold weight used to accept or reject the discarded particles.

K = The step coefficient.

nj = Repetition rate of each particle xa_k if doing systematic resampling.

xsa_k = The accepted particles from the discarded particles at k th time.

L = The rational step for the Euclidean distance.

Algorithm 11: LOCR pseudo-code [93].

Heuristic Kalman Algorithm Resampling

The typical resampling methods often generate only a small number of particles that tend to have exceedingly large weights. Thus, most of the recursive calculations in the transition and observation equations tend to get wasted on these abundant particles. If the sample size of the data set is small and a non-informative prior (with wide range) is used, then the particles may have very limited chance to cluster around the true state. When the likelihood lies in the tail of the prior distribution, the resampling step can lead to sample impoverishment whereby important samples are dropped and the unimportant ones are replicated [92]. To enhance the fraction of meaningful particles, the Heuristic Kalman Algorithm can be used to generate new superior sample sets, see Algorithm 12. After the posterior weight calculation, the Heuristic Kalman Algorithm is used to optimize the fitness function ($fit = p(y_i | x_i^{(i)})$).

The Heuristic Kalman Algorithm will move the mean of the random number generator towards the region with significant fitness value (high likelihood value). The random generator of the Heuristic Kalman Algorithm spits a new sample set when the distance between the samples is below a defined threshold and/or a maximum number of iterations is exceeded. Then, a resampling step is executed to select and replicate particles with larger weights. The optimized particles tend to cluster around the

high likelihood regions conditioned on the recent observation; therefore, their weights are significant. As a result, the problem of impoverishment is avoided. On the other hand, the Heuristic Kalman Algorithm drives particles that are far away from true states to move towards the region where true states may be present with a higher probability. Thus, sample degeneracy is also avoided [92].

$\left[\{x_k^j\}_{j=1}^{N_\xi}\right] \leftarrow HKA\left(\{x_k^i\}_{i=1}^\rho, \text{costf}, \mathbf{u}_k, \varphi_{th}, \alpha, N_\xi\right)$

- 1: $\varphi \leftarrow \mathbf{inf}$
- 2: $\boldsymbol{\mu}_k \leftarrow (\bar{\mathbf{x}}_k + \underline{\mathbf{x}}_k)/2$
- 3: $\mathbf{P}_k^- \leftarrow (\bar{\mathbf{x}}_k + \underline{\mathbf{x}}_k)/6$
- 4: **while** $\varphi > \varphi_{th}$
- 5: $\mathbf{x}_k \leftarrow \mathcal{N}(\boldsymbol{\mu}_k, \mathbf{P}_k^-)$
- 6: $\xi_k \leftarrow 1/N_\xi \cdot \sum_{i=1}^{N_\xi} \text{costf}(x_k^i, \mathbf{u}_k)$
- 7: $\mathbf{V}_k \leftarrow \text{var}\left(\{\text{costf}(x_k^i, \mathbf{u}_k)\}_{i=1}^{N_\xi}\right)$
- 8: $\mathbf{L}_k \leftarrow \mathbf{P}_k^- \cdot (\mathbf{P}_k^- + \text{diag}(\mathbf{V}_k))$
- 9: $\mathbf{a}_k = \alpha \cdot \min\left(1, \left(\text{mean}(\sqrt{\mathbf{V}_k})\right)^2\right) / \left(\min\left(1, \left(\text{mean}(\sqrt{\mathbf{V}_k})\right)^2\right) + \left(\max(\sqrt{\mathbf{P}_k^+})\right)^2\right)$
- 10: $\mathbf{P}_k^+ = (\mathbf{I} - \mathbf{a}_k \mathbf{L}_k) \cdot \mathbf{P}_k^-$
- 11: $\varphi = \max\left(\left\{\sqrt{\max\left(\{\text{costf}(x_k^i, \mathbf{u}_k)\}_{i=1}^{N_\xi}\right)} - \sqrt{\text{costf}(x_k^i, \mathbf{u}_k)}\right\}_{i=1}^{N_\xi}\right)$
- 12: $\boldsymbol{\mu}_k \leftarrow \boldsymbol{\mu}_k + \mathbf{L}_k \cdot (\mathbf{x}_k - \boldsymbol{\mu}_k)$
- 13: $\mathbf{P}_k^- \leftarrow \mathbf{P}_k^- + \mathbf{a}_k \cdot (\sqrt{\mathbf{P}_k^+} - \mathbf{P}_k^-)$
- 14: **end while**

Where

x_k^i = The variables of the defined state space model of i th particle at k th time.
 w_k^i = The weight of i th particle at k th time.
 \mathbf{u}_k = The input at k th time.
 ρ = Amount of particles.
 $\boldsymbol{\mu}_k$ = The mean vector at k th time.
 \mathbf{P}_k^- = The variance vector at k th time.
 $\bar{\mathbf{x}}_k$ = The upper bound of the search box.
 $\underline{\mathbf{x}}_k$ = The lower bound of the search box.
 ξ_k = The perturbed knowledge of the optimum point.
 N_ξ = Number of best candidates.
 \mathbf{V}_k = The variance vector (ignorance about the optimum point) at k th time.
 \mathbf{L}_k = The Kalman gain at k th time.
 \mathbf{a}_k = The slowdown factor at k th time.
 α = The slowdown coefficient.
 \mathbf{P}_k^+ = The variance vector of the posterior-estimation error at k th time.
 φ_{th} = The threshold variable of the stopping rule.
 φ = The stopping rule variable.

Algorithm 12: Heuristic Kalman Algorithm's pseudo-code.

5.2.2.2 Gaussian Process Regression

The Gaussian Process (GP) is based on the statistical learning theory and adapts well to high dimensions, small samples, and nonlinear and other complex problems with a strong generalization ability [51], see Algorithm 13.

In a GP, observations occur in a continuous domain (time or space) and every point is associated with a normally distributed random variable. This supposes that every finite collection of those random variables has a multivariate normal distribution and that every finite linear combination of them is normally distributed. Supported by those assumptions, a GP defines a probability distribution over functions (Eq. (90)) which are composed by a mean function (Eq. (91)) and a covariance function (Eq. (92)). In this way, the degradation trends are learnt from battery data sets with the combination of GP functions.

$$f \sim GP(m(x), k(x, x')) \quad (90)$$

$$m(x) = E(f(x)) \quad (91)$$

$$k(x, x') = E[(f(x) - m(x))(f(x') - m(x')))] \quad (92)$$

Parameters	Description
f	The function that describes the system behaviour.
$m(x)$	The mean function.
$k(x, x')$	The covariance function.
$E(f(x))$	The most probable value of $f(x)$.

Table 132: The Gaussian Process

Typically a GP uses a mean function equal to zero with the aim of describing all the system by the covariance function since the covariance function is flexible enough to model the true mean arbitrarily well [134]. Nonetheless, if there is prior knowledge of the system, it is possible to express that prior information as the most probable result of the systems in form of the mean function. In this way, the covariance function of the GP is able to describe the behaviour of the system that the prior knowledge is not able to capture.

There are many types of mathematical expressions that fulfil the requirements to be a covariance function of a GP. The most common covariance functions are the Squared Exponential (SE) covariance function (Eq. (93)) [126][135], the Matérn (Ma) covariance function (Eq. (94)) [129][135], the periodic covariance function (Eq. (95)) [126][129], the neural network covariance function (Eq. (96)) [128][136] and the combination of them [128][135].

$$k_{SE}(x, x') = \sigma_{SE}^2 \exp\left(-\frac{1}{l^2}(x-x')^2\right) \quad (93)$$

$$k_{Ma}(x, x') = \sigma_{Ma}^2 \frac{2^{1-v}}{\Gamma(v)} \left(\sqrt{2v} \frac{(x-x')}{\rho}\right)^v R_v \left(\sqrt{2v} \frac{(x-x')}{\rho}\right) \quad (94)$$

$$k_{Pe}(x, x') = \sigma_{Pe}^2 \exp\left(-\frac{1}{l^2} \sin^2\left[\frac{\omega}{2\pi}(x-x')\right]\right) \quad (95)$$

$$k_{NN}(x, x') = \sigma_{NN} \cdot \sin^{-1} \left(\frac{2\tilde{x}^T \Sigma \tilde{x}'}{\sqrt{(1 + 2\tilde{x}^T \Sigma \tilde{x})(1 + 2\tilde{x}'^T \Sigma \tilde{x}')}} \right) \quad (96)$$

Parameters	Description
k_{SE}	The Squared Exponential covariance function.
k_{Ma}	The Matérn covariance function.
k_{Pe}	The periodic covariance function.
k_{NN}	The neural network covariance function.
$(x - x')$	The difference between two input values.
$\sigma_{SE}, l, \sigma_{Ma}, \rho, \sigma_{Pe}, \sigma_{NN}, \omega$	The hyper-parameters of the Squared Exponential, Matérn, periodic and Neural Network covariance functions.
v	The smoothness hyper-parameter, typically taken as constant ($v = 3/2$ or $5/2$).
Γ	The gamma function.
R_v	The modified Bessel function of the second kind.
\tilde{x}	A vector that contains the inputs.
Σ	The covariance matrix that emulates the weights of a Neural Network.

Table 133: The covariance functions of the Gaussian Process

The covariance function selection can be an important and difficult problem [137]. On a previous work [119], the characteristics of the Squared Exponential, Matérn and Neural Network covariance

functions have been analysed. The study has shown that the Squared Exponential covariance function can describe perfectly the system's behaviour onto the observed operation window. Nonetheless, it is not interesting for prognosis since it tends to 0 on inputs out of the observed window. The Matérn covariance function can also describe perfectly the system's behaviour onto the operation window. Nonetheless, it is not interesting in prognosis since it increases exponentially on inputs out of the observed window. The Neural Network covariance function shows limitations on describing the behaviour of the system on the observed operation window, at least with the tested hyper-parameter values. However, the captured system's behaviour is kept in a linear way onto future predictions, which in lithium ion battery prognosis problems is interesting (it is assumed that the aging will not have a sudden change).

The distribution over functions obtained by the GP is used as a prior for Bayesian inference (Eq. (97)). The calculated prior does not depend on the training data, but specifies some properties of the functions (the objective is to learn properties of the prior in the light of the training data) [134]. The calculation of the posterior will provide the predictions for unseen test cases. Then, the joint distribution of the desired test set is evaluated where the training set covariance (K), training-test set covariance (K_*) and the test set covariance (K_{**}) are calculated.

Since the values for the training set f are known, the conditional distribution of f_* given f can be calculated (this is the posterior distribution for a specific set of unseen test cases, see Eq. (98)). In the same way, the mean and the variance of the posterior can be deducted from here (Eq. (99) and Eq. (100)).

$$\begin{bmatrix} f \\ f_* \end{bmatrix} \sim \mathcal{N} \left(\begin{bmatrix} \mu \\ \mu_* \end{bmatrix}, \begin{bmatrix} K & K_* \\ K_*^T & K_{**} \end{bmatrix} \right) \quad (97)$$

$$f_* | f \sim \mathcal{N}(\mu_* + K_*^T K^{-1}(f - \mu), K_{**} - K_*^T K^{-1} K_*) \quad (98)$$

$$m_p(x) = m(x) + K_*^T K^{-1}(f - \mu) \quad (99)$$

$$k_p(x, x') = K_{**} - K_*^T K^{-1} K_* \quad (100)$$

Parameters	Description
f	The function that describes the system's behaviour on the training data set.
f_*	The function that describes the system's behaviour on the test data set.
μ	The prior knowledge of the system on the training data set.
μ_*	The prior knowledge of the system on the test data set.
\mathcal{N}	Normal distribution.
K	The training set covariance.
K_*	The training-test set covariance.
K_{**}	The test set covariance.
$m_p(x)$	The mean of the posterior at x .
$m(x)$	The prior knowledge at x .
$k_p(x, x')$	The covariance of the posterior at x .

Table 134: The Bayesian inference on a Gaussian Process

The estimation attained with this Bayesian inference is noiseless but it is something common to have noise in the observations of many applications of regression. In the GP models, such noise is easily taken into account. The easiest way of adding the noise effect in the observation is to assume that the noise is Gaussian and independent. In this scenario, the noise variance is added to the covariance values of each test point respect to the same test point ($k_p(x, x')$; $x = x'$) (see Eq. (101), Eq. (102) and Eq. (103)).

$$K_y = K + \sigma_y I \quad (101)$$

$$m_p(x) = m(x) + K_*^T K_y^{-1} (f - \mu) \quad (102)$$

$$k_p(x, x') = K_{**} - K_*^T K_y^{-1} K_* \quad (103)$$

Parameters	Description
K_y	The noisy training set covariance.
K	The training set covariance.
σ_y	The variance of the observation noise.
I	The identity matrix.
f	The function that describes the system's behaviour on the training data set.
μ	The prior knowledge on the training data set.
K_*	The training-test set covariance.
K_{**}	The test set covariance.
$m_p(x)$	The mean of the posterior at x .
$m(x)$	The prior knowledge at x .
$k_p(x, x')$	The covariance of the posterior at x .

Table 135: The Bayesian Inference on a Gaussian Process considering a Gaussian noise on the measurements

$[\hat{y}_T, \sigma_T] = GP(\mathbf{u}_L, \mathbf{y}_L, \mathbf{u}_T, \mu, \sigma)$

- 1: $K \leftarrow [k(\mathbf{u}_i, \mathbf{u}_j, \sigma)]_{i=1..L, j=1..L}$
- 2: $K_y \leftarrow K + \sigma_y I$
- 3: **for** $i = 1$ **to** T **do**
- 4: $K_* \leftarrow [k(\mathbf{u}_i, \mathbf{u}_j, \sigma)]_{j=1..L}$
- 5: $K_{**} \leftarrow k(\mathbf{u}_i, \mathbf{u}_i, \sigma)$
- 6: $\hat{y}_i \leftarrow \mu_i + K_*^T K_y^{-1} (\mathbf{y}_L - \mu_L)$
- 7: $\sigma_i \leftarrow K_{**} - K_*^T K_y^{-1} K_*$
- 8: **end for**

Where

\mathbf{u}_L = The input variable of the training data set.
 \mathbf{y}_L = Observations of the training data set.
 \mathbf{u}_T = The input variable of the test data set.
 μ = The prior knowledge about the output on the whole evaluated data set.
 σ = The variance of the covariance function.
 \hat{y}_T = The most probable prediction.
 σ_T = The variance of the Gaussian distribution of the prediction.
 K = The covariance matrix.
 $k(x, x', \sigma)$ = The covariance function.
 K_y = The noisy covariance matrix.
 K_* = The training-test set covariance.
 K_{**} = The test set covariance.

Algorithm 13: Gaussian Process Regression.

5.2.2.3 Extended Kalman Filter

The Kalman Filter framework is based on Bayesian parameter estimation (A Bayes estimator allows to estimate parameters based on prior knowledge about the parameter distribution) [138] that requires the use of recursive equations. The taken main assumption is that the measuring noise and process noise are Gaussian, independent of each other and have a zero mean [44]. The Kalman Filter framework uses a series of measurements observed over time to estimate the more probable output variables. This method is composed by two steps: first a prediction state is required and then the estimation is updated (see Eq. (104) and (105)) [20]. Thanks to this, the Kalman Filter provides a theoretically well designed and time proven method to filter measurements of system input and output by producing an intelligent estimation of a dynamic system's state [44].

$$x_{k+1} = Ax_k + Bu_k + a_k \quad (104)$$

$$z_{k+1} = Cx_{k+1} + b_{k+1} \quad (105)$$

Parameters	Description
x	The system's state variable.
u	The control input.
z	A comparison vector.
$k, k + 1$	The actual state and the next state respectively.
A, B, C	The covariance matrix that links x_k to x_{k+1} , x_{k+1} to u_k and x_{k+1} to z_{k+1} respectively.
a, b	The process noise and measurement noise respectively.

Table 136: Space Model used in Kalman Filter [44]

The Extended Kalman Filter linearizes the model at each step and then applies the Kalman Filter [57] by using partial derivatives and Taylor series expansion [8], see Algorithm 14.

Unlike the Kalman Filter, the Extended Kalman Filter is not an optimal estimator due to the first-order linearization (it ignores the high order Taylor expansion terms) [57]. This leads to errors becoming larger [51] and therefore the Extended Kalman Filter cannot deal with systems with highly non-linear characteristics (first order Taylor series approximation cannot give enough accuracy in a highly non-linear case [8]). Another limitation is that a matrix operation is needed where the size of the matrix correspond directly to the number of states of the battery model [20].

$$\hat{x}_{k|k}, P_{k|k} \leftarrow \text{EKFStep}(u_{k-1}, y_k, \hat{x}_{k-1|k-1}, P_{k-1|k-1})$$

- 1: $\hat{x}_{k|k-1} \leftarrow f(\hat{x}_{k-1|k-1}, u_{k-1})$
- 2: $\hat{y}_{k|k-1} \leftarrow h(\hat{x}_{k|k-1})$
- 3: $P_{k|k-1} \leftarrow F_{k-1}P_{k-1|k-1}F_{k-1}^T + Q$
- 4: $P_{yy} \leftarrow H_kP_{k|k-1}H_k^T + R$
- 5: $P_{xy} \leftarrow P_{k|k-1}H_k^T + R$
- 6: $K_k \leftarrow P_{xy}P_{yy}^{-1}$
- 7: $\hat{x}_{k|k} \leftarrow \hat{x}_{k|k-1} + K_k(y_k - \hat{y}_{k|k-1})$
- 8: $P_{k|k} \leftarrow (I - K_kH_k)P_{k|k-1}$

Where

$\hat{x}_{k|k-1}$ = Inner state at time instant k knowing the inner state at time instant $k - 1$.

$\hat{y}_{k|k-1}$ = observation estimation at time instant k knowing the observation estimation at time instant $k - 1$.

$P_{k|k-1}$ = The covariance matrix at time instant k knowing the covariance matrix at time instant $k - 1$.

u_{k-1} = The input vector at time instant $k - 1$.

y_k = The (measured) system output vector at time instant k .

F_{k-1} = The Jacobian transformation of the space state equations (f).

H_k = The Jacobian transformation of the observation equations (h).

P_{yy} = The covariance of the outputs.

P_{xy} = The cross variance.

K_k = The Kalman gain at time instant k .

Q = The assumed process noise covariance.

R = The assumed sensor noise covariance.

Algorithm 14: Extended Kalman Filter pseudo code [57].

The state estimation uncertainty propagation is done analytically by calculating the state estimation covariance matrix (where its diagonal is the variance) at the defined End of Life time instant knowing the estate at the last filtered time instant. However, computing the uncertainty of the observation is not trivial from an analytical point of view [138]. There is also no information that suggests that the observation at the EOL time instant will be Normal distributed. In this scenario, the probability density function of the observation at the EOL time instant is approximated using computational statistics methods such as the one described previously in the "Uncertainty propagation method" section.

5.2.2.4 Unscented Kalman Filter

The Unscented Kalman Filter is a version of the Kalman Filter that approximates the state distribution using the unscented transform. This procedure maintains the nonlinear functions exactly as they are, eliminating the need to calculate Jacobians as in Extended Kalman Filter [57]. Instead,

deterministically selected weighted samples, called sigma points, are generated. These sigma points capture the mean and covariance of the state distribution, which can be propagated to calculate the posterior mean and covariance of the state distribution [54].

There are several methods to select the sigma points, such as the symmetric unscented transform, the minimal skew simplex transform and the spherical simplex unscented transform, from which the commonly used method is the symmetric unscented transform [57], see Eq. (106) and Eq. (107).

$$w^i = \begin{cases} \frac{ki}{n_x + ki}, & i = 0 \\ \frac{ki}{2(n_x + ki)}, & i = 1, \dots, 2n_x \end{cases} \quad (106)$$

$$\mathcal{X}^i = \begin{cases} \bar{x}, & i = 0 \\ \bar{x} + \left(\sqrt{(n_x + ki)P_{xx}}\right), & i = 1, \dots, n_x \\ \bar{x} - \left(\sqrt{(n_x + ki)P_{xx}}\right), & i = n_x + 1, \dots, 2n_x \end{cases} \quad (107)$$

Parameters	Description
ki	It is a free parameter that can be used to tune the higher order moments of the distribution [57].
w^i	The weight of the i th sigma point.
n_x	Amount of states.
P_{xx}	The covariance of the original distribution.
\mathcal{X}^i	The mean of the i th sigma point.

Table 137: Sigma point calculation by Symmetric Unscented Transformation

The main merit of the Unscented Kalman Filter comparing with the Extended Kalman Filter is that the Unscented Kalman Filter is accurate to the third-order Taylor series expansion for any nonlinearity. Some other merits are that the Unscented Kalman Filter is robust to noise because it takes the measurement and process uncertainties into account and that it has the ability to self-correct [54].

The main limitation of the Unscented Kalman Filter is that the use of the it alone can lead to poor prediction performance if the initial state estimation is modelled incorrectly [139].

$$\hat{\mathbf{x}}_{k|k}, \mathbf{P}_{k|k} \leftarrow \mathbf{UKFStep}(\mathbf{u}_{k-1}, \mathbf{y}_k, \{\hat{\mathcal{X}}_{k-1|k-1}^i, \mathbf{w}^i\}_{i=1}^{n_s}, \mathbf{P}_{k-1|k-1})$$

- 1: $\hat{\mathcal{X}}_{k|k-1}^i \leftarrow f(\hat{\mathcal{X}}_{k-1|k-1}^i, \mathbf{u}_{k-1}), i = 1, \dots, n_s$
- 2: $\hat{\mathcal{Y}}_{k|k-1}^i \leftarrow h(\hat{\mathcal{X}}_{k|k-1}^i), i = 1, \dots, n_s$
- 3: $\hat{\mathbf{x}}_{k|k-1} \leftarrow \sum_i^{n_s} w^i \mathcal{X}_{k|k-1}^i$
- 4: $\hat{\mathbf{y}}_{k|k-1} \leftarrow \sum_i^{n_s} w^i \mathcal{Y}_{k|k-1}^i$
- 5: $\mathbf{P}_{k|k-1} \leftarrow \mathbf{Q} + \sum_i^{n_s} w^i (\mathcal{X}_{k|k-1}^i - \hat{\mathbf{x}}_{k|k-1})(\mathcal{X}_{k|k-1}^i - \hat{\mathbf{x}}_{k|k-1})^T$
- 6: $\mathbf{P}_{yy} \leftarrow \mathbf{R} + \sum_i^{n_s} w^i (\mathcal{Y}_{k|k-1}^i - \hat{\mathbf{y}}_{k|k-1})(\mathcal{Y}_{k|k-1}^i - \hat{\mathbf{y}}_{k|k-1})^T$
- 7: $\mathbf{P}_{xy} \leftarrow \sum_i^{n_s} w^i (\mathcal{X}_{k|k-1}^i - \hat{\mathbf{x}}_{k|k-1})(\mathcal{Y}_{k|k-1}^i - \hat{\mathbf{y}}_{k|k-1})^T$
- 8: $\mathbf{K}_k \leftarrow \mathbf{P}_{xy} \mathbf{P}_{yy}^{-1}$
- 9: $\hat{\mathbf{x}}_{k|k} \leftarrow \hat{\mathbf{x}}_{k|k-1} + \mathbf{K}_k (\mathbf{y}_k - \hat{\mathbf{y}}_{k|k-1})$
- 10: $\mathbf{P}_{k|k} \leftarrow \mathbf{P}_{k|k-1} - \mathbf{K}_k \mathbf{P}_{yy} \mathbf{K}_k^T$

Where

$\hat{\mathcal{X}}_{k|k-1}^i$ = The i th sigma point at time instant k knowing the i th sigma points at time instant $k - 1$.

$\hat{\mathcal{Y}}_{k|k-1}^i$ = The estimated observation with the i th sigma point at time instant k knowing the i th sigma points at time instant $k - 1$.

n_s = The amount of sigma points.

$\hat{\mathbf{x}}_{k|k-1}$ = Inner state at time instant k knowing the inner state at time instant $k - 1$.

$\hat{\mathbf{y}}_{k|k-1}$ = observation estimation at time instant k knowing the observation estimation at time instant $k - 1$.

$\mathbf{P}_{k|k-1}$ = The covariance matrix at time instant k knowing the covariance matrix at time instant $k - 1$.

\mathbf{u}_{k-1} = The input vector at time instant $k - 1$.

\mathbf{y}_k = The (measured) system output vector at time instant k .

w^i = The weight of the i th sigma point.

Q = The assumed process noise covariance.

R = The assumed sensor noise covariance.

P_{yy} = The covariance of the outputs.

P_{xy} = The cross variance.

K_k = The Kalman gain at time instant k .

Algorithm 15: The Unscented Kalman Filter pseudo-code [57].

As in the Extended Kalman Filter, the state estimation uncertainty propagation is done analytically by calculating the state estimation covariance matrix (where its diagonal is the variance) at the defined End of Life time instant knowing the state at the last filtered time instant. However, computing the uncertainty of the observation is not trivial from an analytical point of view [138]. To overcome this difficulty, the probability density function of the observation at the EOL time instant is approximated using computational statistics methods, such as the one described previously in “Uncertainty propagation method” section.

5.2.3 Evaluation

Several prediction stochastic algorithms are evaluated. For that, firstly, it is necessary to determine the inputs of the algorithms used on the evaluation exercises. These inputs consist on the data and on the prior knowledge about the performance of the system. Secondly, it is necessary to define the characteristics of the analysed algorithms. There are many elements that affect significantly the performance rate of these algorithms, so their performance evaluation cannot be done without the proper definition of the selected algorithm configuration. Thirdly, it is necessary to determine the used hyper-parameters. The hyper-parameters are the tuning elements and affect greatly the performance of the algorithm under evaluation. In this case, the hyper-parameters are not fixed by expertise, but estimated with a parametrization algorithm based on the defined “Universal parameterization criterion”. Therefore, the inputs of the applied parametrization algorithm need to be defined instead of the hyper-parameters themselves.

Once all the variables of the defined algorithm are properly defined, the simulations are run and the evaluation results are obtained.

5.2.3.1 Input

In this proposal, the input of the algorithm refers to the information of the system that is under evaluation. In other words, the information about the lithium ion battery that is introduced on the stochastic algorithm to predict the event of interest: the data used on the prognosis and the prior knowledge that models the behavioural trends of the data. As a result of the available input combinations, a trial matrix has been designed, see Table 139.

- **Data**

The selected data for the evaluation of the prognosis tools consists on the dischargeable capacity of a lithium ion battery at different state of health defined by the evolution of the applied cycles. The data set has been taken from NASA’s data repository [140], a repetitively used public data source on evaluating lithium ion battery RUL prognosis algorithms. The selected NASA’s data sets consist on rechargeable 18650 Gen 2 Li-ion cells with a rated capacity of 2Ah. The experiment was conducted through three different operational profiles (charge, discharge and impedance) at room temperature. Charging was performed in a constant current at 1.5A until the battery voltage reached 4.2V and continued in constant voltage mode until the charge current dropped to 20mA. The discharge runs were stopped at 2.7V. The experiments were conducted until the capacity decreased to the specified EOL criteria of 1.4Ah [141].

Among the different data sets available on the selected NASA’s data repository, the proposed evaluation framework requires using two data sets with different uncertainty levels on the data itself. For that, it is considered that the uncertainty on the input data comes from the effects that the proposed models on the prior knowledge section (next section) cannot describe, such as the capacity

recovery events. The selected data set with high uncertainty is “B0018” and the selected data set with low uncertainty is “B0007”, see Figure 107.

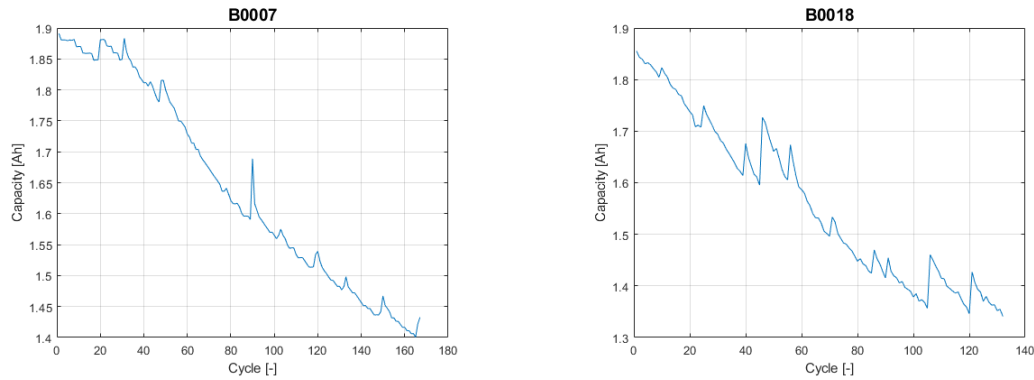


Figure 107: The input data of the evaluated stochastic algorithm.

▪ **Prior knowledge**

The behavioural aspect that needs to be modelled by the prior knowledge would be the dischargeable capacity evolution of the battery until, at least, the defined EOL event. The dischargeable capacity of the battery suffers a decreasing evolution or a decay. This thesis proposes to use two semi-empirical capacity decrease models that have different uncertainty levels on describing the system’s behaviour. In the literature, it has been proved that the capacity decay is not linear [142] and that a double exponential expression is able to describe it with a high level of confidence [93][92][47]. Therefore, a double exponential model is taken as the prior knowledge with low uncertainty (Eq. (108)), and a linear model is taken as the prior knowledge with high uncertainty (Eq. (109)).

$$cap(t) = a \cdot exp^{b \cdot t} + c \cdot exp^{d \cdot t} \quad (108)$$

$$cap(t) = a \cdot t + b \quad (109)$$

$$x_{k+1} = x_k + u_k, \quad x \in [a, b, c, d] \quad (110)$$

Parameters	Description
$cap(t)$	The function that describes the dischargeable capacity evolution at the input t .
a, b, c, d	The free variables.
x_k	The hidden state at time instant k .
u_k	The state space model’s noise at time instant k .

Table 138: The proposed capacity decay models

The defined prior knowledge can be also used to build the state space model required by the stochastic filters. An state space model is a model that uses state variables to describe a system by a set of first-order differential or difference equations [143]. It also describes an observed process with a hidden state process [41]. On one hand, the observation of the applicable state space model can be defined as the dischargeable capacity. The observation equations are already defined as the prior knowledge: Eq. (108) and Eq. (109). On the other hand, the hidden states can be defined as the variables a, b, c, d used on Eq. (108) and Eq. (109). The hidden state process is unknown, but it can be claimed that the hidden state process is kept constant (when the observation equations are able to capture correctly the dischargeable capacity evolution trend, the hidden states remain constant in time). Therefore, a linear stochastic process is proposed as the state transition model (also referred as the hidden state process), see Eq. (110).

Test n°	Stochastic tool	Aging model	Cell
1	Particle Filter	Eq. (108)	“B0007”
2			“B0018”

3		Eq. (109)	"B0007"
4			"B0018"
5	Gaussian Process	Eq. (108)	"B0007"
6			"B0018"
7		Eq. (109)	"B0007"
8	"B0018"		
9	Extended Kalman Filter	Eq. (108)	"B0007"
10			"B0018"
11		Eq. (109)	"B0007"
12			"B0018"
13	Unscented Kalman Filter	Eq. (108)	"B0007"
14			"B0018"
15		Eq. (109)	"B0007"
16			"B0018"

Table 139: Trial matrix definition for every algorithm under evaluation

5.2.3.2 Algorithm configuration

The selected Particle Filter configuration consists on a simple Particle Filter with a proposal distribution method based on the previous iteration's distribution and a systematic resampling method. An initial parameter definition step has been done based on experience and on the literature [144]. The defined parameters are resumed in Table 140.

Parameters	Value	Description
ρ	500	Particle quantity [144].
N_r	50	Resampling threshold % respect to the particle quantity.

Table 140: Affecting parameters on the Particle Filter

The selected Gaussian Process configuration consists on a Gaussian Process algorithm that uses the results obtained from the aging model as the prior knowledge. The selected covariance function is the neural network covariance function, a covariance function that emulates the behaviour of a Neural Network algorithm (Eq. (96)).

The Extended Kalman Filter and the Unscented Kalman Filter are completely defined by themselves; they do not require any further definition. These two algorithms are particular configurations of a general Kalman Filter.

5.2.3.3 Parametrization

The algorithms under evaluation have some variables that need to be determined, especially the so called hyper-parameters. The proper definition and fitting of these variables affects greatly the performance level that the stochastic algorithms have. This is why, it has been proposed a parametrization exercise that mixes literature research, use case experience and the parametrization criterion described on "Universal parameterization criterion".

▪ Particle Filter

The parameterization of the hyper-parameters of the Particle Filter is performed based on Algorithm 16. It starts initializing the inner states at each time instant. For that, a "least squares optimization" of the training data and the capacity decay model is conducted using MATLAB's "lsqcurvefit" function. Once this is done, the algorithm's hyper-parameters at each time step (Table 141) are achieved by grid search optimization.

Parameters	Description
σ_u	The variance of the state model's Gaussian noise.
σ_v	The variance of the observation model's Gaussian noise.
σ_{ini}	The variance of the initial Gaussian distribution of the particles.

Table 141: Hyper-parameters on the Particle Filter with basic resampling methods

The grid for each hyper-parameter is designed based on the rule of delimiting as much as possible the tested values without losing interesting options. For that, a sensibility analysis would be required, but in this case, the design of the grid is based on previous engineering experience. The obtained

results have led to define the limits of the grids as well as defining the grid delta values. The created grid is shown in Table 142.

Parameters	High limit	Intervals	Low limit
σ_u	1.5	0.6, 0.1, 0.05, 0.02, 0.01, 0.005, 0.002, 0.001	0.0005
σ_v	1.5	0.6, 0.1, 0.05, 0.02, 0.01, 0.005, 0.002, 0.001	0.0005
σ_{ini}	0.1	0.05	0.01

Table 142: Grid Search Optimization grid on the Particle Filter with basic resampling methods

The results obtained with every configuration on the grid are evaluated to find the optimal hyper-parameters. This is done running C_V times each grid configuration and finding the case with the lowest variation among the run cases with the lowest Root Mean Squared Error, which in this case it has been set to 10.

$\{\theta_{optimum}^\lambda\}_{\lambda=1}^{E_\lambda} \leftarrow \text{PARAMETERIZATION}(\{x_\lambda^0, y_\lambda, u_\lambda, N_\lambda\}_{\lambda=1}^{E_\lambda}, \theta)$

```

1: for  $\lambda = 1$  to  $E_\lambda$ 
2:   for  $j = 1$  to  $C_V$  do
3:     for  $s = 1$  to  $size(\vartheta_u)$  do
4:       for  $r = 1$  to  $size(\vartheta_v)$  do
5:         for  $q = 1$  to  $size(\vartheta_{ini})$  do
6:            $\sigma_u \leftarrow \vartheta_u^s$ 
7:            $\sigma_v \leftarrow \vartheta_v^r$ 
8:            $\sigma_{ini} \leftarrow \vartheta_{ini}^q$ 
9:            $x_1 \leftarrow \mathcal{N}(x_\lambda^0, \sigma_{ini})$ 
10:           $w_1 \leftarrow \mathcal{U}(\mathbf{0}, \mathbf{1}/\rho)$ 
11:          for  $k = 2$  to  $N_\lambda$  do
12:             $[\{x_k^i, w_k^i\}_{i=1}^\rho, \hat{x}_k] \leftarrow \text{PFstep}(\{x_{k-1}^i, w_{k-1}^i\}_{i=1}^\rho, \sigma_u, \sigma_v, y_k^t)$ 
13:          end for
14:           $\hat{y}_\lambda \leftarrow f(\{\hat{x}_k\}_{k=1}^{N_\lambda}, u_\lambda)$ 
15:           $RMSE^{j,s,r,q} \leftarrow RMSE(y_\lambda, \hat{y}_\lambda)$ 
16:        end for
17:      end for
18:    end for
19:  end for
20:   $\vartheta_{top10}^{j,\lambda} \leftarrow \{\min(RMSE^{j,s,r,q})\}_{j=1}^{C_V}$ 
21:   $\vartheta_{optimum}^\lambda \leftarrow \min(\text{var}(\vartheta_{top10}^{j,\lambda}))$ 
22: end for

```

Where

E_λ = Amount of prediction time instants.

x_λ^0 = The initialization of the hidden states at prediction time instant λ .

y_λ = Observations at prediction time instant λ .

u_λ = The inputs of the observation equation on the test data set f at prediction time instant λ .

N_λ = Amount of learning points at prediction time instant λ .

θ = The entire hyper-parameter grid.

C_V = Amount of repetitions of each configuration on the grid.

σ_u = The variance of the state model's Gaussian noise.

σ_v = The variance of the observation model's Gaussian noise.

σ_{ini} = The variance of the initial Gaussian distribution of the particles.

ϑ_x = The grid of the hyper-parameter σ_x .

x_k^i = The hidden state of i particle at time instant k .

w_k^i = The weight of the hidden state of i particle at time instant k .

\hat{x}_k = most probable hidden state at time instant k .

\hat{y}_λ = prediction of the system's output at prediction time instant λ on the validation data set.

$RMSE^{j,s,r,q}$ = Root Mean Square Error in each iteration of the grid search optimization.

$RMSE$ = Root Mean Square Error equation.

$\vartheta_{top10}^{j,\lambda}$ = The top ten hyper-parameters at prediction time instant λ in each repetition j .

$\vartheta_{optimum}^\lambda$ = The optimum hyper-parameters at prediction time instant λ .

Algorithm 16: Parametrization of the PF.

- **Gaussian Process**

The parameterization of the hyper-parameters of the Gaussian Process is performed based on Algorithm 17. The algorithm's hyper-parameters at each time step (Table 143) are achieved by grid search optimization.

Parameters	Description
σ_{NN}	The signal variance.
Σ	The covariance matrix that emulates the weight matrix on a Neural Network system.
σ_y	The noise variance.

Table 143: Hyper-parameters on the Gaussian Process with Neural Network covariance function

The grid for each hyper-parameter is designed based on the rule of delimiting as much as possible the tested values without losing interesting options. For that, a sensibility analysis would be required, but in this case, the design of the grid is based on previous engineering experience. The obtained results have led to define the limits of the grids as well as defining the intermediate values of the grid. The created grid is shown in Table 144.

Parameters	High limit	Intervals	Low limit
σ_{NN}	10	1,0.5,0.1,0.05,0.02,0.01,0.005,0.001	0.0001
$\Sigma(1)$	10	1,0.5,0.1,0.05,0.02,0.01,0.005,0.001	0.0001
$\Sigma(2)$	10	1,0.5,0.1,0.05,0.02,0.01,0.005,0.001	0.0001
σ_y	1	0.1	0.01

Table 144: Grid Search Optimization grid on the Gaussian Process with a Neural Network covariance function

The results obtained with every configuration on the grid are evaluated to find the optimal hyper-parameters. This is done running just one time each grid configuration. The results obtained with the Gaussian Process are stable so there is no need of doing extra effort on finding the most stable option. The hyper-parameter combination that achieves the lowest Root Mean Squared Error is determined the optimum set of hyper-parameters.

$$\left[\{\theta_{Optimum}^\lambda\}_{\lambda=1}^{E_\lambda} \right] \leftarrow \text{PARAMETERIZATION} \left(\{u_L^\lambda, y_L^\lambda, u_T^\lambda, y_T^\lambda, \mu_{L,T}^\lambda\}_{\lambda=1}^{E_\lambda}, \theta \right)$$

```

1: for  $\lambda = 1$  to  $E_\lambda$ 
2:   for  $j = 1$  to  $size(\vartheta_{NN})$  do
3:     for  $s = 1$  to  $size(\vartheta_{\Sigma 1})$  do
4:       for  $r = 1$  to  $size(\vartheta_{\Sigma 2})$  do
5:         for  $q = 1$  to  $size(\vartheta_y)$  do
6:            $\sigma_{NN} \leftarrow \vartheta_{NN}^j$ 
7:            $\Sigma(1) \leftarrow \vartheta_{\Sigma 1}^s$ 
8:            $\Sigma(2) \leftarrow \vartheta_{\Sigma 2}^r$ 
9:            $\sigma_y \leftarrow \vartheta_y^q$ 
10:           $[\hat{y}_T^\lambda, \sigma_T^\lambda] \leftarrow GP(u_L^\lambda, y_L^\lambda, u_T^\lambda, \mu_{L,T}^\lambda, \sigma_{NN}, \Sigma, \sigma_y)$ 
11:           $RMSE^{j,s,r,q} \leftarrow RMSE(y_T^\lambda, \hat{y}_T^\lambda)$ 
12:        end for
13:      end for
14:    end for
15:  end for
16:   $\vartheta_{Optimum}^\lambda \leftarrow \min(RMSE^{j,s,r,q})$ 
17: end for
    
```

Where

E_λ = Amount of prediction time instants.

u_L^λ = The input variable of the training data set at prediction time instant λ .

y_L^λ = Observations of the training data set at prediction time instant λ .

u_T^λ = The input variable of the test data set at prediction time instant λ .

$\mu_{L,T}^\lambda$ = The prior knowledge about the output on the whole evaluated data set.

y_T^λ = Observations of the test data set at prediction time instant λ .

θ = The entire hyper-parameter grid.

ϑ_x = The grid of the hyper-parameter σ_x .

C_V = Amount of repetitions of each configuration on the grid.
 $RMSE^{j,s,r,q}$ = Root Mean Square Error in each iteration of the grid search optimization.
 $RMSE$ = Root Mean Square Error equation.
 \hat{y}_T^λ = prediction of the system's output at prediction time instant λ on the test data set.
 σ_T^λ = variance of the Gaussian distribution of the predictions of the system's output at prediction time instant λ on the test data set.
 $\vartheta_{optimum}^\lambda$ = The optimum hyper-parameters at prediction time instant λ .

Algorithm 17: Parametrization of the Gaussian Process.

▪ **Extended Kalman Filter**

The parameterization of the hyper-parameters of the Extended Kalman Filter is performed based on Algorithm 18. It starts initializing the inner states at each time instant. For that, a "least squares optimization" of the training data and the capacity decay model is conducted using MATLAB's "lsqcurvefit" function. Once done this, the algorithm's hyper-parameters at each time step (Table 145) are achieved by grid search optimization.

Parameters	Description
q	Covariance of the process.
r	Covariance of the measurement.

Table 145: Hyper-parameters on the Extended Kalman Filter

The grid for each hyper-parameter is designed based on the rule of delimiting as much as possible the tested values without losing interesting options. For that, a sensibility analysis would be required, but in this case, the design of the grid is based on previous engineering experience. The obtained results have led to define the limits of the grids as well as defining the intermediate values of the grid. The created grid is shown in Table 146.

Parameters	High limit	Intervals	Low limit
q	0.1	0.01,0.001,0.0001,0.00001,0.000001,0.0000001,0.00000001,0.000000001	0.000000001
r	0.1	0.01,0.001,0.0001,0.00001,0.000001,0.0000001,0.00000001,0.000000001	0.000000001

Table 146: Grid Search Optimization grid on the Extended Kalman Filter

The results obtained with every configuration on the grid are evaluated to find the optimal hyper-parameters. The results obtained with the Extended Kalman Filter didn't use to be stable. The response of this algorithm typically needs a multi-result evaluation step like the Particle Filter. However, this is done running just one time each grid configuration because the state model noise and the measurement noises are set to zero. This means that the results obtained with the Extended Kalman Filter becomes stable and reproducible. There is no need of doing an extra effort on finding the most stable option. As a result, the hyper-parameter combination that achieves the lowest Root Mean Squared Error is determined the optimum set of hyper-parameters.

$$\left[\{\vartheta_{optimum}^\lambda\}_{\lambda=1}^{E_\lambda} \right] \leftarrow \text{PARAMETERIZATION} \left(\{x_\lambda^0, y_\lambda, u_\lambda, N_\lambda\}_{\lambda=1}^{E_\lambda}, \theta \right)$$

```

1: for  $\lambda = 1$  to  $E_\lambda$ 
2:   for  $j = 1$  to  $size(\vartheta_q)$  do
3:     for  $s = 1$  to  $size(\vartheta_r)$  do
4:        $q \leftarrow \vartheta_q^s$ 
5:        $r \leftarrow \vartheta_r^s$ 
6:        $\hat{x}_1 \leftarrow x_\lambda^0$ 
7:        $P_1 \leftarrow \{I \cdot q, r\}$ 
8:       for  $k = 2$  to  $N_\lambda$  do
9:          $[\hat{x}_k, P_k] \leftarrow \text{EKFstep}(u_{k-1}, y_k, \hat{x}_{k-1}, P_{k-1})$ 
10:      end for
11:       $\hat{y}_\lambda \leftarrow f(\{\hat{x}_k\}_{k=1}^{N_\lambda}, u_\lambda)$ 
12:       $RMSE^{j,s,r} \leftarrow RMSE(y_\lambda, \hat{y}_\lambda)$ 
13:    end for
14:  end for
15:   $\vartheta_{optimum}^\lambda \leftarrow \min(RMSE^{j,s,r})$ 
16: end for
  
```

Where

- E_λ = Amount of prediction time instants.
- x_λ^0 = The initialization of the hidden states at prediction time instant λ .
- y_λ = Observations at prediction time instant λ .
- u_λ = The inputs of the observation equation on the test data set f at prediction time instant λ .
- N_λ = Amount of learning points at prediction time instant λ .
- θ = The entire hyper-parameter grid.
- q = Covariance of the process.
- r = Covariance of the measurement.
- P_k = The covariance matrix at time instant k .
- ϑ_x = The grid of the hyper-parameter σ_x .
- x_k^i = The hidden state of i particle at time instant k .
- w_k^i = The weight of the hidden state of i particle at time instant k .
- \hat{x}_k = most probable hidden state at time instant k .
- \hat{y}_λ = prediction of the system's output at prediction time instant λ on the validation data set.
- $RMSE^{j,s,r}$ = Root Mean Square Error in each iteration of the grid search optimization.
- $RMSE$ = Root Mean Square Error equation.
- $\theta_{optimum}^\lambda$ = The optimum hyper-parameters at prediction time instant λ .

Algorithm 18: Parametrization of the Extended Kalman Filter.

▪ **Unscented Kalman Filter**

The parameterization of the hyper-parameters of the Extended Kalman Filter is performed based on Algorithm 19. It starts initializing the inner states at each time instant. For that, a “least squares optimization” of the training data and the capacity decay model is conducted using MATLAB’s “lsqcurvefit” function. Once done this, the algorithm’s hyper-parameters at each time step (Table 147) are achieved by grid search optimization.

Parameters	Description
q	Covariance of the process.
r	Covariance of the measurement.
ki	A free variable that determines the scaling factor.

Table 147: Hyper-parameters on the Unscented Kalman Filter

The grid for each hyper-parameter is designed based on the rule of delimiting as much as possible the tested values without losing interesting options. For that, a sensibility analysis would be required, but in this case, the design of the grid is based on previous engineering experience. The obtained results have led to define the limits of the grids as well as defining the intermediate values of the grid. The created grid is shown in Table 148.

Parameters	High limit	Intervals	Low limit
q	0.01	0.001,0.0001,0.00001,0.000001,0.0000001,0.00000001	0.000000001
r	0.01	0.001,0.0001,0.00001,0.000001,0.0000001,0.00000001	0.000000001
ki	10	2,1,0.1,0.01,0.001,0.0001	0.0000001

Table 148: Grid Search Optimization grid on the Unscented Kalman Filter

The results obtained with every configuration on the grid are evaluated to find the optimal hyper-parameters. The results obtained with the Unscented Kalman Filter didn't use to be stable. The response of this algorithm typically needs a multi-result evaluation step like the Particle Filter. However, this is done running just one time each grid configuration because the state model noise and the measurement noises are set to zero. This means that the results obtained with the Unscented Kalman Filter becomes stable and reproducible. There is no need of doing an extra effort on finding the most stable option. As a result, the hyper-parameter combination that achieves the lowest Root Mean Squared Error is determined the optimum set of hyper-parameters.

$$\left[\{\theta_{optimum}^\lambda\}_{\lambda=1}^{E_\lambda} \right] \leftarrow \text{PARAMETERIZATION} \left(\{x_\lambda^0, n_s, y_\lambda, u_\lambda, N_\lambda\}_{\lambda=1}^{E_\lambda}, \theta \right)$$

- 1: for $\lambda = 1$ to E_λ
 - 2: for $j = 1$ to $size(\vartheta_q)$ do
 - 3: for $s = 1$ to $size(\vartheta_r)$ do
 - 4: for $t = 1$ to $size(\vartheta_{ki})$ do
-

```

5:       $q \leftarrow \vartheta_u^j$ 
6:       $r \leftarrow \vartheta_r^s$ 
7:       $ki \leftarrow \vartheta_{ki}^t$ 
8:       $P_1 \leftarrow \{I \cdot q, r\}$ 
9:       $\hat{x}_1 \leftarrow x_\lambda^0$ 
10:      $n_x \leftarrow (n_s/2) - 1$ 
11:      $\{w^i\}_{i=1}^{n_s} \leftarrow \begin{cases} \frac{ki}{n_x+ki}, & i = 0 \\ \frac{ki}{2(n_x+ki)}, & i = 1, \dots, 2n_x \end{cases}$ 
12:     for  $k = 2$  to  $N_\lambda$  do
13:          $\{\hat{x}_{k-1}^i\}_{i=1}^{n_s} \leftarrow \begin{cases} \hat{x}_{k-1}, & i = 0 \\ \hat{x}_{k-1} + (\sqrt{(n_x + ki)P_{k-1}}), & i = 1, \dots, n_x \\ \hat{x}_{k-1} - (\sqrt{(n_x + ki)P_{k-1}}), & i = n_x + 1, \dots, 2n_x \end{cases}$ 
14:          $[\hat{x}_k, P_k] \leftarrow EKfstep(u_{k-1}, y_k, \{\hat{x}_{k-1}^i, w^i\}_{i=1}^{n_s}, P_{k-1})$ 
15:     end for
16:      $\hat{y}_\lambda \leftarrow f(\{\hat{x}_k\}_{k=1}^{N_\lambda}, u_\lambda)$ 
17:      $RMSE^{j,s,r,q} \leftarrow RMSE(y_\lambda, \hat{y}_\lambda)$ 
19: end for
20: end for
19: end for
21:  $\vartheta_{optimum}^\lambda \leftarrow \min(RMSE^{j,s,t})$ 
22: end for

```

Where

E_λ = Amount of prediction time instants.

x_λ^0 = The initialization of the hidden states at prediction time instant λ .

y_λ = Observations at prediction time instant λ .

u_λ = The inputs of the observation equation on the test data set f at prediction time instant λ .

N_λ = Amount of learning points at prediction time instant λ .

θ = The entire hyper-parameter grid.

q = Covariance of the process.

r = Covariance of the measurement.

ki = A free variable that determines the scaling factor.

n_s = The amount of sigma points.

\hat{X}_k^i = The i th sigma point at time instant k .

w^i = The weight of the i th sigma point.

P_k = The covariance matrix at time instant k .

ϑ_x = The grid of the hyper-parameter σ_x .

x_k^i = The hidden state of i particle at time instant k .

w_k^i = The weight of the hidden state of i particle at time instant k .

\hat{x}_k = most probable hidden state at time instant k .

\hat{y}_λ = prediction of the system's output at prediction time instant λ on the validation data set.

$RMSE^{j,s,r}$ = Root Mean Square Error in each iteration of the grid search optimization.

$\vartheta_{optimum}^\lambda$ = The optimum hyper-parameters at prediction time instant λ .

Algorithm 19: Parametrization of the Unscented Kalman Filter.

5.2.3.4 Results

The trials described in Table 139 are simulated. For that, some common simulation variables are defined based on experience and on the literature [115][117], see Table 149.

Parameters	Value	Description
T_{min}	10%	Minimum training data set $(N(1) + L)$.
β	50%	The minimum acceptable probability mass [117].
α	5%	The relative error [115].
L	4%	Validation data set.
EOL	7/8	End of Life time instant situation on the data set.
$\Delta\lambda$	1	The delta from one time instant to the next one.

Table 149: Simulation variables

The achieved prognosis results in all the trials are summarized thanks to tables that gather the obtained evaluation metrics and the figures that assist the qualitative evaluation of the obtained metrics. On one hand, Table 150 synthetizes just on three metrics the timeliness, precision, accuracy and the computational burden thanks to the Prognosis Horizon (PH), Convergence of the Relative Accuracy (CRA) and FLOP count. On the other hand, the Table 164, Table 165, Table 166 and Table 167 placed on "Annex 1" gathers all the details about the accuracy, precision and timeliness of the algorithm response at each tested prediction-time-instant. Those tables are considered as additional documentation because of the lack of synthesis (there are too many values that hinder the evaluation). In this scenario, a qualitative aid was proposed in form of a figure that displays the PH and α - λ accuracy, see Figure 108.

Test	PH	CRA	FLOP counts
1	129	65.2671	54 59 580
2	103	71.0676	4 289 670
3	128	84.1564	2 379 860
4	102	69.7007	1 869 890
Average	115.5	72.54	3 499 750

Table 150: The obtained evaluation metrics of Particle Filter on all training data sets

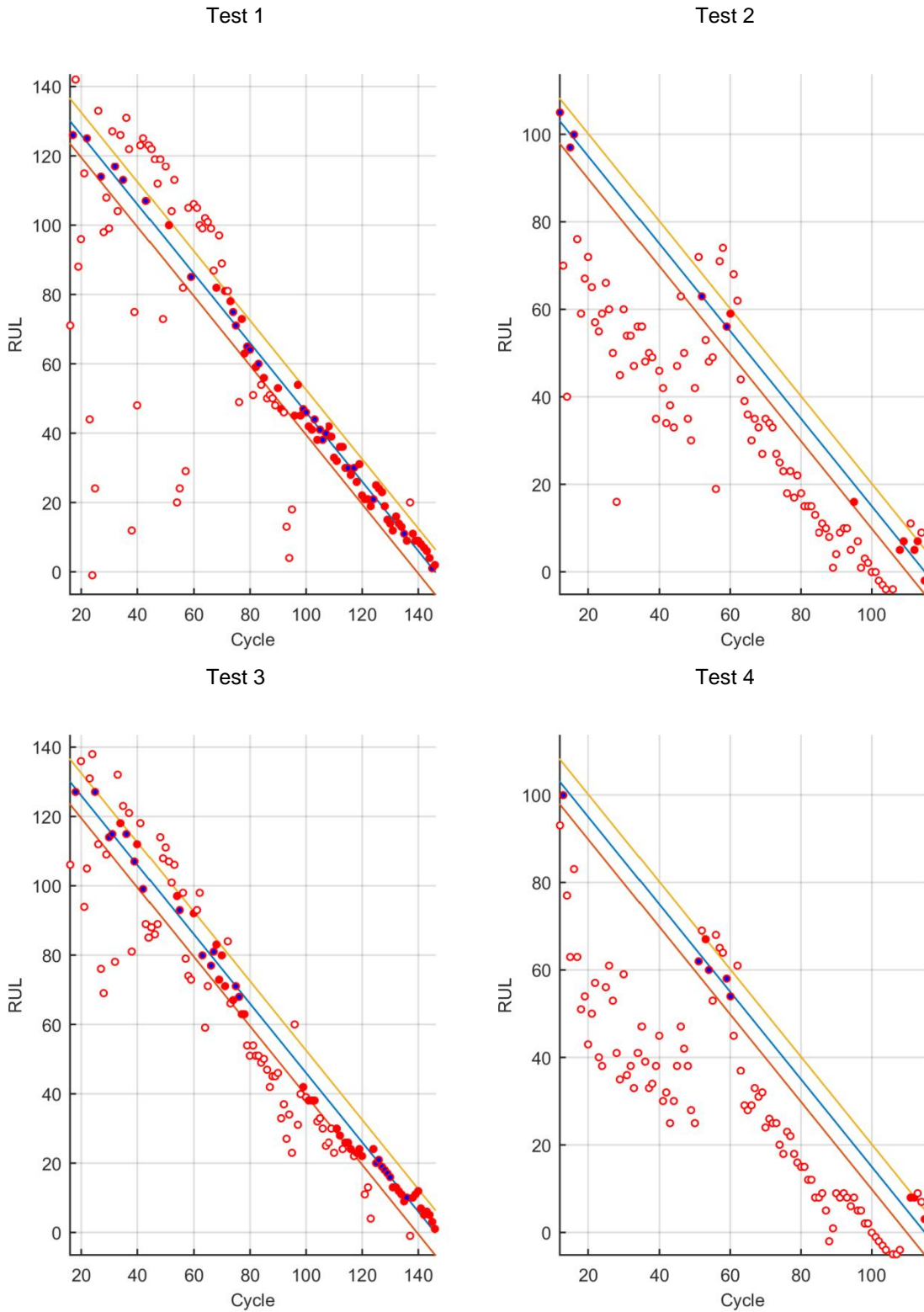


Figure 108: PH and α - λ accuracy visualization of the evaluated Particle Filter

Test	PH	CRA	FLOP counts
5	94	57.6241	933 408 615
6	45	77.9644	360 141 100
7	94	74.8617	933 408 615
8	99	72.9784	360 141 100
Average	83	70.85	646 774 857

Table 151: The obtained evaluation metrics of Gaussian Process on all training data sets

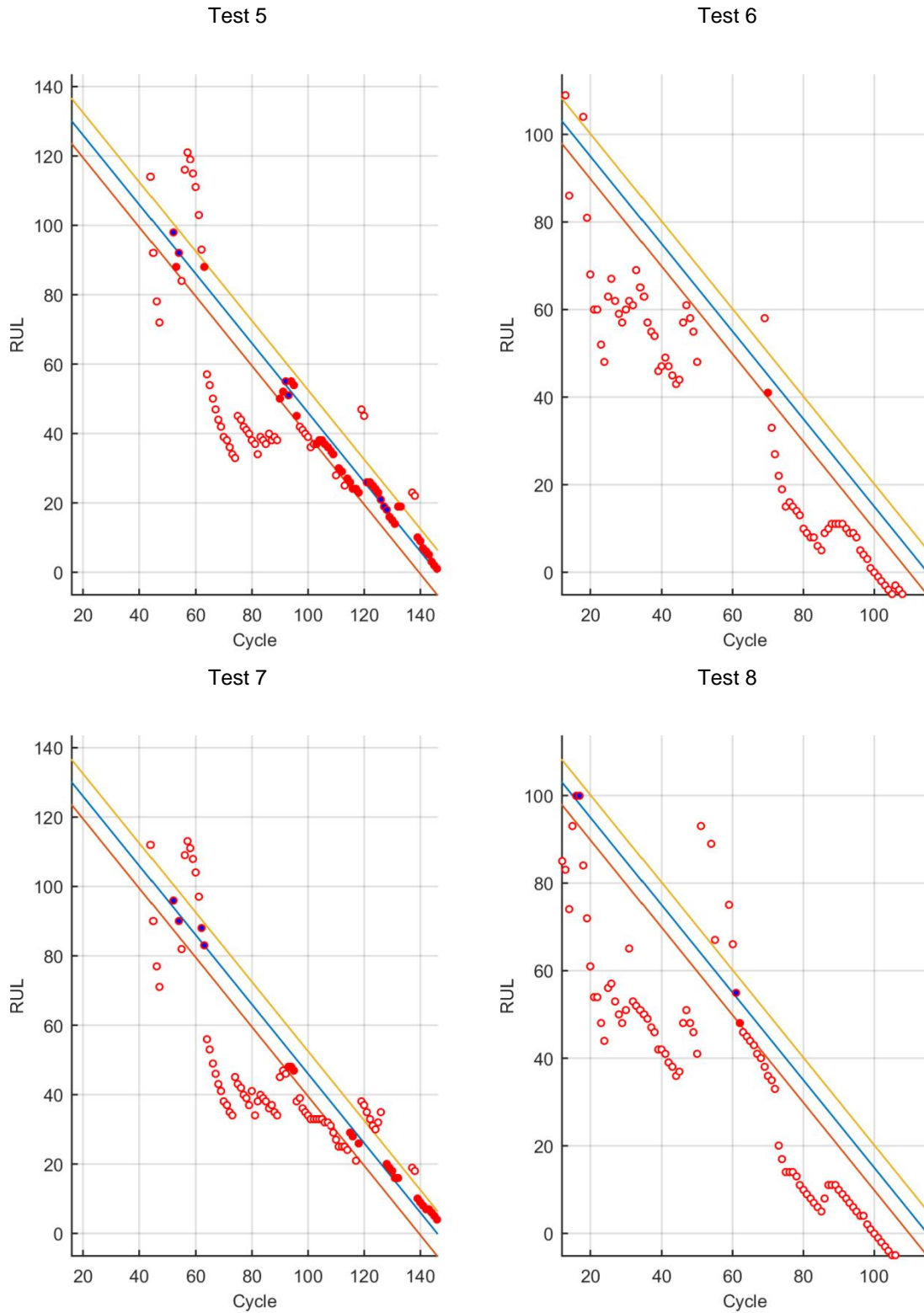


Figure 109: PH and α - λ accuracy visualization of the evaluated Gaussian Process

Test	PH	CRA	FLOP counts
9	78	42.2972	75 600
10	97	66.8369	59 400
11	76	32.2774	10 360
12	100	68.8150	8 140
Average	87.75	52.55	38 375

Table 152: The obtained evaluation metrics of Extended Kalman Filter on all training data sets

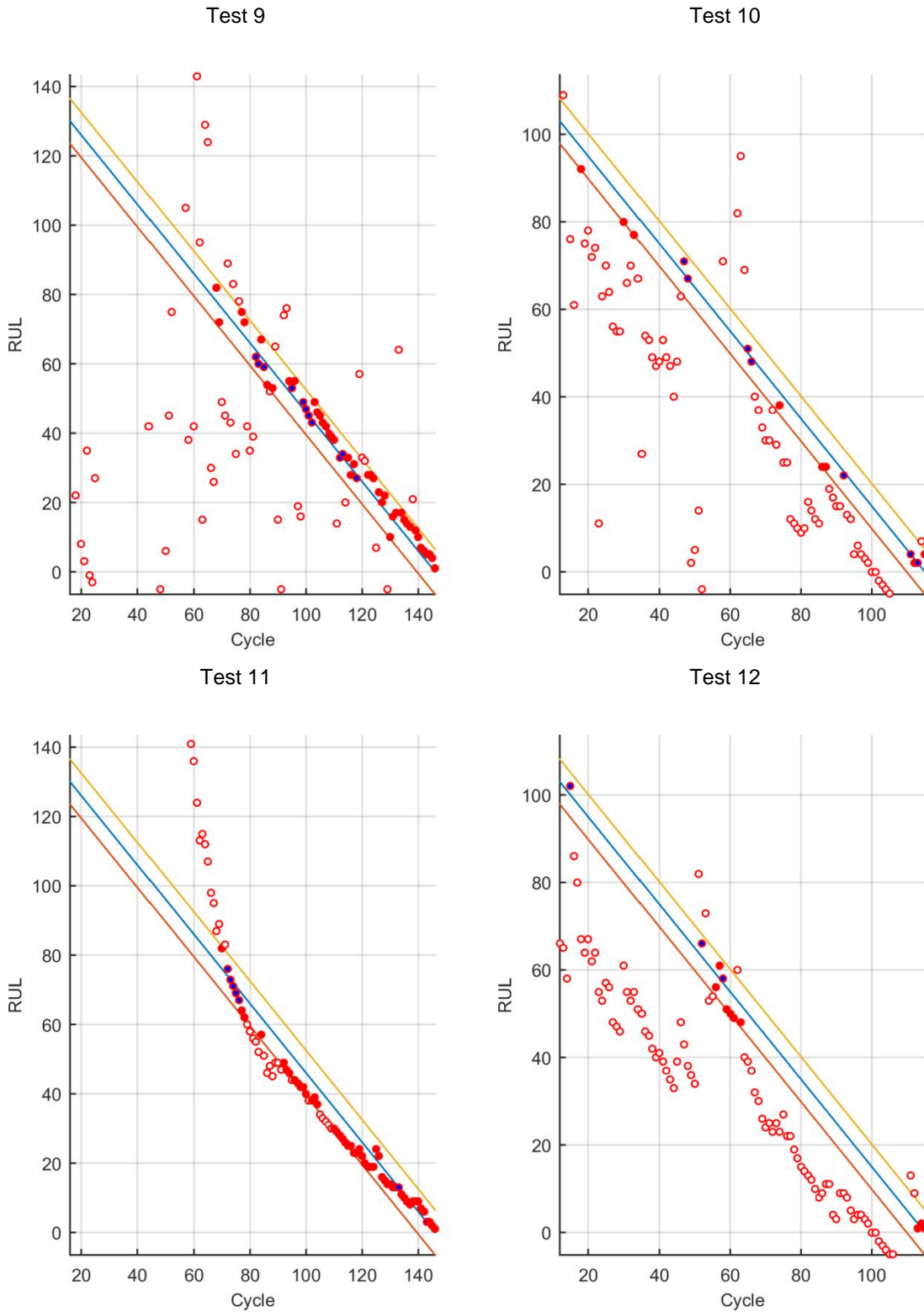


Figure 110: PH and α - λ accuracy visualization of the evaluated Extended Kalman Filter

Test	PH	CRA	FLOP counts
13	78	60.5296	1 209 600
14	68	66.9505	950 400
15	73	29.5973	165 760
16	103	70.4614	130 240
Average	80.5	56.88	614 000

Table 153: The obtained evaluation metrics of Unscented Kalman Filter on all the training data sets

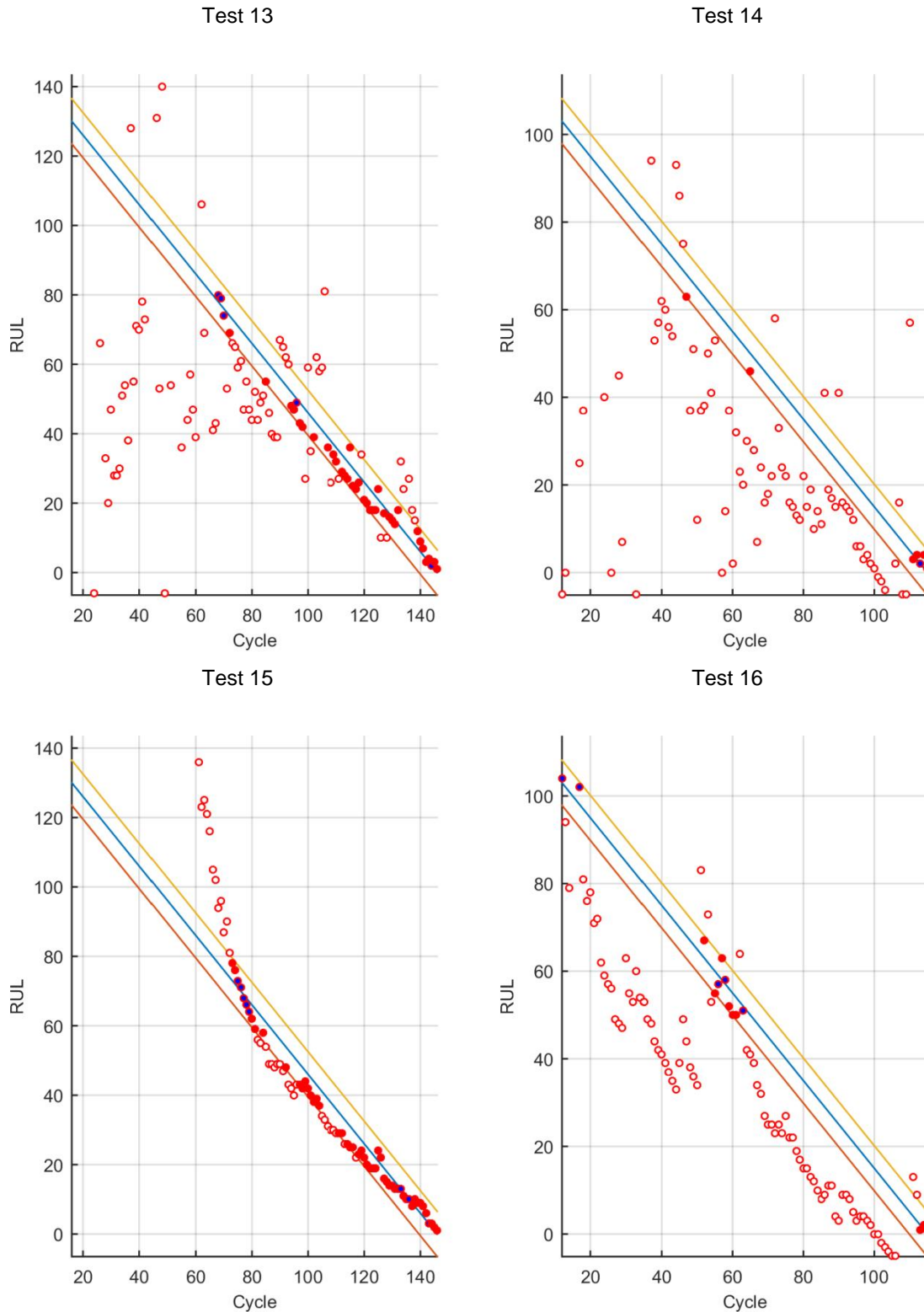


Figure 111: PH and α - λ accuracy visualization of the evaluated stochastic Unscented Kalman Filter

5.2.4 Comparison

The average values of the evaluated stochastic algorithms applied on a lithium ion battery prognosis problem with different levels of uncertainty are gathered in Table 155.

Test	PH	CRA	FLOP counts
Particle Filter	115.5	72.54	3 499 750
Gaussian Process	83	70.85	646 774 857
Extended Kalman Filter	87.75	52.55	38 375
Unscented Kalman Filter	80.5	56.88	614 000

Table 154: The average evaluation metrics of the evaluated 4 stochastic algorithms

In average, the Particle Filter has the highest Prognosis Horizon and the Extended Kalman Filter has the lowest Convergence of the Relative Accuracy and the lowest FLOP counts. This means that in an average sense:

- The Particle Filter is the stochastic algorithm among the evaluated ones that can predict accurately the earliest. The minimum data points that the Particle Filter requires for accurate estimations is the lowest among the tested stochastic algorithms.
- The Extended Kalman Filter is the stochastic algorithm among the evaluated ones that has the greatest accuracy improvement potential. The increase rate on the accuracy level that the Extended Kalman Filter achieves respect to the increase of the training data points is the greatest among the evaluated algorithms.
- The Extended Kalman Filter is the stochastic algorithm among the evaluated ones that has the lowest computational cost.

In an average sense, the most interesting prognosis stochastic algorithm at early prognosis is the evaluated Particle Filter configuration when there is no computational restriction. The evaluated Particle Filter configuration needs to do 3 million simple numerical operations to get just one prediction. This amount of numerical operations could be critical on On-board prognosis solutions but it is not on off-board applications. On the other hand, at late predictions would be the Extended Kalman Filter since it shows the greatest accuracy improvement when increasing the training data points. Besides, the Extended Kalman Filter has the lowest computational cost among all the evaluated algorithms, which makes it interesting for on-board applications.

Checking on the best cases, the highest Prognosis Horizon value is obtained with the Particle Filter, the low uncertain data set and the low uncertain prior knowledge; the lowest Convergence of the Relative Accuracy is obtained with the Unscented Kalman Filter (close to the minimum value obtained with the Extended Kalman Filter with the trial configuration), the low uncertain data set and the high uncertain prior knowledge (simplest model); and the lowest FLOP count is obtained with the Extended Kalman Filter, the high uncertain data (shorter data set) set and the high uncertain prior knowledge (simplest model). The results show that the highest timeliness is obtained with the Particle Filter, the highest correctness improvement is obtained with the Unscented Kalman Filter close to the values obtained with the Extended Kalman Filter and the lowest computational cost has the Extended Kalman Filter. These results are aligned with the ones obtained in an average sense.

The Prognosis Horizon is delimited by the initial remaining useful life; this is why the highest value is obtained with the larger data set (the low uncertain data set). On the Extended Kalman Filter, the maximum prognosis horizons are obtained with the smaller data set (the high uncertain data set), but the maximum obtainable Prognosis Horizon resides on the larger data set, as shown in the Particle Filter.

On the same hand, the convergence of the relative accuracy depends on the evolution of the obtained accuracy. Initial low accuracy and final high accuracy leads to have a low convergence value. The lower Convergence of Relative Accuracy values are obtained on the tests 11 and 15, which shows real high initial errors and low final errors, see Figure 112. The contrary increases the convergence. There could be cases with high accuracy estimations at every prediction-time-instants and have low convergence values, since they do not experience an improvement with the time. The

maximum Convergence of Relative Accuracy is obtained on test 3, which in a first glance it is the test with the most uniform and stable predictions (it has the lowest maximum errors on the lowly accurate predictions) and the one with the lowest initial errors (it has the highest Prognosis Horizon). However, test 3 has not as many highly accurate values as test 1 (the accuracy is kept similar all the prediction time instants). This means that the actual accuracy level is not shown by this metric, but rather the relative difference between the initially obtained accuracy values and the ones obtained lastly. Therefore, this metric does not defines the correctness but rather the improvement potential.

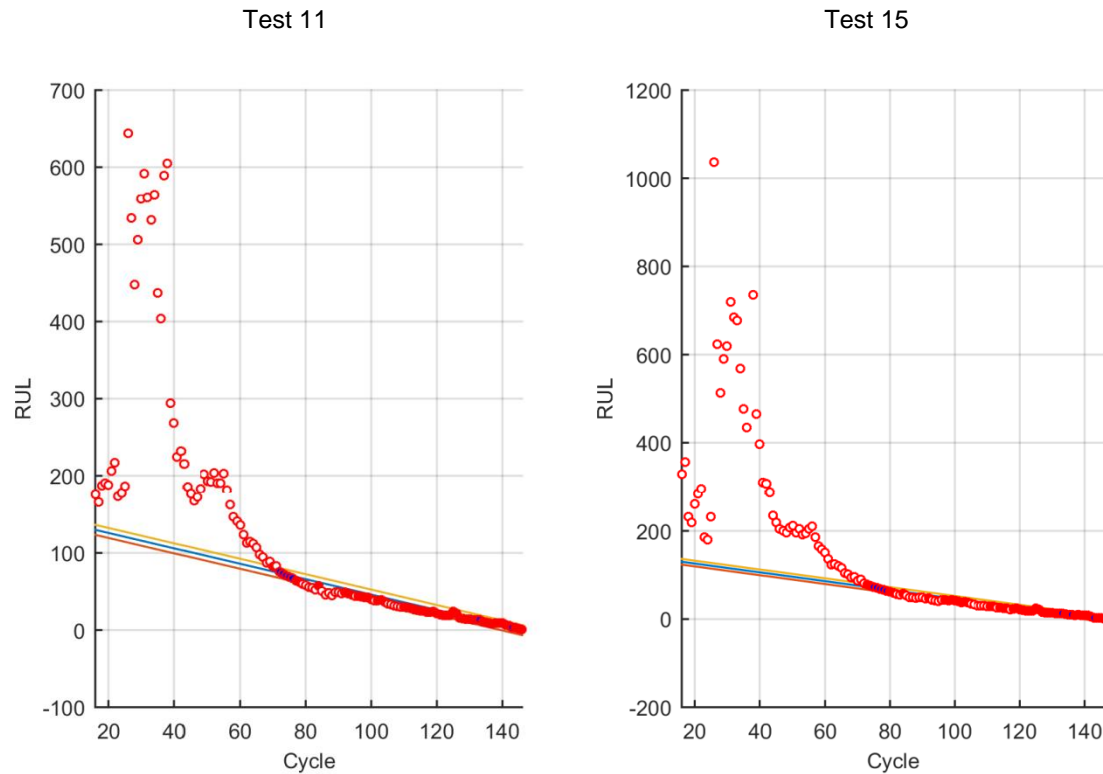


Figure 112: Illustrative example of the Remaining Useful Life predictions that are out of the displayed window.

As for the flop counting on the evaluated Stochastic Filters, the simplest prior knowledge and the smaller data set leads to the lower value (low uncertain data set and low uncertain prior knowledge). In case of the evaluated stochastic process (Gaussian Process), the complexity of the prior knowledge does not affect the computational burden of the algorithm. The prior knowledge is counted as 1 numerical operation indifferently to the used expression (exponential and lineal equations are considered as a unique numerical operation). This is why the FLOP count is kept the same on tests 6-8 and tests 5-7.

Checking on the qualitative figures in general, firstly, it can be seen that there is a clear effect on the uncertainty of the utilized data set. All the tests with the low uncertain data set gather more remaining useful life estimations inside the Prognosis Horizon boundaries than the tests run with the high uncertain data set. This means that the quality of the data determines greatly the accuracy level the evaluated prognosis algorithms will be able to obtain.

Secondly, it can be seen that in general the Prognosis Horizon is not determining what theoretically it determines, at least on most of the run tests. There are tests with high Prognosis Horizon values but with huge prediction errors from this point onwards. This metric should indicate the prediction-time-instant from which the predictions are done inside the boundaries of the Prognosis Horizon, but the figures show that this is only happening on the tests 11 and 15, where the accuracy of the predictions is kept almost always inside the Prognosis Horizon from the calculated Prognosis Horizon onwards. The rest have punctual accurate predictions with huge amount of continuous inaccurate predictions, especially on the tests run with the high uncertain data set.

Thirdly, it can be seen that the evaluated stochastic Filters (the Particle Filter, the Extended Kalman Filter and the Unscented Kalman Filter) shows a lower dispersion of the obtained remaining useful life estimations respect to the real remaining useful life with the simplest aging model (high uncertain model). The estimations done with the linear model shows less maximum errors than the estimations done with the double exponential model (low uncertain prior knowledge). This is attributed to the sensibility of the filtered hidden states. A slight change on the filtered hidden states of the double exponential equation has a great effect on the final remaining useful life estimation, what could lead to have punctual increased estimation errors.

And fourthly, the figures of the tests from 5 to 16 show some prediction-time-periods without visualization of the realized remaining useful life estimations. This issue is checked on the un-synthesized metrics. It has been detected two possible cases. On the first cases, there are some remaining useful life estimations that are out of the defined visualization window. It is especially appreciable on the tests 11 and 15, see Figure 112. On the second cases, the generated extrapolations show a growing behavior. On those cases, the end of life threshold is not crossed and therefore there is not a mathematical result for the remaining useful life prediction. These cases are put on black on the un-synthesized tables and the prediction-time-instants with no result are displayed on Figure 113. These results show how odd events that happen at the initial observations or odd events that generate a huge change on the evolution of the observed system could lead to incongruities on the evaluated stochastic algorithms.

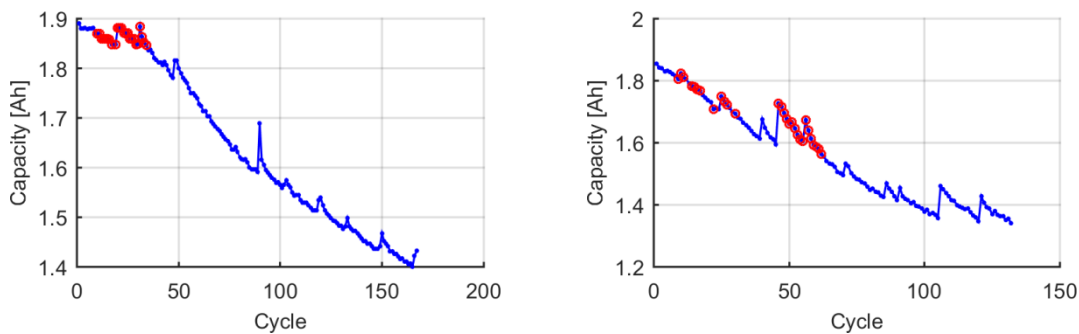


Figure 113: Conflicting points

To sum up, the best candidate for early predictions is the Particle Filter; the best candidate to achieve a uniform accuracy level is the Particle Filter used with a simple mathematical expression; the best candidate for late predictions is the Unscented Kalman Filter; and the best candidate for on-board prediction is the Extended Kalman Filter.

5.2.5 Validation

The prediction algorithm will solve the loss of reliability of the constructed aging models. The proposal consists on correcting and improving the constructed aging models with data obtained from the real life application.

The selected case scenario is the test 8, which has mixed operation conditions. The aging paths of the health indicators of the test 8 have been already modelled using the data from the tests 5, 6 and 7 on the validation section of the “Sizing Energy Storage Systems” chapter. Explicitly, the prediction algorithm is applied on the pure ohmic resistance evolution. The pure ohmic resistance on test 8 suffers an unexpected decrease on the second check-up, which cannot be described by the constructed aging model. The proposed pure ohmic resistance increase aging model has a monotonic characteristic, so it cannot describe a resistance decrease event (an odd event in the point of view of the proposed model). As a consequence, it ends committing huge prediction errors. This thesis proposes to apply a prognosis algorithm to eliminate, or at least reduce, the effect of those odd events on describing the aging behaviour of the system.

The best applicable algorithm on this case would be an algorithm that obtains early accurate predictions since the odd event happens in between the first and second observations. On the same

hand, the prediction algorithm is applied off-board, so there is not a computational restriction. On this scenario, the most appropriate stochastic algorithm among the evaluated ones would be the evaluated Particle Filter configuration.

Once the prediction algorithm is selected, how this algorithm is applied must be determined. For that, the input, the algorithm configuration and the parametrization of the algorithm are analysed.

The input is composed by data and prior knowledge. The data, on this use case, consists on the pure ohmic resistance observations done on test 8. The prior knowledge consists on the knowledge that describes the evolution of the observations. For this study, this knowledge has been defined as the calculated aging path of test 8 on the “Sizing Energy Storage Systems” chapter instead of the constructed aging model itself. The calculated aging path has been selected above the aging model in order to prove that the calculated aging path would have been able to describe the aging observed on test 8 if there were not an odd event.

In addition to this, due to the characteristics of the Particle Filter, a state space model needs to be constructed as part of the prior knowledge. On this case, the calculated aging path is used instead of the aging model itself. This means that there are not variables that can be used as the hidden variables required on a state space model such as the used on the evaluation section. The prior knowledge on this case is given in form of data. On this scenario, the aging variables are not modified. Instead, the improvement is believed to come from the correction of the initial value. The initial pure ohmic resistance value is left as the free variable on the prediction environment. The approach is described by Eq. (112).

$$R = R_{ini} + R_{path} \quad (111)$$

$$R_{ini,k+1} = R_{ini,k} + u_k \quad (112)$$

Parameters	Description
R	The most probable pure ohmic resistance.
R_{ini}	The initial value of the pure ohmic resistance.
R_{path}	The calculated pure ohmic resistance evolution of test 8.
u_k	The state space model's noise at time instant k .

Table 155: The mathematical framework to apply the Particle Filter on test 8

The algorithm configuration would be the same as the one determined on this evaluation section: a simple Particle Filter used along with a Systematic resampling method. An initial parameter definition step has been done based on experience and on the literature [144]. The defined parameters are resumed in Table 156.

Parameters	Value	Description
ρ	500	Particle quantity [144].
N_r	50	Resampling threshold % respect to the particle quantity.

Table 156: Affecting parameters on the Particle Filter

The odd event happens between the first and second observations. The odd event has already happened for the third observation and the evolution of the pure ohmic resistance from the second and third observations is aligned with the calculated aging path. Therefore, the third observation has been selected as the prediction time instant.

On this case, the amounts of observations used for the selected prediction time instant are only three. There are not enough data points to apply the proposed parametrization method (it requires having some data points for the selection of the hyper-parameters). The algorithm is parametrized based on the gathered experience with the application of the proposed parametrization method on NASA's data sets, see Table 157. On one hand, we have the initial and posterior variances of the state model's Gaussian noise. Those two variances can be related with the amplitude of the error on the estimations; the proposed expression can be transformed into a linear stochastic expression

where the uncertainty is expressed by the hidden variable; its variance could be assumed to be the variance of the error. There is an error below 10 between the estimated and observed second relative pure ohmic resistance value. Therefore, their variance is set between 1 and 2. On the other hand, we have the variance of the observation model's Gaussian noise. The observations are supposed to be accurate. Therefore, this hyper-parameter is set to a much lower value than the observed values.

Parameters	Value	Description
σ_u	1.54	The variance of the posterior state model's Gaussian noise.
σ_v	0.0370	The variance of the observation model's Gaussian noise.
σ_{ini}	1.73	The variance of the initial state model's Gaussian noise.

Table 157: Hyper-parameters on the Particle Filter applied on the validation

The algorithm has been applied on the defined framework and the prediction has been done, see Figure 114.

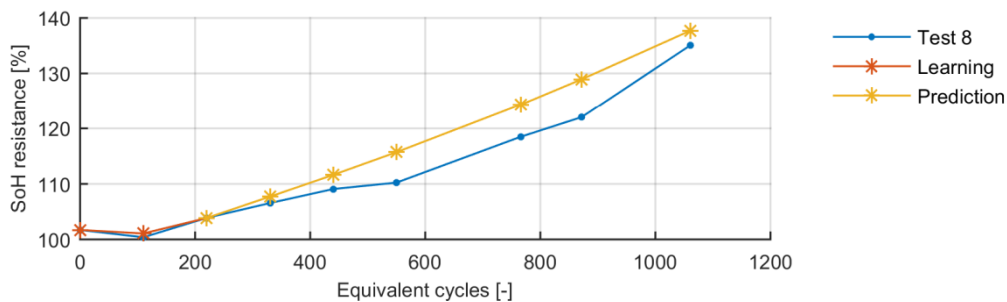


Figure 114: Correction of the calculated aging path of the pure ohmic resistance evolution of test 8 with a Particle Filter prognosis algorithm

The results show that the estimated aging path accuracy increases significantly with the addition of a prediction algorithm and that the effect of odd events can be practically erased from the real aging path. On the same hand, the results prove that the response of the constructed aging model is able to describe the aging behaviour of the pure ohmic resistance evolution and therefore, the second hypothesis on the “Sizing Energy Storage Systems” chapter is validated.

5.3 Sudden performance decay prediction

The proposed aging model assumes that the aging mechanisms behind the evolution of the modelled health indicators don't change in the future. The proposed aging models can only extrapolate the same trends observed on the training data sets. They cannot guess unobserved performances. However, many studies point to the incorrectness of this assumption [145][146]. The extrapolation of the observed aging trends on the validation section of “Sizing Energy Storage Systems” chapter has exhibited this phenomenon. There are cases that aging trend changes appear.

The aging trend is physically produced by many different aging mechanisms that coexist inside the cell, see Figure 115. The proper determination and modelling of these aging mechanisms is complex and their effect cannot be de-convoluted at will. Besides, the effect of some aging mechanisms are not observable until certain condition is met (their effect is hidden until a cumulative deterioration surpasses some threshold [27]). In this scenario, there is no easy way to properly determine the contribution of each aging mechanism on the performance decay of the cell.

A complex electrochemical model that describes all the chemical reactions that generate the performance decay of the cell would solve any problem related with extrapolations, but this is out of the scope of this thesis. Instead, this thesis proposes to fill the data sets with enough data to avoid extrapolations. This way, there will not be any unobserved aging trends and the error will be decreased significantly. There are two options to achieve this. The first option consists on increasing the data sets by lengthening the testing time. This is the ideal case. The data sets are increased to levels where the extrapolation is not demanded. Nonetheless, there are cases where the time required to get that data could be unaffordable, such as in the case of the data gathered from the

evaluated High-Power battery (after testing them for 3 years, the degradation is less than 5% on all the cases). For those cases, a second option is proposed, which consists on filling artificially the data sets.

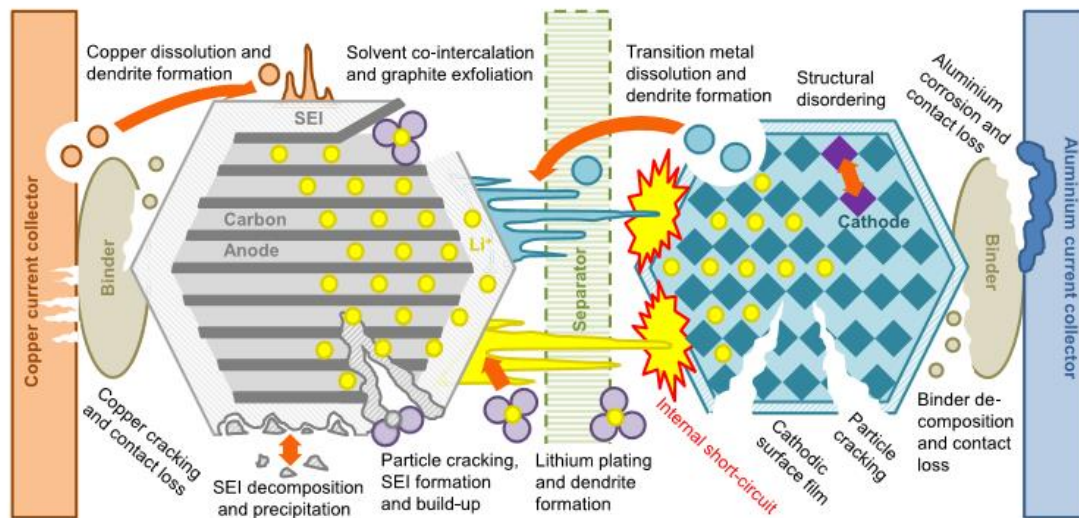


Figure 115: The different degradation modes of a lithium ion cell [31].

Electrode level data, also referred as Half-cell data, is used to generate the data required to fill the training data sets of the aging model. The data from the negative electrode is expected to be relevant enough to predict the change of the aging rate and to model it. For that, Half-cell data is required. However, the Half-cell data is obtained from building coin cells that contain samples of the selected battery and the data is obtained from destructive tests (the cell is opened and chopped), which means that Half-cell data cannot be obtained on the check-ups of an aging test. As a consequence, Half-cell data at a fresh state and the full-cell observations done at the check-ups need to be correlated. This is done by the fitting of the convoluted positive and negative OCV profiles. From the fitting, health indicators are recorded and modelled with which the artificial data is generated.

5.3.1 Electrode level data acquisition

Electrode level data cannot be obtained from the cell itself. The responses of the electrodes are convoluted on the response of the full cell and they cannot be separated intuitively. Besides, there is a destructive measurement methodology behind the acquisition of this kind of data, impeding the acquisition of this kind of data on intermediate checkups of the aging test. This is why this type of data is solely extracted from fresh cells (cells at the SOH delivered by the battery supplier) or dead cells (cells that have already finished an aging test). This thesis focuses on obtaining electrode level data at a fresh state and assumes that the main characteristics of the electrode are kept invariant.

The proposed electrode level data acquisition methodology consists on constructing a testable one electrode level cell from which that electrode level data can be obtained. In this scenario, coin format small cells are built by facing samples of each electrode against lithium. In this way, the effect of each electrode is isolated. For that, firstly, the battery is opened in a safety environment (destructive measurement process) [147][148]; secondly, samples of the electrodes are extracted and processed [148]; and thirdly, the coin cells are mounted [149][150]. The know-how of the whole process required to build coin cells with samples of electrodes taken from a commercial cell is described by chemists on the literature [147][148][149][150] (the construction of coin cells is systematic and well-known by CIDETEC). The main steps are the following ones:

- Cut the part of the holder of the battery that has no contact with the electrodes.
- Retire the excess of electrolyte.
- Retire completely the holder by twisting it.
- Chop the electrodes.
- Wash the chopped parts with typical electrolyte solvents such as DMC [148].

- Dry the chopped electrodes.
- Retire the active material on one side of the chopped electrodes. Depending on the solution, the active material needs to be removed with water or with a dissolvent (NMP) [151].
- Dry the chopped electrodes.
- Die-cut cylindrical samples of the electrodes.
- Die-cut cylindrical lithium samples.
- Build the coin cells with the electrodes samples and the lithium samples.

Once the coin cells are constructed, these coin cells are tested. A close to equilibrium OCV measurement test is performed to measure the OCV of each electrode. The voltage window defined on these tests are kept the same on each composition of electrode (every coin cell with graphite based negative electrode is tested from 2.5V to 0V). However, the current applied on these tests is chemistry and size dependent. The current density (or current rate) that experiences the electrode needs to be the same on both tests: the test done at commercial cell and the test that will be done at coin cell. The current rate applied to the commercial cell is 20 times smaller than the nominal current rate (C/20). The current rate applied on the coin cell must be the same, 20 times smaller than the nominal current rate, but in this case the current rate refers to the coin cell's current rate. This current rate needs to be calculated. This calculus is done by multiplying the mass and the theoretical specific capacity of the active material used on the coin cell.

Then, the tests are performed. An example of an OCV profile of a commercial graphite-LMO cell and the OCV profiles that belong to the electrodes of that same commercial graphite-LMO cell is shown in Figure 116 and Figure 117.

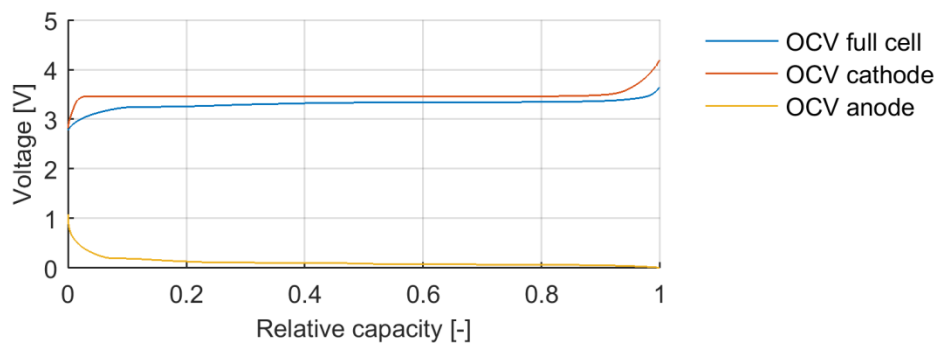


Figure 116: Charge full-cell and half-cell OCV profiles of a fresh SAMSUNG 18650 26F battery.

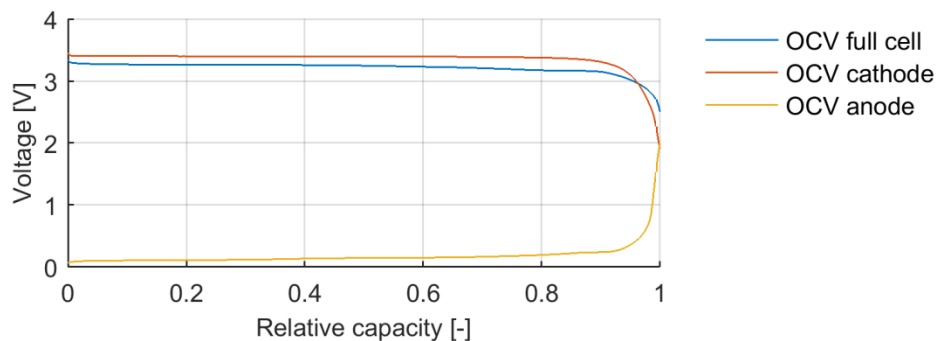


Figure 117: Discharge full-cell and Half-cell OCV of a fresh SAMSUNG 18650 26F battery.

5.3.2 Electrode level health indicator estimation

The half-cell test is a destructive type test. Electrode level data cannot be obtained on middle checkups of an aging test. As a consequence, the tracking of the health indicators of the electrodes cannot be observed directly. Instead, it needs to be estimated based on observations done on the checkups.

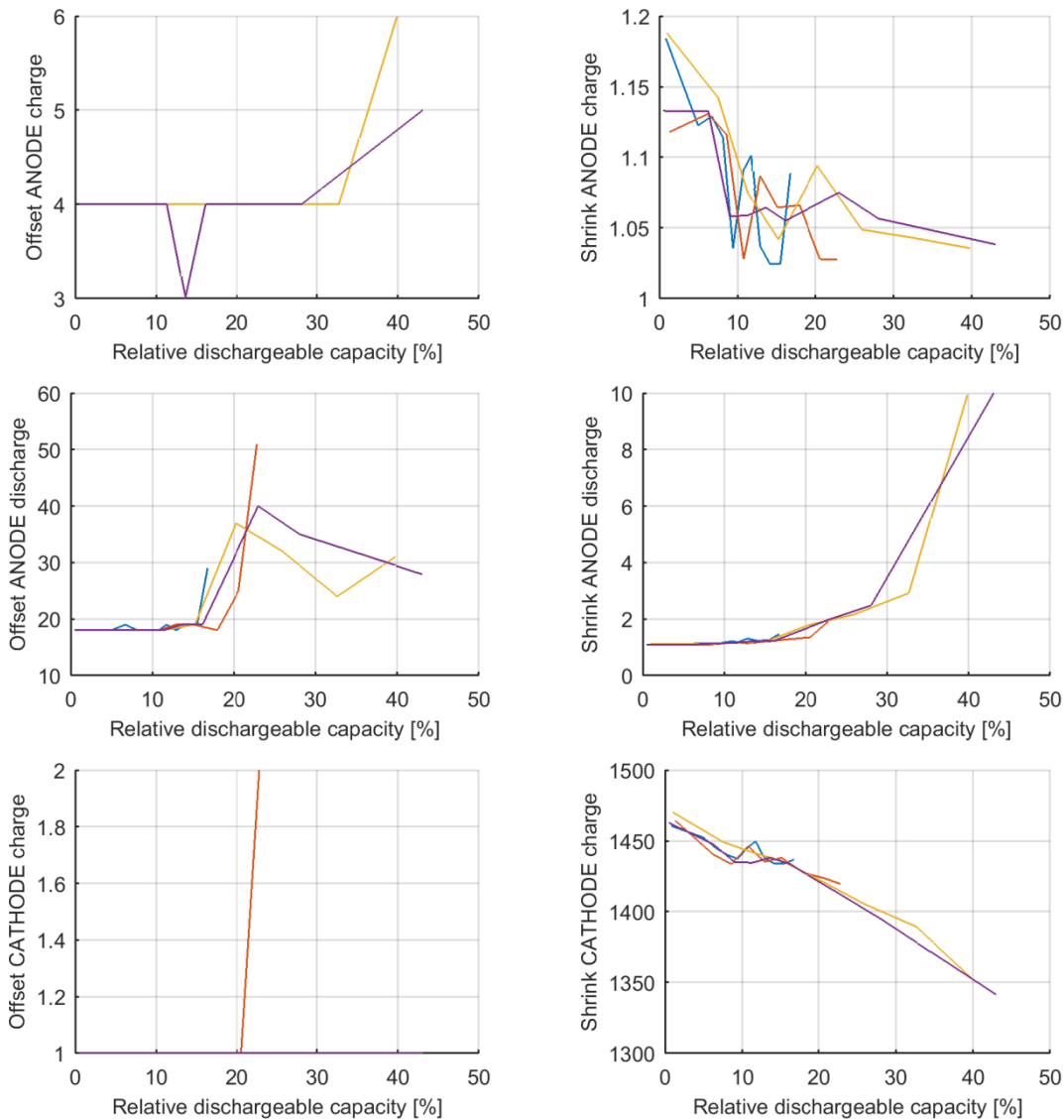
This thesis proposes to use the observed full-cell OCV profiles to estimate the health indicators of the electrodes. For that, a quadratic optimization environment is developed where the error between the convolution of the electrode level OCV profiles and the observed full-cell OCV profile is minimized. The convolution of both electrode level OCV profiles requires a scaling factor (describes the proportion and dimension mismatch of electrodes by adjusting the stoichiometric window) and a balancing factor (describes the start and the end of the voltage window of each electrode) [152][153], see Eq. (113) and (114). These two convolution factors are used as the free variables on the optimization environment and as the health indicators of the electrodes. The evolution of these variables is faced against a health indicator of the full-cell: the decay of the dischargeable capacity. Thanks to this, the health indicators of the half-cells and the full-cell are correlated, see Figure 118.

$$OCV_{cell}(t) = OCV_{MAno}(t) - OCV_{MCat}(t) \tag{113}$$

$$AH_{Mx}(t) = scale_x \cdot AH_x(t + off_x) \tag{114}$$

Parameters	Description
$OCV_{cell}(t)$	The Open Circuit Voltage of the full cell at time instant t .
OCV_{Mx}	The modified Open circuit Voltage of the electrode x , being x anode (<i>Ano</i>) or cathode (<i>Cat</i>).
$AH_{Mx}(t)$	The modified cumulative capacity at time instant t of electrode x .
$scale_x$	The shrink factor or scaling factor of the electrode x .
off_x	The offset or balancing factor of the electrode x .

Table 158: Convolution of both electrode level OCV profiles



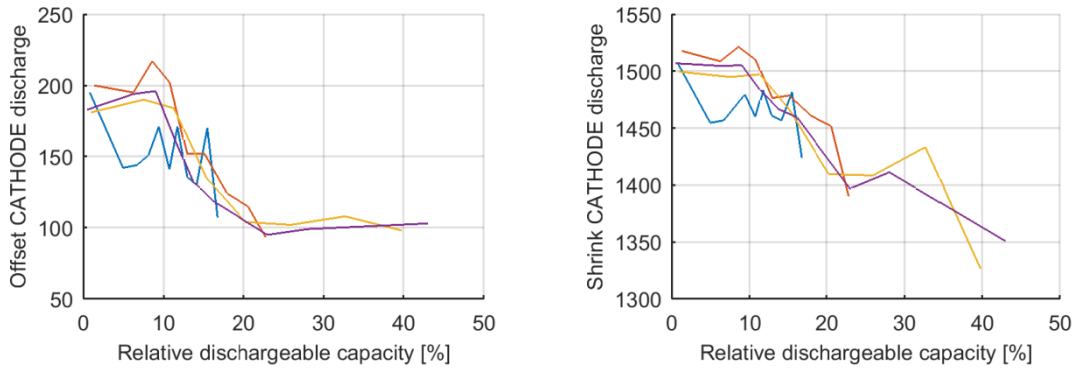


Figure 118: Evolution of the Electrode level Health Indicators. The blue line refers to Test 5, the red line refers to Test 6, the yellow line refers to Test 7 and the purple line refers to Test 8.

5.3.3 Electrode level health indicator modelling

The Mechanistic aging models are the typical models that employ Half-cell data as an input [154][155]. Mechanistic aging models are supported by half-cell information with the aim of identifying and quantifying the degradation mechanisms [35].

Dubarry et al. [35] proposed a mechanistic model composed of 2 layers: a sub-layer and a top layer. The sub-layer describes the electrode behavior by half-cell modules modelled by equivalent circuit approaches. It can handle electroactive ohmic resistance increase, faradic rate degradation and formation of parasitic phases. The top layer assemble the two electrodes into a full cell configuration taking into account the electrode composition and loading ratio matching (similar to the offset and scaling factors used on 'Electrode level health indicator estimation) [35].

Marongiu et al. [156] developed a mechanistic model based on the online collection of information relative to the characteristics of the plateaus of the voltage curve to describe degradation modes [18]. The length of the plateau represents sufficient information in order to calculate the battery capacity.

Birkl et al. [31] proposed a mechanistic degradation model based on a semi-empirical OCV model developed by Birkl et al. [78]. This degradation model aims to estimate the extent of the different degradation modes at any point in a cell's life by fitting the cell's OCV. For that, Birkl et al. assumed that the parameters of the OCV model remain unaltered and that the degradation does not impact the individual phases of the electrode materials in different ways.

The mechanistic aging model approach offers unique high-fidelity simulation to address path dependency of the battery degradation [31]. However, the mechanistic model requires good understanding of battery degradation processes and failure mechanisms (out of the scope of the thesis to determine and quantify the contribution of each battery degradation process).

In this scenario, this thesis proposal consists on modelling the trends of the extracted Health Indicators of the electrodes. In concrete, the health indicators that show a clear trend: the scaling factor of the anode OCV profile at discharge and the scaling factor of the cathode OCV profile at charge. The model is built following the methodology described in the 'Aging: Testing and Modelling' chapter, specifically the modelling methodology described on the phase 1. Some example results are displayed in Figure 119.

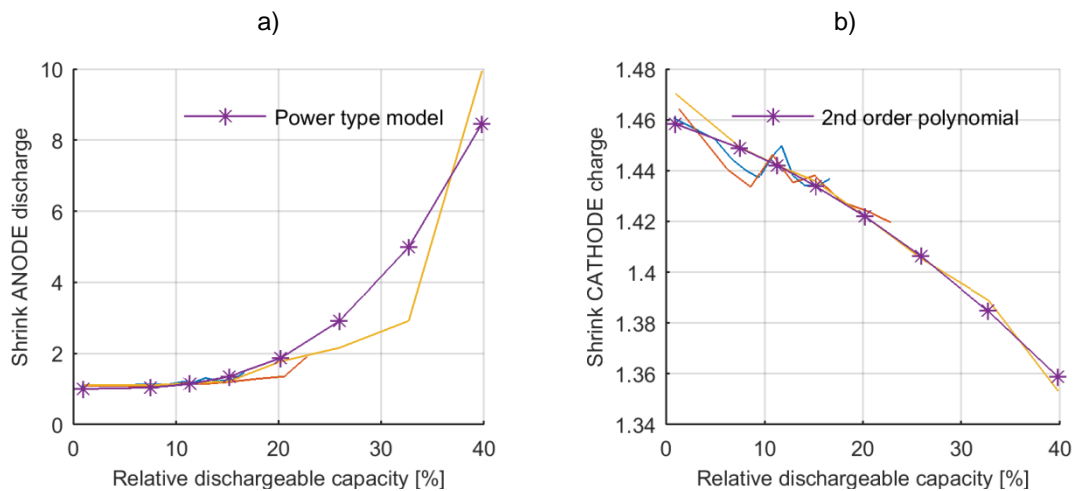


Figure 119: Models of the health indicators obtained from the Half-cell data. A) refers to the scaling factor of the anode at discharge and B) refers to the scaling factor of the cathode at charge.

5.3.4 Artificial data generation

The proposal of generating data in an artificial way consists on transposing the modelled trends of the half-cell health indicators to the trends of the full-cell health indicators. However, this is not a trivial task. In this scenario, this artificial data generation proposal has focused on developing the bridge of a specific case rather than finding a common rule. The case under evaluation is found on the tests 5 and 6, where a significant increase of the error on extrapolations in time appears.

The results from modelling the scaling factors of the anode at discharge and the anode at charge show that is likely that test 5, 6 and 7 have the same behavior at electrode level. The trends observed on the negative electrode at discharging and on the positive electrode at the charging are practically identical, the longest observed case being the test 7. Based on this, it could be assumed that the aging behavior of the cells from the tests 5 and 6 will have the same trend changes at the same deterioration levels as the cell from the test 7. This could be translated to a common aging master curve [95] for those three tests based on the observation done on the test 7, see Figure 120.

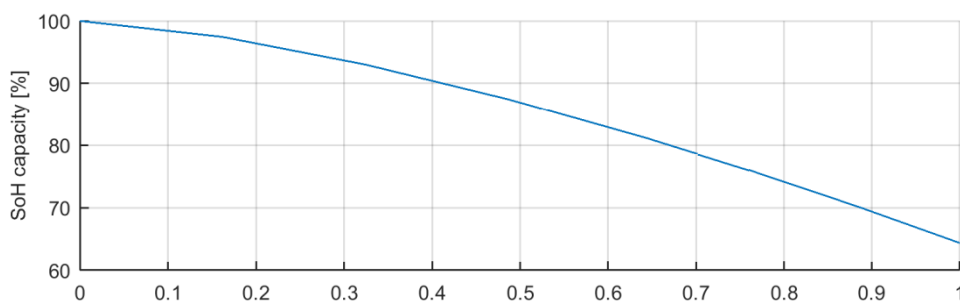


Figure 120: Aging master curve of tests 5, 6 and 7 taken from test 7.

The data we lack is generated from this aging master curve. The changes of the aging rate will come at the same deterioration levels. Nonetheless, the required discharged energy to generate the same deterioration level is not the same. Each test has its degradation speed, which can be described by a scale factor and an initial offset between the different aging paths, see Eq.(115). The equation is placed on a quadratic optimization environment solved with the function “Isqcurvefit” of MATLAB. The obtained initial offsets and scale factors are gathered in Table 160.

$$\begin{aligned}
 Y_i &= offset_i + Y_{MASTER} \\
 X_i &= X_{MASTER} * scale_i
 \end{aligned}
 \tag{115}$$

Parameters	Description
Y_i	The relative dischargeable capacity values of test i obtained from the master curve.
X_i	The equivalent cycles of test i corresponding to the calculated Y_i .

$offset_i$	The initial offset of the test i .
$scale_i$	The scaling factor that connects the aging master curve with the aging path of test i .
Y_{MASTER}	The relative dischargeable capacity values of the aging master curve of tests 5, 6 and 7.
X_{MASTER}	The equivalent cycles of the aging master curve related with Y_{MASTER} .

Table 159: Scaling equation

	Scale factor	Offset
Test 5	1.78	-5.92
Test 6	1.62	-6.68

Table 160: Scaling variables of test 5 and 6

Once the scale factors are obtained, the aging master curve is applied and the lacking data is obtained, see Figure 121.

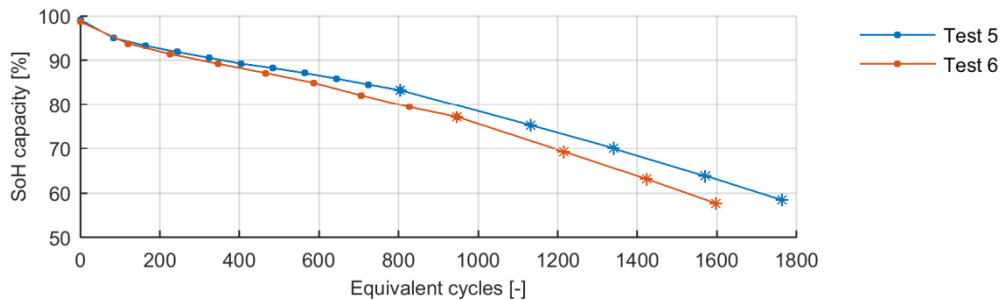


Figure 121: Lengthened data sets of test 5 and 6.

5.3.5 Validation

The correctness of the artificially generated data is studied in this case. The extrapolation errors generated with the constructed aging model on the validation section of the “Sizing Energy Storage Systems” chapter are corrected with the construction of aging models with the lengthened data sets of the tests 5 and 6. For that, the dischargeable capacity evolution and the discharged energy are modelled following the steps detailed on the first phase of the proposed aging modelling methodology.

The first phase of the proposed modelling methodology consists on choosing the mathematical expression that fits better the dischargeable capacity. The tested mathematical expressions are shown in Table 161.

Aging	Linear	Exponential	Logarithmic	Power type	2 nd order polynomial
Cycling	x	x	x	x	x

Table 161: Selection of mathematical expressions that can be applied to describe the aging trend of the dischargeable capacity evolution

The fitting accuracy is measured with the Root Mean Square Error (RMSE) metric between the measurements and the estimation done with the fitted mathematical expression. This metric has been calculated on the artificially lengthened tests 5 and 6 for the dischargeable capacity evolution, see Table 162.

	Linear	Exponential	Logarithmic	Power type	2 nd order polynomial
Test 5	0,01345	0,02069	0,09611	0,01033	0,00867
Test 6	0,01200	0,02172	0,09708	0,00972	0,00797

Table 162: Fitting RMSE of the lengthened dischargeable capacity evolution data sets of the tests 5 and 6

The fitting of the data of the dischargeable capacity evolution shows that the mathematical expression that fits better all the results is the 2nd order polynomial. However, the power type equation has been selected because between the power type equation and the 2nd order polynomial there is less than an increase of 50% and because the power type equation has been used on the rest constructed aging models. The reconstructed cycling aging models are added linearly in a

complete new aging model, see Eq. (74). The aging on test 12 is estimated and displayed in Figure 122.

$$Q = Q_{ini} - (1.16e^{-5} \cdot cyc_1^{1.23} + 2.12e^{-5} \cdot cyc_2^{1.17} + 4.16e^{-6} \cdot cyc_3^{1.44}) \quad (116)$$

Parameters	Description
Q	The dischargeable capacity.
Q_{ini}	The dischargeable capacity value at Beginning of life (initial value).
cyc_i	The discharged energy in Ah related to the test $i + 4$.
R	The pure ohmic resistance.
R_{ini}	The pure ohmic resistance value at Beginning of life (initial value).

Table 163: Parameters of the reconstructed complete aging model

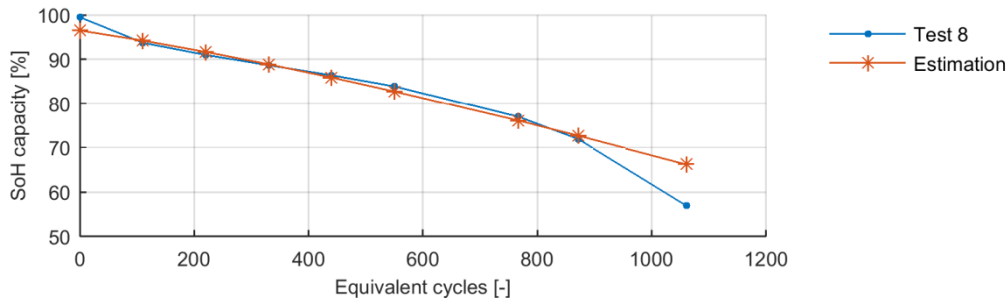


Figure 122: Comparison of the observed dischargeable capacity evolution in the test with dynamic operation conditions (dots) and the estimated one with the complete aging model (stars) with artificial data points.

The results show an improvement of predictions on extrapolated values in time. The error on the last extrapolation in time has been reduced by 33%. Nonetheless, it is still far from perfection since there is still a huge estimation error (an error of 10%).

5.4 Conclusions

This chapter aims at increasing the accuracy of the constructed aging models. For that, two types of sources on the prediction error are evaluated. Firstly, the contribution on the prediction error of deviations on the expectations is evaluated. Specifically, the deviation on the monotonic performance expectation of the system is evaluated. The reduction of the pure ohmic resistance and the raise of the dischargeable capacity are events that the proposed aging model cannot describe. In this scenario, the solution is thought to come from updating the calculated aging path with data from the real application. Early measurements of the modelled health indicator are used to minimize the prediction error due to this kind of event. For that, a prognosis algorithm is required. There are many different prognosis algorithms, and there is no specific algorithm that overcomes the rest in performance. The algorithms need to be evaluated based on the adaptation rate of the algorithm to the application in order to determine the most appropriate algorithm. We need to select the best candidate for our application. This is why an evaluation framework is developed and afterwards applied to the identified most relevant prognosis algorithms on lithium ion battery remaining useful life problems: Particle Filter and Gaussian Process. In addition to these most relevant prognosis algorithms, the Extended Kalman Filter and the Unscented Kalman Filter are also evaluated. The evaluation framework consists on calculating 7 quantitative metrics and a qualitative diagram. The results have shown that the evaluated Particle Filter configuration gets the earliest accurate predictions, that the Particle Filter gets the most stable predictions, that the Unscented Kalman Filter has the greatest improvement rate on the achievable prediction accuracy and that the Extended Kalman Filter has the lowest computational cost. These results can be interpreted as being the algorithms based on Kalman Filter more appropriate for posterior estimations; and the Particle Filter more appropriate for prediction and prognosis.

Secondly, the contribution of uncomplete aging data sets on the prediction error is evaluated. There is a significant prediction error when extrapolating in time an aging path that suffers an unobserved aging trend change. On those cases, the gathered data is considered not enough to describe the aging behaviour of the system when extrapolating in time. Data that shows the change of the aging

trend is required. For that, a methodology that generates artificially the lacking data is introduced. The proposed methodology is based on the correlation of the state of health of the electrodes with the state of health of the full-cell. This approach uses the OCV profiles of fresh electrodes and the OCV profiles of the full-cell observed at different check-ups (at different state of healths). The trends detected on the health indicators of the electrodes are transposed to the health indicators of the full cell, generating like this the lacking data. The methodology has been applied to the data gathered on the aging tests 5 and 6. In particular, some dischargeable capacity values below 80% have been generated on those data sets. As a result, the constructed model achieves higher prediction accuracy on the last predicted value.

CHAPTER 6:

6 Conclusion and Future Research Lines

This chapter presents the main conclusions already drawn all along this thesis. After the conclusions, a section with the future research lines is developed.

6.1 Conclusion

The main objective of this thesis consists on determining accurately the most profitable size of an Energy Storage System based on lithium ion batteries considering the lifespan of the batteries. In order to meet this objective, this thesis presents the development of all the necessary elements on a simulation environment where the levelized costs of a set of size values are calculated. The proposed methodology is shown in Figure 7.

Firstly, the methodology to calculate the combinational value of some Health Indicators at which the battery stops fulfilling the requirements defined by the application is presented (the End of Life). In this case, the health indicators of interests are the dischargeable capacity decrease and the pure resistance increase. It has been validated that the constructed End of Life map with the selected Health Indicators is able to determine accurately the real End of Life of the battery, showing that the most restrictive and significant health indicator is the dischargeable capacity decrease. Therefore the intuitive hypothesis that the End of Life of a battery is application dependent has also been validated.

Secondly, the health indicators of interest, the dischargeable capacity decay and the pure ohmic resistance increase, are modelled based on the most relevant stress factors. The methodology to acquire the aging data and the construction of the posterior empirical models are presented. The whole methodology has been tested on a High-Power and on a High-energy application.

On one hand, the methodology used to generate the aging test matrix has been evaluated. It has been seen that a proper aging analysis contains just too many testing cases. It is necessary to reduce the required amount of testing cases. As a consequence, hypotheses about the aging behaviour that allows to reduce the amount of testing cases needs to be adopted. The final sizing results will be conditioned by the assumed hypotheses. In case those are not correct, the constructed aging model will not give accurate results on the operation conditions. Therefore, those hypotheses need to be listed and validated as much as possible.

On the other hand, the methodology used to generate the aging models is evaluated as we have seen on chapter 3. It has been found that the proposed aging modelling methodology is completely dependent to the aging testing matrix. The aging test matrix limits the applicable mathematical expressions as well as the operation window that the model will be able to describe. Besides, the quality of the obtained data will conditions greatly the response of the model and will determine the most appropriate mathematical expression. The worse the data is, the simpler the mathematical expression needs to be. Among the evaluated data sets, it has been found that the data sets containing the pure ohmic resistance evolution are susceptible to be noisy.

Nonetheless, it has been discovered that the proposed aging modelling methodology is able to capture the effect of the stress factors on the trend of the selected health indicators even though having little data. It has been validated as well the correctness, interpolation ability and real life applicability of the developed aging models. In addition to this, it has been validated in chapter 3 that the cycling aging and the calendar aging can be linearly added. Thanks to this, it has been proved that it is possible to describe the degradation that the battery experiences on real life applications using a model constructed uniquely on data obtained from tests done at lab level with static operation conditions.

Thirdly, the simulation environment for sizing exercises of lithium ion battery energy storage systems has been developed. The evaluated use cases have shown that the smaller sizing option doesn't need to be the most profitable sizing option. The most profitable option could be a bigger one than the minimum applicable sizing. This confirms that the thought of adding the lifespan prediction to the sizing exercise was correct when calculating the most profitable one.

In addition to this, firstly, the cumulative behaviour of the aging has been confirmed and secondly, the effect of short rest times on the aging has been presented, supporting like this the assumed hypotheses on the development of the simulation environment.

Fourthly, the error done by the constructed aging models is minimized (chapter 5). The error of the aging models is minimized by focusing on the errors done when extrapolating in time and when facing odd events. On one hand, electrode level data is analysed to generate data artificially and reduce the errors when extrapolating in time. On the other hand, a prognosis stochastic algorithm is selected and employed with real life data to deal with the effect that odd events have on the evolution of the health indicators. Both accuracy improvement methods require validation or real life data, which means that they are restricted to the data availability. Nonetheless, it has been seen that these methods have a great potential and that are interesting enough to spend resources researching them.

6.2 Future work

The development of this thesis has given place to the identification of the following future research lines:

- It has been assumed that the resistance is increased uniformly at the whole SOC range. However, it has been found that this is not fully correct and in this work a 20% margin on the resistance increase has been added in order to add the uncertainty on the resistance values at different SOC from the one measured. This 20% has been given by considering the maximum difference on the evaluated cases. A study of the uncertainty on the resistance increase on different SOC would be of great interest.
- The EOL map of the application has been defined with the cell level values. Testing this evaluation on a solution level where additional resistances appear due to the connections, the wires and the intermediate electronics is of great interest.
- The dynamic behaviour of stress factor is a source of uncertainty. The validation of the correctness of using the mean stress factor simplifying the dynamic behaviour of it is of great interest.
- The use of physical and electrochemical knowledge on the definition and selection of the mathematical expression that describe the effect the stress factor have on the trend of the health indicators is of high interest.
- The developed aging test matrix design methodology uses experiences from already developed aging models. Further implementation of the proposed methodology and feedback from real-life application of the constructed aging models is of high interest.
- The observed operation conditions used to generate the aging models have been scarce. The constructed aging models have limitations on the operation conditions that those models can describe. More data about unobserved operation conditions is of high interest.
- Further development of the use of electrode level data to predict changes on the aging trend is of high interest.
- There are key prediction time instants on the used data sets that could lead to more synthesized and significant results. The definition of the criteria to select the prediction time instants of interest when evaluating these kinds of algorithms is of high interest.
- The evaluated algorithm configurations have been conditioned by their design and the applied parametrization. There are many design and parametrization aspects that could change completely the obtainable prediction accuracy level on each prediction time instant. The evaluation of different configurations of these algorithms is of high interest.
- The creation of a reliable prognosis algorithm which could give accurate prediction on each prediction time instant is of great interest.
- The evaluated prognosis algorithms can be applied on real applications. The implementation of the evaluated Particle Filter configuration on an on-board Electric Vehicle application as an on-board prognosis tool is of high interest.
- The whole sizing methodology is focused on lithium ion batteries because of the expertise of CIDETEC. Nonetheless, the developed methodologies are applicable to any Energy Storage System that shows a monotonic deterioration over time. The validation of the whole proposed methodology on a different Energy Storage System is of high interest.

- The developed methodologies have been implemented on MATLAB's scripts. The consolidation of all the created simulation and visualization scripts on a user-friendly executable is of high interest.
- The operation of lithium ion batteries on energy balancing applications has multiple variables that affect the income-cost balance (weather uncertainty, price changes on the market of the electricity, etc.). The further development of the proposed simulation environment to evaluate the effect of those variables is of high interest.
- The implementation of the defined control of lithium ion batteries on real life energy balancing applications is of high interest.

References

- [1] T. M. I. Mahlia, T. J. Saktisahdan, A. Jannifar, M. H. Hasan, and H. S. C. Matseelar, "A review of available methods and development on energy storage; technology update," *Renew. Sustain. Energy Rev.*, vol. 33, pp. 532–545, 2014.
- [2] United States Environmental Protection Agency (EPA), "Global Greenhouse Gas Emissions Data | Greenhouse Gas (GHG) Emissions | US EPA." [Online]. Available: <https://www.epa.gov/ghgemissions/global-greenhouse-gas-emissions-data>. [Accessed: 07-Dec-2018].
- [3] M. Sandelic, D.-I. Stroe, and F. Iov, "Battery Storage-Based Frequency Containment Reserves in Large Wind Penetrated Scenarios: A Practical Approach to Sizing," *Energies*, vol. 11, no. 11, p. 3065, 2018.
- [4] European Commission, "European Battery Alliance." [Online]. Available: https://ec.europa.eu/growth/industry/policy/european-battery-alliance_es. [Accessed: 14-Dec-2018].
- [5] I. Buchmann and Cadex Electronics Inc., *Batteries in a portable world: a handbook on rechargeable batteries for non-engineers*. Cadex Electronics, 2001.
- [6] D. O. Akinyele and R. K. Rayudu, "Review of energy storage technologies for sustainable power networks," *Sustain. Energy Technol. Assessments*, vol. 8, pp. 74–91, 2014.
- [7] Boltta, "LITHIUM ION | Boltta," 2019. [Online]. Available: <http://boltta.com/lithium-ion/>. [Accessed: 17-Dec-2019].
- [8] J. Zhang and J. Lee, "A review on prognostics and health monitoring of Li-ion battery," *J. Power Sources*, vol. 196, no. 15, pp. 6007–6014, 2011.
- [9] T. B. Reddy and D. Linden, *Linden's handbook of batteries*. McGraw-Hill, 2011.
- [10] R. J. Masaki, Yoshio, Kozawa, Akiya, Brodd, *Lithium-Ion Batteries*, vol. 53, no. 9. 2013.
- [11] E. Sarasketa-Zabala, "A novel approach for lithium-ion battery selection and lifetime prediction," Mondragon Unibertsitatea, 2014.
- [12] M.-T. F. Rodrigues *et al.*, "A materials perspective on Li-ion batteries at extreme temperatures," *Nat. Energy*, vol. 2, no. July, p. 17108, 2017.
- [13] N. Omar, P. Van den Bossche, T. Coosemans, and J. Van Mierlo, "Peukert revisited-critical appraisal and need for modification for lithium-ion batteries," *Energies*, 2013.
- [14] Battery University, "Basic to Advanced Battery Information from Battery University." [Online]. Available: <http://batteryuniversity.com/>. [Accessed: 31-Jan-2017].
- [15] R. V. Bugga and M. C. Smart, "Lithium Plating Behavior in Lithium-Ion Cells," in *ECS Transactions*, 2010, vol. 25, no. 36, pp. 241–252.
- [16] R. Spotnitz, "Simulation of capacity fade in lithium-ion batteries," *J. Power Sources*, vol. 113, no. 1, pp. 72–80, 2003.
- [17] S. Schwunk, N. Armbruster, S. Straub, J. Kehl, and M. Vetter, "Particle filter for state of charge and state of health estimation for lithium-iron phosphate batteries," *J. Power Sources*, vol. 239, pp. 705–710, 2013.
- [18] J. Groot, "State-of-health estimation of Li-ion batteries: cycle life test methods," *PhD, CHALMERS Univ. Technol.*, p. 138, 2012.
- [19] A. Eddahech, O. Briat, N. Bertrand, J.-Y. Deléage, and J.-M. Vinassa, "Behavior and state-of-health monitoring of Li-ion batteries using impedance spectroscopy and recurrent neural networks," *Int. J. Electr. Power Energy Syst.*, vol. 42, no. 1, pp. 487–494, 2012.
- [20] M. Bercibar, I. Gandiaga, I. Villarreal, N. Omar, J. Van Mierlo, and P. Van Den Bossche, "Critical review of state of health estimation methods of Li-ion batteries for real applications," *Renew.*

Sustain. Energy Rev., vol. 56, pp. 572–587, 2016.

- [21] W. Waag, S. Käbitz, and D. U. Sauer, “Experimental investigation of the lithium-ion battery impedance characteristic at various conditions and aging states and its influence on the application,” *Appl. Energy*, vol. 102, pp. 885–897, 2013.
- [22] Y. Merla, B. Wu, V. Yufit, N. P. Brandon, R. F. Martinez-Botas, and G. J. Offer, “Novel application of differential thermal voltammetry as an in-depth state-of-health diagnosis method for lithium-ion batteries,” *J. Power Sources*, vol. 307, pp. 308–319, Mar. 2016.
- [23] J. Xu, L. Binghe, L. Wang, and S. Shang, “Dynamic mechanical integrity of cylindrical lithium-ion battery cell upon crushing,” *Eng. Fail. Anal.*, vol. 53, pp. 97–110, 2015.
- [24] J. Xu *et al.*, “Coupling Effect of State-of-Health and State-of-Charge on the Mechanical Integrity of Lithium-Ion Batteries,” *Exp. Mech.*, vol. 58, no. 4, pp. 633–643, Apr. 2018.
- [25] A. Guha and A. Patra, “State of Health Estimation of Lithium-Ion Batteries Using Capacity Fade and Internal Resistance Growth Models,” *IEEE Trans. Transp. Electr.*, vol. 4, no. 1, pp. 135–146, Mar. 2018.
- [26] H. Wenzl *et al.*, “Life prediction of batteries for selecting the technically most suitable and cost effective battery,” *J. Power Sources*, vol. 144, no. 2, pp. 373–384, 2005.
- [27] M. Dubarry, C. Truchot, and B. Y. Liaw, “Cell degradation in commercial LiFePO₄ cells with high-power and high-energy designs,” *J. Power Sources*, vol. 258, pp. 408–419, 2014.
- [28] M. Dubarry, “Path Dependence in Lithium-Ion Batteries Degradation : A Comparison of Cycle and Calendar Aging,” in *PRIME*, 2016, no. 808, pp. 1–14.
- [29] S. F. Schuster *et al.*, “Nonlinear aging characteristics of lithium-ion cells under different operational conditions,” *J. Energy Storage*, vol. 1, no. 1, pp. 44–53, 2015.
- [30] S. Käbitz *et al.*, “Cycle and calendar life study of a graphite|LiNi_{1/3}Mn_{1/3}Co_{1/3}O₂ Li-ion high energy system. Part A: Full cell characterization,” *J. Power Sources*, vol. 239, pp. 572–583, 2013.
- [31] C. R. Birkl, M. R. Roberts, E. Mcturk, P. G. Bruce, and D. A. Howey, “Degradation Diagnostics for Lithium Ion Cells,” *J. Power Sources*, vol. 341, pp. 1–35, 2016.
- [32] Q. Zhang and R. E. White, “Calendar life study of Li-ion pouch cells. Part 2: Simulation,” *J. Power Sources*, vol. 179, no. 2, pp. 785–792, 2008.
- [33] S. Grolleau *et al.*, “Calendar aging of commercial graphite/LiFePO₄ cell – Predicting capacity fade under time dependent storage conditions,” *J. Power Sources*, vol. 255, pp. 450–458, 2014.
- [34] C. Pastor-Fernández, K. Uddin, G. H. Chouchelamane, W. D. Widanage, and J. Marco, “A Comparison between Electrochemical Impedance Spectroscopy and Incremental Capacity-Differential Voltage as Li-ion Diagnostic Techniques to Identify and Quantify the Effects of Degradation Modes within Battery Management Systems,” *J. Power Sources*, vol. 360, pp. 301–318, 2017.
- [35] M. Dubarry, C. Truchot, and B. Y. Liaw, “Synthesize battery degradation modes via a diagnostic and prognostic model,” *J. Power Sources*, vol. 219, pp. 204–216, 2012.
- [36] M. Dubarry and B. Y. Liaw, “Identify capacity fading mechanism in a commercial LiFePO₄ cell,” *J. Power Sources*, vol. 194, no. 1, pp. 541–549, 2009.
- [37] D. Anseán, M. Dubarry, A. Devie, and B. Y. Liaw, “Lithium Plating Quantification in Commercial Graphite || LiFePO₄ batteries,” in *PRIME*, 2016, no. 808, pp. 1–13.
- [38] Z. Ma, J. Jiang, W. Shi, W. Zhang, and C. C. Mi, “Investigation of path dependence in commercial lithium-ion cells for pure electric bus applications: Aging mechanism identification,” *J. Power Sources*, vol. 274, pp. 29–40, 2015.
- [39] P. Liu *et al.*, “Aging Mechanisms of LiFePO₄ Batteries Deduced by Electrochemical and Structural Analyses,” *J. Electrochem. Soc.*, vol. 157, no. 4, p. A499, 2010.
- [40] X.-S. Si, Z.-X. Zhang, and C.-H. Hu, *Data-Driven Remaining Useful Life Prognosis Techniques Stochastic Models, Methods and Applications*. China: Springer Series in Reliability Engineering,

2016.

- [41] X. S. Si, W. Wang, C. H. Hu, and D. H. Zhou, "Remaining useful life estimation - A review on the statistical data driven approaches," *Eur. J. Oper. Res.*, vol. 213, no. 1, pp. 1–14, 2011.
- [42] A. K. S. Jardine, D. Lin, and D. Banjevic, "A review on machinery diagnostics and prognostics implementing condition-based maintenance.pdf," *Mech. Syst. Signal Process.*, 2006.
- [43] A. Heng, S. Zhang, A. C. C. Tan, and J. Mathew, "Rotating machinery prognostics: State of the art, challenges and opportunities," *Mech. Syst. Signal Process.*, vol. 23, no. 3, pp. 724–739, 2009.
- [44] S. M. Rezvanianiani, Z. Liu, Y. Chen, and J. Lee, "Review and recent advances in battery health monitoring and prognostics technologies for electric vehicle (EV) safety and mobility," *J. Power Sources*, vol. 256, pp. 110–124, Jun. 2014.
- [45] S. Sepasi, R. Ghorbani, and B. Y. Liaw, "A novel on-board state-of-charge estimation method for aged Li-ion batteries based on model adaptive extended Kalman filter," *J. Power Sources*, vol. 245, pp. 337–344, 2014.
- [46] F. Li and J. Xu, "A new prognostics method for state of health estimation of lithium-ion batteries based on a mixture of Gaussian process models and particle filter," *Microelectron. Reliab.*, vol. 55, no. 7, pp. 1035–1045, 2015.
- [47] C. Chen and M. Pecht, "Prognostics of lithium-ion batteries using model-based and data-driven methods," *Proc. IEEE 2012 Progn. Syst. Heal. Manag. Conf. PHM-2012*, 2012.
- [48] C. Lin, A. Tang, and W. Wang, "A Review of SOH Estimation Methods in Lithium-ion Batteries for Electric Vehicle Applications," *Energy Procedia*, vol. 75, pp. 1920–1925, Aug. 2015.
- [49] J. Wang *et al.*, "Cycle-life model for graphite-LiFePO₄ cells," *J. Power Sources*, vol. 196, no. 8, pp. 3942–3948, 2011.
- [50] N. Gorjian, L. Ma, M. Mittinty, P. Yarlagadda, and Y. Sun, "A review on degradation models in reliability analysis," in *Engineering Asset Management*, 2009, no. September, pp. 28–30.
- [51] L. Wu, X. Fu, and Y. Guan, "Review of the Remaining Useful Life Prognostics of Vehicle Lithium-ion Batteries Using Data-Driven Methodologies," *Appl. Sci.*, vol. 6, no. 6, p. 166, 2016.
- [52] D. Wang, Q. Miao, and M. Pecht, "Prognostics of lithium-ion batteries based on relevance vectors and a conditional three-parameter capacity degradation model," *J. Power Sources*, vol. 239, pp. 253–264, 2013.
- [53] S. Sepasi, R. Ghorbani, and B. Y. Liaw, "Inline state of health estimation of lithium-ion batteries using state of charge calculation," *J. Power Sources*, vol. 299, pp. 246–254, 2015.
- [54] W. He, N. Williard, C. Chen, and M. Pecht, "State of charge estimation for electric vehicle batteries using unscented kalman filtering," *Microelectron. Reliab.*, vol. 53, no. 6, pp. 840–847, 2013.
- [55] Y. Cui *et al.*, "Prediction Model and Principle of End-of-Life Threshold for Lithium Ion Batteries Based on Open Circuit Voltage Drifts," *Electrochim. Acta*, vol. 255, pp. 83–91, Nov. 2017.
- [56] B. Saha, S. Poll, K. Goebel, and J. Christophersen, "An integrated approach to battery health monitoring using bayesian regression and state estimation," *2007 IEEE Autotestcon*, no. July, pp. 646–653, 2007.
- [57] K. Goebel, M. Daigle, A. Saxena, S. Sankararaman, I. Roychoudhury, and J. Celaya, *Prognostics : the science of prediction*. 2017.
- [58] M. Oyarbide, "Development and implementation of SOC and SOH estimators for lithium based energy storage systems," Arrasate Unibertsitatea, 2013.
- [59] G. Vertiz-Navarro, "Gestión térmica de sistemas de almacenamiento de energía basados en baterías litio-ion," Mondragon Unibertsitatea, 2015.
- [60] P. Shen, M. Ouyang, L. Lu, J. Li, and X. Feng, "The Co-estimation of State of Charge, State of Health and State of Function for Lithium-ion Batteries in Electric Vehicles," *IEEE Trans. Veh. Technol.*, vol. 9545, no. c, pp. 1–1, 2017.

- [61] N. Watrin, B. Blunier, and A. Miraoui, "Review of adaptive systems for lithium batteries state-of-charge and state-of-health estimation," *2012 IEEE Transp. Electr. Conf. Expo, ITEC 2012*, no. 3, 2012.
- [62] M. Chen and G. A. Rincon-Mora, "Accurate Electrical Battery Model Capable of Predicting Runtime and I-V Performance," *IEEE Trans. Energy Convers.*, vol. 21, no. 2, pp. 504–511, Jun. 2006.
- [63] C. Forgez, D. Vinh Do, G. Friedrich, M. Morcrette, and C. Delacourt, "Thermal modeling of a cylindrical LiFePO₄/graphite lithium-ion battery," *J. Power Sources*, vol. 195, no. 9, pp. 2961–2968, 2010.
- [64] P. Keil and A. Jossen, "Calendar Aging of NCA Lithium-Ion Batteries Investigated by Differential Voltage Analysis and Coulomb Tracking," *J. Electrochem. Soc.*, vol. 164, no. 1, pp. A6066–A6074, 2017.
- [65] L. a. Escobar and W. Q. Meeker, "A Review of Accelerated Test Models," *Stat. Sci.*, vol. 21, no. 4, pp. 552–577, 2007.
- [66] V. Ruiz, A. Kriston, A. Pfrang, and L. Brett, "Overview of standardised battery ageing methods and summary of battery degradation processes," 2016.
- [67] B. P. Weaver, "Methods for planning repeated measures degradation tests," Iowa State University, 2011.
- [68] D. I. Stroe, M. Swierczynski, A. I. Stan, R. Teodorescu, and S. J. Andreasen, "Accelerated lifetime testing methodology for lifetime estimation of lithium-ion batteries used in augmented wind power plants," *IEEE Trans. Ind. Appl.*, vol. 50, no. 6, pp. 4006–4017, 2014.
- [69] H. Lim and B.-J. Yum, "Optimal design of accelerated degradation tests based on Wiener process models," *J. Appl. Stat.*, vol. 38, no. 2, pp. 309–325, Feb. 2011.
- [70] Woodbank Communications Ltd, "Battery Testing, Test Methods and Procedures," *Electropaedia*, 2005. [Online]. Available: <https://www.mpoweruk.com/testing.htm>. [Accessed: 04-Oct-2019].
- [71] M. Santhakumar and T. Asokan, "Application of robust design techniques for underwater vehicle control," in *Proceedings of the Eighth ISOPE Ocean Mining Symposium*, 2009, pp. 285–289.
- [72] GMPUA, "Quality by Design." [Online]. Available: <http://www.gmpua.com/World/Manu/07/i.htm>. [Accessed: 07-Nov-2017].
- [73] J. Schmalstieg, S. Käbitz, M. Ecker, and D. U. Sauer, "A holistic aging model for Li(NiMnCo)O₂ based 18650 lithium-ion batteries," *J. Power Sources*, vol. 257, pp. 325–334, Jul. 2014.
- [74] A. Eddahech, O. Briat, and J. M. Vinassa, "Performance comparison of four lithium-ion battery technologies under calendar aging," *Energy*, vol. 84, pp. 542–550, 2015.
- [75] M. Lewerenz, J. Münnix, J. Schmalstieg, S. Käbitz, M. Knips, and D. U. Sauer, "Systematic aging of commercial LiFePO₄/Graphite cylindrical cells including a theory explaining rise of capacity during aging," *J. Power Sources*, vol. 345, pp. 254–263, 2017.
- [76] F. Geifes, C. Bolsinger, P. Mielcarek, and K. P. Birke, "Determination of the entropic heat coefficient in a simple electro-thermal lithium-ion cell model with pulse relaxation measurements and least squares algorithm," *J. Power Sources*, vol. 419, pp. 148–154, Apr. 2019.
- [77] M. Klett *et al.*, "Non-uniform aging of cycled commercial LiFePO₄/graphite cylindrical cells revealed by post-mortem analysis," *J. Power Sources*, vol. 257, pp. 126–137, 2014.
- [78] C. R. Birkl, E. McTurk, M. R. Roberts, P. G. Bruce, and D. A. Howey, "A Parametric Open Circuit Voltage Model for Lithium Ion Batteries," *J. Electrochem. Soc.*, vol. 162, no. 12, pp. A2271–A2280, 2015.
- [79] J. Meng *et al.*, "An overview of online implementable soc estimation methods for lithium-ion batteries," *Proc. - 2017 Int. Conf. Optim. Electr. Electron. Equipment, OPTIM 2017 2017 Intl Aegean Conf. Electr. Mach. Power Electron. ACEMP 2017*, pp. 573–580, 2017.
- [80] M. A. Roscher and D. U. Sauer, "Dynamic electric behavior and open-circuit-voltage modeling of LiFePO₄-based lithium ion secondary batteries," *J. Power Sources*, vol. 196, no. 1, pp. 331–336,

- 2011.
- [81] A.-I. Stroe, V. Knap, and D.-I. Stroe, "Comparison of lithium-ion battery performance at beginning-of-life and end-of-life," *Microelectron. Reliab.*, vol. 88–90, pp. 1251–1255, Sep. 2018.
- [82] M. Ecker *et al.*, "Development of a lifetime prediction model for lithium-ion batteries based on extended accelerated aging test data," *J. Power Sources*, vol. 215, pp. 248–257, Oct. 2012.
- [83] B. Xu, "Degradation-limiting Optimization of Battery Energy Storage Systems Operation," *Power Syst. Lab. ETH Zurich*, no. September 2013, 2013.
- [84] G. Saldaña, J. I. San Martín, I. Zamora, F. J. Asensio, and O. Oñederra, "Analysis of the Current Electric Battery Models for Electric Vehicle Simulation," *Energies*, vol. 12, no. 14, p. 2750, 2019.
- [85] M. Scarfogliero *et al.*, "Lithium-ion batteries for electric vehicles: A review on aging models for vehicle-to-grid services," in *2018 International Conference of Electrical and Electronic Technologies for Automotive*, 2018, pp. 1–6.
- [86] A. Millner, "Modeling lithium ion battery degradation in electric vehicles," *2010 IEEE Conf. Innov. Technol. an Effic. Reliab. Electr. Supply, CITRES 2010*, no. October 2010, pp. 349–356, 2010.
- [87] J. Purewal, J. Wang, J. Graetz, S. Soukiazian, H. Tataria, and M. W. Verbrugge, "Degradation of lithium ion batteries employing graphite negatives and nickel-cobalt-manganese oxide + spinel manganese oxide positives: Part 1, aging mechanisms and life estimation," *J. Power Sources*, vol. 272, pp. 1154–1161, 2014.
- [88] M. Schimpe, M. E. von Kuepach, M. Naumann, H. C. Hesse, K. Smith, and A. Jossen, "Comprehensive Modeling of Temperature-Dependent Degradation Mechanisms in Lithium Iron Phosphate Batteries," *J. Electrochem. Soc.*, vol. 165, no. 2, pp. A181–A193, Jan. 2018.
- [89] W. Diao, S. Saxena, and M. Pecht, "Accelerated cycle life testing and capacity degradation modeling of LiCoO₂-graphite cells," *J. Power Sources*, vol. 435, p. 226830, Sep. 2019.
- [90] L. Zhang and C. Lyu, "Decomposition Study of Degradation Reasons for LiCoO₂ -Based 14500 Lithium-Ion Batteries Using a Nondestructive Method," *IEEE Access*, vol. 6, pp. 44417–44432, 2018.
- [91] B. Xu, A. Oudalov, A. Ulbig, G. Andersson, and D. S. Kirschen, "Modeling of Lithium-Ion Battery Degradation for Cell Life Assessment," *IEEE Trans. Smart Grid*, vol. 9, no. 2, pp. 1131–1140, Mar. 2018.
- [92] P. L. T. Duong and N. Raghavan, "Heuristic Kalman optimized particle filter for remaining useful life prediction of lithium-ion battery," *Microelectron. Reliab.*, vol. 81, no. December 2017, pp. 232–243, 2018.
- [93] H. Zhang, Q. Miao, X. Zhang, and Z. Liu, "An improved unscented particle filter approach for lithium-ion battery remaining useful life prediction," *Microelectron. Reliab.*, vol. 81, no. 24, pp. 288–298, 2018.
- [94] S. Zhang and X. Hu, "Adaptively coordinated optimization of battery aging and energy management in plug-in hybrid electric buses," *Appl. Energy*, vol. 256, no. 174, p. 113891, 2019.
- [95] E. Cuervo-Reyes and R. Flückiger, "One Law to Rule Them All: Stretched Exponential Master Curve of Capacity Fade for Li-Ion Batteries," *J. Electrochem. Soc.*, vol. 166, no. 8, pp. A1463–A1470, May 2019.
- [96] F. Yang, D. Wang, Y. Xing, and K.-L. Tsui, "Prognostics of Li(NiMnCo)O₂-based lithium-ion batteries using a novel battery degradation model," *Microelectron. Reliab.*, no. 70, pp. 70–78, 2017.
- [97] S. Zhang, "A new method for lithium-ion battery's SOH estimation and RUL prediction," in *2018 13th IEEE Conference on Industrial Electronics and Applications (ICIEA)*, 2018, pp. 2693–2697.
- [98] B. Rumberg, K. Schwarzkopf, B. Epping, I. Stradtman, and A. Kwade, "Understanding the different aging trends of usable capacity and mobile Li capacity in Li-ion cells," *J. Energy Storage*, vol. 22, pp. 336–344, Apr. 2019.
- [99] J. Aldersey-Williams and T. Rubert, "Levelised cost of energy – A theoretical justification and

- critical assessment," *Energy Policy*, vol. 124, no. October 2018, pp. 169–179, 2019.
- [100] Vrije Universiteit Brussel, "Green Energy Park - Collaborating Today On Tomorrow's Solutions." [Online]. Available: <https://greenenergypark.be/en/>. [Accessed: 29-Oct-2018].
- [101] C. S. Lai *et al.*, "Levelized cost of electricity for photovoltaic/biogas power plant hybrid system with electrical energy storage degradation costs," *Energy Convers. Manag.*, vol. 153, no. October, pp. 34–47, 2017.
- [102] M. Bruck, P. Sandborn, and N. Goudarzi, "A Levelized Cost of Energy (LCOE) model for wind farms that include Power Purchase Agreements (PPAs)," *Renew. Energy*, vol. 122, pp. 131–139, 2018.
- [103] S. Alberici *et al.*, "Subsidies and costs of EU energy.," 2014.
- [104] I. Pawel, "The cost of storage - How to calculate the levelized cost of stored energy (LCOE) and applications to renewable energy generation," *Energy Procedia*, vol. 46, pp. 68–77, 2014.
- [105] W. Sinvert, "Three-phase inverters for grid-connected photovoltaic systems SINVERT PV Inverter - SINVERT 60 M - SINVERT 1700 MS." 2008.
- [106] A. Rohatgi, "WebPlotDigitizer," 2018. [Online]. Available: <https://automeris.io/WebPlotDigitizer>. [Accessed: 13-Nov-2018].
- [107] MathWorks, "payper - Periodic payment of loan or annuity," *MathWorks*, 2019. [Online]. Available: <https://es.mathworks.com/help/finance/payper.html>. [Accessed: 14-Oct-2019].
- [108] M. Arrinda, M. Berecibar, M. Oyarbide, H. Macicior, E. Muxika, and M. Messagie, "Levelized Cost of Electricity Calculation of the Energy Generation Plant of a CO₂ Neutral Micro-grid," *Energy*, 2020.
- [109] Y. Miyaki, "Method of estimating battery life, battery life estimation device, electric vehicle, and electric supply apparatus," US 2017/0291500 A1, 2017.
- [110] A. Widodo, M.-C. Shim, W. Caesarendra, and B.-S. Yang, "Intelligent prognostics for battery health monitoring based on sample entropy," *Expert Syst. Appl.*, vol. 38, no. 9, pp. 11763–11769, 2011.
- [111] S. Li, S. Pischinger, C. He, L. Liang, and M. Stapelbroek, "A comparative study of model-based capacity estimation algorithms in dual estimation frameworks for lithium-ion batteries under an accelerated aging test," *Appl. Energy*, vol. 212, no. December 2017, pp. 1522–1536, 2018.
- [112] X. Zhang, Q. Miao, and Z. Liu, "Remaining useful life prediction of lithium-ion battery using an improved UPF method based on MCMC," *Microelectron. Reliab.*, 2017.
- [113] Y. Zhou and M. Huang, "On-board capacity estimation of lithium-ion batteries based on charge phase," *J. Electr. Eng. Technol.*, vol. 13, no. 2, 2018.
- [114] S. Sankararaman, A. Saxena, and K. Goebel, "Are current prognostic performance evaluation practices sufficient and meaningful?," *PHM 2014 - Proc. Annu. Conf. Progn. Heal. Manag. Soc. 2014*, 2014.
- [115] K. Pugalenthi and N. Raghavan, "A holistic comparison of the different resampling algorithms for particle filter based prognosis using lithium ion batteries as a case study," *Microelectron. Reliab.*, vol. 91, no. December 2017, pp. 160–169, 2018.
- [116] D. E. Acuña and M. E. Orchard, "Prognostic Algorithms Design Based on Predictive Bayesian Cramér-Rao Lower Bounds," *IFAC-PapersOnLine*, vol. 50, no. 1, pp. 4719–4726, 2017.
- [117] A. Saxena, J. R. Celaya, B. Saha, S. Saha, and K. Goebel, "On Applying the Prognostic Performance Metrics," *Annu. Conf. Progn. Heal. Manag. Soc.*, pp. 1–16, 2009.
- [118] S. Sankararaman, M. Daigle, A. Saxena, and K. Goebel, "Analytical algorithms to quantify the uncertainty in remaining useful life prediction," *IEEE Aerosp. Conf. Proc.*, 2013.
- [119] M. Arrinda, M. Oyarbide, H. Macicior, and E. Muxika, "Comparison of Stochastic capacity estimation tools applied on remaining useful life prognosis of Lithium ion batteries," *PHM Soc. Eur. Conf.*, vol. 4, no. 1, Jul. 2018.

- [120] A. Saxena, J. Celaya, B. Saha, S. Saha, and K. Goebel, "Metrics for Offline Evaluation of Prognostic Performance," *Int. J. Progn. Heal. Manag.*, no. 1, pp. 1–20, 2010.
- [121] Q. Miao, L. Xie, H. Cui, W. Liang, and M. Pecht, "Remaining useful life prediction of lithium-ion battery with unscented particle filter technique," *Microelectron. Reliab.*, vol. 53, no. 6, pp. 805–810, 2013.
- [122] G. Dong, Z. Chen, J. Wei, and Q. Ling, "Battery health prognosis using brownian motion modeling and particle filtering," *IEEE Trans. Ind. Electron.*, vol. 65, no. 11, pp. 8646–8655, 2018.
- [123] L. Zhang, Z. Mu, and C. Sun, "Remaining Useful Life Prediction for Lithium-Ion Batteries Based on Exponential Model and Particle Filter," *IEEE Access*, vol. 6, pp. 17729–17740, 2018.
- [124] J. L. Doob, "STOCHASTIC PROCESSES AND STATISTICS," in *Proceedings of the National Academy of Sciences of the United States of America*, 1934, pp. 376–379.
- [125] B. Saha and K. Goebel, "Modeling Li-ion battery capacity depletion in a particle filtering framework," *Proc. Annu. Conf. Progn. Heal. Manag. Soc.*, pp. 2909–2924, 2009.
- [126] D. Liu, J. Pang, J. Zhou, Y. Peng, and M. Pecht, "Prognostics for state of health estimation of lithium-ion batteries based on combination Gaussian process functional regression," *Microelectron. Reliab.*, vol. 53, no. 6, pp. 832–839, 2013.
- [127] R. R. Richardson, C. R. Birkl, M. A. Osborne, and D. A. Howey, "Gaussian Process Regression for In-situ Capacity Estimation of Lithium-ion Batteries," pp. 1–12, 2017.
- [128] D. Zhou *et al.*, "Prognostics for state of health of lithium-ion batteries based on gaussian process regression," 2018.
- [129] Y. Zhang, H. Zhang, and Z. Tian, "The Application of Gaussian Process Regression in State of Health Prediction of Lithium Ion Batteries," in *2018 IEEE 3rd Advanced Information Technology, Electronic and Automation Control Conference (IAEAC)*, 2018, pp. 515–519.
- [130] M. S. Arulampalam, S. Maskell, N. Gordon, and T. Clapp, "A tutorial on particle filters for online nonlinear/non-Gaussian Bayesian tracking," *IEEE Trans. Signal Process.*, vol. 50, no. 2, pp. 174–188, 2002.
- [131] K. Goebel, B. Saha, A. Saxena, J. R. Celaya, and J. P. Christophersen, "Prognostics in Battery Health Management," *IEEE Instrum. Meas. Mag.*, pp. 33–40, 2008.
- [132] R. Douc, O. Cappé, and E. Moulines, "Comparison of Resampling Schemes for Particle Filtering," 2005.
- [133] T. Li, M. Bolic, and P. M. Djuric, "Resampling Methods for Particle Filtering," *IEEE Signal Process. Mag.*, no. May, pp. 70–86, 2015.
- [134] C. E. Rasmussen, "Gaussian processes for machine learning," *Int. J. Neural Syst.*, vol. 14, no. 2, pp. 69–106, 2006.
- [135] R. R. Richardson, M. A. Osborne, and D. A. Howey, "Gaussian process regression for forecasting battery state of health," 2017.
- [136] Z. Wang, J. Ma, and L. Zhang, "State-of-Health Estimation for Lithium-Ion Batteries Based on the Multi-Island Genetic Algorithm and the Gaussian Process Regression," *IEEE Access*, vol. 5, pp. 21286–21295, 2017.
- [137] B. Long, W. Xian, L. Jiang, and Z. Liu, "An improved autoregressive model by particle swarm optimization for prognostics of lithium-ion batteries," *Microelectron. Reliab.*, vol. 53, no. 6, pp. 821–831, 2013.
- [138] A. Saxena, K. Goebel, M. Field, M. Field, and E. K. Filter, "Uncertainty Representation and Interpretation in Model-based Prognostics Algorithms based on Kalman Filter Estimation," in *Annual Conference of the Prognostics and Health Management Society 2012*, 2012, pp. 1–10.
- [139] X. Zheng and H. Fang, "An integrated unscented kalman filter and relevance vector regression approach for lithium-ion battery remaining useful life and short-term capacity prediction," *Reliab. Eng. Syst. Saf.*, vol. 144, pp. 74–82, 2015.

- [140] B. Saha and K. Goebel, "Battery Data Set", NASA Ames Prognostics Data Repository, Moffett Field, CA," 2007. [Online]. Available: <http://ti.arc.nasa.gov/project/prognostic-data-repository>.
- [141] L. Tao *et al.*, "Lithium-ion battery capacity fading dynamics modelling for formulation optimization: A stochastic approach to accelerate the design process," *Appl. Energy*, vol. 202, pp. 138–152, 2017.
- [142] B. Saha, K. Goebel, and J. Christophersen, "Comparison of prognostic algorithms for estimating remaining useful life of batteries," *Trans. Inst. Meas. Control*, vol. 31, no. 3–4, pp. 293–308, Jun. 2009.
- [143] MathWorks, "What Are State-Space Models?" [Online]. Available: <https://es.mathworks.com/help/ident/ug/what-are-state-space-models.html>. [Accessed: 22-Aug-2017].
- [144] J. Qi, A. Mauricio, M. Sarrazin, K. Janssens, and K. Gryllias, "Enhanced Particle Filter and Cyclic Spectral Coherence based Prognostics of Rolling Element Bearings," in *Prognosis and Health Management European conference 2018*, 2018, pp. 1–10.
- [145] G. Baure and M. Dubarry, "Synthetic vs. Real Driving Cycles: A Comparison of Electric Vehicle Battery Degradation," *Batteries*, vol. 5, no. 2, p. 42, May 2019.
- [146] M. Johnen, S. Pitzten, U. Kamps, M. Kateri, and D. U. Sauer, "Modeling long-term capacity degradation of lithium-ion batteries," Jul. 2019.
- [147] N. Williard, B. Sood, M. Osterman, and M. Pecht, "Disassembly methodology for conducting failure analysis on lithium-ion batteries," *J. Mater. Sci. Mater. Electron.*, vol. 22, no. 10, pp. 1616–1630, Oct. 2011.
- [148] T. Waldmann *et al.*, "Review—Post-Mortem Analysis of Aged Lithium-Ion Batteries: Disassembly Methodology and Physico-Chemical Analysis Techniques," *J. Electrochem. Soc.*, vol. 163, no. 10, pp. A2149–A2164, Aug. 2016.
- [149] A. Kayyar, J. Huang, M. Samiee, and J. Luo, "Construction and testing of coin cells of lithium ion batteries.," *J. Vis. Exp.*, no. 66, p. e4104, Aug. 2012.
- [150] V. Murray, D. S. Hall, and J. R. Dahn, "A Guide to Full Coin Cell Making for Academic Researchers," *J. Electrochem. Soc.*, vol. 166, no. 2, pp. A329–A333, Jan. 2019.
- [151] S. Sun *et al.*, "Accelerated aging and degradation mechanism of LiFePO₄ /graphite batteries cycled at high discharge rates," *RSC Adv.*, vol. 8, no. 45, pp. 25695–25703, Jul. 2018.
- [152] S. Lee, P. Mohtat, J. B. Siegel, and A. G. Stefanopoulou, "Beyond Estimating Battery State of Health: Identifiability of Individual Electrode Capacity and Utilization," in *2018 Annual American Control Conference (ACC)*, 2018, pp. 2288–2293.
- [153] Y. Gao, J. Jiang, C. Zhang, W. Zhang, and Y. Jiang, "Aging mechanisms under different state-of-charge ranges and the multi-indicators system of state-of-health for lithium-ion battery with Li(NiMnCo)O₂ cathode," *J. Power Sources*, vol. 400, pp. 641–651, Oct. 2018.
- [154] J. Christensen and J. Newman, "Cyclable Lithium and Capacity Loss in Li-Ion Cells," *J. Electrochem. Soc.*, vol. 152, no. 4, pp. A818–A829, 2005.
- [155] J. Christensen and J. Newman, "Effect of Anode Film Resistance on the Charge/Discharge Capacity of a Lithium-Ion Battery," *J. Electrochem. Soc.*, vol. 150, no. 11, p. A1416, 2003.
- [156] A. Marongiu, N. Nlandi, Y. Rong, and D. U. Sauer, "On-board capacity estimation of lithium iron phosphate batteries by means of half-cell curves," *J. Power Sources*, vol. 324, pp. 158–169, 2016.

Annex 1: Un-synthesized evaluation metrics.

Test	Prediction RMSE	RA	P value	PDF width	Test	Prediction RMSE	RA	P value	PDF width	Test	Prediction RMSE	RA	P value	PDF width	Test	Prediction RMSE	RA	P value	PDF width
1	0.18903	0.54615	0.00000	6	2	0.04144	0.98058	0.00105	0	3	0.07651	0.81538	0.00000	11	4	0.04402	0.90291	0.00249	22
	0.03283	0.97674	0.00134	62		0.10362	0.68627	0.00002	15		0.04310	0.83721	0.00000	0		0.04434	0.98039	0.00171	127
	0.03260	0.89063	0.00006	15		0.26402	0.39604	0.00000	0		0.03183	0.99219	0.08875	0		0.07933	0.76238	0.00143	133
	0.12141	0.69291	0.00000	6		0.03800	0.97000	0.00136	209		0.04102	0.84252	0.00029	23		0.15366	0.63000	0.00076	122
	0.09438	0.76190	0.00000	2		0.04146	0.98990	0.00165	155		0.03082	0.92063	0.00070	26		0.05634	0.83838	0.00084	146
	0.04915	0.92000	0.00000	0		0.06685	0.77551	0.00113	86		0.09853	0.75200	0.00000	1		0.13677	0.64286	0.00079	92
	0.03338	0.99194	0.00104	12		0.13092	0.60825	0.00062	56		0.06162	0.84677	0.00000	0		0.22149	0.52577	0.00038	49
	0.28560	0.35772	0.00000	16		0.09162	0.69792	0.00149	48		0.03270	0.93496	0.00000	0		0.18804	0.56250	0.00090	44
	0.53898	-0.00820	0.00000	0		0.07158	0.75789	0.00132	116		0.03771	0.86885	0.00000	10		0.27706	0.45263	0.00056	113
	0.37721	0.19835	0.00000	0		0.09401	0.69149	0.00104	114		0.02734	0.95041	0.00000	0		0.20890	0.53191	0.00055	34
	0.02929	0.89167	0.00132	341		0.12387	0.61290	0.00111	83		0.03290	0.93333	0.00118	266		0.14331	0.61290	0.00089	146
	0.02723	0.95798	0.00152	189		0.12738	0.59783	0.00117	82		0.15103	0.63866	0.00059	116		0.29348	0.43478	0.00074	55
	0.06436	0.83051	0.00082	161		0.10869	0.64835	0.00119	81		0.20274	0.58475	0.00008	46		0.30807	0.41758	0.00044	46
	0.03516	0.92308	0.00152	204		0.07542	0.73333	0.00000	3		0.03223	0.93162	0.00141	187		0.13383	0.62222	0.00000	4
	0.05018	0.85345	0.00183	126		0.09240	0.67416	0.00094	169		0.02754	0.98276	0.00160	104		0.10429	0.68539	0.00122	126
	0.02913	0.89565	0.00145	240		0.13436	0.56818	0.00000	0		0.02540	1.00000	0.00142	250		0.14087	0.60227	0.00146	77
	0.02125	0.97368	0.00170	209		0.41363	0.18391	0.00000	0		0.12481	0.68421	0.00056	41		0.22787	0.47126	0.00067	79
	0.04005	0.92035	0.00193	170		0.15520	0.52326	0.00083	52		0.05252	0.83186	0.00108	309		0.29181	0.40698	0.00000	3
	0.03283	0.87500	0.00174	232		0.07957	0.70588	0.00151	75		0.02770	0.69463	0.00136	246		0.09386	0.69412	0.00088	69
	0.02091	0.98198	0.00173	164		0.10240	0.64286	0.00145	66		0.03896	0.89189	0.00651	27		0.27418	0.42857	0.00079	73
	0.04324	0.80909	0.00158	222		0.10099	0.65060	0.00075	58		0.02728	0.95455	0.00149	238		0.24231	0.45783	0.00073	90
	0.04944	0.88073	0.00117	759		0.13130	0.57317	0.00113	44		0.03173	0.88991	0.00134	357		0.28622	0.40244	0.00055	62
	0.47981	0.11111	0.00000	0		0.08045	0.69136	0.00087	92		0.08892	0.75000	0.00087	1168		0.18240	0.50617	0.00085	251
	0.09623	0.70093	0.00180	249		0.07931	0.70000	0.00105	101		0.02847	1.00000	0.00172	159		0.13387	0.58750	0.00105	0
	0.20460	0.45283	0.00000	0		0.10734	0.60759	0.00013	24		0.03315	0.94340	0.00133	286		0.18568	0.49367	0.00062	41
	0.04214	0.82857	0.00176	157		0.09417	0.64103	0.00117	158		0.04227	0.87619	0.00187	172		0.24337	0.42308	0.00104	69
	0.03728	0.79808	0.00003	57		0.08904	0.63636	0.00081	36		0.03191	0.95192	0.00248	125		0.22182	0.44156	0.00093	75
	0.02550	0.96117	0.00086	117		0.17056	0.46053	0.00023	31		0.04936	0.86408	0.00187	107		0.16841	0.50000	0.00120	85
	0.03600	0.79412	0.00134	581		0.09908	0.61333	0.00000	1		0.05786	0.83333	0.00166	104		0.11944	0.60000	0.00086	35
	0.03784	0.79208	0.00127	0		0.11191	0.56757	0.00000	3		0.04394	0.87129	0.00270	81		0.22218	0.40541	0.00000	14
	0.03411	0.81000	0.00124	976		0.14527	0.46575	0.00000	0		0.04704	0.43800	0.00207	96		0.20057	0.43836	0.00005	28
	0.02885	0.86869	0.00141	243		0.12077	0.52778	0.00000	11		0.03861	0.89899	0.00228	103		0.25787	0.34722	0.00099	54
	0.03667	0.78571	0.00160	243		0.15006	0.46479	0.00085	42		0.03765	0.83673	0.00130	335		0.20035	0.42254	0.00000	11
	0.07714	0.75258	0.00058	30		0.07785	0.67143	0.00073	37		0.02951	0.88660	0.00163	314		0.13531	0.54286	0.00066	39
	0.03732	0.78125	0.00138	351		0.03835	0.91304	0.00000	2		0.03656	0.84375	0.00143	272		0.08337	0.68116	0.00053	22
	0.01896	0.94737	0.00108	19		0.06124	0.73529	0.00000	2		0.03055	0.87368	0.00139	319		0.10553	0.61765	0.00064	30
	0.02395	0.89362	0.00156	279		0.12540	0.52239	0.00062	51		0.02567	0.92553	0.00167	238		0.12104	0.56716	0.00068	27
	0.03812	0.78495	0.00174	211		0.13903	0.45455	0.00000	0		0.03312	0.86022	0.00134	353		0.19170	0.42424	0.00001	24
	0.23354	0.21739	0.00000	2		0.08115	0.64615	0.00000	6		0.03993	0.94565	0.00157	235		0.20025	0.38462	0.00000	0
	0.26693	0.26374	0.00000	0		0.05626	0.87500	0.00193	136		0.03608	0.97802	0.00161	212		0.05657	0.96875	0.00197	105
	0.02802	0.91111	0.00149	53		0.05201	1.00000	0.00178	128		0.04046	0.91111	0.00154	243		0.05710	0.90476	0.00292	43

0.19061	0.32584	0.00000	4	0.04837	0.85484	0.00218	91	0.04484	0.88764	0.00167	157	0.06055	0.91935	0.00252	90
0.03631	0.80682	0.00146	231	0.05347	0.78689	0.00158	110	0.05468	0.84091	0.00163	157	0.04764	0.98361	0.00238	65
0.02080	0.97701	0.00189	45	0.04576	0.81667	0.00168	132	0.05227	0.83908	0.00170	128	0.04891	0.88333	0.00246	59
0.03927	0.76744	0.00130	553	0.16123	0.32203	0.00000	0	0.03717	0.93023	0.00193	189	0.06206	0.84746	0.00202	95
0.03849	0.76471	0.00130	1312	0.05097	0.77586	0.00182	157	0.02654	0.90588	0.00156	243	0.05898	0.87931	0.00062	8
0.03059	0.80952	0.00181	235	0.05241	0.70175	0.00130	772	0.03566	0.83333	0.00128	901	0.05942	0.87719	0.00284	43
0.03203	0.80723	0.00157	333	0.03562	1.00000	0.00109	4	0.02849	0.96386	0.00139	280	0.05061	0.96429	0.00187	99
0.03680	0.75610	0.00151	321	0.03854	0.92727	0.00088	10	0.08299	0.71951	0.00167	95	0.04614	0.98182	0.00192	97
0.03731	0.75309	0.00123	2492	0.07902	0.74074	0.00217	118	0.04188	0.87654	0.00137	154	0.07500	0.83333	0.00050	60
0.03548	0.76250	0.00173	223	0.05991	0.83019	0.00159	167	0.02816	0.96250	0.00164	231	0.06929	0.84906	0.00190	68
0.02374	0.89873	0.00226	32	0.04100	0.84615	0.00211	105	0.02455	0.97468	0.00323	27	0.07346	0.71154	0.00207	25
0.01758	0.94872	0.00046	12	0.04896	0.76471	0.00148	465	0.02337	0.93590	0.00475	31	0.10345	0.56863	0.00108	20
0.03653	0.74026	0.00170	39	0.05384	0.72000	0.00119	106	0.02674	0.94805	0.00225	70	0.11822	0.56000	0.00291	52
0.02708	0.82895	0.00162	35	0.07085	0.61224	0.00162	227	0.02111	0.94737	0.00035	5	0.07536	0.59184	0.00179	127
0.01824	0.92000	0.00160	187	0.04633	0.72917	0.00167	84	0.02837	0.94667	0.00303	62	0.06262	0.68750	0.00001	13
0.01808	0.90541	0.00219	30	0.04786	0.70213	0.00169	83	0.02500	0.86486	0.00009	7	0.06519	0.65957	0.00000	3
0.01694	0.93151	0.00169	180	0.06347	0.58696	0.00150	42	0.03209	0.90411	0.00000	0	0.06130	0.69565	0.00015	9
0.01633	0.95833	0.00249	27	0.03977	0.77778	0.00085	11	0.02858	0.93056	0.00000	3	0.09367	0.53333	0.00000	6
0.01766	1.00000	0.00330	0	0.03721	0.77273	0.00161	161	0.02014	1.00000	0.00206	13	0.07368	0.59091	0.00117	32
0.07340	0.70000	0.00204	45	0.03928	0.76744	0.00008	8	0.02293	0.97143	0.00270	22	0.07345	0.58140	0.00241	38
0.01505	0.94203	0.00212	29	0.05225	0.64286	0.00038	13	0.02985	0.91304	0.00149	11	0.06964	0.59524	0.00248	57
0.02583	0.92647	0.00270	59	0.05460	0.60976	0.00000	0	0.02660	0.92647	0.00191	14	0.09163	0.48780	0.00100	30
0.02085	0.97015	0.00297	58	0.06131	0.57500	0.00000	4	0.04945	0.80597	0.00000	0	0.09216	0.45000	0.00000	9
0.01986	0.96970	0.00230	26	0.08590	0.46154	0.00167	179	0.05605	0.77273	0.00000	0	0.06928	0.58974	0.00149	35
0.04737	0.78462	0.00221	80	0.05848	0.60526	0.00242	53	0.04461	0.83077	0.00241	53	0.06926	0.57895	0.00269	40
0.02698	0.92188	0.00152	0	0.06884	0.45946	0.00145	34	0.04922	0.79688	0.00253	72	0.08487	0.48649	0.00000	0
0.02249	0.95238	0.00339	24	0.05329	0.61111	0.00037	14	0.04695	0.80952	0.00198	43	0.09276	0.44444	0.00000	1
0.03335	0.87097	0.00231	99	0.06444	0.51429	0.00226	74	0.04946	0.79032	0.00185	36	0.09432	0.42857	0.00000	11
0.02721	0.91803	0.00247	19	0.06917	0.44118	0.00214	40	0.04535	0.81967	0.00134	20	0.08483	0.44118	0.00000	0
0.03934	0.83333	0.00250	85	0.06730	0.45455	0.00112	28	0.04856	0.78333	0.00000	2	0.09735	0.36364	0.00000	0
0.03319	0.86441	0.00003	0	0.06643	0.46875	0.00171	32	0.06408	0.71186	0.00200	50	0.09636	0.37500	0.00000	3
0.03315	0.86207	0.00210	22	0.07004	0.41935	0.00000	3	0.05168	0.77586	0.00006	9	0.11300	0.25806	0.00000	3
0.03617	0.84211	0.00230	99	0.08450	0.30000	0.00000	1	0.04877	0.78947	0.00303	41	0.10596	0.26667	0.00235	36
0.02393	0.94643	0.00148	5	0.06990	0.37931	0.00000	2	0.04074	0.82143	0.00000	4	0.09538	0.31034	0.00000	3
0.03391	0.85455	0.00000	12	0.07497	0.35714	0.00004	4	0.08246	0.60000	0.00000	13	0.11798	0.17857	0.00356	33
0.03326	0.85185	0.00104	42	0.07581	0.29630	0.00000	7	0.06554	0.68519	0.00028	14	0.16326	-0.07407	0.00000	0
0.15602	0.24528	0.00000	12	0.12850	0.03846	0.00043	25	0.10178	0.50943	0.00000	9	0.13021	0.03846	0.00000	2
0.19021	0.07692	0.00000	25	0.08793	0.16000	0.00056	0	0.06987	0.65385	0.00044	24	0.08371	0.36000	0.00000	0
0.12535	0.35294	0.00170	46	0.06389	0.37500	0.00150	21	0.13760	0.45098	0.00000	23	0.08043	0.33333	0.00074	18
0.02781	0.90000	0.00240	81	0.05678	0.43478	0.00331	44	0.05380	0.80000	0.00262	111	0.07327	0.39130	0.00146	26
0.01597	0.89796	0.00468	48	0.05546	0.45455	0.00000	3	0.08374	0.63265	0.00234	57	0.07546	0.36364	0.00000	2
0.02131	0.93750	0.00225	101	0.07813	0.23810	0.00147	21	0.04253	0.83333	0.00323	43	0.08040	0.28571	0.00306	32
0.01598	1.00000	0.00298	20	0.04392	0.80000	0.00000	16	0.02916	0.89362	0.00024	6	0.06681	0.40000	0.00164	11
0.01659	1.00000	0.00194	52	0.05723	0.36842	0.00385	35	0.03357	0.84783	0.00094	10	0.07649	0.26316	0.00330	51
0.02181	0.93333	0.00223	22	0.07627	0.05556	0.00352	44	0.03382	0.84444	0.00052	8	0.07110	0.27778	0.00000	4
0.02177	0.93182	0.00300	20	0.06612	0.17647	0.00016	10	0.03057	0.86364	0.00000	2	0.08398	0.11765	0.00000	0

0.01511	0.97674	0.00125	2	0.06950	0.12500	0.00011	10	0.02981	0.88372	0.00000	2	0.08085	0.12500	0.00004	9
0.02426	0.90476	0.00003	4	0.07033	0.00000	0.00000	2	0.04704	0.76190	0.00000	0	0.08142	0.00000	0.00295	26
0.01596	1.00000	0.00230	4	0.06955	0.00000	0.00226	0	0.03796	0.80488	0.00000	0	0.08543	-0.07143	0.00244	31
0.02040	0.95000	0.00040	3	0.07260	-0.15385	0.00000	4	0.04672	0.75000	0.00000	2	0.08766	-0.15385	0.00000	1
0.01435	0.97436	0.00108	28	0.06984	-0.25000	0.00000	1	0.06842	0.64103	0.00273	54	0.08799	-0.25000	0.00000	0
0.01056	0.89474	0.00153	11	0.07692	-0.36364	0.00000	0	0.05599	0.68421	0.00280	63	0.08785	-0.36364	0.00000	0
0.01523	0.94595	0.00250	97	0.08244	-0.60000	0.00000	0	0.03770	0.81081	0.00266	50	0.09386	-0.60000	0.00434	44
0.02353	0.91667	0.00328	63	0.06719	-0.44444	0.00000	5	0.06228	0.63889	0.00282	67	0.08541	-0.55556	0.00000	0
0.02349	0.91429	0.00202	209	0.09105	-1.25000	0.00000	0	0.03385	0.85714	0.00299	37	0.10990	-0.62500	0.00331	15
0.01360	0.94118	0.00316	7	0.03434	0.71429	0.00122	18	0.03424	0.82353	0.00004	5	0.07482	-0.57143	0.00000	0
0.01193	0.90909	0.00122	5	0.02769	0.83333	0.04382	0	0.04435	0.72727	0.00258	106	0.09657	-1.33333	0.00000	1
0.02102	0.93750	0.00176	18	0.07637	-1.80000	0.00000	2	0.03648	0.81250	0.00226	17	0.10094	-1.80000	0.00347	143
0.02000	0.96774	0.00270	91	0.01959	-0.75000	0.00332	63	0.03450	0.83871	0.00370	49	0.02045	0.00000	0.00478	49
0.02090	0.93333	0.00240	9	0.02283	0.33333	0.00300	153	0.03428	0.80000	0.00127	8	0.02000	-0.66667	0.00474	28
0.01496	0.96552	0.00196	10	0.01904	-1.50000	0.00364	82	0.04051	0.75862	0.00199	31	0.02225	-2.50000	0.00000	0
0.02214	0.92857	0.00210	0	0.02192	-7.00000	0.00397	58	0.03312	0.82143	0.00000	2	0.02127	-5.00000	0.00000	3
0.01179	0.85185	0.00095	5					0.02843	0.88889	0.00000	2				
0.02771	0.84615	0.00157	26					0.03129	0.84615	0.00000	0				
0.02900	0.84000	0.00531	7					0.06942	0.44000	0.00000	2				
0.02594	0.87500	0.00123	5					0.05975	0.54167	0.00000	4				
0.02958	0.82609	0.00179	38					0.09116	0.17391	0.00000	0				
0.02127	0.95455	0.00122	12					0.02107	0.90909	0.00281	92				
0.01375	0.80952	0.00339	80					0.02588	0.95238	0.00406	58				
0.01256	0.80000	0.00171	41					0.02192	0.95000	0.00281	49				
0.01449	0.78947	0.00271	128					0.02831	1.00000	0.00401	52				
0.01716	0.94444	0.00305	42					0.02310	1.00000	0.00361	36				
0.02386	0.88235	0.00316	85					0.02324	1.00000	0.00042	0				
0.02455	0.87500	0.00310	36					0.02238	1.00000	0.00258	3				
0.02767	0.80000	0.00243	16					0.02862	0.86667	0.00130	7				
0.01372	0.85714	0.00213	9					0.02541	0.92857	0.00048	1				
0.01776	0.92308	0.00162	5					0.02403	0.92308	0.00158	2				
0.01748	0.91667	0.00185	10					0.02633	0.91667	0.00041	2				
0.02143	1.00000	0.00106	4					0.03064	0.81818	0.00087	0				
0.02413	0.90000	0.00104	15					0.02399	1.00000	0.00163	2				
0.02000	-0.22222	0.00000	16					0.06642	-0.11111	0.00175	12				
0.01536	0.62500	0.00000	3					0.01917	0.75000	0.00194	7				
0.01773	0.71429	0.00403	101					0.01703	0.42857	0.00439	46				
0.01581	0.50000	0.00258	32					0.01447	0.00000	0.00007	7				
0.01587	0.40000	0.00345	95					0.01973	0.60000	0.00184	8				
0.01650	0.25000	0.00217	16					0.02261	0.75000	0.00227	15				
0.01735	0.00000	0.00387	89					0.01957	0.00000	0.00168	8				
0.01954	0.00000	0.00368	30					0.02036	-0.50000	0.00000	8				
0.02436	1.00000	0.00430	81					0.01919	-1.00000	0.00106	4				

Table 164: The obtained evaluation metrics on all the tests and training data sets with the evaluated Particle Filter configuration

T.	Prediction RMSE	RA	P value	PDF width	T.	Prediction RMSE	RA	P value	PDF width	T.	Prediction RMSE	RA	P value	PDF width	T.	Prediction RMSE	RA	P value	PDF width
5	0.13290	-0.20769	0.00110	511	6	0.07495	0.75728	0.00789	35	7	0.12546	0.06154	0.00158	378	8	0.06036	0.82524	0.00068	866
	0.12900	-0.15504	0.00092	639		0.04807	0.93137	0.01147	7		0.12135	0.10078	0.00137	456		0.06388	0.81373	0.00950	76
	0.10929	0.17969	0.00048	1204		0.04824	0.85149	0.00137	11		0.09811	0.39844	0.00098	655		0.09487	0.73267	0.00000	8
	0.10004	0.29921	0.00000	38		0.29863					0.09125	0.48819	0.00006	38		0.04303	0.93000	0.00000	1
	0.10488	0.27778	0.00000	4		0.30102					0.09138	0.50000	0.00000	4		0.04744	0.98990	0.48394	1
	0.10762	0.24000	0.00000	3		0.15200	0.01020	0.00015	66		0.09459	0.47200	0.00000	2		0.04915	0.97959	0.00886	1
	0.11224	0.19355	0.00000	3		0.04472	0.92784	0.00000	>65535		0.09991	0.42742	0.00000	3		0.04745	0.86598	0.00167	402
	0.10170	0.30081	0.00000	2		0.04700	0.84375	0.00073	789		0.08793	0.52033	0.00000	2		0.07750	0.75000	0.00237	301
	0.09847	0.32787	0.00000	3		0.08109	0.71579	0.00000	>65535		0.08429	0.54918	0.00000	2		0.11675	0.64211	0.00058	975
	0.09883	0.32231	0.00000	3		0.10526	0.63830	0.00000	>65535		0.08476	0.54545	0.00000	2		0.14423	0.57447	0.00071	819
	0.36211					0.10119	0.64516	0.00000	>65535		0.23550	-0.57500	0.00034	1606		0.14130	0.58065	0.00084	705
	0.32671					0.13194	0.56522	0.00000	>65535		0.23991	-1.10924	0.00084	499		0.17589	0.52174	0.00106	578
	0.30088					0.14945	0.52747	0.00000	>65535		0.22802	-1.64407	0.00000	104		0.19658	0.48352	0.00133	478
	0.29173					0.08519	0.70000	0.00136	20		0.22180	-1.97436	0.00000	30		0.12966	0.62222	0.00000	9
	0.29374					0.06976	0.75281	0.01563	44		0.22412	-2.43103	0.00053	597		0.12311	0.64045	0.00000	2
	0.29563					0.08304	0.70455	0.00000	0.00280		0.25601	-3.31304	0.00000	>65535		0.14427	0.60227	0.00000	1
	0.29617					0.09120	0.67816	0.00000	0.00258		0.24169	-3.15789	0.00022	2379		0.15539	0.57471	0.00000	0.00253
	0.29685					0.09678	0.66279	0.00000	0.00239		0.25480	-3.26549	0.00000	>65535		0.16262	0.55814	0.00000	0.00234
	0.29751					0.07968	0.70588	0.00000	0.00224		0.23804	-3.13393	0.00000	12		0.13666	0.60000	0.00000	0.0022
	0.26608					0.07095	0.73810	0.00000	0.00211		0.23002	-2.65766	0.00000	1.04E-08		0.07146	0.77381	0.00362	200
	0.24502					0.06886	0.73494	0.00000	1		0.19095	-1.77273	0.00026	1992		0.11499	0.63855	0.00000	0.00204
	0.30024					0.04566	0.84146	0.00001	6		0.24232	-3.63303	0.00000	21		0.11621	0.63415	0.00073	21
	0.30142					0.05067	0.80247	0.00000	5		0.24613	-3.94444	0.00000	21		0.11606	0.62963	0.00034	19
	0.27768					0.05481	0.78750	0.00000	4		0.24438	-3.72897	0.00000	20		0.11586	0.62500	0.00011	17
	0.24752					0.07178	0.72152	0.00000	4		0.24096	-3.38679	0.00000	18		0.11891	0.62025	0.00004	16
	0.15938	-3.00000	0.00000	>65535		0.07381	0.70513	0.00000	3		0.17620	-1.71429	0.00035	1463		0.12122	0.60256	0.00001	14
	0.11972	-0.99038	0.00000	>65535		0.07756	0.70130	0.00000	3		0.15655	-1.21154	0.00041	1231		0.12569	0.59740	0.00000	12
	0.05589	0.48544	0.00000	>65535		0.10357	0.60526	0.00000	>65535		0.05394	0.53398	0.00000	>65535		0.14106	0.55263	0.00000	65535
	0.01745	0.88235	0.00000	>65535		0.09422	0.62667	0.00000	>65535		0.01632	0.90196	0.00000	>65535		0.13673	0.56000	0.00087	650
	0.02897	0.91089	0.00000	>65535		0.08558	0.66216	0.00000	1		0.03184	0.89109	0.00000	>65535		0.13679	0.55405	0.00000	0.00119
	0.05652	0.78000	0.00000	>65535		0.08928	0.64384	0.00000	0.00116		0.06013	0.77000	0.00000	>65535		0.14335	0.53425	0.00000	1
	0.06883	0.72727	0.00000	>65535		0.09369	0.62500	0.00000	0.00111		0.07291	0.71717	0.00000	>65535		0.14899	0.52778	0.00000	0.00109
	0.07579	0.24490	0.00171	292		0.09811	0.60563	0.00000	0.00106		0.07099	0.36735	0.00225	228		0.15458	0.50704	0.00000	0.00104
	0.11503	-0.18557	0.00028	1832		0.08958	0.62857	0.00000	0.00102		0.10982	0.02062	0.00062	872		0.14167	0.52857	0.00000	0.00101
	0.10992	-0.10417	0.00034	1535		0.10495	0.82609	0.00000	>65535		0.10437	0.09375	0.00070	781		0.08204	0.69565	0.00134	435
	0.11786	-0.16842	0.00082	638		0.04333	0.89706	0.00000	>65535		0.11171	0.05263	0.00127	431		0.06969	0.75000	0.00141	412
	0.04096	0.95745	0.00000	>65535		0.04604	0.86567	0.00000	>65535		0.04018	0.97872	0.00000	>65535		0.07451	0.71642	0.00155	378
	0.03873	0.94624	0.00000	>65535		0.04934	0.83333	0.00000	>65535		0.11980	0.04301	0.00000	37		0.07926	0.69697	0.00171	348
	0.03864	1.00000	0.00000	>65535		0.06242	0.73846	0.00000	>65535		0.03917	0.97826	0.00000	>65535		0.09604	0.63077	0.00197	309
	0.02995	0.92308	0.00000	>65535		0.18861					0.03450	0.90110	0.00000	>65535		0.09810	0.54688	0.00141	386
	0.03805	0.71111	0.00000	>65535		0.33022					0.03294	0.78889	0.00000	>65535		0.21242	-0.33333	0.00114	438
	0.04645	0.64045	0.00000	>65535		0.25267					0.04090	0.73034	0.00000	>65535		0.27887	-0.93548	0.00101	463
	0.04561	0.64773	0.00000	>65535		0.18436					0.03993	0.73864	0.00065	820		0.10668	0.54098	0.00499	35
	0.04358	0.67816	0.00000	>65535		0.15670					0.03784	0.75862	0.00071	750		0.05916	0.88333	0.00885	78
	0.04070	0.70930	0.00000	>65535		0.17343					0.03498	0.79070	0.00078	684		0.19477	-1.79661	0.00000	>65535

0.03237	0.78824	0.00000	>65535	0.17505		0.02742	0.85882	0.00088	613	0.20483	-2.01724	0.00000	>65535
0.02190	0.89286	0.00000	>65535	0.17139		0.02043	0.95238	0.00102	538	0.20129	-2.01754	0.00000	>65535
0.01903	0.93976	0.00000	>65535	0.16247		0.02084	1.00000	0.00116	480	0.08567	0.66071	0.00525	113
0.08156	0.69512	0.00000	>65535	0.15853		0.08979	0.68293	0.00000	>65535	0.06799	0.80000	0.01085	58
0.09041	0.66667	0.00000	>65535	0.16632		0.09898	0.65432	0.00000	>65535	0.04769	0.98148	0.05976	13
0.10548	0.62500	0.00000	>65535	0.16969		0.11445	0.61250	0.00000	>65535	0.04229	0.90566	0.03271	22
0.11772	0.59494	0.00000	>65535	0.16860		0.12706	0.58228	0.00000	>65535	0.04183	0.88462	0.03807	17
0.13351	0.56410	0.00000	>65535	0.16418		0.14327	0.55128	0.00000	>65535	0.04216	0.88235	0.03764	16
0.14058	0.54545	0.00000	>65535	0.15947		0.15066	0.53247	0.00000	>65535	0.04251	0.88000	0.03764	16
0.15188	0.51316	0.00000	>65535	0.15410		0.16233	0.50000	0.00000	>65535	0.04291	0.87755	0.03764	16
0.15482	0.50667	0.00000	>65535	0.14609		0.16557	0.49333	0.00000	>65535	0.04351	0.85417	0.03654	15
0.16230	0.48649	0.00000	>65535	0.12572	-3.21277	0.00000			3	0.04425	0.85106	0.03457	14
0.16870	0.46575	0.00000	>65535	0.06318	0.73913	0.00000			>65535	0.04533	0.82609	0.02966	14
0.17276	0.45833	0.00000	>65535	0.04650	0.91111	0.01354			52	0.04666	0.80000	0.02610	13
0.08460	0.63380	0.01492	39	0.05609	0.75000	0.03075			19	0.04798	0.79545	0.02109	13
0.08773	0.62857	0.01263	31	0.07319	0.62791	0.00225			11	0.04956	0.76744	0.01658	12
0.09071	0.60870	0.00832	26	0.09493	0.52381	0.00000			6	0.12097	0.47619	0.00000	5
0.09318	0.60294	0.00408	22	0.11406	0.46341	0.00000			4	0.13863	0.41463	0.00000	4
0.09507	0.59701	0.00224	20	0.15968	0.37500	0.00000			4	0.18556	0.35000	0.00000	3
0.09648	0.57576	0.00074	17	0.12436	0.41026	0.00000			4	0.14674	0.35897	0.00000	3
0.09775	0.56923	0.00016	15	0.12119	0.39474	0.00000			3	0.14273	0.36842	0.00000	2
0.11220	0.53125	0.00000	>65535	0.12562	0.37838	0.00000			2	0.14627	0.35135	0.00000	2
0.08158	0.61905	0.00204	297	0.13060	0.36111	0.00000			2	0.15041	0.30556	0.00000	2
0.08118	0.61290	0.00253	248	0.17826	0.28571	0.00000			2	0.15512	0.28571	0.00000	2
0.08209	0.60656	0.00333	197	0.18202	0.26471	0.00000			2	0.15782	0.26471	0.00000	2
0.06973	0.66667	0.00000	4	0.18565	0.24242	0.00000			1	0.16052	0.24242	0.00000	2
0.07215	0.64407	0.00000	3	0.14780	0.25000	0.00000			1	0.16258	0.21875	0.00000	2
0.06584	0.67241	0.00000	2	0.15095	0.19355	0.00000			1	0.16562	0.19355	0.00000	1
0.06653	0.66667	0.00000	2	0.15499	0.16667	0.00000			1	0.16956	0.16667	0.00000	1
0.03032	0.89286	0.00000	1	0.09639	0.31034	0.00000			1	0.11393	0.27586	0.00000	0.00420
0.02364	0.94545	0.08066	6	0.08128	0.35714	0.00000			1	0.08688	0.39286	0.00048	10
0.01846	0.98148	0.00000	0.00135	0.07617	0.40741	0.00225			11	0.07609	0.40741	0.00003	8
0.02401	0.96226	0.03612	22	0.07030	0.42308	0.00000			1	0.07384	0.42308	0.00000	0.00079
0.01747	0.94231	0.00000	0.00095	0.06304	0.44000	0.00000			4	0.07486	0.40000	0.00000	2
0.01726	0.94118	0.01748	3	0.05715	0.45833	0.00000			5	0.07421	0.37500	0.00000	2
0.02687	0.90000	0.00000	1	0.05986	0.43478	0.00000	0.00184			0.07449	0.34783	0.00000	2
0.03170	0.85714	0.00899	85	0.06055	0.40909	0.00000	>65535			0.07513	0.31818	0.00000	2
0.03158	0.85417	0.00000	0.00211	0.05881	0.42857	0.00000			1	0.07638	0.28571	0.00000	2
0.03197	0.85106	0.00000	0.00203	0.05815	0.40000	0.00000	0.00105			0.07809	0.25000	0.00000	2
0.03242	0.84783	0.00000	0.00196	0.06529	0.26316	0.00000			3	0.07726	0.21053	0.00000	1
0.03882	0.80000	0.00000	1	0.07375	0.22222	0.00000			1	0.07786	0.22222	0.00000	1
0.03358	0.84091	0.01210	65	0.07260	0.17647	0.00000	>65535			0.08032	0.11765	0.00000	0.00088
0.02915	0.86047	0.00000	1	0.07358	0.06250	0.00000			3	0.08145	0.06250	0.01767	19
0.02592	0.90476	0.02700	4	0.08227	0.00000	0.00000			4	0.08429	0.00000	0.00000	0.00100
0.02299	0.92683	0.00000	0.00110	0.08259	-0.07143	0.00000			4	0.08429	-0.07143	0.00000	1
0.02370	0.92500	0.00000	0.00107	0.08387	-0.15385	0.00000			4	0.08601	-0.15385	0.00000	0.00044

0.02299	0.92308	0.06476	4	0.08499	-0.25000	0.00000	4	0.03907	0.82051	0.00000	2	0.08695	-0.25000	0.00000	1
0.02344	0.92105	0.06476	4	0.08617	-0.36364	0.00000	3	0.03909	0.81579	0.00000	2	0.08807	-0.36364	0.00000	1
0.02474	0.91892	0.00000	1	0.08811	-0.50000	0.00000	3	0.04123	0.78378	0.00000	0.00061	0.08999	-0.50000	0.00000	0.00079
0.03846	0.77778	0.00000	1	0.06672	-0.33333	0.00000	0.00056	0.04756	0.75000	0.00000	0.00257	0.08859	-0.55556	0.00000	1
0.03016	0.85714	0.00032	3	0.06840	-0.50000	0.00000	0.00055	0.05108	0.71429	0.00286	7	0.09037	-0.87500	0.00000	1
0.03058	0.85294	0.00032	3	0.06993	-0.71429	0.00000	0.00053	0.04568	0.73529	0.00001	4	0.09186	-1.00000	0.00000	1
0.03958	0.75758	0.00000	1	0.07153	-1.00000	0.00000	0.00047	0.04355	0.75758	0.03025	16	0.09349	-1.33333	0.00000	1
0.02971	0.84375	0.00000	2	0.07342	-1.60000	0.00000	1	0.04380	0.75000	0.00000	0.00058	0.09552	-2.00000	0.00000	1
0.03163	0.83871	0.00032	3	0.06943	-2.00000	0.00000	0.00049	0.02311	0.93548	0.12099	4	0.09051	-2.50000	0.00000	1
0.03212	0.80000	0.00032	3	0.06600	-2.66667	0.00000	0.00048	0.02351	0.93333	0.12099	4	0.07349	-3.33333	0.00000	0.00124
0.03106	0.82759	0.00000	2	0.05503	-4.50000	0.00000	1	0.04472	0.72414	0.00000	0.00051	0.05992	-5.00000	0.00000	1
0.03151	0.82143	0.00000	2	0.04450	-9.00000	0.00000	0.00135	0.02451	0.92857	0.06632	3	0.04932	-9.00000	0.00000	0.00135
0.01897	0.25926	0.00000	>65535					0.01201	0.59259	0.01295	20				
0.01837	0.26923	0.00000	>65535					0.01178	0.57692	0.01322	18				
0.01671	0.96000	0.00886	1					0.01128	0.60000	0.01619	16				
0.01540	0.91667	0.07598	9					0.01077	0.62500	0.01665	13				
0.01552	0.91304	0.00000	0.00025					0.01066	0.65217	0.01658	12				
0.01572	0.90909	0.00000	0.00024					0.01074	0.63636	0.01632	11				
0.01556	0.90476	0.00000	0.00024					0.01215	0.47619	0.00966	13				
0.01767	0.95000	0.24197	2					0.01576	0.25000	0.00350	15				
0.01937	1.00000	0.03970	20					0.02421	-9.68421	0.00000	>65535				
0.02115	1.00000	0.48394	1					0.01520	0.88889	0.05399	2				
0.02262	0.94118	0.25159	3					0.01487	0.88235	0.05399	2				
0.02281	0.93750	0.25159	3					0.01478	0.87500	0.05399	2				
0.02368	0.93333	0.00000	0.00041					0.01557	0.93333	0.02957	23				
0.00978	0.64286	0.00000	>65535					0.01530	0.85714	0.05399	2				
0.01006	0.53846	0.00000	2					0.02640	-15.07692	0.00042	1106				
0.03006	65535	0.00000	>65535					0.02572	-15.66667	0.00043	1083				
0.02885	65535	0.00000	>65535					0.02464	-15.90909	0.00000	>65535				
0.02816	65535	0.00000	>65535					0.02408	-16.60000	0.00000	>65535				
0.01571	-0.55556	0.00002	7					0.01170	-0.11111	0.00000	4				
0.01545	-0.75000	0.00000	6					0.01168	-0.25000	0.00000	4				
0.01710	0.57143	0.08832	7					0.01511	0.57143	0.00000	1				
0.01722	0.50000	0.00000	0.00020					0.01473	0.50000	0.00000	1				
0.01831	0.60000	0.00000	0.00023					0.01459	0.40000	0.00000	1				
0.01906	0.50000	0.00000	0.00027					0.01467	0.25000	0.00000	1				
0.02038	0.33333	0.00886	1					0.01272	-0.33333	0.04839	10				
0.02067	0.50000	0.08386	9					0.01276	-1.00000	0.04839	10				
0.02139	0.00000	0.00000	0.00014					0.01297	-3.00000	0.04839	10				

Table 165: The obtained evaluation metrics on all the tests and training data sets with the evaluated Gaussian Process configuration

Test	Prediction RMSE	RA	P value	PDF width	Test	Prediction RMSE	RA	P value	PDF width	Test	Prediction RMSE	RA	P value	PDF width	Test	Prediction RMSE	RA	P value	PDF width
9	229.574	0.53846	0.00040	2620	10	0.07827	0.73786	0.00042	1996	11	0.07204	0.64615	0.00000	2658	12	0.14279	0.64078	0.00017	2066
	1.50955	-0.00775	0.00000	7		0.04795	0.93137	0.00013	2071		0.06231	0.71318	0.00106	0		0.14221	0.63725	0.00005	2086
	49868	0.17188	0.00006	2641		0.04452	0.84158	0.00101	1478		0.08563	0.53906	0.00101	0		0.18329	0.57426	0.00014	2078
	103.526	0.34646	0.00050	262		0.06693	0.76000	0.00102	1468		0.09029	0.50394	0.00009	0		0.05299	0.98000	0.00044	2031
	1.12839	0.06349	0.00013	107		0.12462	0.61616	0.00030	2009		0.08961	0.50794	0.00000	2655		0.05174	0.86869	0.00011	0
	580466	0.02400	0.00007	56		0.13396	0.23469	0.00000	0		0.10675	0.35200	0.00030	2492		0.06241	0.81633	0.00048	2047
	7690.5	0.28226	0.00014	2625		0.03743	0.94845	0.00072	2035		0.11732	0.25000	0.00077	2548		0.10811	0.69072	0.00018	2063
	1.43508	-0.00813	0.00011	16		0.06261	0.78125	0.00104	0		0.07858	0.58537	0.00070	2545		0.11774	0.66667	0.00017	0
	1.51395	-0.02459	0.00000	4		0.05284	0.82105	0.00000	0		0.08410	0.54098	0.00059	0		0.10228	0.70526	0.00060	2035
	0.66490	0.22314	0.00030	2620		0.06642	0.76596	0.00106	0		0.09422	0.46281	0.00077	2575		0.12219	0.65957	0.00017	0
	0.39885					0.05783	0.79570	0.00104	1473		0.24297	-3.36667	0.00099	0		0.10840	0.68817	0.00020	2064
	0.39051					89.96647	0.11957	0.00035	74		0.23000	-2.48739	0.00089	1838		0.14892	0.59783	0.00025	2058
	0.37649					0.09082	0.69231	0.00108	0		0.21380	-1.79661	0.00000	0		0.15485	0.58242	0.00019	2074
	0.32453					0.06112	0.77778	0.00108	1473		0.22499	-2.32479	0.00127	2487		0.12529	0.63333	0.00072	980
	0.31884					0.07701	0.71910	0.00099	0		0.23351	-2.81897	0.00121	2341		0.12618	0.62921	0.00058	2040
	0.31939					0.10822	0.63636	0.00000	4		0.23612	-3.14783	0.00009	2636		0.17219	0.54545	0.00006	0
	0.27668					0.10551	0.63218	0.00000	6		0.23554	-2.92105	0.00011	2631		0.17355	0.54023	0.00010	2065
	0.29178	-125.5575	0.00000	0		0.10262	0.63953	0.00000	6		0.23262	-2.70796	0.00014	2634		0.17021	0.53488	0.00011	2060
	0.25342	-6.13393	0.00000	11		0.03728	0.94118	0.00003	2065		0.23573	-3.03571	0.00023	2631		0.08443	0.71765	0.00012	2065
	0.23979	-4.26126	0.00036	2481		0.05671	0.78571	0.00101	1421		0.21814	-1.93694	0.00159	2422		0.10876	0.65476	0.00076	2028
	0.22509	-2.97273	0.00011	2620		0.04634	0.84337	0.00000	0		0.21177	-1.67273	0.00092	2382		0.11355	0.63855	0.00015	2073
	0.27510	-16.60550	0.00082	2612		0.03645	0.93902	0.00000	0		0.24424	-3.40367	0.00139	0		0.09993	0.67073	0.00024	0
	0.27590	-16.37963	0.00090	2623		0.04765	0.82716	0.00000	0		0.24707	-3.60185	0.00090	1835		0.11959	0.62963	0.00040	0
	0.26812	-11.04673	0.00000	5		0.32305	0.33750	0.00077	0		0.18663	-0.74766	0.00000	2471		0.11896	0.62500	0.00022	2061
	0.22162	-2.66038	0.00078	2337		0.08304	0.68354	0.00113	1465		0.17551	-0.52830	0.00111	1846		0.13643	0.58228	0.00113	1452
	0.20559	-2.09524	0.00000	0		0.08228	0.67949	0.00112	0		0.14969	-0.13333	0.00113	2205		0.13467	0.57692	0.00018	2052
	0.18582	-1.18269	0.00094	2280		0.09394	0.63636	0.00114	0		0.15649	-0.23077	0.00114	0		0.14944	0.54545	0.00012	2060
	1.16470	0.02913	0.00041	107		0.09950	0.61842	0.00000	0		0.14598	-0.08738	0.00016	2508		0.15593	0.52632	0.00028	0
	1.72998	0.41176	0.00061	2591		0.08927	0.64000	0.00104	1423		0.12170	0.18627	0.00114	1848		0.14101	0.54667	0.00078	2020
	1.05116	0.04950	0.00041	69		0.06847	0.71622	0.00108	1433		0.11493	0.24752	0.00115	0		0.14977	0.52703	0.00082	2025
	0.70218	0.14000	0.00033	2610		0.08053	0.67123	0.00104	1402		0.10718	0.32000	0.00017	2602		0.16000	0.50685	0.00084	1230
	0.32125	0.38384	0.00046	2609		0.08563	0.65278	0.00101	0		0.11392	0.25253	0.00017	2586		0.16684	0.48611	0.00071	2026
	4.98e13	-0.05102	0.00000	2620		0.10731	0.56338	0.00000	8		0.12177	0.13265	0.00008	13		0.17329	0.46479	0.00075	2020
	3.76e8	-0.05155	0.00036	77		0.07635	0.68571	0.00116	1459		0.13943	-0.08247	0.00003	2578		0.12678	0.55714	0.00079	2028
	0.94636	0.06250	0.00047	103		0.03886	0.91304	0.00102	0		0.13326	-0.01042	0.00110	0		0.07973	0.69565	0.00109	900
	0.23763	0.47368	0.00089	636		0.03814	0.95588	0.00104	1385		0.13268	-0.02105	0.00113	2467		0.09745	0.63235	0.00109	766
	0.07070	0.79787	0.00046	2567		0.03984	1.00000	0.00108	0		0.14448	-0.17021	0.00007	2548		0.11849	0.56716	0.00098	2018
	0.60653	0.16129	0.00049	116		0.86246	0.03030	0.00066	2045		0.13495	-0.04301	0.00025	0		0.12333	0.54545	0.00072	2027
	1.20e8	-0.01087	0.00026	2588		0.61595	0.07692	0.00038	2050		0.13490	-0.06522	0.00037	2529		0.13382	0.52308	0.00086	2013
	1.19216	0.01099	0.00000	17		0.46591	0.21875	0.00047	2045		0.14847	-0.23077	0.00016	2567		0.08247	0.71875	0.00017	0
1.15928	0.02222	0.00000	18	2.72e6	-0.06349	0.00042	2037	0.13535	-0.01111	0.00119	1838	0.05428	0.95238	0.00020	1944				
0.04949	0.82022	0.00061	2565	0.14873	-3.29032	0.00106	1450	0.11848	0.16854	0.00068	2551	0.06981	0.82258	0.00113	1997				
0.25228	0.43182	0.00091	681	0.62113				0.10155	0.32955	0.00052	0	0.04534	0.86885	0.00015	1999				
0.66075	0.13793	0.00062	82	0.51610				0.09610	0.37931	0.00017	2583	0.04440	0.90000	0.00031	2012				
0.18977	0.48837	0.00088	2554	0.47539				0.09073	0.41860	0.00009	45	0.04549	0.94915	0.00033	2020				

0.91535	0.05882	0.00016	34	0.41767		0.07502	0.54118	0.00010	2580	0.05419	0.94828	0.00061	2
0.03790	0.86905	0.00072	2545	0.05691	0.75439	0.00000	0.00000	0.00008	35	0.05120	0.98246	0.00036	1978
4.58112	0.18072	0.00059	2537	0.13026	-1.46429	0.00052	0.00000	0.00011	32	0.04644	0.91071	0.00011	1710
1.05413	0.02439	0.00008	22	0.11553	-0.83636	0.00021	0.00000	0.00012	2583	0.04561	0.90909	0.00129	1815
1.03630	0.02469	0.00005	26	0.45883					3	0.04320	0.90741	0.00019	1991
0.63097	0.37500	0.00034	2487	0.09019	0.45283	0.00116	0.00000	0.00000	0	0.06663	0.86792	0.00024	1982
1.27316	0.32911	0.00010	2342	0.07617	0.17308	0.00116	0.00000	0.00000	3	0.04847	0.92308	0.00029	2017
0.02068	0.94872	0.00044	2580	0.05459	0.64706	0.00017	0.00000	0.00000	5	0.05256	0.78431	0.00129	0
0.03553	0.93506	0.00041	2500	0.03997	0.98000	0.00000	0.00000	0.00000	3	0.05353	0.78000	0.00034	2008
0.11019	0.64474	0.00051	2561	0.03849	0.97959	0.00001	0.00000	0.00000	3	0.05530	0.75510	0.00027	2016
0.12802	0.60000	0.00047	2548	0.03864	0.83333	0.00124	0.00000	0.00000	5	0.06624	0.66667	0.00008	110
0.02696	0.79730	0.00000	3	0.04168	0.78723	0.00132	0.00000	0.00114	3	0.07087	0.63830	0.00020	1942
0.20451	0.58904	0.00048	0	0.04875	0.71739	0.00000	0.00000	0.00000	0	0.08418	0.56522	0.00047	2010
0.02091	0.84722	0.00000	0	0.05371	0.66667	0.00003	0.00000	0.00000	3	0.08864	0.53333	0.00091	1997
0.43023	0.47887	0.00029	2543	0.05036	0.68182	0.00000	0.00000	0.00000	3	0.07981	0.56818	0.00128	1989
0.01701	0.88571	0.00000	0	0.03172	0.86047	0.00002	0.00000	0.00000	0	0.08292	0.53488	0.00037	0
0.01528	0.91304	0.00000	0	0.04906	0.69048	0.00009	0.00000	0.00000	3	0.07099	0.59524	0.00126	1997
0.01476	0.94118	0.00000	3	0.02786	0.92683	0.00037	0.00000	0.00238	3	0.07675	0.56098	0.00028	1775
0.09851	0.62687	0.00052	2528	0.06730	0.62500	0.00008	0.00000	0.00000	5	0.05938	0.67500	0.00105	2001
0.13849	0.53030	0.00079	2558	0.05518	0.64103	0.00137	0.00000	0.00000	3	0.07574	0.56410	0.00117	2002
0.14044	0.60000	0.00038	2528	0.28589	0.31579	0.00009	0.00000	0.00000	3	0.07230	0.57895	0.00120	1995
0.02142	0.96875	0.00088	2563	0.27115	0.29730	0.00027	0.00000	0.00000	16	0.08254	0.51351	0.00046	1999
0.02170	0.95238	0.00000	3	0.27798	0.27778	0.00034	0.00000	0.00000	0	0.08769	0.47222	0.00023	1612
0.01415	0.91935	0.00116	1771	0.14056	0.25714	0.00119	0.00000	0.00048	21	0.09331	0.42857	0.00043	1993
0.02156	0.96721	0.00066	2551	0.12099	0.29412	0.00112	0.00000	0.00000	3	0.09119	0.41176	0.00089	1986
0.02849	0.90000	0.00000	37	0.06821	0.48485	0.00000	0.00000	0.00000	0	0.09461	0.39394	0.00024	1792
0.03066	0.88136	0.00000	0	0.06986	0.43750	0.00142	0.00000	0.00011	21	0.09599	0.37500	0.00053	1972
0.02774	0.91379	0.00000	0	0.07611	0.38710	0.00000	0.00000	0.00000	3	0.10270	0.32258	0.00033	798
0.01423	0.85965	0.00132	0	0.06936	0.36667	0.00119	0.00000	0.00013	0	0.10344	0.26667	0.00034	1767
0.24656	0.26786	0.00042	0	0.02505	0.82759	0.00130	0.00000	0.00135	2094	0.09507	0.31034	0.00033	1877
1623	-0.09091	0.00058	2500	0.02939	0.85714	0.00127	0.00000	0.00039	2540	0.08189	0.39286	0.00121	1989
0.03010	0.62963	0.00126	1803	0.03546	0.70370	0.00138	0.00000	0.00039	2532	0.07667	0.40741	0.00056	1974
0.01683	0.98113	0.00121	1774	0.03775	0.65385	0.00129	0.00000	0.00095	0	0.10794	0.15385	0.00029	36
0.01499	0.94231	0.00112	1699	0.04058	0.60000	0.00126	0.00000	0.00046	2535	0.10975	0.12000	0.00038	0
0.01577	0.96078	0.00114	0	0.03764	0.62500	0.00124	0.00000	0.00090	2524	0.07853	0.37500	0.00028	27
0.01168	0.90000	0.00110	0	0.02520	0.95652	0.00141	0.00000	0.00101	2519	0.07401	0.39130	0.00011	27
0.16739	0.38776	0.00070	2539	0.03469	0.59091	0.00133	0.00000	0.00038	2503	0.07470	0.36364	0.00009	11
0.32559	0.33333	0.00056	0	0.03601	0.57143	0.00131	0.00000	0.00033	2449	0.08279	0.23810	0.00019	36
0.01329	0.95745	0.00000	3	0.06998	0.20000	0.00147	0.00000	0.00000	3	0.08916	0.15000	0.00031	46
0.01433	0.97826	0.00000	3	0.05285	0.31579	0.00007	0.00000	0.00000	3	0.07971	0.21053	0.00046	1809
0.01597	1.00000	0.00000	0	0.06493	0.22222	0.00006	0.00000	0.00000	3	0.07898	0.22222	0.00140	1975
0.01817	0.97727	0.00000	0	0.06389	0.17647	0.00011	0.00000	0.00050	5	0.07977	0.17647	0.00155	1977
0.00957	0.86047	0.00119	1725	0.06658	0.12500	0.00000	0.00000	0.00090	2516	0.08051	0.12500	0.00146	1978
0.01137	0.90476	0.00133	1795	0.07157	0.00000	0.00155	0.00000	0.00105	2517	0.08487	0.00000	0.00170	1971
0.01156	0.90244	0.00133	0	0.06906	0.00000	0.00152	0.00000	0.00056	2492	0.08072	0.00000	0.00177	1969
0.01230	0.92500	0.00128	1779	0.07413	-0.15385	0.00147	0.00000	0.00089	2513	0.08800	-0.15385	0.00189	1967

0.01225	0.92308	0.00128	0	0.07435	-0.25000	0.00000	2	0.03802	0.82051	0.00052	2508	0.08838	-0.25000	0.00031	15
0.01303	0.94737	0.00123	1752	0.07558	-0.36364	0.00000	8	0.03844	0.81579	0.00092	2511	0.08916	-0.36364	0.00035	0
0.01376	0.94595	0.00146	0	0.07629	-0.50000	0.00134	1368	0.03800	0.81081	0.00041	2441	0.09161	-0.50000	0.00032	1083
0.01364	0.94444	0.00122	1728	0.03446	-0.77778	0.00138	1381	0.03559	0.83333	0.00051	2468	0.08671	-0.55556	0.00000	2
0.13925	0.40000	0.00080	0	0.06718	-0.87500	0.00014	13	0.03527	0.82857	0.00071	0	0.09439	-0.87500	0.00045	0
0.01889	0.97059	0.00000	65535	0.06819	-1.14286	0.00000	23	0.03472	0.82353	0.00000	3	0.09219	-1.00000	0.00000	0
0.01511	0.96970	0.00128	0	0.06307	-1.66667	0.00006	0	0.03653	0.81818	0.00043	2388	0.09458	-1.33333	0.00035	0
0.06067	0.62500	0.00114	2504	0.16876	-1.60000	0.00145	1957	0.03671	0.81250	0.00097	2503	0.09938	-2.00000	0.00048	1716
0.01365	0.93548	0.00133	0	0.07069	1.00000	0.00145	1953	0.03653	0.80645	0.00036	2369	0.02440	-1.25000	0.00202	1956
0.02262	0.93333	0.00000	3	0.07725	0.66667	0.00168	1955	0.03153	0.83333	0.00125	2507	0.02059	-1.00000	0.00196	1958
0.01446	0.93103	0.00000	16	0.07898	1.00000	0.00155	0	0.03818	0.79310	0.00117	0	0.03286	0.50000	0.00039	61
0.02063	0.96429	0.00149	1800	0.01927	-5.00000	0.00015	8	0.03236	0.82143	0.00115	2486	0.02761	0.00000	0.00021	34
0.01261	0.88889	0.00144	1792					0.02810	0.88889	0.00134	2499				
0.01123	0.73077	0.00128	1744					0.02979	0.84615	0.00136	2493				
0.01128	0.72000	0.00135	0					0.03296	0.80000	0.00105	2499				
0.01219	0.83333	0.00135	1766					0.03436	0.79167	0.00129	2492				
0.01098	0.78261	0.00140	1776					0.03223	0.82609	0.00111	2506				
0.01117	0.77273	0.00129	1736					0.02868	0.86364	0.00118	2470				
0.18926	0.33333	0.00058	2432					0.01536	0.85714	0.00027	61				
0.01319	0.85000	0.00144	1784					0.01751	0.90000	0.00055	2358				
0.02261	0.94737	0.00138	2500					0.03070	0.84211	0.00080	0				
0.01250	0.77778	0.00000	65535					0.03000	0.83333	0.00132	2481				
13.9093	-0.29412	0.00086	2474					0.02973	0.82353	0.00087	2462				
0.04857	0.62500	0.00115	2478					0.02969	0.87500	0.00075	2433				
0.01734	0.93333	0.00000	5					0.02779	0.86667	0.00056	3				
0.01189	0.78571	0.00000	13					0.02490	0.92857	0.00115	2481				
0.01122	0.61538	0.00132	0					0.02413	1.00000	0.00141	0				
0.01196	0.58333	0.00135	0					0.02521	0.91667	0.00142	2480				
0.01268	0.63636	0.00137	1739					0.02666	0.90909	0.00132	2480				
0.01280	0.60000	0.00141	1750					0.02505	0.90000	0.00126	2479				
0.01262	0.55556	0.00143	1758					0.02765	0.88889	0.00097	2438				
0.01425	-0.62500	0.00000	32					0.02079	0.87500	0.00143	2479				
0.01152	0.28571	0.00159	1779					0.01856	0.71429	0.00130	2467				
0.01395	0.33333	0.00135	1707					0.01821	0.50000	0.00042	67				
0.02396	0.60000	0.00062	2415					0.02021	0.60000	0.00000	3				
0.02214	0.50000	0.00030	2228					0.02201	0.50000	0.00000	3				
0.01755	0.33333	0.00153	1763					0.02621	1.00000	0.00120	2433				
0.01611	-0.50000	0.00003	2017					0.02609	0.50000	0.00133	0				
0.01704	-2.00000	0.00151	0					0.02632	0.00000	0.00139	2448				

Table 166: The obtained evaluation metrics on all the tests and training data sets with the evaluated Extended Kalman Filter

Test	Prediction RMSE	RA	P value	PDF width	Test	Prediction RMSE	RA	P value	PDF width	Test	Prediction RMSE	RA	P value	PDF width	Test	Prediction RMSE	RA	P value	PDF width
13	1.64205				14	1.37693	-0.04854	0.00018	2105	15	0.16886	-0.52308	0.00015	2658	16	0.04685	0.99029	0.00145	169
	1.64050					1.18810	0.00000	0.00022	2100		0.17927	-0.75969	0.00123	2491		0.04332	0.92157	0.00181	108
	1.63899					1.55035					0.12254	0.17969	0.00041	2545		0.07389	0.78218	0.00086	359
	1.63746					1.54787					0.11458	0.26772	0.00000	13		0.12129	0.53000	0.00004	2098
	1.63591					1.54551					0.14101	-0.07143	0.00085	556		0.07067	0.84848	0.00005	2094
	1.63433					0.49818	0.25510	0.00006	2096		0.15442	-0.28000	0.00075	685		0.05292	0.95918	0.00005	0
	1.63273					0.36628	0.38144	0.00009	2094		0.16015	-0.37903	0.00069	727		0.05508	0.83505	0.00016	0
	1.63119					1.53877					0.09137	0.48780	0.00099	2526		0.06803	0.79167	0.00009	2086
	0.96203	-0.04918	0.00000	2644		1.53652					0.08678	0.52459	0.00097	2521		0.05947	0.82105	0.00014	0
	1.62804					1.53432					0.12916	0.07438	0.00084	407		0.07996	0.75532	0.00021	0
	0.19487	0.55000	0.00007	2642		1.53211					0.26465	-6.64167	0.00100	2271		0.07088	0.77419	0.00015	2088
	2.01394					0.93215	-0.08696	0.00000	2084		0.23990	-3.24370	0.00000	118		0.11214	0.67391	0.00008	2084
	0.46904	0.27966	0.00030	72		0.18387	0.43956	0.00000	2075		0.22407	-2.34746	0.00080	2243		0.12135	0.64835	0.00036	0
	0.64154	0.17094	0.00016	0		0.63498	-0.07778	0.00000	2081		0.23514	-3.04274	0.00000	219		0.12427	0.63333	0.00000	0
	0.32371	0.40517	0.00010	2631		0.46402	0.00000	0.00000	0		0.23686	-3.33621	0.00078	2208		0.12618	0.62921	0.00000	4
	0.50245	0.24348	0.00040	2618		2.75e25					0.24667	-4.26087	0.00144	2337		0.16679	0.55682	0.00084	295
	0.49230	0.24561	0.00047	2612		0.14331	0.51724	0.00000	2058		0.24524	-4.00877	0.00002	788		0.16837	0.55172	0.00082	235
	0.46163	0.26549	0.00026	0		0.33664	0.08140	0.00012	2075		0.24514	-3.99115	0.00082	2081		0.16523	0.54651	0.00077	329
	0.25904	0.45536	0.00033	2615		1.23e23					0.23737	-3.08036	0.00000	165		0.07971	0.74118	0.00100	533
	0.23773	0.48649	0.00032	2615		6.01e25					0.22443	-2.28829	0.00000	104		0.10826	0.65476	0.00000	4
	0.35797	0.34545	0.00049	80		1.54e27					0.21755	-1.95455	0.00000	93		0.11332	0.63855	0.00124	0
	0.04443	0.82569	0.00104	0		0.44864	-0.06098	0.00057	2069		0.32693					0.08046	0.73171	0.00031	2065
	0.21283	0.50926	0.00033	2615		0.40850	-0.11111	0.00009	0		0.25780	-4.81481	0.00000	88		0.10007	0.66667	0.00005	2065
	0.11996	0.66355	0.00158	61		1.49857					0.22566	-2.34579	0.00000	41		0.10028	0.66250	0.00013	2067
	0.12008	0.66038	0.00019	21		0.09999	0.24051	0.00123	891		0.21208	-1.74528	0.00000	30		0.11830	0.62025	0.00019	2046
	0.08315	0.74286	0.00241	56		0.05320	0.79487	0.00215	169		0.18578	-0.95238	0.00000	18		0.11744	0.61538	0.00002	0
	0.09626	0.70192	0.00155	110		0.07926	0.68831	0.00205	47		0.18657	-0.94231	0.00000	19		0.13295	0.57143	0.00042	2041
	0.19712	-2.04854	0.00161	2350		0.06483	0.75000	0.00099	2010		0.17877	-0.78641	0.00016	2604		0.14030	0.55263	0.00022	2033
	0.08978	0.44118	0.00073	89		0.05058	0.82667	0.00113	1999		0.15262	-0.30392	0.00020	2519		0.14097	0.54667	0.00000	2
	0.08958	0.42574	0.00063	68		0.05410	0.81081	0.00107	2005		0.14411	-0.17822	0.00013	0		0.14979	0.52703	0.00000	2
	0.05985	0.69000	0.00293	70		0.06187	0.76712	0.00092	2010		0.13471	-3.05000	0.00006	2594		0.16009	0.50685	0.00000	0
	0.17760	0.53535	0.00098	585		0.06411	0.75000	0.00094	0		0.13379	-0.02020	0.00096	2485		0.16696	0.48611	0.00000	2
	0.07356	0.57143	0.00161	65		0.05982	0.69014	0.00122	0		0.13021	0.00000	0.00015	2508		0.17344	0.46479	0.00000	0
	1.34e21	-0.06186	0.00010	39		0.05771	0.77143	0.00118	1993		0.14297	-0.14433	0.00094	2484		0.12668	0.55714	0.00000	3
	2.33e8	-0.09375	0.00000	13		0.04385	0.91304	0.00117	1999		0.14428	-0.20833	0.00085	0		0.07489	0.71014	0.00000	3
	0.15051	0.56842	0.00140	75		0.04142	0.92647	0.00104	2005		0.13521	-0.06316	0.00000	18		0.09541	0.64706	0.00000	0
	0.14791	-0.42553	0.00107	443		0.10795	0.55224	0.00045	2041		0.14558	-0.18085	0.00098	461		0.11835	0.56716	0.00000	2
	0.13215	-0.15054	0.00102	294		0.05793	0.77273	0.00108	2008		0.13587	-0.05376	0.00102	440		0.12321	0.54545	0.00000	0
	0.09244	0.39130	0.00066	69		0.57678	0.18462	0.00000	6		0.13740	-0.10870	0.00113	763		0.13373	0.52308	0.00000	0
	0.28162	0.39560	0.00063	42		0.11711	0.57813	0.00152	59		0.14946	-0.25275	0.00091	570		0.08407	0.70313	0.00127	931
	0.21245	-5.93333	0.00195	2388		0.11159	0.60317	0.00143	268		0.15306	-0.34444	0.00010	2436		0.05445	0.93651	0.00170	151
	0.19128	0.49438	0.00004	27		0.05697	0.80645	0.00118	1015		0.13544	-0.08989	0.00008	0		0.07018	0.82258	0.00000	4
	0.11050	0.64773	0.00151	92		0.07730	0.67213	0.00132	317		0.11767	0.11364	0.00023	2524		0.04500	0.86885	0.00228	73
	0.16049	0.54023	0.00113	81		0.24105	0.88333	0.00141	15		0.11146	0.18391	0.00000	2121		0.04427	0.91667	0.00271	70
	0.21281	0.45349	0.00001	20		1.39651					0.10535	0.24419	0.00005	1803		0.04562	0.96610	0.00240	74

0.12599	-0.71765	0.00083	2492	0.39283	0.00000	0.00098	133	0.08875	0.40000	0.00013	2441	0.05584	0.91379	0.00000	1955
0.04490	0.73810	0.00181	28	6.45586	0.24561	0.00000	1896	0.07220	0.53571	0.00020	2471	0.05122	0.98246	0.00196	147
0.04813	0.83133	0.00227	0	0.08082	0.66071	0.00265	61	0.07655	0.49398	0.00122	2496	0.04643	0.92857	0.00180	118
0.10194	-0.26829	0.00106	2511	0.71723	0.03636	0.00000	9	0.07279	0.52439	0.00009	1741	0.04553	0.90909	0.00237	67
0.08487	0.04938	0.00093	0	0.07605	0.59259	0.00141	145	0.06714	0.56790	0.00023	2220	0.04305	0.92593	0.00270	55
0.15824	0.51250	0.00201	72	0.16051	0.43396	0.00150	302	0.05093	0.68750	0.00002	2420	0.07179	0.79245	0.00000	0
0.13973	0.54430	0.00166	96	0.17914	0.38462	0.00116	243	0.04719	0.70886	0.00024	13	0.04854	0.98077	0.00066	2
0.01895	0.97436	0.00756	21	0.08575	0.58824	0.00212	71	0.03455	0.79487	0.00024	2420	0.04783	0.82353	0.00000	0
0.02008	0.97403	0.00626	26	0.03295	0.92000	0.00105	0	0.03983	0.75325	0.00127	2489	0.04868	0.82000	0.00000	2
0.02120	0.97368	0.00607	22	0.08096	0.57143	0.00127	1997	0.02717	0.85526	0.00009	2350	0.05016	0.79592	0.00000	0
0.07419	0.70667	0.00282	54	0.35317	0.14583	0.00120	1051	0.03277	0.80000	0.00129	2506	0.05979	0.70833	0.00000	0
0.02573	0.93243	0.00543	21	0.08598	0.51064	0.00136	1995	0.02175	0.90541	0.00000	11	0.06429	0.68085	0.00000	0
0.02880	0.90411	0.00535	18	0.15474	0.34783	0.00201	55	0.01922	0.93151	0.00022	0	0.07729	0.58696	0.00000	3
0.03022	0.90278	0.00461	20	0.12948	0.40000	0.00000	9	0.01847	0.94444	0.00048	1632	0.08186	0.55556	0.00000	0
0.04275	0.83099	0.00057	2564	0.08799	0.50000	0.00207	116	0.01820	0.97183	0.00054	0	0.07882	0.56818	0.00000	0
0.03420	0.87143	0.00480	19	0.03931	0.65116	0.00213	22	0.01862	0.98571	0.00013	0	0.08294	0.53488	0.00206	74
0.07575	0.68116	0.00049	16	0.04272	0.78571	0.00302	43	0.02019	0.98551	0.00028	0	0.07053	0.59524	0.00000	4
0.04507	0.80882	0.00213	126	0.06979	0.58537	0.00167	28	0.02209	0.97059	0.00023	0	0.07637	0.56098	0.00165	38
0.06983	0.70149	0.00055	17	0.07566	0.55000	0.00111	21	0.02402	0.95522	0.00031	2129	0.05859	0.67500	0.00014	11
0.07770	0.66667	0.00045	17	0.11106	0.41026	0.00204	31	0.02619	0.93939	0.00000	0	0.07531	0.56410	0.00000	4
0.04517	0.80000	0.00243	16	0.10896	0.39474	0.00154	32	0.02905	0.90769	0.00000	0	0.07189	0.57895	0.00000	4
0.06990	0.68750	0.00072	19	0.11620	0.35135	0.00230	34	0.03487	0.87500	0.00140	1401	0.07724	0.51351	0.00000	0
0.05029	0.77778	0.00150	15	0.11794	0.33333	0.00285	42	0.03559	0.87302	0.00045	2350	0.08247	0.47222	0.00000	2
0.04188	0.82258	0.00333	22	0.04500	0.62857	0.00237	118	0.02572	0.93548	0.00191	165	0.08817	0.42857	0.00000	3
0.02882	0.90164	0.00207	208	0.07898	0.44118	0.00266	89	0.03361	0.88525	0.00007	2353	0.08730	0.44118	0.00000	0
0.05181	0.76667	0.00224	18	0.04810	0.57576	0.00208	173	0.04367	0.81667	0.00000	2500	0.08976	0.39394	0.00000	0
0.06907	0.67797	0.00305	74	0.10161	0.31250	0.00257	84	0.04191	0.83051	0.00149	1070	0.09128	0.37500	0.00000	0
0.06931	0.67241	0.00208	150	0.05725	0.45161	0.00252	163	0.04248	0.82759	0.00033	2401	0.09810	0.32258	0.00000	3
0.06743	0.68421	0.00273	50	0.07264	0.36667	0.00000	10	0.03513	0.85965	0.00181	155	0.10340	0.26667	0.00252	59
0.02385	0.80357	0.00392	73	0.02705	0.58621	0.00148	1957	0.03452	0.87500	0.00223	45	0.09401	0.31034	0.00037	8
0.02102	0.81818	0.00395	75	0.03972	0.67857	0.00356	62	0.03721	0.85455	0.00119	14	0.08137	0.39286	0.00000	9
0.01861	0.85185	0.00436	69	0.04219	0.62963	0.00371	54	0.03255	0.88889	0.00217	40	0.07616	0.40741	0.00102	22
0.01706	0.86792	0.00383	66	0.04536	0.57692	0.00408	54	0.04210	0.81132	0.00084	14	0.10789	0.15385	0.00267	54
0.02521	0.92308	0.00426	51	0.03473	0.36000	0.00360	45	0.04373	0.80769	0.00081	14	0.10970	0.12000	0.00250	57
0.02673	0.92157	0.00544	46	0.03628	0.66667	0.00395	23	0.04546	0.78431	0.00052	13	0.07848	0.37500	0.00283	73
0.01884	0.98000	0.00364	52	0.03530	0.65217	0.00281	152	0.03316	0.86000	0.00162	14	0.07397	0.39130	0.00305	71
0.02950	0.87755	0.00475	28	0.03408	0.63636	0.00283	217	0.03184	0.87755	0.00246	46	0.07406	0.36364	0.00037	13
0.02835	0.87500	0.00432	28	0.03775	0.57143	0.00258	165	0.03145	0.87500	0.00222	42	0.08275	0.23810	0.00315	65
0.08866	0.57447	0.00067	26	0.05947	0.30000	0.00171	15	0.02405	0.93617	0.00026	2041	0.08894	0.15000	0.00247	30
0.01412	0.71739	0.00193	0	0.05591	0.31579	0.00214	15	0.02567	0.91304	0.00023	2041	0.07950	0.21053	0.00354	29
0.04139	0.77778	0.00484	50	0.08816	0.16667	0.00371	66	0.02790	0.88889	0.00025	2297	0.07875	0.22222	0.00000	4
0.02839	0.88636	0.00707	13	0.05648	0.23529	0.00286	198	0.03058	0.86364	0.00000	11	0.07955	0.17647	0.00000	4
0.02111	0.55814	0.00236	200	0.05944	0.12500	0.00343	184	0.02740	0.90698	0.00019	4	0.08030	0.12500	0.00000	4
0.01768	0.61905	0.00240	184	0.06689	0.06667	0.00367	23	0.02854	0.88095	0.00080	7	0.08479	0.00000	0.00000	2
0.02061	0.56098	0.00230	211	0.06351	-0.07143	0.00323	150	0.03765	0.82927	0.00177	34	0.08033	0.00000	0.00000	0
0.04047	-0.02500	0.00216	296	0.09088	-0.15385	0.00361	18	0.03849	0.82500	0.00202	30	0.08762	-0.15385	0.00000	2

0.02428	0.92308	0.00503	43	0.05860	-0.33333	0.00377	150	0.03943	0.79487	0.00203	32	0.08735	-0.25000	0.00019	13
0.03173	0.68421	0.00143	2539	0.06132	-0.54545	0.00352	167	0.03981	0.78947	0.00174	32	0.08821	-0.36364	0.00048	0
0.02377	0.91892	0.00435	42	0.07469	-0.60000	0.00470	18	0.03933	0.81081	0.00208	33	0.09145	-0.50000	0.00333	27
0.02756	0.88889	0.00619	22	0.04220	0.22222	0.00685	28	0.03929	0.80556	0.00164	32	0.08579	-0.55556	0.00051	13
0.03794	0.77143	0.00453	21	0.02764	0.00000	0.00445	52	0.03593	0.82857	0.00188	39	0.09425	-0.87500	0.00455	24
0.03107	0.85294	0.00658	13	0.35346	-0.71429	0.00000	0	0.02996	0.85294	0.00055	8	0.09135	-1.00000	0.00004	11
0.03071	0.84848	0.00501	25	0.34491	-0.83333	0.00000	0	0.03716	0.78788	0.00267	38	0.09388	-1.33333	0.00059	15
0.03076	0.84375	0.00538	23	0.04268	-9.40000	0.00207	0	0.03732	0.81250	0.00256	37	0.09926	-2.00000	0.00474	21
0.01030	0.83871	0.00225	326	0.07849	0.75000	0.00084	3	0.03713	0.80645	0.00207	38	0.02451	-1.25000	0.00000	3
0.03051	0.83333	0.00604	12	0.03920	0.66667	0.00430	65	0.03094	0.83333	0.00002	0	0.02059	-1.00000	0.00000	3
0.03233	0.82759	0.00527	24	0.06326	1.00000	0.00283	13	0.04234	0.75862	0.00268	27	0.03276	0.50000	0.00552	38
0.02151	0.92857	0.00488	42	0.02218	-2.00000	0.00708	16	0.03240	0.82143	0.00079	7	0.02752	0.00000	0.00433	39
0.01009	0.74074	0.00266	184					0.02616	0.88889	0.00323	31				
0.03170	0.80769	0.00694	0					0.02944	0.84615	0.00022	4				
0.03373	0.80000	0.00696	13					0.03300	0.80000	0.00071	6				
0.03581	0.75000	0.00654	14					0.03364	0.79167	0.00189	29				
0.03367	0.78261	0.00640	15					0.03047	0.82609	0.00259	29				
0.03039	0.81818	0.00736	15					0.02700	0.86364	0.00290	30				
0.01479	0.85714	0.00847	16					0.01502	0.85714	0.00254	172				
0.07560	0.50000	0.00328	91					0.01746	0.90000	0.00372	62				
0.02591	0.89474	0.00264	240					0.03114	0.84211	0.00183	11				
0.05901	0.55556	0.00522	20					0.03042	0.83333	0.00183	12				
0.02359	0.94118	0.00473	33					0.03014	0.82353	0.00216	12				
0.02357	0.93750	0.00473	33					0.03009	0.87500	0.00200	12				
0.02419	0.93333	0.00973	13					0.03034	0.86667	0.00181	13				
0.01144	0.71429	0.00431	84					0.02466	0.92857	0.00172	4				
0.02502	-0.46154	0.00427	61					0.02256	1.00000	0.00259	30				
0.01623	0.00000	0.00342	55					0.02524	0.91667	0.00200	6				
0.04630	-89.72727	0.00479	2425					0.02669	0.90909	0.00197	6				
0.02210	-0.70000	0.00303	60					0.02390	1.00000	0.00207	30				
0.01152	0.00000	0.00386	45					0.02768	0.88889	0.00212	7				
0.01069	0.12500	0.00607	39					0.01975	0.75000	0.00328	30				
0.01118	0.28571	0.00418	34					0.01858	0.71429	0.00134	7				
0.01444	0.50000	0.00520	52					0.01818	0.50000	0.00479	51				
0.01999	0.60000	0.00693	20					0.01850	0.40000	0.00025	11				
0.03583	0.75000	0.00811	18					0.02030	0.50000	0.00013	19				
0.01983	0.66667	0.00665	35					0.02646	1.00000	0.00276	11				
0.02861	1.00000	0.00866	16					0.02634	0.50000	0.00266	11				
0.02109	-1.00000	0.01123	12					0.02656	0.00000	0.00266	10				

Table 167: The obtained evaluation metrics on all the tests and training data sets with the evaluated Unscented Kalman Filter

